RIGA TECHNICAL UNIVERSITY

Sabīne Greivule

AUGU EĻĻAS IZCELSMES FOTOCIETĒJOŠU POLIMĒRU SVEĶU SINTĒZE UN PIELIETOJUMI

Promocijas darbs

SYNTHESIS AND APPLICATIONS OF VEGETABLE OIL-BASED PHOTO-CURABLE POLYMER RESINS

Doctoral Thesis

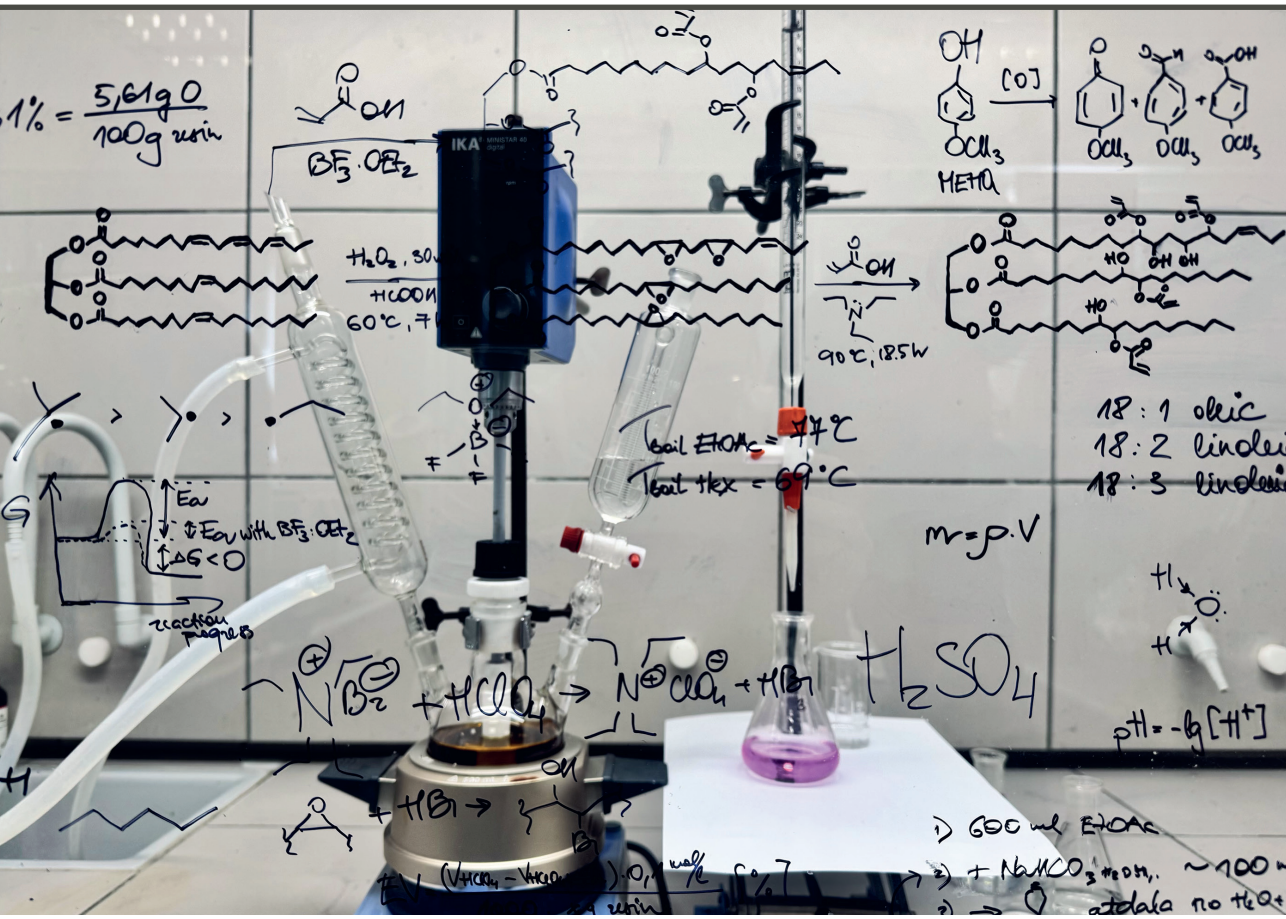

RTU Izdevniecība
RTU Press
Rīga 2026

RĪGAS TEHNISKĀ UNIVERSITĀTE

Dabaszinātņu un tehnoloģiju fakultāte
Ķīmijas un ķīmijas tehnoloģijas institūts

RIGA TECHNICAL UNIVERSITY

Faculty of Natural Sciences and Technology
Institute of Chemistry and Chemical Technology

Sabīne Greivule

Doktora studiju programmas "Ķīmija, materiālzinātne un tehnoloģijas" doktorante
Doctoral Student of the Study Programme "Chemistry, Materials Science and Engineering"

AUGU EĻĻU IZCELSMES FOTOCIETĒJOŠU POLIMĒRU SVEĶU SINTĒZE UN PIELIETOJUMI

Promocijas darbs

SYNTHESIS AND APPLICATIONS OF VEGETABLE OIL-BASED PHOTO-CURABLE POLYMER RESINS

Doctoral Thesis

Zinātniskais vadītājs / Scientific supervisor
Profesors / Professor *Dr. sc. ing.* SERGEJS GAIDUKOVS

Zinātniskais konsultants / Scientific consultant
Dr. ir. TOINE BIEMANS

RTU Izdevniecība / RTU Press
Rīga 2026 / Riga 2026

Greivule, S. Augu eļļas izcelsmes fotocietējošu polimēru sveķu sintēze un pielietojumi. Promocijas darba kopsavilkums. Rīga: RTU Izdevniecība, 2026. 94 lpp.

Greivule, S. Synthesis and Applications of Vegetable Oil-Based Photo-Curable Polymer Resins. Summary of the Doctoral Thesis. Riga: RTU Press, 2026. 94 p.

Publicēts saskaņā ar promocijas padomes "RTU P-02" 2026. gada 16. marta lēmumu, protokols Nr. 04030- 9.2/9.

Published in accordance with the decision of the Promotion Council "RTU P-02" of 16 March 2026, Minutes No. 04030-9.2/9.

Savienojumi un materiāli tika sintezēti, izstrādāti un testēti Rīgas Tehniskās universitātes Ķīmijas un ķīmijas tehnoloģijas institūtā.

The compounds and materials were synthesised, developed and tested at Riga Technical University Institute of Chemistry and Chemical Technology.

Promocijas darba pētījumu atbalstīja:

- Eiropas Sociālā fonds, projekts Nr. 8.2.2.0/20/I/008 "Rīgas Tehniskās universitātes un Banku augstskolas doktorantu un akadēmiskā personāla stiprināšana stratēģiskās specializācijas jomās" īstenošanai, saskaņā ar darbības programmas «Izaugsme un nodarbinātība» specifiskā atbalsta mērķi 8.2.2 "Stiprināt augstākās izglītības institūciju akadēmisko personālu stratēģiskās specializācijas jomās";
- Rīgas Tehniskās universitātes doktorantu stipendiju programma;
- ES Atveseļošanas un noturības mehānisms, projekts Nr. 5.2.1.1.i.0/2/24/I/CFLA/003 "Konsolidācijas un pārvaldības izmaiņu ieviešana RTU, LiepU, Rēzeknes Tehnoloģiju akadēmijā un Latvijas Jūras akadēmijā un Liepājas Jūrniecības koledžā virzībai uz izcilību augstākajā izglītībā, zinātnē un inovācijās" akadēmiskās karjeras doktoranta stipendijas ietvaros (ID 1097);

- ES Atveseļošanas un noturības mehānisms, projekta Nr. 5.2.1.1.i.0/2/24/I/CFLA/003 “Konsolidācijas un pārvaldības izmaiņu ieviešana RTU, LiepU, Rēzeknes Tehnoloģiju akadēmijā un Latvijas Jūras akadēmijā un Liepājas Jūrniecības koledžā virzībai uz izcilību augstākajā izglītībā, zinātnē un inovācijās” pētniecības un attīstības granta apakšprojekta – inovāciju konsolidācijas granta ietvaros (ID 4835).

This research was supported by:

- the European Social Fund within the Project No. 8.2.2.0/20/I/008 “Strengthening of PhD students and academic personnel of Riga Technical University and BA School of Business and Finance in the strategic fields of specialization” of the Specific Objective 8.2.2 “To Strengthen Academic Staff of Higher Education Institutions in Strategic Specialization Areas” of the Operational Programme “Growth and Employment”;
- Riga Technical University’s Doctoral Grant program;
- the EU Recovery and Resilience Facility within Project No. 5.2.1.1.i.0/2/24/I/CFLA/003 “Implementation of consolidation and management changes at Riga Technical University, Liepaja University, Rezekne Academy of Technology, Latvian Maritime Academy and Liepaja Maritime College for the progress towards excellence in higher education, science and innovation” academic career doctoral grant (ID 1097);
- the EU Recovery and Resilience Facility within Project No. 5.2.1.1.i.0/2/24/I/CFLA/003 “Implementation of consolidation and management changes at Riga Technical University, Liepaja University, Rezekne Academy of Technology, Latvian Maritime Academy and Liepaja Maritime College for the progress towards excellence in higher education, science and innovation” research and development grant sub-grant innovation consolidation grant (ID 4835).

PATEICĪBAS

Vislielākais paldies manam atbalstošajam vīram Ģirtam, kurš ar savu mīlestību, iedrošinājumu un humoru mani vienmēr uzmundrinājis un motivējis darboties! Liels paldies manai ģimenei – mammai Edītei, tētim Verneram, brālim Reinim un visam kuplajam radu skaitam –, kas caur maniem stāstiem dzīvojuši līdz visiem šiem gadiem fakultātē! Liels paldies maniem kolēģiem un doktorantūras līdzgaitniekiem par tik patīkamo atmosfēru darbā, par kopīgi pavadīto laiku ārzemēs, par smiekliem, padomiem, palīdzību eksperimentos un datu apstrādē! Paldies manām draudzenēm un bijušajām kursabiedrenēm, kas vienmēr interesējās par mana darba progresu un notikumiem fakultātē!

Pateicos savam mentoram 2023./2024. gadā (uzņēmumā *Worlée*, Vācijā) – *Toine Biemans* – par tik daudz skaidrojumiem un padomiem darba izstrādē, kā arī par palīdzību Vācijā ar ikdienišķām lietām. Paldies institūta direktorei Inesei Mieriņai par palīdzību un uzņemtajiem KMR spektriem!

No sirds pateicos savam darba vadītājam profesoram Sergejam Gaidukovam par iespēju strādāt lieliskā kolektīvā, par motivāciju, idejām, padomiem un atbalstu visā darba tapšanas laikā! Pateicos arī par fantastisko iespēju piedalīties ārzemju treniņskolās, redzēt zinātni ārpus Latvijas robežām, kā arī apceļot pasauli un iepazīt ārvalstu kultūru!

"Jo Dievs nav mums devis bailības garu,
bet spēka, mīlestības un savaldības garu."
/2. Tim. 1:7/

ACKNOWLEDGEMENTS

My deepest gratitude goes to my supportive husband, Ģirts, whose love, encouragement, and humour have always uplifted and motivated me to keep going. Many thanks go to my family – my mother Edīte, my father Verners, my brother Reinis, and my entire extended family – who have shared in my journey throughout all these years at the faculty. I am also very grateful to my colleagues and my fellow PhD students for creating a pleasant working atmosphere, for the time spent together abroad, for the laughter, advice, and help with experiments and data processing. I am grateful to my friends and former coursemates, who have always been interested in the progress of my work and events at the faculty.

I would like to thank my mentor during 2023/2024 (in the company Worlée, Germany), Toine Biemans, for his many explanations and advice in developing this work, as well as for helping me with everyday matters in Germany. I am grateful to the institute director, Inese Mieriņa, for her assistance and for taking the NMR spectra.

I would like to thank my supervisor, Professor Sergejs Gaidukovs, for the opportunity to work in a wonderful team, for the motivation, ideas, guidance, and support throughout the entire process of this work. I am also thankful for the fantastic opportunity to participate in international training schools, to see science beyond Latvia's borders, to travel the world and experience foreign cultures.

PROMOCIJAS DARBS IZVIRZĪTS ZINĀTNES DOKTORA GRĀDA IEGŪŠANAI RĪGAS TEHNISKAJĀ UNIVERSITĀTĒ

Promocijas darbs zinātnes doktora (*Ph. D.*) grāda iegūšanai tiek publiski aizstāvēts 2026. gada 25. maijā plkst. 10 Rīgas Tehniskās universitātes Dabaszinātņu un tehnoloģiju fakultātē, Paula Valdena ielā 3, 272. auditorijā.

OFICIĀLIE RECENZENTI

Asociētais profesors *Dr. chem.* Ingars Reinholds,
Latvijas Universitāte, Latvija

Profesors *Ph. D. Marco Sangermano*,
Turīnas Politehniskā universitāte, Itālija

Profesore *Ph. D. Minna Hakkarainen*,
Karaliskais Tehnoloģiju institūts, Zviedrija

APSTIPRINĀJUMS

Apstiprinu, ka esmu izstrādājusi šo promocijas darbu, kas iesniegts izskatīšanai Rīgas Tehniskajā universitātē zinātnes doktora (*Ph. D.*) grāda iegūšanai. Promocijas darbs zinātniskā grāda iegūšanai nav iesniegts nevienā citā universitātē.

Sabīne Greivule ……. (paraksts)

Date: ……

Promocijas darbs sagatavots kā tematiski vienota zinātnisko publikāciju kopa. Tajā ir kopsavilkums latviešu un angļu valodā un piecas *SCI* publikācijas. Publikācijas uzrakstītas angļu valodā, to kopējais apjoms ir 67 lpp.

ANOTĀCIJA

Promocijas darbā risināta problēma, kas saistīta ar naftas produktu pārmērīgu izmantošanu polimērmateriālu industrijā un to nepietiekamu pārstrādi. Šāda atkarība veicina resursu izsīkumu, vides piesārņojumu un rada papildu izaicinājumus atkritumu apsaimniekošanā, jo tradicionālajiem termoreaktīvajiem polimēriem ir ierobežotas pārstrādes iespējas. Lai demonstrētu to, ka pāreja uz ilgtspējīgākiem risinājumiem ir iespējama, pētījumā izmantotas rapšu, linsēklu un vīnogu kauliņu eļļas kā atjaunojami dabas izcelsmes resursi polimērmateriālu izstrādei. Augu eļļas un to polimēru atvasinājumi (taukskābju modificēti poliesteri jeb alkīdi) tika pārveidoti fotoaktīvos savienojumos, modificējot tos ar akrilātiem, un pētīti UV gaismas inducētā cietēšanas procesā, kas ir ātra, energoefektīva un videi draudzīga alternatīva tradicionālajai termiskajai cietēšanai.

Fotoaktīvie augu eļļu akrilāti sintezēti, izmantojot vienpakāpes vai divpakāpes sintēzes metodes, optimizējot reakcijas parametrus un izvērtējot to ietekmi uz UV cietēšanas kinētiku. Vienlaikus fotoaktīvo akrilgrupu ieviešana pielāgota arī linsēklu eļļas izcelsmes alkīdiem – industriāli nozīmīgam pārklājumu sektoram –, izmantojot epoksīda gredzena atvēršanās reakciju, būtiski paātrinot alkīdu cietēšanu, samazinot nepieciešamību pēc šķīdinātājiem un saglabājot mehānisko izturību. Tika izstrādātas UV cietējošas sveķu formulācijas ar dažādiem, tostarp dabas izcelsmes, reaktīvajiem atšķaidītājiem, lai samazinātu sveķu viskozitāti un uzlabotu šķērssaistīto polimērmateriālu fizikālās un (termo)mehāniskās īpašības. Sveķu piemērotība koksnes pārklājumiem tika pētīta, nosakot adhēzijas stiprību, svārsta cietību un iespiešanās dziļumu. Šķērssaistīto materiālu mehānisko īpašību uzlabošanai darba gaitā tika izstrādāti kompozītmateriāli ar celulozes stiegrojumu, saglabājot izejvielu atjaunojamo izcelsmi. Visbeidzot, darbā tika demonstrēta UV cietējošu vitrimēru izstrāde no akrilētas epoksidētas rapšu eļļas, kontrolējot struktūrā dinamiski kovalento saišu saturu. Iegūtie materiāli tika termiski atkārtoti pārstrādāti un 3D drukāti, kā arī tiem tika pierādīta struktūras atjaunošanās, kas būtiski paplašina to otrreizējās izmantošanas iespējas.

Promocijas darba rezultāti demonstrē augu eļļu akrilātu un to atvasinājumu potenciālu ilgtspējīgu, funkcionālu un pārstrādājamu polimērmateriālu izstrādei, piedāvājot videi draudzīgu alternatīvu naftas izcelsmes polimērmateriāliem un paplašinot UV cietējošo materiālu praktiskās pielietojuma iespējas.

IZMANTOTIE SAĪSINĀJUMI

3D	trīsdimensionāls
A. u.	patvaļīgas vienības
AA	akrilskābe
AESO	akrilēta epoksidēta sojas pupiņu eļļa
AERO	akrilēta epoksidēta rapšu eļļa
AGO	akrilēta vīnogu kauliņu eļļa
ALO-A	akrilētas linsēklu eļļas alkīds
ALO	akrilēta linsēklu eļļa
ARO	akrilēta rapšu eļļa
Ats.	atsauce
AV	skābes skaitlis
BHT	butilēts hidroksitoluols
DBC	dubultsaišu konversija
DLP	digitālās gaismas apstrāde
DMA	dinamiski mehāniskā analīze
DS	dielektriskā spektroskopija
DSC	diferenciāli skenējošā kalorimetrija
E	elastības modulis
E′	uzkrājuma modulis (DMA mērījumos)
E″	zudumu modulis (DMA mērījumos)
EEW	epoksīda masas ekvivalents
ELO-A	epoksidētas linsēklu eļļas alkīds
ERO	epoksidēta rapšu eļļa
EtOAc	etilacetāts
EV	epoksīda skaitlis
FTIR	Furjē transformācijas infrasarkanā spektroskopija
G′	uzkrājuma modulis (fotoreoloģijas mērījumos)
G″	zudumu modulis (fotoreoloģijas mērījumos)
$G_{(t)}/G_0$	normalizētais sprieguma relaksācijas modulis
GDA	glicerīna 1,3-diglicerolāta diakrilāts
GPT	glicerīna propoksitriakrilāts
h	stundas
HDDA	heksāndiola diakrilāts
HPPA	2-hidroksi-3-fenoksipropil akrilāts
HQ	hidrohinons
IBOA	izobornilakrilāts
Izn.	iznākums
KMR	kodolmagnētiskā rezonanse
MEHQ	4-metoksifenols
NP	nanopapīrs

ppm	miljonās daļas
RO	rapšu eļļa
SEC	izmēru izslēgšanas hromatogrāfija
SEM	skenējošā elektronu mikroskopija
SLA	stereolitogrāfija
T	temperatūra
T_g	stiklošanās temperatūra
t_{gel}	gelpunkts
Tanδ	zudumu faktors
TEA	trietilamīns
TGA	termogravimetriskā analīze
TMPTMA	trimetilolpropāna trimetakrilāts
TPGDA	tripropilēnglikola diakrilāts
TPP	trifenilfosfīns
UES	nepiesātināts esteris
UV-Vis	ultravioletās redzamās gaismas spektroskopija
VOC	gaistošie organiskie savienojumi
ε	deformācija
ε_B	deformācija sagraušanas brīdī
η	viskozitāte
σ	spriegums
σ_B	sagraušanas robežspriegums
τ*	relaksācijas laiks

SATURS

Pielikums IV Platnieks, O., Briede, S., Grase, L., Thakur, V., J., & Gaidukovs, S. (2023). Fully Bio-Based Thermoset Composites from UV Curable Prepregs: Vegetable Oil Acrylate Impregnated Hemp Nanopaper. *Polymer Composites*, 44(9), 5721-5733.

Pielikums V Briede, S., Besprozvannaja I., Porcarello M., & Gaidukovs, S. (2026). Reprocessable and Repairable Bio-Based Vitrimers from Acrylated Epoxidized Rapeseed Oil for Additive Manufacturing. *Macromolecular Materials and Engineering*. doi: 10.1002/mame.70228. (Pieņemts).

PROMOCIJAS DARBA VISPĀRĒJS RAKSTUROJUMS

Ievads un literatūras apskats

Mūsdienās polimērmateriālu industrija saskaras ar vairākām problēmām, kas galvenokārt saistītas ar pārmērīgu neatjaunojamo resursu izmantošanu un salīdzinoši lēnu inovatīvu tehnoloģisko procesu ieviešanu industrijā. 2019. gadā naftas izcelsmes plastmasas ražošanas apjomi pasaulē sasniedza gandrīz 370 miljonus tonnu, un tikai aptuveni 9 % no tiem tika pārstrādāti, kas liecina par būtiskiem trūkumiem esošajā aprites sistēmā [1]. Ņemot vērā Eiropas Savienības "zaļā kursa" ("*Green Deal*") mērķi līdz 2050. gadam panākt klimata neitralitāti, pāreja uz atjaunojamām izejvielām kļūst aktuāla, lai mazinātu atkarību no naftas produktiem un nodrošinātu materiālu atgriešanu apritē. Kā ilgtspējīgs atjaunojamais biopolimēru avots pēdējos gados plaši tiek pētītas augu eļļas. Interese par augu eļļu izmantošanu polimērmateriālu industrijā ir strauji pieaugusi, un kopš 2015. gada publikāciju skaits par to pielietojumu biopolimēru izstrādē ir palielinājies par vairāk nekā 250 %. Piemēram, Latvijas klimata apstākļiem piemērotā rapšu eļļa šajā kontekstā ir nozīmīgs atjaunojamais resurss un pieejama alternatīva izejviela polimērmateriālu izstrādei.

Vēsturiski augu eļļas, piemēram, linsēklu eļļa, plaši izmantotas polimēru industrijā, galvenokārt laku un pārklājumu ražošanā. Pēdējās desmitgadēs interese par augu eļļām ir ievērojami pieaugusi, paplašinoties tehnoloģiskajai attīstībai un biomasas pielietošanas jomām [2], [3]. Augu eļļas galvenokārt sastāv no triglicerīdiem (ap 95 %); mazā daudzumā sastopami monoglicerīdi un diglicerīdi, brīvās taukskābes, fosfolipīdi, tokoferoli, polifenoli un citi savienojumi [4]. Triglicerīdu molekulā esošie reakciju aktīvie centri – dubultsaites, estergrupas, alilgrupas un bisalilgrupas – nodrošina plašas struktūras modifikācijas iespējas. Turklāt augu eļļu viskozitāte (η) padara tās piemērotas UV cietējošiem sveķiem, nodrošinot labu plūstamību.

Lai rapšu un citas augu eļļas efektīvi izmantotu biopolimēru ražošanā, īpaša uzmanība tiek pievērsta to apstrādes tehnoloģijām. Viens no mūsdienīgiem un moderniem risinājumiem polimēru ražošanas procesā ir fotoinducēta jeb ultravioletās (UV) gaismas inducēta cietēšanas tehnoloģija, kas kā alternatīva termiskajai cietēšanai nodrošina ātrāku reakciju, mazāku enerģijas patēriņu un mazākas gaistošo organisko savienojumu (VOC) emisijas. UV cietēšana augu eļļām iespējama pēc to taukskābju atlikumos esošo nepiesātināto dubultsaišu modificēšanas, ieviešot tajās fotoaktīvas akrilgrupas.

Augu eļļu akrilēšanu var panākt, izmantojot vairākus sintēzes ceļus, no kurām visplašāk izmantotā ir tradicionālā divpakāpju epoksidēšanas-akrilēšanas metode. Ir ziņotas arī alternatīvas pieejas, piemēram, tieša dubultsaišu vienpakāpes akrilēšana, taču tā ir mazāk pētīta. Sintēzes metodes izvēle ietver kompromisus starp reakcijas apstākļiem, kontroli un blakusreakciju iespējamību. Divpakāpju metode ir labi atstrādāta un ļauj pakāpeniski kontrolēt funkcionālo grupu veidošanos, lai gan tas prasa precīzu gan epoksidēšanas, gan sekojošās gredzena uzšķelšanas reakciju optimizāciju. Savukārt tieša dubultsaišu akrilēšana ir īsāka un atomu ziņā efektīvāka sintēzes metode, bet parasti pieprasa spēcīgu katalizatoru klātbūtni un var būt jutīgāka pret reakcijas apstākļiem.

Augu eļļu akrilēšana divpakāpju sintēzē sākas ar triglicerīda taukskābju atlikumos esošo dubultsaišu epoksidēšanu, kam seko oksirāna gredzena uzšķelšana ar akrilskābi (AA) (1. a att.). Dubultsaišu epoksidēšana jeb Priļežajeva reakcija caur *in situ* ģenerētu peroksiskābi ir plaši lietota epoksidētas sojas pupiņu eļļas iegūšanai [5]. Nekontrolētos apstākļos viegli iespējamas blakusreakcijas, piemēram, epoksīda gredzena atvēršanās ar skābi vai ūdeni un citas nevēlamas reakcijas (piemēram, H_2O_2 sadalīšanās), kas var notikt gan ūdens fāzē, gan eļļas fāzē, gan uz robežvirsmas [6]. Publikācijās 60 °C temperatūra atzīta par optimālu epoksidēšanas reakcijai [7]. *Kousaalya* un līdzautori novēroja, ka reakcijas temperatūras paaugstināšana no 40 °C līdz 60 °C palielināja epoksidēšanas iznākumu no 58 % līdz 88 %. Savukārt tālākajos eksperimentos, mērot α-glikola vērtības, autori novēroja, ka, turpinot palielināt temperatūru, palielinājās arī nevēlamā epoksīda gredzena atvēršanās reakciju daudzums [8]. *Turco* un līdzautori norādīja, ka linsēklu eļļas epoksidēšana jāveic zemākā temperatūrā, lai izvairītos no epoksīda gredzena atvēršanās. Izmantojot kinētisko modeli, autori aprēķināja, ka lielā linolēnskābes atlikuma daudzuma dēļ triglicerīda struktūrā linsēklu eļļa ir 1,5 reizes reaktīvāka nekā sojas pupiņu eļļa; līdz ar to epoksidēšanas laikā gredzena atvēršanās reaktivitāte bija aptuveni četras reizes augstāka nekā sojas pupiņu eļļai [9]. H_2O_2 pievienošanas ātruma ietekme uz reakcijas iznākumu literatūrā nav plaši pētīta, un galvenokārt H_2O_2 tiek pievienots 30 min līdz 60 min laikā. *Santacesaria* un līdzautori pierādīja, ka H_2O_2 pievienošanas ātruma ietekme dubultsaišu konversijai un iznākumam ir maznozīmīga, salīdzinot ar reakcijā izmantoto H_2O_2 un dubultsaišu molāro attiecību [10]. Kā katalizators visbiežāk tiek izmantota skudrskābe vai etiķskābe. Daži autori kā katalizatoru iesaka pievienot H_2SO_4 vai – lai sasniegtu augstāku augu eļļas epoksidēšanas iznākumu – pievienot šķīdinātāju vai pat papildu brīvās taukskābes [11], [12]. Interesanti, ka atšķirībā no lielākās daļas zinātnisko rakstu, kuros minēts, ka epoksidēšanas procesa ātruma limitējošā reakcija ir peroksiskābes veidošanās, tas pats autors ziņoja, ka pati epoksidēšanas reakcija ir piecas reizes lēnāka nekā peroksiskābes veidošanās [13]. Nepilnīgu reakcijas iznākumu, atstājot neizreaģējušas taukskābju atlikumos esošās dubultsaites, var izraisīt stēriski apgrūtināta piekļuve reakcijas centriem, nekontrolēti reakcijas apstākļi (temperatūras, laika, reaģentu molārās attiecības) vai pat, kā ziņo *La Scala* un līdzautori, dažādas taukskābju reaģētspējas [14]. Epoksidēšanas iznākums parasti tiek ziņots kā epoksīda skaitlis (EV, mol epoksīda/100 g sveķu) vai epoksīda masas ekvivalents (EEW, g sveķu/mol epoksīda), kas visbiežāk tiek noteikts, titrējot ar *in situ* ģenerētu HBr [15]. Atkarībā no taukskābju atlikuma sadalījuma triglicerīdā parasti EV ir robežās no 0,250 mol epoksīda/100 g sveķu līdz 0,613 mol epoksīda/100 g sveķu. Šo raksturojošo parametru saistība ir šāda: EV = 100/EEW. Epoksidēšanas reakciju salīdzinājums dažādām augu eļļām gan pēc izejvielu molārajām attiecībām, gan reakciju apstākļiem apkopots 1. tabulā.

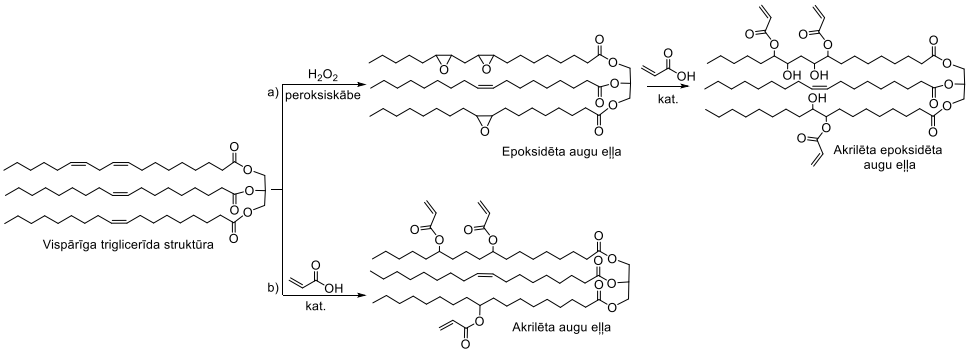

1. att. Akrilētu augu eļļu sintēze a) divos soļos, caur epoksidēšanu; b) vienā solī ar katalizatoru.

1. tabula

Dažādu augu eļļu epoksidēšanas reakcijas salīdzinājums pēc izejvielu molārajām attiecībām un reakcijas apstākļiem

Izmantotā augu eļļa	Ziņotais joda skaitlis (g I_2/100 g produkta)	Aprēķinātais C=C skaits/ taukskābes atlikumā	Molārā attiecība, (mol/mol)		Laiks (h)	T (°C)	EV (mol epoksīda/ 100 g sveķu)[a]	Izn. %	Ats.
			$n_{H2O2}/n_{C=C}$	$n_{HCOOH}/n_{C=C}$					
Linsēklu eļļa	174	2,01	1,4	0,2	5–9	45–60	0,375–0,531[b]	55–77	[9]
Jatrofas eļļa	105	1,21	4,1	0,2	5–6	60–65	0,252[c]	61	[16]
Sojas pupiņu eļļa	–	1,53[d]	2,0	0,6	1–7	45–55	0,288–0,481[e]	55–92	[17]
Sojas pupiņu eļļas alkīds	57,63	0,96	3,0	2,9	6	0	0,298[f]	–	[18]
Sojas pupiņu eļļa	–	–	1,8	0,8	7	50	0,383[g]	–	[19]
Perilla eļļa	196,9	2,27	10,3	3,4	8	40–60	0,610[h]	91	[8]

[a] Pārskatāmībai un salīdzināšanai reakciju iznākumi tabulā pārrēķināti un norādīti kā EV, kur raksturojošo parametru attiecības ir šādas: EV = 100/EEW un EV = Oksirāna skābekļa saturs/16.
[b] Ziņotā vērtība: oksirāna skābekļa saturs = 6–8,5 g O/100 g sveķu.
[c] Ziņotā vērtība: EEW = 397 g sveķu/mol epoksīda.
[d] Ziņotā vērtība: sākuma dubultsaišu skaits = 4,60.
[e] Ziņotā vērtība: 2,4–4,6 epoksīda grupas/molekulā.
[f] Ziņotā vērtība: EEW = 335,7 g sveķu/mol epoksīda.
[g] Ziņotā vērtība: oksirāna skābekļa saturs = 6,13 %.
[h] Ziņotā vērtība: EEW = 164 g sveķu/mol epoksīda.

Savukārt 2011. gadā pirmoreiz tika aprakstīta epoksidētas sojas pupiņu eļļas akrilēšana ar AA trietilamīna (TEA) klātbūtnē UV cietējošu koksnes pārklājumu pielietojuma izpētei [19]. Epoksidētas sojas pupiņu eļļas akrilēšanas reakcija tika veikta 80 °C temperatūrā 15 h. Epoksidētas augu eļļas un AA akrilgrupu molārā attiecība literatūrā tiek ziņota no 1 : 0,165 līdz pat 1 : 10, un tā ir atkarīga no triglicerīda taukskābju atlikuma satura [20]. Liels AA pārākums

palielina reakcijas iespējamību, tomēr pastāv risks tās polimerizācijai par poliakrilskābi. *Maassen* un līdzautori novēroja AA polimerizāciju 95 °C temperatūrā trīs situācijās: 1) izmantojot vairāk nekā divus AA ekvivalentus (attiecībā uz 1 ekvivalentu epoksīda gredzena); 2) veicot reakciju ilgāk par 7 h; 3) mērogojot reakciju uz lielākiem apjomiem [21]. Turklāt AA atlikums pēc sintēzes arī apgrūtina reakcijas neitralizēšanu, un tās atlikums akrilētos augu eļļas sveķos var ietekmēt UV cietējošā gala pārklājuma īpašības. Literatūrā epoksidētu taukskābju atlikumu akrilēšanas reakcijas temperatūra ir robežās no 60 °C līdz 120 °C. Jāpiezīmē, ka 110 °C tiek uzskatīti par akrilēšanas temperatūras "griestiem", jo tas var izraisīt AA polimerizāciju [22], kam pretēji *Chu* un līdzautori 120 °C temperatūru ziņoja kā optimālu epoksidētas sojas pupiņu eļļas akrilēšanai [23]. Turklāt arī akrilēšanas laiks ievērojami atšķiras literatūrā minētajos sintēžu aprakstos un ir minēts robežās no 2,3 h līdz 40 h [20]. Epoksidētas augu eļļas akrilēšanas kvantitatīvs iznākums pēc sintēzes lielākoties netiek noteikts. Parasti pētnieki vadās pēc EV vērtības samazināšanās vai pēc izlietotā AA daudzuma, nosakot skābes skaitli ar KOH etanola šķīduma titrēšanu [24]. *Saithai* un līdzautori noteica kvantitatīvu akrilētas sojas pupiņu eļļas (AESO) iznākumu pēc ^{1}H-KMR spektroskopijas, ar iznākumu 1,54–2,76 akrilgrupas uz molekulu atkarībā no sojas pupiņu eļļas epoksidēšanas iznākuma [17]. Akrilēšanas reakciju salīdzinājums dažādām epoksidētām augu eļļām gan pēc izejvielu molārajām attiecībām, gan reakciju apstākļiem apkopots 2. tabulā.

2. tabula

Dažādu epoksidētu augu eļļu akrilēšanas reakcijas salīdzinājums pēc izejvielām un reakcijas apstākļiem

Izmantotā epoksidētā augu eļļa	Aprēķinātais EV (mol epoksīda/ 100 g sveķu)	Molārā attiecība $n_{AA}/n_{epoksīds}$, (mol/mol)	Katalizators	Inhibitors	Laiks (h)	T (°C)	Ziņotās reakcijas beigas/ iznākums	Ats.
Epoksidēta sojas pupiņu eļļa	0,250	1,41	TPP, 1 masas %	BHT, 0,03 masas %	6	90–95	AV = 1,15 mg KOH/g sveķu, Oksirāna skābekļa saturs = 0,012 g O/100 g sveķu	[24]
Epoksidēta sojas pupiņu eļļa	0,425	1,25	Trifenilfosfīna oksīds, 1,5 masas %	4-terc-butilkatehols, 0,15 masas %	6	120	AV = 5 mg KOH/g sveķu, 95 %	[23]
Epoksidēta sojas pupiņu eļļa	0,288	10	–	HQ	7	110	1,54–2,76 akrilgrupas/ molekulā	[17]
Epoksidēta linsēklu eļļa	0,563	0,89	TPP, 0,059 masas %	HQ, 0,5 masas %	2,3	60–75	–	[25]
Epoksidēta sojas pupiņu eļļa	0,375	4	TEA, 1 masas %	MEHQ, 0,5 masas %	40	80–110	AV = 10 mg KOH/g sveķu, EV = 0,15 g O_2/100 g sveķu	[22]
Epoksidēta sojas pupiņu eļļa	0,383	0,6	TEA	HQ	15	80	AV = 6,2 mg KOH/g sveķu	[19]

2013. gadā *Zhang* un līdzautori nāca klajā ar tiešu AA pievienošanos triglicerīda skābju atlikumos esošajām dubultsaitēm $BF_3{\cdot}OEt_2$ katalizatora klātbūtnē (1. b att.) [26]. Šīs sintēzes priekšrocības ir laika un atomu ekonomija, salīdzinot ar divpakāpju sintēzi izmantojot epoksidēšanu. Turklāt pēc sintēzes bija iespējams atgūt līdz pat 86 % sākotnējo izejvielu (nereaģējušo akrilskābi un katalizatoru). Autori ar ^{1}H-KMR analīzi pierādīja 3,09 akrilgrupas uz vienu triglicerīda molekulu, kas ir 76 % augsts iznākums, pieņemot 4,08 kā vidējo taukskābju atlikuma dubultsaišu skaitu sojas pupiņu eļļā. Vēlāk, veicot literatūras analīzi par dažādiem karbonilgrupas un alkēnu dubultsaišu reakciju katalizatoriem, šie paši autori sojas pupiņu eļļas tiešai akrilēšanai izmēģināja arī citus katalizatorus [27]. Autori novēroja, ka gan Brensteda, gan Luisa skābēm sojas pupiņu eļļas akrilēšanā bija no skābuma atkarīga katalītiskā aktivitāte šādā secībā: $BF_3{\cdot}OEt_2 > FeCl_3 > SnCl_4 > TiCl_4$ un *p*TsOH > MsOH > Amberlyst 15. Augsta katalizatora koncentrācija ne tikai paātrināja reakciju, bet arī nodrošināja augstāku reakcijas iznākumu – līdz pat 3,26 akrilgrupām molekulā. Autori papildus izpētīja reakcijas apstākļus, secinot, ka, temperatūrai palielinoties virs 80 °C, notiek blakusreakcijas, tostarp AA polimerizācija. Vēlāk cita zinātnieku grupa šo sintēzes metodi izmantoja, lai sintezētu dažādus augu eļļu akrilātus, tajā skaitā palmu, olīvu, zemesriekstu, rapšu, kukurūzas un vīnogu kauliņu eļļas akrilātus [28]. Autori novēroja, ka pēc reakcijas akrilgrupu skaits molekulā palielinājās, palielinoties augu eļļu nepiesātinājuma pakāpei, savukārt reakcijas ātrums samazinājās stērisko traucējumu dēļ, kas kavēja tālāku akrilgrupu pievienošanos. Pēc UV cietēšanas eļļas ar augstāku akrilgrupu daudzumu uzrādīja augstāku šķērssaišu blīvumu, kas ir kvantitatīvs lielums un raksturo šķērssasistīto mezglu skaitu polimēra tilpuma vienībā (mol/m^3).

Augstāks šķērssaišu blīvums ietekmēja materiālu termomehāniskās un mehāniskās īpašības, un tā rezultātā palielinājās stiklošanās temperatūra (T_g), sagraušanas robežspriegums (σ_B) un elastības modulis (E). Augstāko T_g (50 °C), stiepes moduli (8,94 MPa) un iznākumu ar 2,17 akrilgrupām uz molekulu pēc ^{1}H-KMR spektroskopijas uzrādīja akrilēta vīnogu kauliņu eļļa.

Apkopojot, divpakāpju epoksidēšanas-akrilēšanas sintēzes metode laika gaitā ir pilnveidota un plašāk izmantota dažādu augu eļļu modificēšanai. Tomēr tā ietver divus reakcijas soļus. Vienpakāpes augu eļļu akrilēšana nodrošina īsāku sintēzes laiku, taču tās efektivitāte un selektivitāte lielā mērā ir atkarīga no katalizatora izvēles un reakcijas apstākļiem. Līdz ar to izvēle starp šīm pieejām ir atkarīga no vēlamā kompromisa starp procesa vienkāršību un funkcionālo grupu kontroli, jo šie faktori ietekmē iegūto materiālu struktūru, reaģētspēju un piemērotību pielietojumiem.

Līdz ar ilgtspējības koncepta paplašināšanos sveķu formulāciju izstrāde kļūst arvien būtiskāka, jo mūsdienu materiāliem jāatbilst ne tikai ekoloģiskajiem kritērijiem, bet arī progresīvu ražošanas tehnoloģiju prasībām. Strauji attīstoties industriālajiem procesiem, ir nostiprinājusies ceturtā industriālā revolūcija jeb "Industrija 4.0", kuras pamatā ir digitālo un automatizācijas tehnoloģiju integrācija ražošanā [29]. Viens no nozīmīgākajiem virzieniem šajā kontekstā ir aditīvā ražošana, kas raksturojama kā trīsdimensionālu (3D) objektu veidošana no digitāla modeļa, pakāpeniski uzklājot materiālu slāņos, izmantojot digitāli vadāmu aprīkojumu. Aditīvās ražošanas tehnoloģijas ietver materiāla ekstrūziju, saistvielas strūklas uzklāšanu, pulveru slāņa sakausēšanu, loksņu laminēšanu, vannas tipa fotopolimerizāciju u. c. [30]. Starp vannas tipa polimerizācijas metodēm plaši lietota ir digitālās gaismas apstrādes (DLP) un stereolitogrāfijas (SLA) 3D druka, kurā UV starojuma inducēta polimerizācija norit slāni pa

slānim, vienlaikus vai punktveidā ar lāzerstaru izgaismojot šķidro sveķu slāni [31]. UV cietējošo sveķu 3D drukas tehnoloģija nodrošina augstu izšķirtspēju, izcilu virsmas kvalitāti, kā arī izejvielu efektīvu izmantošanu, kas padara to piemērotu sarežģītu detaļu ražošanai [32]. Lielākā daļa UV aktīvo sveķu ir akrilātu atvasinājumi, un tie veido aptuveni pusi no 3D drukāšanas polimērmateriālu tirgus [33]. Literatūrā jau publicēti daži raksti, kuros minēts, ka akrilētu augu eļļu saturoši 3D drukāti materiāli mehānisko īpašību ziņā spēj sacensties ar komerciāli pieejamajiem naftas monomeru saturošiem 3D drukātiem materiāliem. Piemēram, 3D drukātam sojas pupiņu eļļas metakrilātam ar 78 % dabas izcelsmes saturu ziņots σ_B = 43,7 MPa [34]. Savukārt 3D drukāti AESO oligomēri, kas sintezēti vienā solī, uzrādījuši lieliskas termomehāniskās īpašības ar T_g 128–130 °C. Turklāt UV gaismas iespiešanās dziļums bija 0,277 mm, kas ir lielāks nekā plaši izmantotajos komerciālajos sveķos [35]. Šie ir lieliski un reprezentatīvi piemēri augu eļļu pielietošanas potenciālam 3D drukā. Šādas ražošanas tehnoloģijas attīstība būtiski paaugstina prasības pret fotoaktīvo sveķu formulāciju izstrādi un to parametru optimizāciju konkrētiem pielietojumiem, piemēram, viskozitātes, reaģētspējas un galamateriāla mehānisko īpašību pielāgošanu.

Akrilētām augu eļļām raksturīga augsta viskozitāte, kas var pārsniegt pat 17000 mPa·s [36]. Augstā viskozitāte rodas molekulu garo alkilķēžu dēļ, jo iespējama to sapīšanās, kas palielina plūsmas pretestību, kā arī starpmolekulāro mijiedarbības spēku rezultātā, tostarp ūdeņraža saišu veidošanās starp hidroksil-, akrilāta un estera grupām. Augsta viskozitāte ierobežo sveķu apstrādes iespējas gan 3D drukas procesos, gan virsmas pārklājumu izstrādē, jo tajos nepieciešama vienmērīga materiāla plūsma. Šīs problēmas risināšanai UV cietējošajās formulācijās parasti tiek izmantoti reaktīvie atšķaidītāji – zemas viskozitātes monomēri un oligomēri, kas ne tikai samazina sistēmas viskozitāti, bet arī piedalās fotoiniciētā šķērssaistīšanās reakcijā [19]. To lietošana ļauj izvairīties no šķīdinātāju izmantošanas un nodrošina visu komponenšu integrāciju polimēru tīklā. Parasti tiek izvēlēti mono-, di- vai daudzfunkcionāli (met)akrilāti, piemēram, izobornilakrilāts (IBOA), tripropilēnglikola diakrilāts (TPGDA), trimetilolpropāna tri(met)akrilāts (TMPT(M)A), 1,6-heksāndiola diakrilāts (HDDA) u. c. [37]. Reaktīvo atšķaidītāju izvēle balstās optimālā līdzsvarā starp viskozitāti, reaģētspēju un UV cietinātā materiāla termomehāniskajām īpašībām, pielāgojot sveķu formulāciju konkrētam pielietojumam. Diemžēl lielākā daļa komerciāli pieejamo reaktīvo atšķaidītāju ir iegūti no naftas, radot bažas par ilgtspējību un toksicitāti. Tāpēc jaunākie pētījumi arvien vairāk koncentrējas uz alternatīvu dabas izcelsmes reaktīvo atšķaidītāju izstrādi. Literatūrā aprakstīta reaktīvo atšķaidītaju sintēze un pielietojums UV cietējošās sistēmās no tādām dabas izcelsmes izejvielām kā ricinolskābe [38], kardanols [39], furāns [40], rīcineļļa [41], eugenols [42] u. c. Literatūrā nereti ziņots arī par iekšējo dubultsaišu saturošu esteru kā reaktīvo atšķaidītāju izmantošanu UV cietējošos sveķos, visbiežāk maleīnskābes un fumārskābes atvasinājumu formā [43], [44]. Lai gan iekšējo dubultsaišu reaģētspēja UV cietēšanā ir zemāka par terminālo dubultsaišu reaģētspēju (galvenokārt sterisko, π-elektronu delokalizācijas un blakusesošo elektronakceptoro grupu dēļ), tās tiek plaši lietotas, jo spēj nodrošināt nepieciešamo estera ķēžu integrāciju polimēra tīklā un ietekmēt galaprodukta īpašības. Interesantu pētījumu veica *Northrop* un līdzautori, salīdzinot četrus savienojumus ar iekšējām dubultsaitēm brīvo radikāļu tiol-ēna "*klik*" reakcijā. Autori novēroja šādu reaģētspēju: norbornēns > fumarāts > maleimīds > krotonāts [45]. Iekšējo dubultsaišu klātbūtne makromolekulā var piešķirt zināmu elastīgumu vai mīkstinošu efektu, tāpēc šādus esterus bieži

kombinē ar citiem akrilātiem, lai paaugstinātu kopējo fotopolimerizācijas ātrumu un polimēra šķērssaišu blīvumu [46]. Turklāt, izmantojot dabas izcelsmes esterus, ir iespējams samazināt no naftas iegūto akrilātu īpatsvaru formulācijās. Šī pieeja, kā arī ietekme uz fotopolimerizācijas procesu un šķērssaistītā materiāla īpašībām tika detalizēti analizēta darba trešajā daļā.

Akrilāti tiek plaši izmantoti arī kā galvenā komponente virsmas aizsargpārklājumos, iegūstot izturīgu un estētisku polimērmateriāla slāni. Turklāt to funkcionalitāte ļauj regulēt pārklājumu īpašības, piemēram, adhēziju, cietību un elastību. Pārklājumu nozarē īpaši turpina pieaugt pieprasījums pēc produktiem ar zemāku VOC, tostarp šķīdinātāju, saturu, jo to izraisītās emisijas ir otrajā vietā aiz automobiļu emisijām kā galvenais gaisa piesārņojuma avots [47]. UV cietējošie pārklājumi parasti tiek formulēti bez šķīdinātājiem, nodrošinot ātru cietēšanu istabas temperatūrā (22 °C), kas ļauj palielināt ražošanas ātrumu, turklāt ietaupot arī vietu ražošanas telpā. Lai gan UV cietējošo pārklājumu tirgus straujākā izaugsme novērojama Āzijā, arī Eiropā un Ziemeļamerikā tā prognozētā izaugsme ir aptuveni 9 % gadā, kas ir ievērojami augstāka nekā tradicionālo pārklājumu industrijas vidējais pieauguma temps [48]. Pielāgojoties arvien pieaugošajām vides normām, biomasas, t. sk. augu eļļu, iekļaušana UV cietējošās pārklājumu formulācijās kļūst arvien populārāka tēma gan zinātnē, gan industrijas sektorā [49]. Literatūrā jau ziņots par augu eļļu atvasinājumu perspektīvu kā UV cietējošu pārklājumu avotu, t. sk. ziņots par rīcineļļas [50], tungas [51], jatrofas un palmu eļļu atvasinājumiem [52]. Tie tiek izmantoti koksnes, metāla, plastmasas un papīra virsmu aizsardzībai no korozijas, ķīmisko vielu un atmosfēras iedarbības [53]. Izmantojot augu eļļas UV cietējošos pārklājumos, iespējams iegūt plašu mehānisko īpašību spektru, ieskaitot augstu cietību, adhēziju, elastību un citus fizikālos parametrus. Šādi pārklājumi pētīti tādiem specifiskiem mērķiem kā antimikrobiāli [54], liesmu slāpējoši [55], augstas veiktspējas [56] un nanokompozītu pārklājumi [57].

UV cietējošo materiālu potenciāls tiek izvērtēts arī strukturālu materiālu sistēmās. Polimēra matricas un stiegrojuma kompozītmateriāli ir būtiska materiālzinātnes joma, nodrošinot īpašību kombinācijas, kas nav sasniedzamas ar katru komponenti atsevišķi. Lai gan visbiežāk lietotie kompozītmateriāli ir ar augstu mehānisko veiktspēju, to ražošana balstās naftas izcelsmes polimēru matricās (epoksīdi, poliestera sveķi) un stikla vai oglekļa šķiedru stiegrojumā, kuru iegūšana ir energoietilpīga [58]. Šādu kompozītmateriālu izmantošana ilgtermiņā ir pretēja aprites ekonomikas principiem. Alternatīvu kompozītmateriālu izstrāde, kas balstās atjaunojamās izejvielās, pēdējā desmitgadē ir kļuvusi par nozīmīgu materiālzinātnes virzienu. Kaņepju šķiedras ir daudzsološas dabiskās šķiedras sintētisko šķiedru aizvietošanā. Tās ir mehāniski izturīgas, ar lielu celulozes saturu, un to iegūšanai nepieciešams ievērojami mazāk enerģijas nekā stikla vai oglekļa šķiedrām – literatūrā ziņots, ka enerģijas ietaupījums var sasniegt līdz pat 80 % [59]. Jāņem vērā tas, ka dabisko šķiedru trūkums, salīdzinot ar sintētiskajām, ir to neviendabība – šķiedru īpašības ievērojami atšķiras atkarībā no audzēšanas apstākļiem, klimata un apstrādes. Šo trūkumu iespējams mazināt, pagatavojot homogēnākas šķiedru struktūras, piemēram, papīru. Nanopapīrs (NP), kas iegūts, fibrillējot celulozes nanoizmēra šķiedras, nodrošina vienmērīgu šķiedru sadalījumu un augstu virsmas laukumu. Šāda struktūra ir labi piemērota matricu impregnācijai, piemēram, ar dabas izcelsmes sveķiem, jo kapilārie efekti un porainība spēj nodrošināt efektīvu sveķu iekļūšanu šķiedru tīklā [60]. NP sagatavošana ir ekonomiski īpaši izdevīga dažādu atkritumproduktu gadījumā, kas satur

dabiskās šķiedras, jo tos iespējams viegli apstrādāt (malt, liet, presēt), izmantojot pārbaudītas un vienkāršas metodes [61]. Kompozītu izstrāde, izmantojot UV cietējošu augu eļļu impregnēšanas pieeju, aplūkota darba ceturtajā daļā.

Neraugoties uz progresu dabas izcelsmes sveķu izstrādē un pielietojumos, būtisks izaicinājums joprojām ir to otrreizējā pārstrāde. Tradicionālie UV cietējošie termoreaktīvie materiāli pēc fotopolimerizācijas veido neatgriezenisku 3D makromolekulāru šķērssaistītu tīklu, kas būtiski ierobežo to plūstamību un pārstrādes potenciālu [62]. Pēdējos gados arvien lielāka uzmanība tiek pievērsta dinamiski kovalento saišu ieviešanai termoreaktīvajos polimēros, lai izstrādātu otrreizēji pārstrādājamus materiālus [63]. Šādas struktūras, kas pazīstamas kā vitrimēri, apvieno termoreaktīvo polimēru mehānisko un termisko izturību ar termoplastu pārstrādājamību. Vitrimēros dinamiski kovalentās saites paaugstinātā temperatūrā piedalās apmaiņas reakcijās, ļaujot materiālam veikt topoloģiskās pārkārtošanās. Transesterifikācija izceļas kā viena no visplašāk pētītajām apmaiņas reakcijām, pateicoties vieglai esteru un hidroksilgrupu iekļaušanai termoreaktīvajās sistēmās [64], [65]. Visbiežāk ziņots par termiskās cietēšanas procesā izstrādātiem vitrimēriem, kas ir gan energoietilpīgs, gan laikietilpīgs process, un tā cietēšana var aizņemt pat 12 h [66]. Zems enerģijas patēriņš un īsāks apstrādes laiks, kas raksturīgs UV cietēšanas procesam, padara to par efektīvu un ilgtspējīgu metodi vitrimēru izstrādē [67]. Turklāt UV cietējoši vitrimēri ir īpaši perspektīvi modernām ražošanas tehnoloģijām, piemēram, 3D drukai, apvienojot iespēju veidot sarežģītas ģeometrijas un nodrošinot materiālu atkārtotu izmantošanu pēc nolietojuma [68]. Šī pieeja ir īpaši perspektīva dabas izcelsmes polimērmateriālu izstrādē, jo tā nodrošina iespēju apvienot ilgtspējīgas izejvielas ar otrreizēju materiālu pārstrādi.

Veiktais pētījums ir vērsts uz iepriekšminēto problēmu risināšanu, sintezējot un formulējot no atjaunojamām izejvielām iegūtus UV cietējošus sveķus ar mērķtiecīgi pielāgotu molekulāro struktūru, kas ļauj kontrolēt cietēšanas kinētiku, iegūt materiālus ar pielāgojamām (termo)mehāniskajām īpašībām un nodrošināt materiālu pārstrādes potenciālu. Lai to paveiktu, tika izvirzīti konkrēti soļi UV cietējošo sveķu izstrādes procesā.

Pirmkārt, svarīgākie faktori UV cietējošo sveķu izstrādē ir piemērota izejmateriālu izvēle un to ķīmiskā funkcionalitāte. Šīs īpašības nosaka sveķu reaģētspēju UV cietēšanas procesā un galamateriāla īpašības. Kā atjaunojamās izejvielas tika izvēlētas dažādas augu eļļas – rapšu, linsēku un vīnogu kauliņu eļļa, pamatojoties uz to pieejamību, ķīmisko struktūru un potenciālu pielietojumam ilgtspējīgos UV cietējošos materiālos. Rapšu un linsēklu eļļas ir viegli pieejamas un piemērotas kultivēšanai Latvijas klimata apstākļiem. Savukārt vīnogu kauliņu eļļa, lai gan mazāk pieejama, tika izvēlēta, pateicoties tās augstajam dubultsaišu skaitam molekulā. Šāda izejmateriālu izvēle ļauj novērtēt, kā dubultsaišu daudzums ietekmē akrilēšanas sintēzi un tālāko reaģētspēju UV cietēšanas laikā. Pretstatā zinātniskajā literatūrā plaši pētītajai un jau komercializētajai AESO rapšu eļļas akrilēšana un tās izmantošana UV cietējošos materiālos līdz šim ir minēta tikai dažos pētījumos. Tādējādi šis darbs sniedz jaunu ieguldījumu vietējās augu eļļas pielietojuma izpētē.

Otrkārt, fotoaktīvo grupu ieviešana augu eļļu struktūrā un UV cietēšanas koncepts tika pārnests uz jau industriāli attīstītu nozari – alkīdiem. Alkīdi tradicionāli tiek izmantoti pārklājumu materiālos to labās adhēzijas un elastības dēļ, tomēr to cietēšana parasti balstās metālu katalizētā oksidatīvā žūšanā, kas ir laikietilpīgs un energoietilpīgs process. Šajā solī alkīdu struktūra tika modificēta, ieviešot noteiktu daudzumu akrilgrupu un nodrošinot

kontrolējamu UV cietēšanas procesu. Šāda pieeja ļauj apvienot alkīdu raksturīgās ekspluatācijas īpašības ar UV cietēšanas tehnoloģijas priekšrocībām.

Treškārt, tika izstrādātas un optimizētas UV cietējošās sveķu formulācijas, izvēloties un kombinējot reaktīvos atšķaidītājus dažādās masas % attiecībās, lai nodrošinātu noteiktas reoloģiskās un mehāniskās īpašības, t. sk. atbilstošu viskozitāti, cietēšanas ātrumu un mehānisko izturību. Monofunkcionāli reaktīvie atšķaidītāji parasti samazina E un uzlabo šķērssaistītā materiāla plastiskumu, veidojot elastīgus materiālus. Savukārt di- un polifunkcionālie reaktīvie atšķaidītāji palielina E un samazina plastiskumu, veidojot trauslus, bet stingrus materiālus. Augstāka reaktīvā atšķaidītāja funkcionalitāte paātrina cietēšanu un nodrošina augstāku šķērssaišu blīvumu [69]. Piemēram, HDDA un TPGDA ievērojami samazina UV cietējošo formulāciju viskozitāti. TMPTA un TMPTMA, būdami trifunkcionāli monomēri, ievērojami palielina polimēra šķērssaišu blīvumu un līdz ar to T_g. Tāpat T_g palielina reaktīvie atšķaidītāji ar struktūrā esošu apjomīgu grupu, piemēram, IBOA. Turpretī TPGDA un HDDA, būdami lineāras struktūras monomēri, uzlabo materiālu elastību [70], [71]. Reaktīvo atšķaidītāju izvēle un formulāciju optimizācija nodrošina sveķu piemērotību 3D drukas tehnoloģijai un virsmas pārklājumu izstrādei. Lielākā daļa reaktīvo atšķaidītaju tiek iegūti no naftas produktiem, bet arvien lielāka interese parādās par dažādiem reaktīvajiem atšķaidītājiem, kas iegūti no atjaunojamiem resursiem. Piemēram, fotoaktīvi furāna atvasinājumi, salīdzinot ar naftas atvasināto HDDA, uzrādījuši augstāku cietību E un T_g UV cietējošos pārklājumos [40]. Darba trešajā daļā tika analizēts jauns furāna atvasinājums kā dabas izcelsmes reaktīvais atšķaidītājs.

Ceturtkārt, tika novērtēts sintezēto fotoaktīvo augu eļļu atvasinājumu pielietojums trīs virzienos: (1) koksnes virsmas aizsargpārklājumu izstrādē; (2) nanokompozītu izstrādē, izmantojot akrilētas augu eļļas kā saistvielu; (3) DLP-tipa 3D drukā. Tika analizēts sveķu un iegūto produktu cietēšanas ātrums, adhēzija, cietība, termiskās un (termo)mehāniskās īpašības, kā arī novērtēta materiālu piemērotība katrā pielietojumā.

Piektkārt, formulācijās tika kontrolēts dinamiski kovalento saišu saturs, lai izstrādātu vitrimēru materiālus, kas balstās termiski aktivētā transesterifikācijas reakcijā. Šāda pieeja ļauj materiāliem saglabāt mehānisko un termisko stabilitāti, vienlaikus nodrošinot to pārstrādājamību un struktūras atgūšanu pēc bojājuma, pateicoties kovalento saišu apmaiņas reakcijām paaugstinātā temperatūrā. Apmaiņas reakcijām nepieciešamo funkcionālo grupu ieviešana augu eļļu struktūrā ir pirmais solis ceļā uz UV cietējošu vitrimēru iegūšanu. Līdz ar to izmantotā akrilētā epoksidētā rapšu eļļa (AERO) tika sintezēta izmantojot epoksīda gredzena atvēršanās reakciju, nodrošinot papildu -OH grupas struktūrā, kas veicina vitrimēra pārstrādājamību. Iegūtās vitrimēru sveķu formulācijas tika izmantotas 3D drukas tehnoloģijā, demonstrējot materiāla pielietojumu aditīvajā ražošanā. Tika analizēti būtiski produkta izstrādes parametri, t. sk. katalizatora ietekme un materiālu sprieguma relaksācija, kas ir nozīmīgi galaprodukta veiktspējas un pārstrādes nodrošināšanai. Vitrimēru izstrāde, izmantojot AERO, ļauj novērtēt materiālu otrreizējās pārstrādes potenciālu, kas ir būtisks aspekts videi draudzīgu polimērmateriālu izstrādē.

Sintezētajiem un formulētajiem sveķiem un šķērssaistītajiem materiāliem noteiktas plaša spektra īpašības, veicot šādas analīzes un testus: Furjē transformācijas infrasarkanā starojuma spektroskopija (FTIR); kodolmagnētiskā rezonanse (KMR); izmēru izslēgšanas

hromatogrāfija (SEC); reoloģija, fotoreoloģija, fotodiferenciāli skenējošā kalorimetrija (foto DSC); skenējošā elektronu mikroskopija (SEM); dinamiski mehāniskā analīze (DMA); mehāniskās izturības tests stiepē; adhēzijas tests; mikrocietības tests; slīdes berzes tests; svārsta cietības tests; iespieduma dziļuma tests; ultravioletās redzamās gaismas spektroskopija (UV-Vis); termogravimetriskā analīze (TGA); biodegradācija; blīvuma noteikšana; dielektriskā spektroskopija (DS); kontaktleņķa noteikšana; TGA-FTIR kombinētā analīze; optiskā mikroskopija. Ar metožu detalizētiem aprakstiem iespējams iepazīties katras publikācijas metožu sadaļā.

Promocijas darba izstrādē apvienota augu eļļu kā atjaunojamo resursu izmantošana, mūsdienīga un energoefektīva UV cietēšanas tehnoloģija un materiālu struktūras funkcionalitāte, tādējādi radot inovatīvus, videi draudzīgus un otrreizēji pārstrādājamus materiālus. Šāda pieeja ne tikai samazinātu atkarību no neatjaunojamajiem resursiem, bet arī veicinātu aprites ekonomikas principu ieviešanu materiālzinātnē.

Mērķis un uzdevumi

Promocijas darba mērķis ir izstrādāt no augu eļļu atvasinājumiem iegūtus polimēru sveķus ar kontrolējamu molekulāro struktūru pielietojumam UV cietējošos termoreaktīvajos materiālos ar pielāgojamām ekspluatācijas un pārstrādes īpašībām.

Promocijas darbam definēti vairāki uzdevumi.

1. Sintezēt akrilēt rapšu, linsēklu un vīnogu kauliņu eļļu atvasinājumus, izmantojot vienpakāpes vai divpakāpes sintēzes metodes, un optimizēt sintēzes reakcijas parametrus atbilstoši ķīmiskās reakcijas mehānismam.
2. Izstrādāt UV cietējošās sveķu formulācijas ar mērķtiecīgi pielāgotu molekulāro struktūru, izmantojot sintezētos augu eļļu akrilātu atvasinājumus, reaktīvos atšķaidītājus un fotoiniciatorus.
3. Izpētīt UV cietēšanas kinētikas un šķērssaistītā polimēra režģa struktūras ietekmi uz termoreaktīvo polimērmateriālu fizikāli mehāniskajām īpašībām, un izpētīt to pielietojumu koksnes pārklājumu izstrādē un 3D drukā.
4. Kontrolēt dinamiski kovalento saišu saturu šķērssaistītā polimēra režģī, izvērtēt iegūtā vitrimēra atkārtotas pārstrādes un struktūras atjaunošanas potenciālu, izpētīt šādu materiālu pielietojumu 3D drukas tehnoloģijai.

Aizstāvēšanai izvirzītās tēzes

1. Mērķtiecīgi pielāgojot sintēzes metodes, reakcijas parametrus un formulāciju sastāvu, iespējams kontrolēt akrilētu augu eļļu atvasinājumu makromolekulāro struktūru, UV cietēšanas kinētiku un šķērssaistītā polimēra režģa blīvumu, tādējādi iegūstot UV cietējošus sveķus ar pielāgojamām galamateriālu īpašībām.
2. UV cietējošās sveķu formulācijas izstrādātas ar pielietojumam atbilstošu viskozitāti un fizikāli mehāniskajām īpašībām, padarot tās piemērotas augsti šķērssaistītu polimēru pārklājumu izveidei.
3. UV cietējošus akrilētas augu eļļas polimērmateriālus var izmantot kā matricas saistvielu dabisko šķiedru kompozītiem, kur iestrādātais celulozes stiegrojums nodrošina uzlabotas fizikāli mehāniskās īpašības.
4. Kontrolējot dinamiski kovalento saišu saturu šķērssaistīta polimēra režģī, iespējams iegūt 3D drukājamus vitrimeru materiālus, kas, balstoties termiski aktivētā transesterifikācijas reakcijas mehānismā, nodrošina atkārtotu pārstrādi un struktūras atjaunošanu.

Zinātniskā novitāte

1. Optimizētas vienpakāpes un divpakāpes rapšu, linsēklu un vīnogu kauliņu eļļas akrilēšanas sintēzes metodes, kas ļauj mērķtiecīgi pielāgot molekulāro struktūru, iegūstot materiālus ar kontrolējamu fotoaktīvo grupu saturu un UV cietēšanas kinētiku.

2. Pierādīts, ka fotoaktīvo grupu ieviešana alkīdu struktūrā bez halogenētu produktu lietošanas apvieno alkīdiem raksturīgās ekspluatācijas īpašības ar UV cietēšanas tehnoloģijas priekšrocībām, nodrošinot ātru un kontrolējamu cietēšanas procesu.
3. Noteiktas sakarības starp molekulāro struktūru, reaktīvo atšķaidītāju daudzumu, cietēšanas kinētiku un fizikāli mehāniskajām īpašībām, ļaujot mērķtiecīgi regulēt UV cietējošo sveķu šķērssaistīšanās blīvumu un pielāgot materiālus konkrētiem pielietojumiem (koksnes pārklājumiem, 3D drukāšanai).
4. Demonstrēta UV cietējošu augu eļļu izmantošana kā matricas saistviela dabisko šķiedru kompozītiem, uzrādot efektīvu matricas-šķiedru mijiedarbību un būtisku (termo)mehānisko īpašību uzlabošanu.
5. Izstrādāti akrilētas augu eļļas vitrimeru materiāli ar kontrolētu dinamiski kovalento saišu saturu, kur vitrimēra sprieguma relaksācijas īpašības balstās termiski aktivētā transesterifikācijas reakcijā, nodrošinot atkārtotu pārstrādi un struktūras atjaunošanu.
6. Kopumā darbs sniedz jaunu zinātnisko ieguldījumu dabas izcelsmes, UV cietējošu un pārstrādājamu polimēru formulāciju izstrādē, apvienojot sintēzes, molekulārā dizaina un cietēšanas kinētikas aspektus un demonstrējot to pielietojumu pārklājumos, 3D drukā un dabisko šķiedru kompozītmateriālos.

Praktiskā nozīme

1. Sintezētos fotoaktīvos rapšu, linsēklu un vīnogu kauliņu eļļas akrilātus var izmantot augsti šķērssaistītu polimēru pārklājumu izveidē, nodrošinot materiālu ātru cietēšanu, pielāgojamu fizikāli mehānisko īpašību profilu un demonstrējot Latvijā iegūstamu augu eļļu potenciālu aizstāt naftas izcelsmes izejvielas.
2. Darba rezultāti demonstrē halogenētu produktu nesaturošu sintēzes ceļu UV cietējošiem linsēklu eļļas izcelsmes alkīdsveķiem, kas palielina materiālu ilgtspēju, samazina vides piesārņojumu un atbilst mūsdienu ilgtspējīgas ražošanas prasībām.
3. UV cietējošie augu eļļu polimērmateriāli kā matricas saistviela dabisko šķiedru kompozītiem uzrāda pielietojumu materiāliem ar uzlabotām (termo)mehāniskajām īpašībām, kas piemēroti kompozītmateriālu tehnoloģijām.
4. Akrilētas augu eļļas vitrimeru materiāli ar kontrolētu dinamiski kovalento saišu saturu sniedz iespēju izveidot pārstrādājamus, atkārtoti lietojamus un struktūru atjaunojošus termoreaktīvos polimērus, kas piemēroti 3D drukas tehnoloģijai.

Darba struktūra un apjoms

Promocijas darbs izstrādāts kā zinātnisko publikāciju kopa, kas veltīts dabas izcelsmes UV cietējošu sveķu sintēzei, raksturošanai, koksnes pārklājumu, kompozītmateriālu un 3D drukas pielietojuma izpētei, kā arī pārstrādes potenciāla novērtēšanai. Darbs ietver piecas oriģinālās zinātniskās publikācijas, kas publicētas recenzētos zinātniskos (*SCI*) žurnālos. Darba vispārīgā struktūra redzama 2. attēlā.

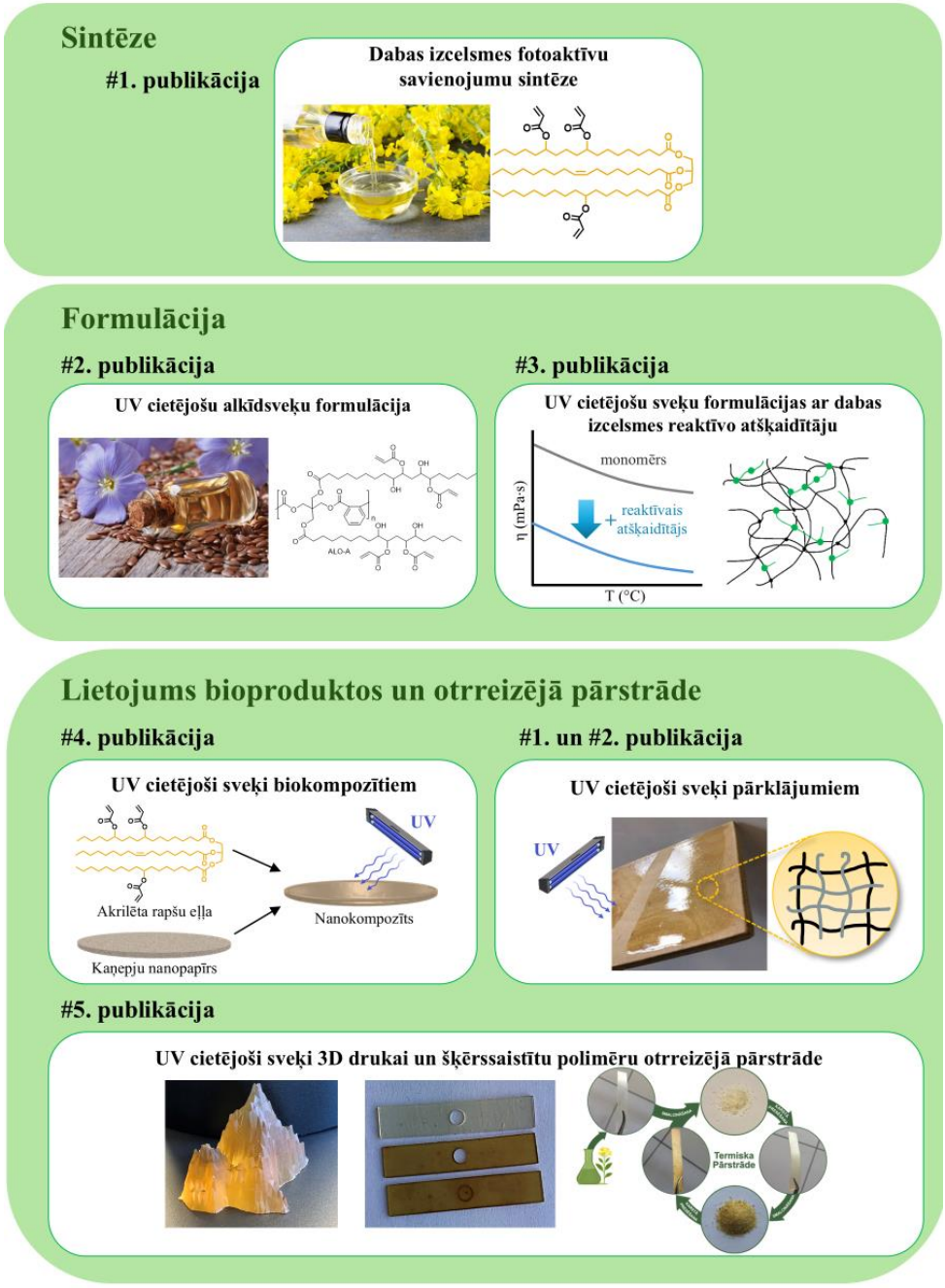

2. att. Darba vispārīga struktūra.

Publikācijas un promocijas darba aprobācija

Promocijas darbā iegūtie rezultāti un sasniegumi publicēti piecās oriģinālās zinātniskās publikācijās. Promocijas darba izstrādes laikā galvenie rezultāti tika prezentēti piecās zinātniskās konferencēs.

SCI publikācijas

1. Briede, S., Platnieks, O., Barkane, A., Sivacovs, I., Leitans, A., Lungevics, J., & Gaidukovs, S. (2023). Tailored Biobased Resins from Acrylated Vegetable Oils for Application in Wood Coatings. *Coatings*, 13 (3), 657. IF=2.8, Q2.
2. Briede, S., Biemans, T., Platnieks, O., & Gaidukovs, S. (2025). Tailored UV-curable acrylated linseed oil-based alkyds: Optimizing crosslinking and coating performance through functionalization and reactive diluent design. *Polymer*, 323, 128227. IF=4.5, Q1.
3. Briede, S., Platnieks, O., Darzina, M., Jirgensons, A., & Gaidukovs, S. (2023). Effect of novel furan-based ester reactive diluent on structure and properties of UV-crosslinked acrylated rapeseed oil. *Journal of Polymer Science*, 61(24), 3318–3328. IF=3.6, Q1.
4. Platnieks, O., Briede, S., Grase, L., Thakur, V., J., & Gaidukovs, S. (2023). Fully Bio-Based Thermoset Composites from UV Curable Prepregs: Vegetable Oil Acrylate Impregnated Hemp Nanopaper. *Polymer Composites*, 44 (9), 5721–5733. IF=4.7, Q1.
5. Greivule, S., Besprozvannaja I., Porcarello M., & Gaidukovs, S. (2026). Reprocessable and Repairable Bio-Based Vitrimers from Acrylated Epoxidized Rapeseed Oil for Additive Manufacturing. *Macromolecular Materials and Engineering*. IF=4.6, Q1, doi: 10.1002/mame.70228. (Pieņemts).

Zinātniskās konferences

1. Briede, S., & Gaidukovs, S. 3D printing and reprocessing of rapeseed oil-based vitrimers. *European Polymer Congress*, Groningen, The Netherlands, June 22–27, 2025.
2. Briede, S., Biemans, T., & Gaidukovs, S. Synthesis of highly functional UV-curable alkyd resins for wood coating application. *European Regional Meeting of the Polymer Processing Society*, Ferrol, Spain, September 30–October 3, 2024.
3. Briede, S., Jurinovs, M., & Gaidukovs, S. Rheological behavior of photoactive vegetable oil for extrusion-based UV-assisted 3D printing. *Nordic Rheology conference*, Aarhus, Denmark, May 31–June 2, 2023.
4. Briede, S., Jurinovs, M., & Gaidukovs, S. Tailored biobased UV-curable resins from acrylated vegetable oils for application in wood coatings. *Renewable Resources & Biorefineries*, Riga, Latvia, April 12–14, 2023.
5. Briede, S., Jurinovs, M., & Gaidukovs, S. Photoactive vegetable oil synthesis for high-performance extrusion UV-light cured 3D printing. *Nordic Polymer Days*, Gothenburg, Sweden, June 1–3, 2022.

Citas zinātniskās publikācijas, kas tapušas promocijas darba izstrādes laikā

1. Platnieks O., Beluns S., Briede S., Jurinovs M., & Gaidukovs S. (2023). Cellulose synergetic interactions with biopolymers: Functionalization for sustainable and green material design. *Industrial Crops and Products*, 204, 117310.
2. Briede, S., Jurinovs, M., Nechausov, S., Platnieks, O., & Gaidukovs, S. (2022). State-of-the-art UV-assisted 3D printing via a rapid syringe-extrusion approach for photoactive vegetable oil acrylates produced in one-step synthesis. *Molecular Systems Design & Engineering*, 7 (11), 1434–1448.
3. Briede, S., Barkane, A., Jurinovs, M., Thakur, V. K., & Gaidukovs, S. (2022). Acrylation of biomass: a review of synthesis process–know how and future application directions. *Current Opinion in Green and Sustainable Chemistry*, 35, 100626.
4. Barkane, A., Jurinovs, M., Briede, S., Platnieks, O., Onufrijevs, P., Zelca, Z., & Gaidukovs, S. (2022). Biobased Resin for Sustainable Stereolithography: 3D Printed Vegetable Oil Acrylate Reinforced with Ultra-Low Content of Nanocellulose for Fossil Resin Substitution. *3D Printing and Additive Manufacturing*, 10 (6), 1272–1286.
5. Jurinovs, M., Rukavisnikovs, N., Greivule, S., Starkova, O., Kovalovs, A., Brunāvs, J., Macutkevič, J., Juhnevica, I., Platnieks, O., & Gaidukovs, S. (2026). Nanostructure-reinforced epoxy-acrylate interpenetrated networks for UV-curable high-performance coatings. *Reactive and Functional Polymers*, 221, 106664.

PROMOCIJAS DARBA GALVENIE REZULTĀTI

Akrilētu augu eļļu sintēze, fotopolimerizācijas kinētika un pielietojuma izpēte UV cietējošiem koksnes pārklājumiem (1. publikācija)

Lai izpētītu augu eļļu pielietojumu UV cietējošu koksnes pārklājumu sveķu izstrādei, sākotnēji tika akrilētas trīs augu eļļas – Latvijā plaši pieejamā rapšu eļļa un salīdzinājumam divas ar dubultsaitēm bagātās eļļas – linsēklu eļļa un vīnogu kauliņu eļļa. Akrilētās eļļas tika iegūtas optimizētā vienpakāpes sintēzes procesā, izmantojot $BF_3 \cdot OEt_2$ kā katalizatoru (3. a att.), kā aprakstīts ievaddaļā un līdzīgi kā 2013. gadā publicētajā sintēzes protokolā [26]. Pēc sintēzes akrilētās eļļas nosauktas attiecīgi – ARO, ALO un AGO. Sintēze laboratorijas apstākļos tika optimizēta līdz noteiktam protokolam – apaļkolbā augu eļļa (1 mol C=C) tika sajaukta ar akrilskābi (AA) (2,1 mol) un lēni pievienots katalizators (0,21 mol). Reakcija tika maisīta un uzturēta 80 °C temperatūrā 5 h, pēc tam atstāta istabas temperatūrā (22 °C) uz nakti. Reakcijas beigās tika pievienots heksāns, lai izšķīdinātu organisko fāzi, kas pēc tam tika mazgāta ar $NaHCO_3$ un NaCl ūdens šķīdumiem, lai neitralizētu un aizvāktu atlikušo AA un katalizatoru. Organiskā fāze tika žāvēta virs Na_2SO_4 un nofiltrēta, pēc tam pazeminātā spiedienā tika ietvaicēts šķīdinātājs. ARO, ALO un AGO tika iegūti kā viskozi, tumši dzelteni sveķi. Iegūtie sveķi tika analizēti ar ^{1}H-KMR spektroskopiju, kā reprezentatīvs piemērs – atšifrēti rapšu eļļas (RO) un ARO spektri (3. b att.).

Vispirms tika noteikti svarīgākie augu eļļas fotopolimerizācijas raksturlielumi, kas apkopoti 3. tabulā [72]. Lai izpētītu sintezēto augu eļļu terminēto akrilgrupu dubultsaišu konversiju (DBC) pēc UV cietēšanas, kā arī fotopolimerizācijas kinētiku, tika izmērīta viskozitāte, uzņemti Furjē transformācijas infrasarkanā starojuma (FTIR) spektri dažādos apstarošanas laikos un veikti fotodiferenciāli skenējošās kalorimetrijas (foto DSC) mērījumi. DBC raksturo akrilgrupu dubultsaišu konversijas pakāpi kovalenti saistītā struktūrā UV cietēšanas laikā, norādot tīkla veidošanās efektivitāti. Akrilētu augu eļļu viskozitāte bija robežās no 430 mPa·s līdz 1305 mPa·s (ARO < AGO < ALO) bīdes ātruma robežās no 10 s^{-1} līdz 100 s^{-1}, kas nodrošina optimālu sveķu plūstamību un ir svarīgs parametrs pārklājumu izstrādē [48], [72]. Savukārt DBC bija robežās no 69 % līdz 85 %, ARO uzrādot visaugstāko konversiju, kas korelē ar augstāko reakcijas iznākumu (57 %, 2,14 akrilgrupām molekulā). AGO maksimālais polimerizācijas ātrums tika sasniegts 9,5 s ($t_{max\ ātr.}$) pie 5,1 % konversijas, un tas bija lielākais, kas liecina par ātru sākotnējo reaģētspēju, taču agrīnu difūzijas (molekulu kustības) kontrolētu polimerizāciju, kas kavē turpmāku reakcijas norisi. ARO polimerizācija turpinājās nedaudz ilgāk augstākas akrilātu funkcionalitātes un zemākas viskozitātes dēļ.

3. tabula

Akrilētu augu eļļu raksturlielumi [72]

Akrilētas augu eļļas	Sintēze				UV cietēšana		
	Tauskābes atlikuma dubultsaites (triglicerīdā)	Akrilgrupas molekulā	Reakcijas iznākums (%)	η (mPa·s)	DBC (%)	$t_{max\ ātr.}$ (s)	DBC maks. ātrumā (%)
ARO	3,74	2,14	57	430	85	9,8	4,5
ALO	5,99	1,62	28	1305	69	13,1	2,4
AGO	4,56	1,67	38	1140	76	9,5	5,1

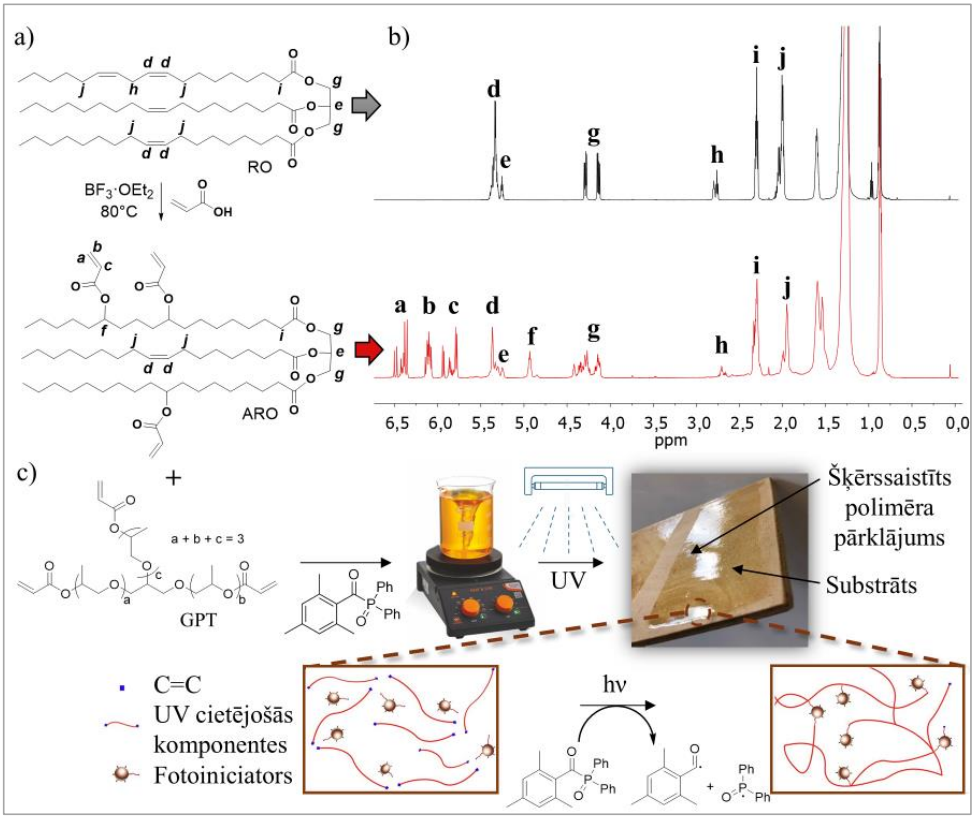

3. att. a) ARO vienpakāpes sintēzes shēma; b) RO un ARO sveķu atšifrēti ^{1}H-KMR spektri [72]; c) UV cietējošu pārklājumu sagatavošanas shematisks attēlojums.

Lai izstrādātu koksnes pārklājumus no sintezētajām eļļām, tika izstrādātas sveķu formulācijas. Šajā darbā ARO, ALO un AGO tika sajauktas ar dabas izcelsmes zemas viskozitātes glicerīna propoksitriakrilātu (GPT) (η = 91 mPa·s, bīdes ātrums – no 10 s^{-1} līdz 100 s^{-1}), kas kalpo kā reaktīvais atšķaidītājs un, būdams trifunkcionāls monomērs, nodrošina lielāku polimēra šķērssaišu blīvumu [73]. GPT polaritāte un savietojamība ar akrilētas augu eļļas sveķiem tika noteika, šķīdinot to istabas temperatūrā dažādās vielās un šķīdinātājos ar pieaugošu polaritāti – rapšu eļļā, akrilētās augu eļļās, etanolā, metanolā, ūdenī. Fotopolimerizācijas ierosināšanai tika pievienots fotoiniciators 2,4,6-trimetilbenzola

difenilfosfīna oksīds. Kopā tika sagatavotas deviņas sveķu formulācijas, kurās divas akrilētās augu eļļas tika sajauktas attiecībā viens pret viens: 1) trīs augu eļļu akrilāti (piemēram, ARO/ALO); 2) trīs augu eļļu akrilāti ar pievienotiem 5 masas % GPT (piemēram, ARO/ALO_GPT5); 3) trīs augu eļļu akrilāti ar pievienotiem 20 masas % GPT (piemēram, ARO/ALO_GPT20). Vienkāršota shēma UV cietējošu koksnes pārklājumu sagatavošanai redzama 3. c attēlā.

(Termo)mehāniskās īpašības tika noteiktas brīvi stāvošām UV cietējošām sveķu plēvītēm. Šādā veidā apstaroti paraugi sniedz informāciju par šķērssaistītā polimēra tīkla veiktspēju, kas palīdz labāk izprast un prognozēt pārklājuma mehānisko un termomehānisko uzvedību uz substrāta (koksnes). Piemēram, augstāks elastības modulis (E) vai stiklošanās temperatūra (T_g) apstarotās brīvi stāvošās plēvītēs bieži korelē ar lielāku izturību pret skrāpējumiem un lielāku ķīmisko izturību, savukārt elastīgākas plēvītes – ar augstāku triecienizturību un noturību pret plaisu veidošanos [74]. Vispirms, izmantojot dinamiski mehānisko analīzi (DMA), tika noteikts uzkrājuma modulis (E′), kas raksturo, cik daudz enerģijas materiāls spēj uzglabāt elastīgajā deformācijā. E′ līkņu vērtības apstarotajiem paraugiem pētītajā temperatūras diapazonā liecināja par stabilu, termiski noturīgu šķērsaistītu polimēra tīku (4. a att.). Pazeminātā temperatūrā, piemēram, –30 °C, GPT pievienošana palielināja E′ vērtību no 805,5 MPa ARO/ALO paraugam līdz 1182,3 MPa ARO/ALO_GPT20 paraugam. Savukārt istabas temperatūrā šiem paraugiem GPT pievienošana palielināja E′ vērtību no 13,7 MPa līdz 34,0 MPa, kas liecina par augstāku polimēra šķērssaišu blīvumu, stingrību un zemāku molekulmasu starp šķērssaitēm. Aprēķinātais šķērssaišu blīvums pēc DMA datiem šiem paraugiem pieauga no $1{,}5 \cdot 10^3$ mol/m^3 līdz $2{,}1 \cdot 10^3$ mol/m^3. Iegūtās E′ vērtības ir raksturīgas šķērssasitītiem UV cietējošiem polimēriem un liecina par materiāla vienlaikus stingro un elastīgo raksturu [75]. Zudumu modulis (E″) raksturo, cik daudz enerģijas materiāls deformācijas laikā zaudē kā siltumu, t. i., materiāla viskozo jeb enerģiju izkliedējošo daļu. Izdalot E″ vērtības ar E′ vērtībām, iegūst zudumu faktora (tanδ) līkni, kas parāda, cik "mobilas" vai "relaksētas" polimēru ķēdes ir noteiktā temperatūrā. Līknes virsotne atspoguļo polimēru ķēžu segmentālās mobilitates relaksācijas sākumu un bieži vien tiek sasaistīta ar T_g. Tomēr jāpiemin, ka joprojām notiek diskusijas par to, vai T_g precīzāk noteikt no E″ līknes virsotnes vai no tanδ līknes virsotnes, jo abi parametri sniedz līdzīgu, bet ne identisku informāciju par polimēra segmentu kustību [76]. Tanδ grafikā (4. b att.) novērojama līknes virsotnes nobīde uz augstākām temperatūras vērtībām līdz ar GPT pievienošanu, kas liecina par ierobežotu ķēžu mobilitāti un palielinātu polimēra šķērssaišu blīvumu. Vienlaikus samazinājās arī tanδ virsotnes augstums, kas atspoguļo relaksācijas procesa intensitātes samazināšanos jeb mazāku segmentu skaitu, kas deformācijas laikā spēj pārvietoties un liecina par stingrāku polimēra tīklu. Visbeidzot, līdz ar GPT pievienošanu tika novērota tanδ līknes platuma palielināšanās, kas atspoguļo šķērssaišu izvietojuma heterogenitāti. Diemžēl tas var radīt arī nevienmērīgu paraugu mehānisko uzvedību [77].

Tālāk tika analizētas UV cietējošo materiālu sprieguma-deformācijas (σ-ε) līknes un aprēķinātās E vērtības (4. c un d att.). GPT pievienošana izraisa nelineāras struktūras – īpašību sakarības. Ir novērojama zināma korelācija starp tanδ līknes virsotnes nobīdi uz augstākām temperatūrām/zemāku tanδ virsotnes intensitāti (no DMA) un lielāku E/sagraušanas robežsprieguma (σ_B) vērtību, tomēr redzama arī pretruna paraugiem ar 5 masas % GPT, jo to mehāniskās izturības vērtības samazinās. Tas liecina par tīkla nevienmērību, iespējamu fāžu

atdalīšanos, GPT monomēram veidojot atsevišķus domēnus. Tas tika izpētīts ar skenējošo elektronu mikroskopiju (SEM) (4. e att.). Reprezentatīvajā SEM šķērsgriezuma attēlā (ii) gadījumā novērojama nevienmērīga mikrostruktūra, kas, iespējams, radusies akrilētu eļļu un GPT fāzu atdalīšanās rezultātā agrīnā cietēšanas stadijā un var būt viens no σ_B samazināšanās iemesliem [78]. Raupja un neviendabīga mikrostruktūra, kas novērojama gan ARO/ALO, gan ARO/ALO_GPT5 paraugos, liecina par iespējamu lokālu sprieguma koncentrēšanos, kur uz fāžu saskares robežām galvenokārt veidojas plaisas. Tas samazina E vērtības, kas šiem paraugiem ir līdzīgas (no 7,1 MPa līdz 10,5 MPa). Savukārt viendabīga morfoloģija ARO/ALO_GPT20 paraugam liecina, ka GPT ir vienmērīgi integrēts polimēra tīklā, nav izteiktu fāžu robežas un stiepes laikā pieliktā slodze netiek lokalizēta. Spriegums tiek sadalīts vienmērīgi visā materiāla tilpumā un līdz ar to, lai iesāktu lūzumu, nepieciešams lielāks spriegums (E līdz 20,3 MPa, σ_B līdz 0,76 MPa).

Lai nodrošinātu efektīvu pārklājuma veiktspēju, tika noteikta formulāciju adhēzija uz bērza saplākšņa. Ņemot vērā to, ka ARO, ALO un AGO dažādo formulāciju ietekme uz (termo)mehāniskajām īpašībām bija mazāk izteikta, datu pārskatāmības un vienkāršības pēc adhēzijas stiprība tika noteikta tikai ARO/ALO formulācijām. Šķidrās sveķu formulācijas tika uzklātas uz saplākšņa un apstarotas, iegūstot 70 % līdz 90 % DBC. Pārklājumu adhēzijas stiprība pakāpeniski palielinājās no 0,56 MPa līdz 1,21 MPa, pieaugot GPT saturam, kas, iespējams, skaidrojams ar starpfāžu saķeres uzlabošanu. Salīdzinot ar literatūru, epoksīda akrilāta un tripropilēnglikola diakrilāts (TPGDA) pārklājumu formulācijas uz koksnes uzrādījušas līdz 1,12 MPa lielu adhēzijas stiprību [79], bet uretāna akrilāta, 1,6-heksāndiola diakrilāts (HDDA), TPGDA un trimetilolpropāna triakrilāts (TMPTA) pārklājumu formulācijas uz polikarbonāta – no 0,52 MPa līdz 2,25 MPa [80]. Jāatzīmē, ka minētie ir mazmolekulāri naftas produkti.

Apkopojot rezultātus, darba pirmajā daļā vienpakāpes sintēzē tika veiksmīgi iegūti rapšu, linsēklu un vīnogu kauliņu eļļas akrilāti, ko iespējams izmantot kā dabas izcelsmes prekursorus UV gaismā cietējošu polimērmateriālu izstrādei. Triglicerīda struktūrā pievienotās akrilgrupas nodrošina pietiekami daudz reakcijas centrus (terminālās dubultsaites), kas ļauj kontrolēt šķērssaistīta polimēra tīkla veidošanos un īpašības. Turklāt akrilētu eļļu viskozitāte (η = 430–1305 mPa·s) nodrošina labu plūstamību pārklājumu formulēšanā ar reaktīvo atšķaidītāju GPT, kas optimālas koncentrācijas gadījumā palielina polimēra šķērssaišu blīvumu, paaugstina T_g, uzlabo mehānisko izturību un stingumu. Šajā darba daļā iegūtie rezultāti demonstrē akrilētu augu eļļu potenciālu koksnes aizsardzības pielietojumos.

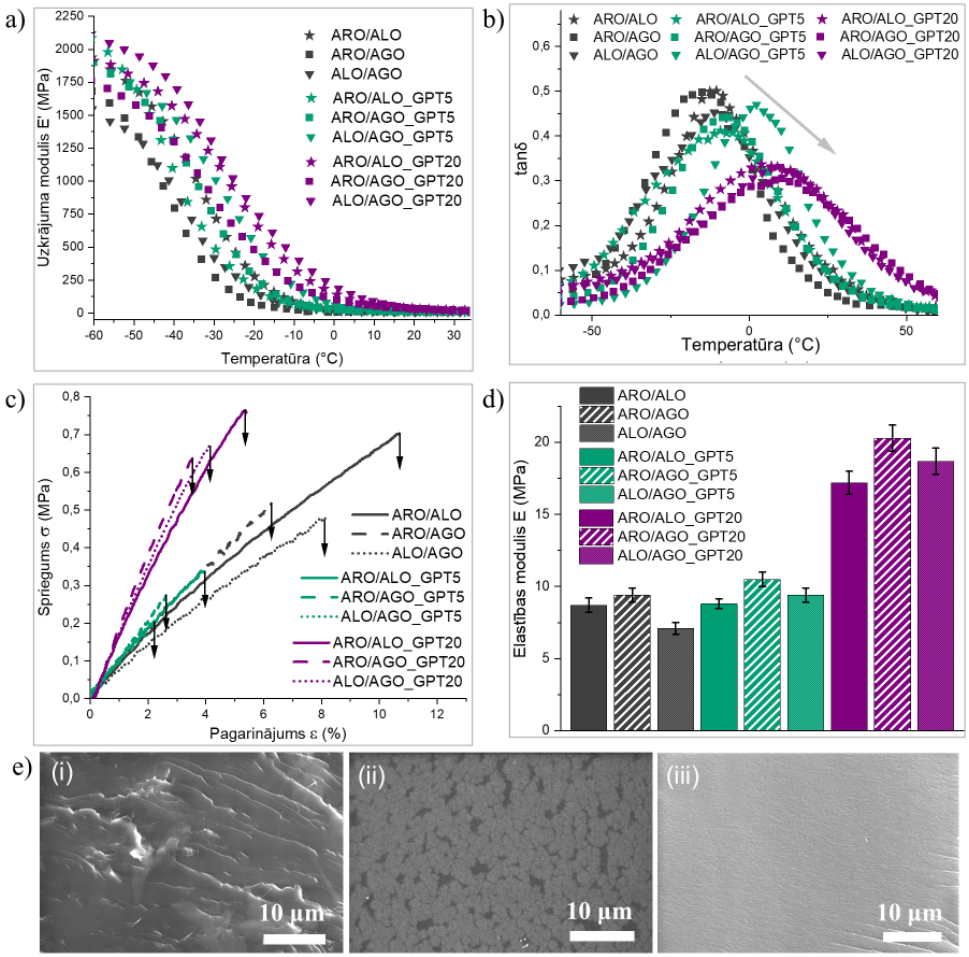

4. att. Šķērssaistīto materiālu a) E′ līknes; b) tanδ līknes; c) σ-ε līknes; d) E grafiks; e) lūzuma virsmu mikrostruktūras morfoloģija – SEM attēli: (i) ARO/ALO, (ii) ARO/ALO_GPT5, (iii) ARO/ALO_GPT20.

Linsēklu eļļas alkīdsveķu sintēze un pielietojuma izpēte UV cietējošiem koksnes pārklājumiem (2. publikācija)

Augu eļļu akrilātu sintēze, to UV cietēšanas process un izstrādāto pārklājumu īpašību izpēte ir būtisks solis atjaunojamo izejvielu izmantošanā koksnes pārklājumos, un iepriekšējā darba daļā iegūtie rezultāti uzrādīja plašu materiālu īpašību spektru. Nākamais solis ir šo zināšanu pārnese uz industriāli nozīmīgu koksnes pārklājumu klasi – alkīdiem. Alkīdi ir sveķi, kas jau daudzus gadus ir vieni no visplašāk izmantotajiem virsmu aizsargpārklājumiem, pateicoties to ķīmiskajām un fizikālajām īpašībām. Tomēr alkīdsveķu pārklājumi žūst lēni, žūšanas procesā nepieciešami metāla katalizatori, un lielākoties sveķi satur organiskos šķīdinātājus (ksilolu, dearomatizētus vai alifātiskus ogļūdeņražus, izoparafīnus u. c.), kas

padara darbu ar tiem potenciāli riskantu. Šos ierobežojumus iespējams novērst, izmantojot UV cietēšanas tehnoloģiju, kas nodrošina ātru cietēšanu bez metāla katalizatoru un organisko šķīdinātāju lietošanas. Tā vietā UV cietējošās sistēmas izmanto fotoiniciatorus, kas apstarošanas laikā ģenerē brīvos radikāļus, ierosinot šķērssaistīšanās reakciju. Līdz ar to darba otrajā solī tika akrilētas alkīdu struktūrā esošās taukskābju atlikumu dubultsaites, izpētīta fotoaktīvo alkīdsveķu UV cietēšanas kinētika, izstrādātas pārklājumu formulācijas un noteiktas to īpašības. Lai to paveiktu, sākotnēji tika sintezēti linsēklu eļļas alkīdsveķi (LO-A), kas satur 73 % linsēklu eļļas taukskābju atlikumu, nodrošinot pietiekami daudz modificējamas iekšējās dubultsaites. Akrilēšana tika veikta divos soļos, izmantojot ievaddaļā aprakstīto epoksidēšanu, lai izvairītos no halogenētu produktu veidošanos [18] un blakusreakcijām, kas varētu būt iespējamas vienpakāpes sintēzē starp alkīda struktūrā esošajām funkcionālajiem fragmentiem un $BF_3{\cdot}OEt_2$ katalizatoru. Epoksidēšanas un sekojošās akrilēšanas reakcijas tika veiktas dažādos apstākļos, līdz sintēzes tika optimizētas līdz vēlamajiem iznākumiem. LO-A divpakāpju akrilēšanas reakcija shematiski redzama 5. a attēlā.

LO-A sveķu epoksidēšana tika veikta H_2O_2 un HCOOH klātbūtnē. Mainot C=C un H_2O_2 molāro attiecību, tika sintezēti divi epoksidēti linsēklu eļļas alkīdsveķi ar atšķirīgu epoksīda saturu – ELO-A (1) un ELO-A (2), lai vēlāk varētu pētīt sekojošo akrilātu UV cietēšanas atšķirības. Pēc sintēzes optimizācijas ELO-A (1) tika noteikta molārā attiecība (mol) bija 1 : 0,4 : 1,8 (taukskābju C=C : HCOOH : H_2O_2), savukārt ELO-A (2) molārā attiecība (mol) tika noteikta 1 : 0,4 : 0,9 (taukskābju C=C : HCOOH : H_2O_2). LO-A tika samaisīts ar HCOOH un karsēts 60 °C apaļkolbā, kas aprīkota ar kondensatoru, pilināmo piltuvi, termopāri un mehānisko maisītāju. 1 h laikā caur pilināmo piltuvi tika lēni pievienots H_2O_2, lai izvairītos no eksotermas reakcijas blakusefektiem. Reakcija turpinājās 6,5 h, un tās progress tika kontrolēts, titrējot epoksīda skaitli (EV), kas pakāpeniski palielinājās, un uzņemot FTIR spektrus. FTIR spektros taukskābju atlikumu dubultsaišu vibrācijas pie 3009 cm^{-1} un 1654 cm^{-1} pēc epoksidēšanas izzuda, savukārt jauna absorbcijas josla parādījās pie 821 cm^{-1}, liecinot par epoksīda gredzena veidošanos. Pēc reakcijas beigām maisījums tika izšķīdināts etilacetātā (EtOAc), organiskā fāze tika mazgāta ar $NaHCO_3$ un NaCl ūdens šķīdumiem, žāvēta virs Na_2SO_4 un nofiltrēta. EtOAc tika atdalīts, destilējot vakuumā. 4. tabulā redzami reakciju iznākumi, ko ietekmē gan izmantoto reaģentu attiecības, gan reakcijas apstākļi. ELO-A (1) un ELO-A (2) tika izmantotas kā izejvielas, lai iegūtu attiecīgi akrilētus linsēklu eļļas alkīdus ALO-A (1) un ALO-A (2).

ELO-A akrilēšana tika veikta AA un katalizatora (1 masas %) klātbūtnē. Eksperimentāli tika salīdzināts reakcijas progress, izmantojot divas dažādas AA molārās attiecības pret epoksīda gredzenu, trietilamīna (TEA) un trifenilfosfīna (TPP) katalītiskā iedarbība, kā arī ELO-A (1) un ELO-A (2) akrilēšanas reakcijas progress. Lai nodrošinātu kontrolētu reakcijas norisi [21], turpmākajos eksperimentos tika izvēlēta epoksīda un AA molārā attiecība (mol) 1 : 1,3. Par katalizatoru tika izvēlēts TEA, jo tas nodrošināja straujāku reakcijas gaitu nekā TPP. Kā tika paredzēts, akrilēšana noritēja lēnāk epoksīdam ar zemāku EV (ELO-A (2)), bet straujāk – epoksīdam ar augstāku EV (ELO-A (1)). ELO-A (1) un ELO-A (2) ir prekursori, lai iegūtu attiecīgi ALO-A (1) un ALO-A (2). ELO-A, TEA un brīvo radikāļu inhibitori butilēts hidroksitoluols (BHT, 600 ppm) un 4-metoksifenols (MEHQ, 600 ppm) tika sajaukti apaļkolbā, kas aprīkota ar kondensatoru, termopāri, mehānisko maisītāju un pilināmo piltuvi. Maisījums tika uzkarsēts līdz 95 °C, kam sekoja AA pievienošana 1 h laikā. Reakcija tika kontrolēta,

titrējot un aprēķinot skābes skaitli (AV). Pēc 18,5 h, kad AV bija mazs vai nemainījās, maisījums tika izšķīdināts EtOAc, organiskā fāze tika mazgāta ar $NaHCO_3$ un NaCl ūdens šķīdumiem, žāvēta virs Na_2SO_4 un nofiltrēta. EtOAc tika atdalīts, destilējot vakuumā, atstājot sveķus ar aptuveno cietvielas saturu 93 %. Akrilēšanas iznākumi apkopoti 4. tabulā. Jāpiemin, ka akrilēšanas laikā EV samazinājās nedaudz straujāk nekā AV, kas varētu liecināt par nevēlamu blakusreakciju – epoksīda gredzena atvēršanos (hidrolīzi).

Reprezentējoši ELO-A (1) un ALO-A (1) ^{1}H-KMR spektri redzami 5. c attēlā. ELO-A (1) spektrā epoksīda gredzena *α*-pozīcijā esošie metilēnprotoni (-**H**COC**H**-) parādījās pie δ = 3,11 ppm un 2,91 ppm. Metilēnprotoni starp divām epoksīda grupām (-COC-C**H₂**-COC-) parādījās pie δ = 1,66–1,83 ppm, un protoni epoksīda gredzena *β*-pozīcijā (-COC-C**H₂**-) parādījās pie δ = 1,47 ppm. Pēc epoksidēšanas protonu signāli, kas atbilst LO-A nepiesātināto taukskābju atlikumu dubultsaitēm (-**H**C=C**H**-), praktiski izzuda. ALO-A (1) ^{1}H-KMR spektrā tika novēroti trīs jauni signāli nobīžu robežās δ = 5,80–6,50 ppm, kas atbilst akrilgrupas protoniem **H₂**C=C**H**-, savukārt epoksīda signāli izzuda.

4. tabula

Sintezēto LO-A, ELO-A un ALO-A raksturlielumi

Sveķi	AV (mg KOH/g sveķu)	OH skaitlis (mg KOH/g sveķu)	mmol C=C/g sveķu	EV (mol epoksīda/100 g sveķu)	mol akrilgrupas /100 g sveķu	Iznākums (%)
LO-A	2,3	69	0,49	–	–	–
ELO-A (1)	3,5	93	0,05	0,34	–	69
ELO-A (2)	4,7	90	0,23	0,27	–	55
ALO-A (1)	48,1	217	0,05	0,01	0,23	68
ALO-A (2)	34,9	183	0,23	0,02	0,18	67

Pirms UV cietēšanas ALO-A (1) un ALO-A (2) sveķi tika sajaukti ar trim dažādiem reaktīvajiem atšķaidītājiem – monofunkcionālu izobornilakrilātu (IBOA), bifunkcionālu tripropilēnglikola diakrilātu (TPGDA) un trifunkcionālu trimetilolpropāna tri(met)akrilātu (TMPTMA) (5. b att.) 10 masas %, 20 masas % un 30 masas %, lai samazinātu viskozitāti (η = 5700–60000 mPa·s) un uzlabotu mehānisko veiktspēju. Katras formulācijas nosaukums veidots, norādot alkīda masas %, reaktīvā atšķaidītāja masas %, atšķaidītāja nosaukumu un izmantoto alkīdu ALO-A (1) vai (2). Piemēram, "90_10 IBOA (1)" ir formulācija ar 90 masas % ALO-A(1) un 10 masas % IBOA.

Akrilētie alkīdsveķi tika raksturoti ar fotoreoloģijas parametriem – uzkrājuma moduli (G′), zudumu moduli (G″) un tanδ līknes vērtībām UV apstarošanas laikā (5. f att.). ALO-A (1) raksturojās ar lielāku polimēra šķērssaišu blīvumu un ātrāku šķērssaistītā tīkla veidošanos nekā ALO-A (2), kas saistīts ar lielāku akrilgrupu skaitu molekulā. Apstarošanas beigās (400 s), ALO-A (1) sasniedza $3{,}9 \cdot 10^7$ Pa lielu G′, savukārt ALO-A (2) – $0{,}6 \cdot 10^7$ Pa. Visām formulācijām ar reaktīvajiem atšķaidītajiem gan G′, gan G″ pēc UV cietēšanas palielinājās līdz ar reaktīvā atšķaidītāja masas % palielināšanos formulācijā, liecinot par blīvāku un stingrāku šķērssaistītā polimēra tīklu (fotoreoloģijas kinētikas dati formulācijām apkopoti tabulā un apskatāmi 2. pielikumā). To pašu apliecina arī tanδ, kas vairumā formulāciju samazinājās. Tomēr pārāk daudz reaktīva atšķaidītāja var ierobežot radikāļu difūziju un kustību, izraisot

priekšlaicīgu polimerizācijas pārtraukšanos [81]. Tāpat visām formulācijām bija novērojama tendence – jo lielāks reaktīvā atšķaidītāja daudzums, jo ātrāk sveķi sasniedza gelpunktu (t_{gel}). Gelpunktā ($G' = G''$ jeb $\tan\delta = 1$) šķidrie sveķi pāriet nepārtrauktā, elastīgā tīklā, materiāls pārstāj uzvesties kā viskozs šķidrums un sāk uzvesties kā elastīgs, ciets ķermenis.

Pēc alkīdsveķu uzvedības noteikšanas fotopolimerzācijas apstākļos formulācijas tika uzklātas uz koka substrāta un apstarotas zem UV gaismas, laižot cauri konvejiera tipa UV lampai (5. e att.). Vizuālā salīdzinājumā ar komerciāli pieejamiem UV cietējošiem sveķiem sintezētie akrilētie alkīdsveķi ALO-A (1) demonstrēja ievērojamu labāku iesūkšanos koksnē, izceļot koksnes toni, vienlaikus nemaskējot arī šķiedru redzamību (5. d att.). Alkīdsveķi ir ķīmiski saderīgi ar celulozi un lignīnu, kas uzlabo to spēju saistīties ar koksnes struktūru un nodrošina dziļāku iesūkšanos. Tas veicina pārklājuma aizsargspēju un samazina deformācijas un plaisāšanas riskus temperatūras un mitruma ietekmē, nodrošinot ilgāku kalpošanas laiku [82].

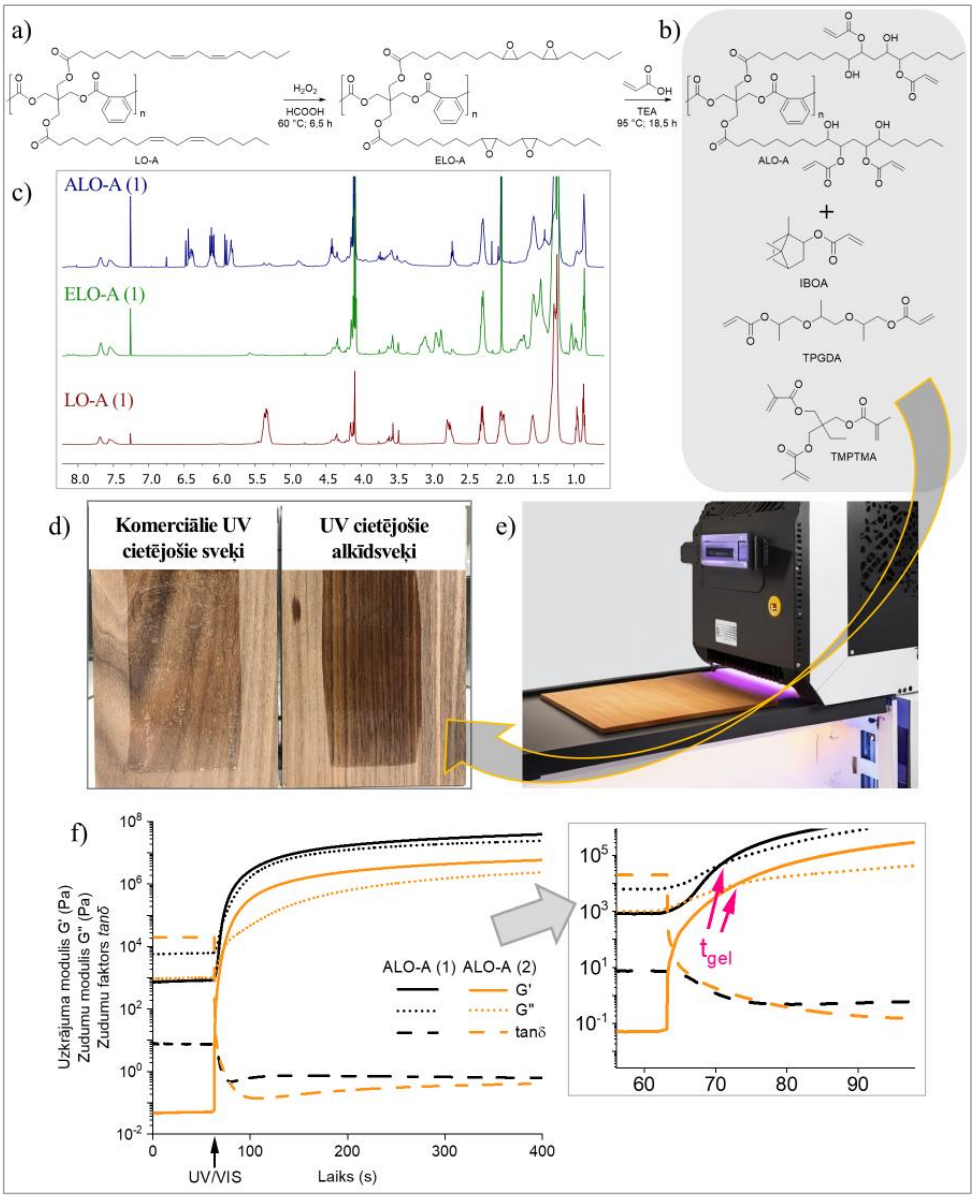

5. att. a) ALO-A sintēze caur epoksidēšanu; b) izmantotie reaktīvie atšķaidītāji; c) LO-A, ELO-A un ALO-A ^{1}H-KMR spektri; d) koksnes nokrāsas efekta salīdzinājums; e) vizualizēts UV cietēšanas process; f) fotoreoloģijas kinētikas līknes ALO-A (1) un (2) ar pietuvinātu grafiku t_{gel} identificēšanai.

Pēc UV apstarošanas tika noteikta pārklājumu svārsta cietība (6. a (i) un (ii) att.), kas atkarīga no molekulu struktūras, akrilgrupu koncentrācijas un polimēra šķērssaišu blīvuma [75]. Akrilētie alkīdsveķi ar dažādiem akrilgrupu daudzumiem uzrādīja 2,2 reižu lielu atšķirību cietībā, ALO-A (1) sasniedzot 103 s augstu cietību. Cietību vēl vairāk palielināja dažādas molekulārās struktūras un akrilgrupu daudzuma saturošu reaktīvo atšķaidītāju pievienošana. Tādējādi akrilēto alkīdsveķu funkcionalitāte un reaktīvo atšķaidītāju izvēle ļāva pielāgot cietības vērtības robežās no 47 s līdz 174 s.

Papildus cietības palielināšanai reaktīvie atšķaidītāji ietekmēja arī elastību, kas tika noteikta, izmantojot *Erichsen* indentācijas testu, mērot iespieduma dziļumu (mm) pārklājumiem, kas uzklāti uz alumīnija metāla substrāta (6. b (i) un (ii) att.). ALO-A (2) ar zemāku šķērssaišu blīvumu nekā ALO-A (1) nodrošināja lielāku polimēra tīkla mobilitāti, un tā rezultātā uzrādīja augstāku elastību ar indentācijas dziļumu 7,0 mm. Reaktīvo atšķaidītāju pievienošana indentācijas dziļumu ietekmēja gan atkarībā no funkcionalitātes, gan atkarībā no struktūras. Monofunkcionālā IBOA struktūrā esošā apjomīgā izobornilgrupa nodrošina brīvu ķēdes kustību, mazina iekšējos spriegumus polimēra matricā un tādējādi palielina elastību. Maksimālais iespiešanās dziļums (7,4 mm) tika novērots paraugam 70_30 IBOA, kas vienlaikus uzrādīja arī augstu svārsta cietību (104 s). Tas apliecina, ka iespējams iegūt pārklājumus ar augstu cietību un elastību vienlaikus bez kompromisa starp šīm īpašībām. Savukārt TPGDA kā bifunkcionāls monomērs nodrošina lielāku polimēra šķērssaišu blīvumu nekā IBOA, bet struktūrā esošās propilgrupas ļauj saglabāt zināmu ķēdes mobilitāti un līdz ar to – mērenu elastību (6,4–7,1 mm).[71] Izmantojot TMPTMA kā reaktīvo atšķaidītāju, iespiešanās dziļums samazinājās līdz 25 mm, jo kā trifunkcionāls monomērs tas veicina blīva šķērssaistīta polimēra tīkla veidošanos, būtiski ierobežojot materiāla spēju deformēties. Iegūtie pārklājuma raksturlielumi liecina, ka, pielāgojot ALO-A funkcionalitāti un izmantojot reaktīvos atšķaidītājus, ir iespējams vienlaikus panākt gan cietības, gan elastības palielināšanos, tādējādi mazinot tradicionāli esošo kompromisu starp mehānisko izturību un elastību [83].

Apkopojot rezultātus, šis darbs demonstrē sistemātisku pieeju no atjaunojamo izejvielu sintēzes līdz galapārklājuma īpašību optimizācijai, izceļot iespēju pielāgot UV cietējošu akrilētu alkīdsveķu struktūru atkarībā no vēlamajām mehāniskajām īpašībām. Formulāciju izpēte ļauj apvienot augstu funkcionalitāti, pielāgojamu mehānisko īpašību spektru un videi draudzīgu tehnoloģiju, piedāvājot risinājumu industriāli nozīmīgam koksnes pārklājumu sektoram.

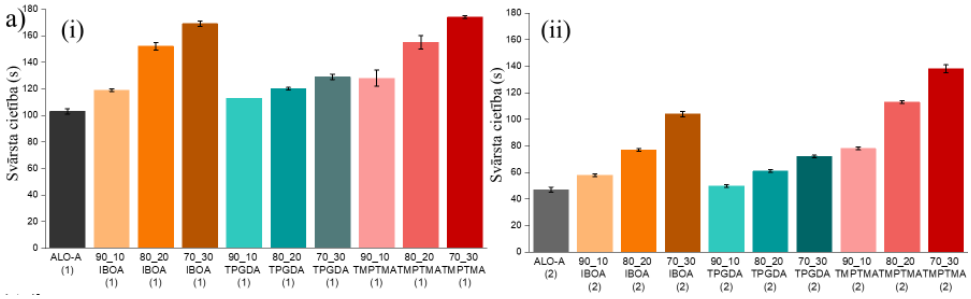

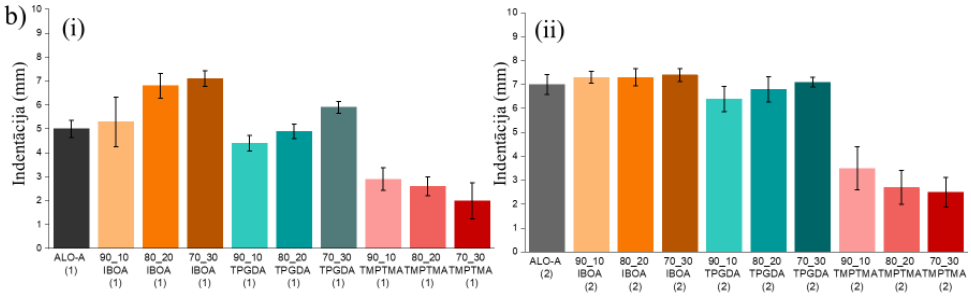

6. att. a) UV cietējošo alkīdsveķu pārklājumu svārsta cietības vērtības, izmantojot (i) ALO-A (1) un (ii) ALO-A (2); b) UV cietējošo alkīdsveķu pārklājumu iespieduma dziļuma vērtības, izmantojot (i) ALO-A (1) un (ii) ALO-A (2).

Jauna no atjaunojamiem resursiem iegūta UV cietējoša reaktīvā atšķaidītāja īpašību izpēte šķērssaistītā akrilētas rapšu eļļas polimēra tīklā (3. publikācija)

Pirmajās divās darba daļās tika izstrādātas un raksturotas UV gaismā cietējošas formulācijas, kurās izmantotas akrilētas augu eļļas un akrilēti alkīdsveķi ar dažādiem reaktīvajiem atšķaidītājiem. Šie pētījumi izceļ sveķu potenciālu kā videi draudzīgus pārklājuma materiālus. Tomēr lielākā daļa komerciālo reaktīvo atšķaidītāju ir naftas izcelsmes akrilāti, kas samazina dabas izcelsmes savienojumu saturu formulācijās un var potenciāli ietekmēt pārklājumu drošumu un ekoloģisko ietekmi. Līdz ar to pieaug interese par dabas izcelsmes reaktīvajiem atšķaidītājiem. Darba trešajā daļā šī problēma tika risināta, izpētot jaunu iekšējās dubultsaites saturošu furāna atvasinājumu – nepiesātinātu esteri (UES).

UES tika iegūts divos soļos elektrosintēzes procesā no furfurilēta etilēnglikola: vispirms elektroķīmiski pārveidojot to par spirociklu, pēc tam pakļaujot elektroķīmiski inducētai pārkārtošanai, veidojot UES. ARO tika iegūts $BF_3{\cdot}OEt_2$ katalizētā vienpakāpes sintēzes reakcijā, kā aprakstīts darba pirmajā daļā. UES tika pievienots ARO kā reaktīvais atšķaidītājs 5 masas % un 20 masas % koncentrācijā (attiecīgi ARO/UES5 un ARO/UES20), samazinot sveķu viskozitāti līdz pat 1,6 reizēm. Tālākā ietekme uz fotopolimerizāciju un šķērssaistītajiem materiāliem tika analizēta ar FTIR un UV redzamās gaismas (UV-Vis) spektroskopiju, stiepes mehānisko analīzi, SEM, DMA un termogravimetrisko analīzi (TGA). Darba beigās tika noteikta materiāla biodegradācijas spēja.

Ir trīs iespējamās reakcijas: (1) šķērssaistīšanās starp ARO un UES; (2) UES homopolimerizācija; (3) ARO homopolimerizācija (7. a att.). Ņemot vērā akrilgrupu reaģētspēju un masas daļu formulācijās, sagaidāms, ka dominē reakcijas, kurās iesaistīts ARO ((1) un (3)), savukārt UES homopolimerizācija (2) ir mazāk ticama. UES pievienošanos ARO polimēra tīklam apstiprināja FTIR spektroskopija, kur pēc UV cietēšanas UES raksturīgā C=C dubultsaites absorbcijas josla pie 1659 cm^{-1} praktiski pilnīga izzuda (7. b att.). Papildus to apliecināja arī optiskās caurlaidības palielināšanās līdz pat 90 % izstrādātajiem šķērssaistītajiem materiāliem UV-Vis apgabalā (7. c un d att.), ko var skaidrot ar UV absorbējošo hromoforu atšķaidīšanu un uzlabotu optisko homogēnitāti.

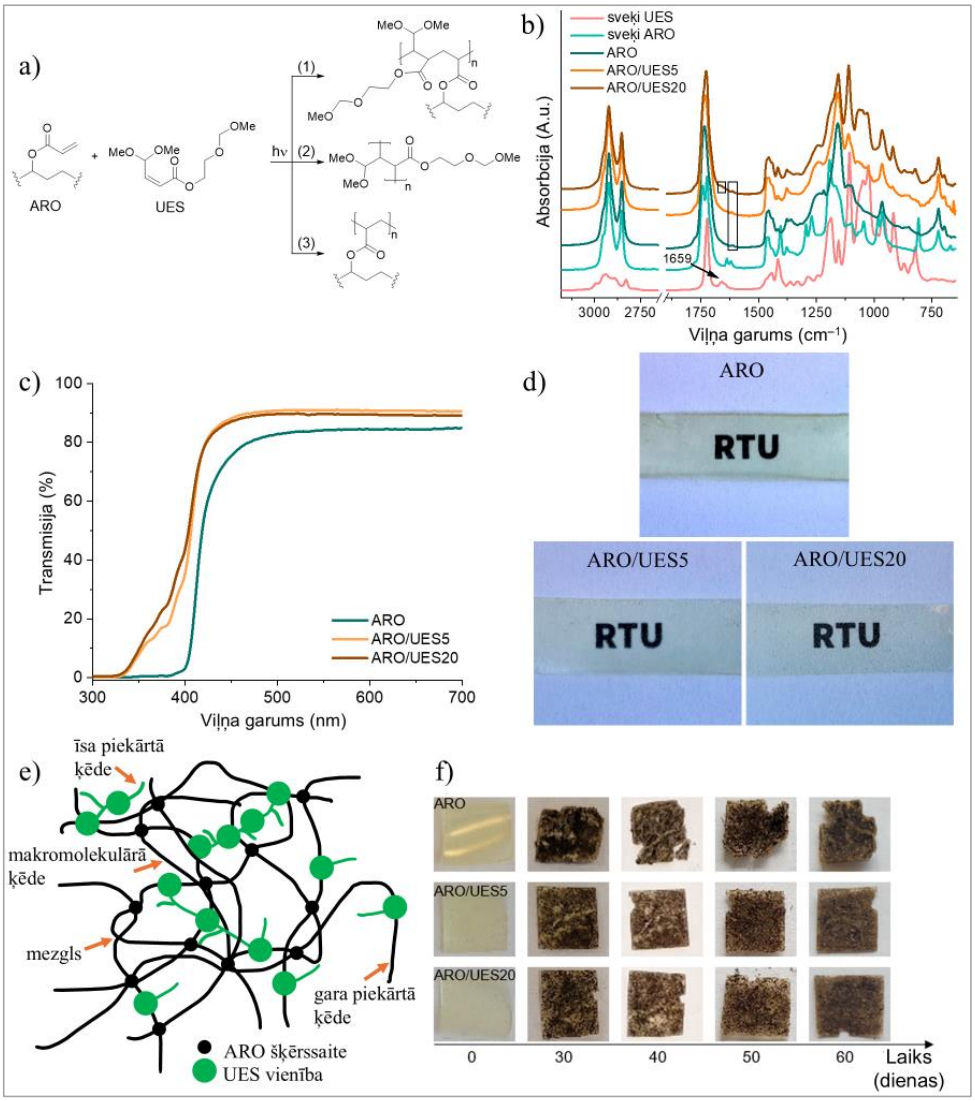

7. att. a) Iespējamās reakcijas starp ARO un UES; b) FTIR spektri ARO, UES un to formulācijām pirms un pēc UV cietēšanas; c) UV-Vis caurejošie spektri šķērssaisstītiem ARO un UES materiāliem; d) optiskās materiālu fotogrāfijas; e) ARO un UES šķērssaistīta tīkla vizualizācija; f) optiskās fotogrāfijas ARO un UES šķērssaistītiem materiāliem biodegradācijas laikā.

Makromolekulārajā tīkla struktūrā triglicerīda alkilķēdes darbojas kā plastifikatori, kas samazina šķērssaistītā materiāla E un σ, savukārt īsās piekārtās UES ķēdes pie lielāka masas % drīzāk palielina materiāla brīvo tilpumu un veicina relaksāciju (7. e att.) [84]. Polimēra šķērssaišu blīvums palielinājās no $1{,}07 \cdot 10^3$ mol/m^3 līdz $1{,}65 \cdot 10^3$ mol/m^3, pievienojot 5 masas % UES. Palielinātais polimēra šķērssaišu blīvums palielināja polimērmateriāla stiepes izturību (σ_B palielinājās no 0,49 MPa līdz 0,55 MPa) un E′ visā temperatūras diapazonā (istabas temperatūrā, 22 °C – no 7,98 MPa līdz 11,8 MPa). Palielinot UES koncentrāciju līdz 20 masas %, stiepes izturība samazinājās, kas liecina par reaktīvā atšķaidītāja pārlieku lielu koncentrāciju; tīkls kļūst pārāk atšķaidīts, trausls un palielinātu segmentu kustīgumu, tāpēc mehāniskā izturība samazinājās.

Papildus priekšrocībai, ka gan ARO, gan UES ir dabas izcelsmes, šajā darbā tika noteikta arī materiālu biodegradācija kontrolētos apstākļos. Paraugu fotogrāfijas pēc izņemšanas no augsnes redzamas 7. f attēlā. Pēc 30 dienu biodegradācijas ARO, ARO/UES5 un ARO/UES20 materiāli uzrādīja 13–15 % materiāla masas zudumu, uzrādot relatīvi stabilu noārdīšanās ātrumu. Nākamo 30 dienu laikā biodegradācijas ātrums samazinājās straujāk ARO šķērssaistītam polimēra tīklam, kas rezultējās kopējā materiāla masas zudumā 18–28 %, pieņemot taukskābju esteru hidrolīzi kā galveno notiekošo reakciju. Biodegradācijas dati uzrāda ļoti labus rezultātus, balstoties literatūrā ziņotajās līdzīgās sistēmās, kur novērots apmēram 14–16 % masas zudums 90 dienu laikā [85]. Turklāt visbiežāk izmantotie reaktīvie atšķaidītaji UV cietējošajos pārklājumos ir naftas produktu atvasinājumi, kuriem biodegradāciju nenovēro [86].

(Termo)mehāniskie testi liecina par iespēju turpmāk pielāgot dabas izcelsmes materiālu mehāniskās īpašības atbilstoši konkrētām prasībām. Materiālu mehāniskās veiktspējas optimizēšanai varētu izmantot vairākas stratēģijas. Piemēram, palielināt T_g un polimēra šķērssaišu blīvumu, izmantojot polifunkcionālus reaktīvos atšķaidītājus, uzlabojot augu eļļas akrilēšanas pakāpi vai optimizējot pēccietēšanas apstākļus [87]. Turklāt materiālu mehāniskās īpašības varētu pastiprināt, ieviešot stiegrojumu un izstrādājot biokompozītmateriālus, kas aplūkots nākamajā darba nodaļā.

Akrilētas augu eļļas impregnētu UV cietējošu nanokompozītmateriālu izstrāde un to īpašību izpēte (4. publikācija)

Šajā darbā tika izstrādāti dabas izcelsmes nanopapīra (NP) kompozītmateriāli, izmantojot kaņepju stublājus (lauksaimniecības atkritumprodukts) un salīdzinot divus augu eļļu akrilātus kā saistvielu – komerciāli pieejamo akrilētu sojas pupiņu eļļu (AESO) un vienpakāpes sintēzē iegūto akrilētu rapšu eļļu (ARO), kas raksturots darba pirmajā sadaļā. Kaņepju šķiedru NP tika sagatavots, mehāniski smalcinot kaņepju stublājus un veidojot viendabīgu šķiedru suspensiju, kas tālāk tika fibrilēta, iegūstot nanofibrilētas celulozes suspensiju (diametrs 86 ± 41 nm). Pēc tam nanofibrilētā suspensija tika ielieta veidnēs, žāvēta kontrolētos apstākļos un presēta, līdz izveidojās blīvs un vienmērīgs NP slānis (80 µm). NP veidošanās procesā fibrilas savstarpēji aglomerējas, veidojot nepārtrauktu struktūru. Nanokompozīta sagatavošanas shēma, kas ilustrē mijiedarbību starp celulozi un ARO vai AESO caur ūdeņraža saitēm, kā arī fizisku celulozes šķiedru ieslēgšanu polimēra matricā, redzamta 8. a attēlā. Iegūtā nanokompozīta fotogrāfija – 8. d attēlā.

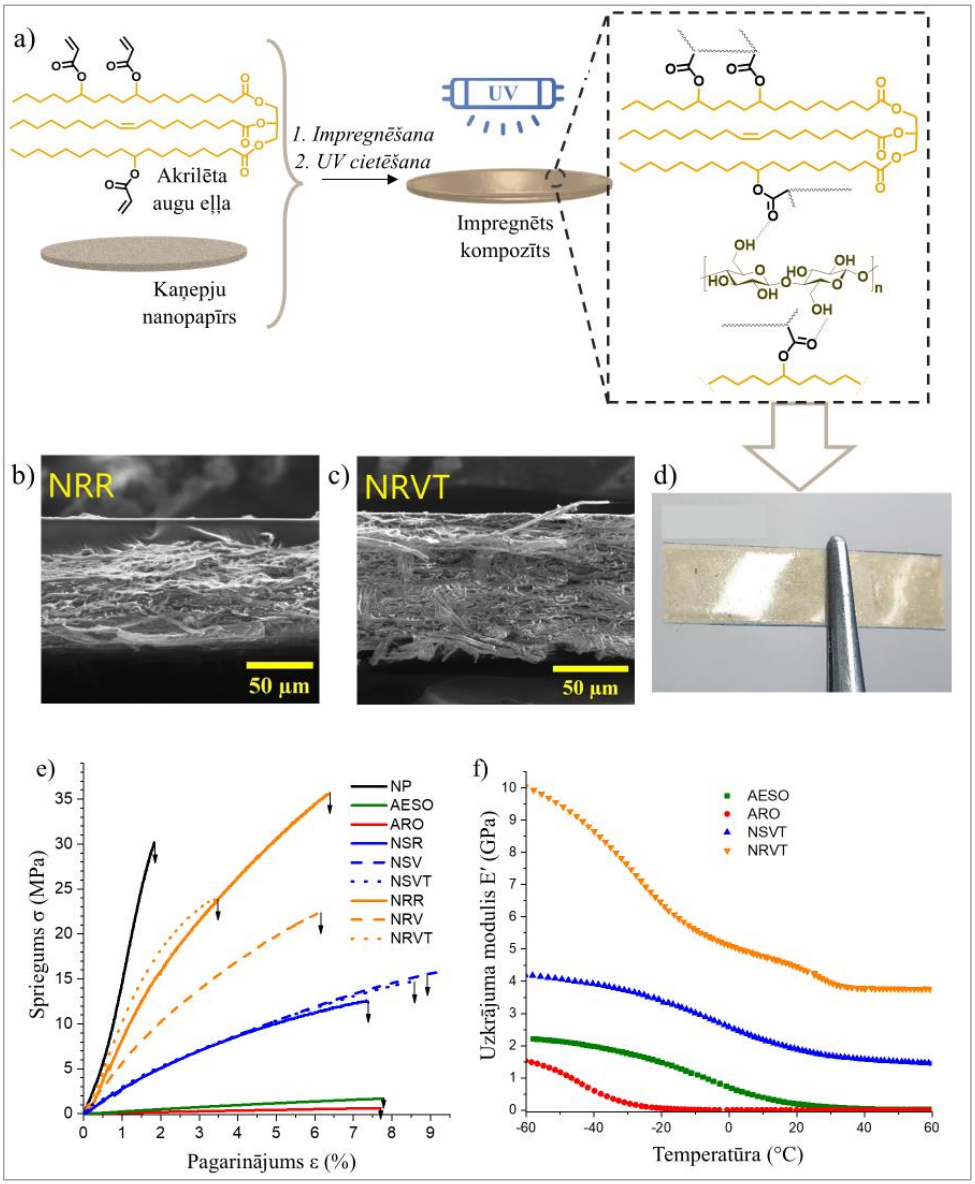

8. att. a) Vienkāršota reprezentējoša shēma dabas izcelsmes nanokompozītmateriālu izstrādei, izmantojot UV cietēšanu; SEM attēli impregnētam NP ar ARO: b) istabas temperatūrā (22 °C); c) 50 °C temperatūrā vakuuma vidē; d) iegūtā nanokompozīta fotogrāfija; e) σ-ε līknes NP, šķērssaistītiem ARO un AESO un to nanokompozītiem; f) E′ līknes šķērssaistītiem ARO un AESO un to impregnētiem nanokompozītiem paaugstinātā temperatūrā vakuuma apstākļos.

NP impregnēšanas process ar ARO un AESO tika analizēts, nosakot sveķu viskozitāti, slapēšanu uz NP virsmas un temperatūras un vakuuma ietekmi. Kompozīta sastāvs tika noteikts sveķu uzsūkšanās impregnēšanas laikā, un tāā rezultātā tika iegūtas 35/65 masas % NP/AESO un 50/50 masas % NP/ARO attiecības, kas izskaidrojamas ar atšķirībām viskozitātē un slapēšanu. Impregnēta NP paraugiem lietots saīsinājums N; ARO vai AESO impregnētiem paraugiem – R vai S; istabas temperatūrā (22 °C) impregnētiem paraugiem – R; vakuumā impregnētiem paraugiem – V; paaugstinātā temperatūrā impregnētiem paraugiem – T. ARO uzrādīja vairāk nekā 20 reizes zemāku viskozitāti gan istabas temperatūrā, gan paaugstinātā temperatūrā (50 °C) bīdes ātruma robežās no 1 s^{-1} līdz 100 s^{-1}, kā arī labāku slapēšanas spēju uz kaņepju NP virsmas nekā AESO, ko apliecina izmērītie kontaktleņķi. ARO kontaktleņķis uz NP samazinājās no 48,2° (5 s) līdz 39,3° (90 s) 20 °C temperatūrā un no 46,5° (5 s) līdz 33,3° (90 s) 50 °C temperatūrā, savukārt AESO kontaktleņķi tādos pašos apstākļos samazinājās attiecīgi no 98,6° līdz 43,7° un no 83,5° līdz 41,1°. Tas nodrošināja dziļāku un vienmērīgāku NP poru piepildījumu ar ARO sveķiem, samazinot gaisa iesprostošanās risku kompozīta struktūrā un uzlabojot matricas-šķiedru mijiedarbību.

Pēc eļļu impregnēšanas NP struktūrā paraugi tika cietināti UV gaismā, iegūstot kompozītus, kuriem tika raksturota struktūra un fizikālās īpašības. Impregnēšanas dziļums un iegūtā kompozīta mikrostruktūra tika novērtēta ar SEM šķērsgriezumu lūzuma vietās, analizējot atlikušā sveķu slāņa biezumu virs substrāta un nosakot poru aizpildījuma pakāpi. AESO gadījumā sveķu slānis (līdz 188 μm istabas temperatūrā) liecināja par ierobežotu impregnēšanos NP struktūrā, savukārt ARO uzrādīja ievērojami dziļāku impregnēšanos ar minimālu atlikušā slāņa biezumu virspusē un augstu porainās struktūras aizpildījumu, ko vēl vairāk uzlaboja impregnēšanas process paaugstinātā temperatūrā (50 °C) un vakuuma vidē.

8. b un c attēlā un redzams SEM attēlu salīdzinājums impregnētam NP ar ARO: b) istabas temperatūrā (NRR); c) 50 °C temperatūrā vakuuma vidē (NRVT). Temperatūras paaugstināšana un impregnēšana vakuumā palielināja arī mehāniskās un termomehāniskās īpašības (8. e un f att.). Vakuumā un 50 °C temperatūrā impregnēts ARO NP (NRVT) uzrādīja 1,3 GPa lielu E, 26,1 MPa lielu σ_B un 4,4 GPa lielu E′ pie 20 °C. Ņemot vērā to, ka ARO un AESO ir salīdzinoši mīksti materiāli, ciklisko slodžu izturību viskozi elastīgajā stāvoklī gandrīz pilnībā nodrošināja NP stiegrojums. Papildus tika veikta dielektriskā spektroskopija (DS), kas atklāja potenciālu izstrādātajiem dabas izcelsmes kompozītiem elektrisko izolatoru pielietojuma jomā, kur dominē epoksīda un papīra sistēmas [88].

Apkopojot rezultātus, šajā pētījumā tika demonstrēta no kaņepju atkritumproduktiem iegūta NP un akrilētas augu eļļas savietojamība, izmantojot UV gaismas cietēšanu. Pētījums parāda perspektīvu virzienu dabas izcelsmes termoreaktīvu kompozītmateriālu attīstībā un akrilētu augu eļļu mehāniskās veiktspējas uzlabošanā, nodrošinot līdzsvaru starp procesu vienkāršību un ilgtspēju.

UV cietējošu akrilētas rapšu eļļas vitrimēru pagatavošana termoreaktīvu materiālu pārstrādei un 3D drukas pielietojumam (5. publikācija)

Balstoties promocijas darba izstrādes gaitā iegūtajos un iepriekšējās darba nodaļās aprakstītajos rezultātos par UV starojumā cietējošām dabas izcelsmes formulācijām, ir redzams, ka šādi materiāli piedāvā plašas pielietojuma iespējas ar daudzveidīgu īpašību spektru. Apskatītie pētījuma virzieni iezīmē vienotu materiālu attīstības ceļu – no atjaunojamo izejvielu ķīmiskās modifikācijas līdz funkcionāliem UV cietējošiem pārklājumiem un kompozītiem. Noslēgumā tika pētītas iespējas materiālu pārstrādei un atkārtotai izmantošanai, izstrādājot vitrimērus. Paplašinot UV cietēšanas tehnoloģiju pielietojumu, tika veikta arī izstrādāto vitrimēru trīdimensionāla (3D) drukāšana.

Lai vitrimēra struktūrā ieviestu papildu -OH grupas un nodrošinātu ātru transesterifikācijas reakciju, rapšu eļļa tika akrilēta caur epoksīda gredzena atvēršanos, veidojot *β*-hidroksilestergrupas (9. a att.). Epoksidēšana tika veikta apaļkolbā, kas aprīkota ar mehānisko maisītāju, termometru un pilināmo piltuvi. Rapšu eļļa (1 mol C=C) tika sajaukta ar HCOOH (0,3 mol), un reakcijas maisījums tika uzkarsēts līdz 60 °C, kam sekoja lēna H_2O_2 (1,8 mol) pievienošana. Reakcija turpinājās 7 h. Reakcijas beigās maisījums tika atdzesēts līdz istabas temperatūrai (22 °C) un izšķīdināts EtOAc, lai ekstrahētu organisko daļu. Tālāk organiskais slānis tika mazgāts ar $NaHCO_3$ un NaCl ūdens šķīdumiem, atbrīvojoties no skābes. Pēc tam organiskā fāze tika žāvēta virs Na_2SO_4, filtrēta un šķīdinātājs tika ietvaicēts pazeminātā spiedienā. Epoksidēta rapšu eļļa (ERO) tika iegūta kā bāli dzelteni sveķi.

ERO akrilēšana tika veikta apaļkolbā, kas aprīkota ar mehānisku maisītāju, termometru un pilināmo piltuvi. ERO (1 mol epoksīda) tika sajaukts ar hidrohinonu (HQ, 300 ppm no AA) kā polimerizācijas inhibitoru un TEA katalizatoru (1 masas % no kopējās sveķu masas), un maisījums tika uzkarsēts līdz 90–95 °C. Pēc tam lēni tika pievienota AA, un reakcijas maisījums tika atstāts uz 18,5 h. Pēc tam tas tika atdzesēts līdz istabas temperatūrai, izšķīdināts EtOAc un mazgāts ar $NaHCO_3$ un NaCl ūdens šķīdumiem. Organiskā fāze tika žāvēta virs Na_2SO_4 un nofiltrēta, šķīdinātājs tika ietvaicēts pazeminātā spiedienā. Akrilēta epoksidēta rapšu eļļa (AERO) tika iegūta kā tumši dzelteni, viskozi sveķi. ^{1}H-KMR spektri redzami 9. b attēlā.

Formulācijas tika izstrādātas, izmantojot 10 masas %, 20 masas % vai 30 masas % AERO, 2-hidroksi-3-fenoksipropilakrilātu (HPPA) un glicerīna 1,3-diglicerolāta diakrilātu (GDA), lai nodrošinātu optimālu -COOR un -OH grupu attiecību un transesterifikācijas reakciju (9. f att.). Tika sagatavotas divas paraugu sērijas – ar $Zn(acac)_2$ transesterifikācijas katalizatoru (10 masas % no kopējās akrilātu masas) un bez tā, lai izvērtētu katalizatora ietekmi uz materiāla īpašībām un pārbaudītu pārstrādes potenciālu vitrimēriem bez katalizatora.

Kopā tika sagatavotas sešas formulācijas, kas satur 70 masas % HPPA un 10 masas %, 20 masas % vai 30 masas % AERO, savukārt GDA saturs bija 10 masas % vai 20 masas %. GDA netika iekļauts formulācijā ar 70 masas % HPPA un 30 masas % AERO. Paraugu sērijām bez katalizatora nosaukumā pievienots saīsinājums "(n/c)". Paraugu nosaukumos norādīts AERO saturs masas %, kā arī katalizatora klātbūtne. Piemēram, "AERO20(n/c)" satur 70 masas % HPPA, 20 masas % AERO un 10 masas % GDA, bet nesatur $Zn(acac)_2$ katalizatoru.

Formulāciju UV cietēšanas kinētika tika pētīta ar foto DSC, kas uzrādīja ātrāku un pilnīgāku fotopolimerizācijas reakciju formulācijām bez pievienotā transesterifikācijas katalizatora (9. c att.). Vitrimēri bez katalizatora uzrādīja 235–241 J/g fotopolimerizācijas

entalpijas vērtības un eksotermisko maksimumu aptuveni 5 s. Turpretī katalizatora saturoši vitrimeri uzrādīja 167–203 J/g fotopolimerizācijas entalpijas vērtības un eksotermisko maksimumu aptuveni 12 s. Samazināto fotopolimerizācijas entalpiju $Zn(acac)_2$ klātbūtnē var skaidrot ar optiskiem efektiem, ko izraisa gaismas izkliede pagatavotajā formulācijā, kas bija duļķaina, samazinot gaismas caurlaidību un līdz ar to radikāļu veidošanos. To apliecināja arī zemākas gela frakcijas, lieconot par mazāk šķērssaistītu polimēra tīklu. Katalizatora saturošajiem vitrimēriem gēla frakcijas vērtības svārstījās no 73 % līdz 79 %, savukārt vitrimeriem bez katalizatora gēla frakcijas vērtības bija robežās no 85 % līdz 96 %.

UV cietējošo vitrimēru sprieguma relaksācija tika veikta, lai izpētītu, cik efektīvi polimēru tīkls spēj atbrīvot uzkrāto iekšējo spriegumu un pielāgoties termiskajiem apstākļiem. Sprieguma relaksācijas ātrumu vitrimēros ietekmē temperatūra, katalizatora veids un koncentrācija, polimēru tīkla struktūra un šķērssaišu blīvums [89]. Savukārt relaksācijas laiks (τ^*) ir laiks, kādā paraugs relaksējas līdz 1/e (~ 37 %) no sākotnējā moduļa. Tika novērots, ka sprieguma relaksācijas ātrums palielinājās līdz ar temperatūras palielināšanos termiski aktivēto dinamisko saišu apmaiņas reakciju dēļ. Piemēram, $Zn(acac)_2$ un 30 masas % AERO saturoša vitrimēra sprieguma relaksācijas laiks no 20 min 180 °C samazinājās līdz 14 min 200 °C. Vitrimēri bez katalizatora attiecīgajā temperatūrā uzrādīja 2–3 reizes lēnāku sprieguma relaksāciju. 9. d attēlā salīdzinātas sprieguma relaksācijas līknes paraugiem ar un bez katalizatora 200 °C temperatūrā.

9. e attēls ilustrē dinamiskās -COOR un -OH apmaiņas reakcijas, kur polimēru tīklā: i) pie lielāka šķērssaišu blīvuma bez katalizatora notiek lēnāka sprieguma relaksācija; ii) pie mazāka šķērssaišu blīvuma $Zn(acac)_2$ paātrina transesterifikācijas reakciju. Literatūrā ziņota gan -COOR, gan -OH grupas pārākuma ietekme uz sprieguma relaksācijas laiku [90], [91]. Atšķirības sprieguma relaksācijas laikā starp paraugiem ar atšķirīgu AERO saturu bija mazāk izteiktas, kas sakrīt ar gela frakciju, liecinot par minimālām atšķirībām polimēra šķērssaišu blīvumā vienas sērijas vitrimēriem.

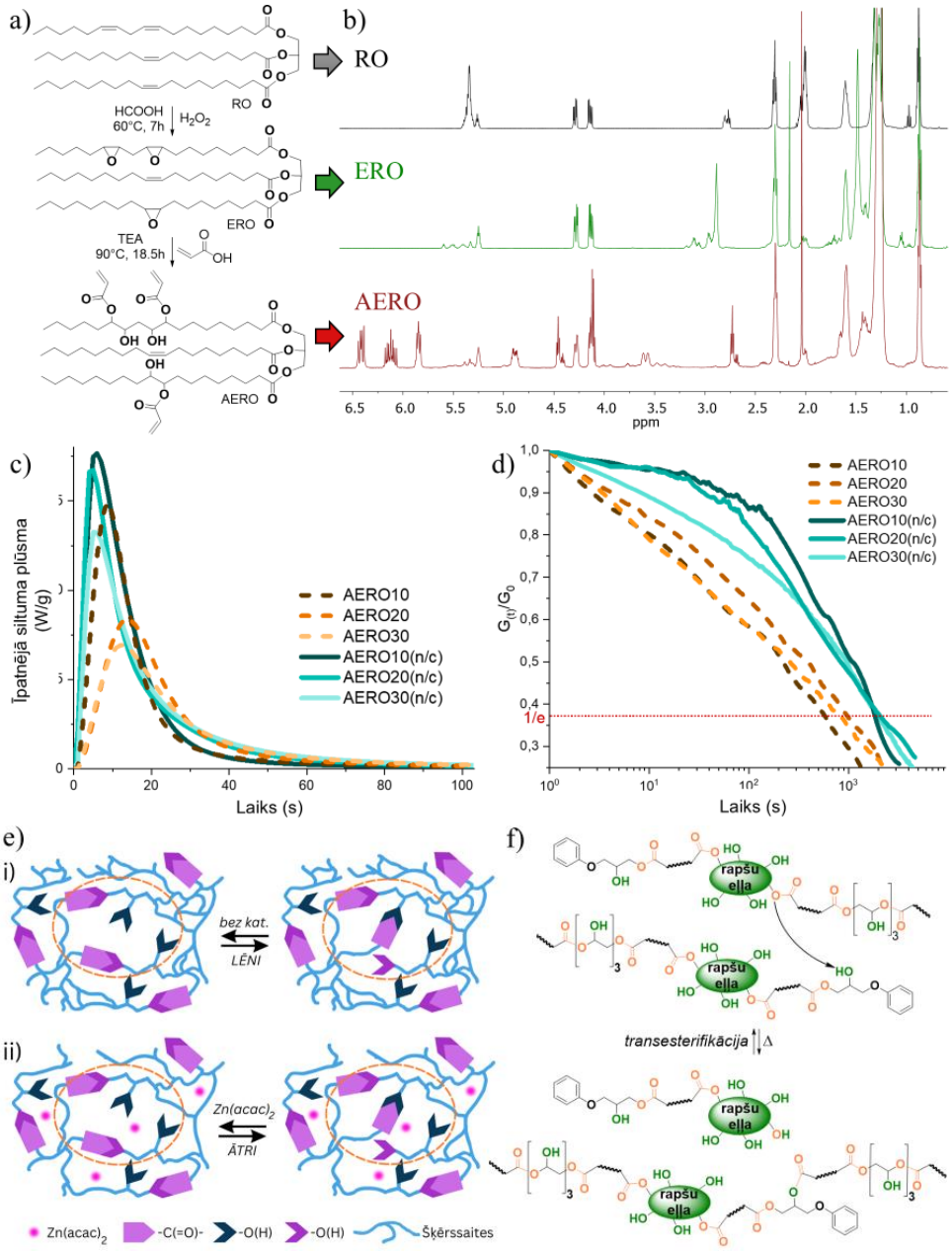

9. att. a) AERO sintēze caur epoksīda gredzena atvēršanās reakciju; b) RO, ERO un AERO ^{1}H-KMR spektri; c) foto DSC līknes; d) sprieguma relaksācijas līknes; e) sprieguma relaksācijas vizualizācija: i) pie lielāka polimēra šķērssaišu blīvuma bez katalizatora; ii) pie mazāka polimēra šķērssaišu blīvuma Zn(acac)$_2$ klātbūtnē; f) viena no iespējamajām termiski ierosinātajām dinamisko saišu apmaiņas reakcijām vitrimēros.

UV cietējošo vitrimēru pārstrādes novērtēšanai abas paraugu sērijas tika sasmalcinātas un sapresētas metāla veidnē (10. a att.). Optimizējot apstākļus, tika noteikts, ka efektīvākā pārstrāde notiek 200 °C temperatūrā 2 h laikā (10. b att.). Šajos apstākļos tika veikti divi secīgi pārstrādes cikli, pēc kuriem tika novērtēta vitrimeru veiktspēja. Pārstrādes laikā vitrimeri saglabāja augstu šķērssaistīšanās pakāpi, par ko liecina sola-gela frakcijas dati (līdz pat 90 %). Tomēr pēc termiskās pārstrādes vitrimēros bez pievienotā katalizatora tika novērotas plaisas, savukārt katalizatora saturošajos paraugos tās neveidojās, apliecinot katalizatora spēju pārkārtot šķērssaistīto tīklu un atjaunot materiāla struktūru (10. b att.). Plaisu veidošanās līdzīgos apstākļos novērota arī citu autoru pētījumos [92]. Pēc termiskās pārstrādes vitrimēru paraugu nosaukumiem tika pievienots pārstrādes cikla kārtas numurs, piemēram, "AERO30_cycle2" apzīmē AERO30 vitrimēru, kas iegūts pēc otrā termiskās pārstrādes cikla.

UV cietējošajiem vitrimēriem tika veikta TGA-FTIR kombinētā analīze, kas vienlaikus nosaka materiāla masas zudumu temperatūras palielināšanās laikā un identificē izdalījušos gāzveida produktus. Iegūtie dati liecināja par pastiprinātu gāzveida produktu izdalīšanos katalizatora saturošiem vitrimēriem, apliecinot atšķirīgus polimēra tīkla pārkārtošanās ceļus paraugiem bez (10. c att.) un ar (10. d att.) katalizatoru. Katalizatora saturošajos vitrimēros gaistošie fragmenti veidojās ievērojami ātrāk dinamisko saišu apmaiņas dēļ un uzrādīja lielāku absorbcijas joslu intensitāti, īpaši CO_2 un C=O reģionos [90]. Līdz ar to katalizatora saturošie vitrimēri uzrādīja zemāku termisko stabilitāti, maksimālajam sadalīšanās ātrumam sasniedzot 370 °C, pretēji vitrimēriem bez katalizatora, kas uzrādīja maksimālo sadalīšanās ātrumu 410 °C temperatūrā. Jāatzīmē, ka termiskā stabilitāte abām vitrimēru sērijām palielinājās ar katru pārstrādes ciklu, kas, visticamāk, saistīts ar mazmolekulāro vai neizreaģējušo komponentu iztvaikošanu termiskās pārstrādes laikā, atstājot materiālu, kas galvenokārt sastāv no stabila šķērssaistīta tīkla.

Tālākie eksperimenti tika veikti katalizatora saturošiem vitrimēriem. Tika novērtēta vitrimēru pārstrādes ietekme uz materiālu (termo)mehāniskajām īpašībām (10. e un f att.). 10. e attēlā redzams, ka E′ vērtības pēc pārstrādes samazinājās visā temperatūras diapazonā, kas atspoguļo stingrības zudumu, visticamāk, tīkla pārkārtošanās, novērotās degradācijas un ķēžu šķelšanās dēļ [93]. Tanδ virsotnes intensitātes samazināšanās liecināja par mazāku molekulāro mobilitāti pie T_g. Vienlaikus neliela tanδ līknes paplašināšanās liecina par lielāku makromolekulārā tīkla heterogenitāti un palielinātu relaksācijas laiku sadalījumu, jo pēc dinamisko saišu apmaiņas reakcijām var veidoties reģioni ar atšķirīgu šķērssaišu blīvumu [94]. Tomēr kopumā vitrimēri pirms un pēc pārstrādes uzrādīja līdzīgu termomehānisko uzvedību, kas liecina, ka materiāls saglabā savas raksturīgākās īpašības. 10. f attēlā redzams, ka mehāniskā izturība pēc pārstrādes pilnībā neatjaunojās, bet tika novērota ievērojama σ_B atgūšana – pēc pirmā cikla 67–98 %, pēc otrā cikla 41–50 % no sākotnējās vērtības. Viens no iemesliem mehāniskās izturības samazinājumam pēc pārstrādes ir kovalentā tīkla bojājumi, kas rodas intensīvas smalcināšanas laikā vitrimēru pārstrādē [95], [96].

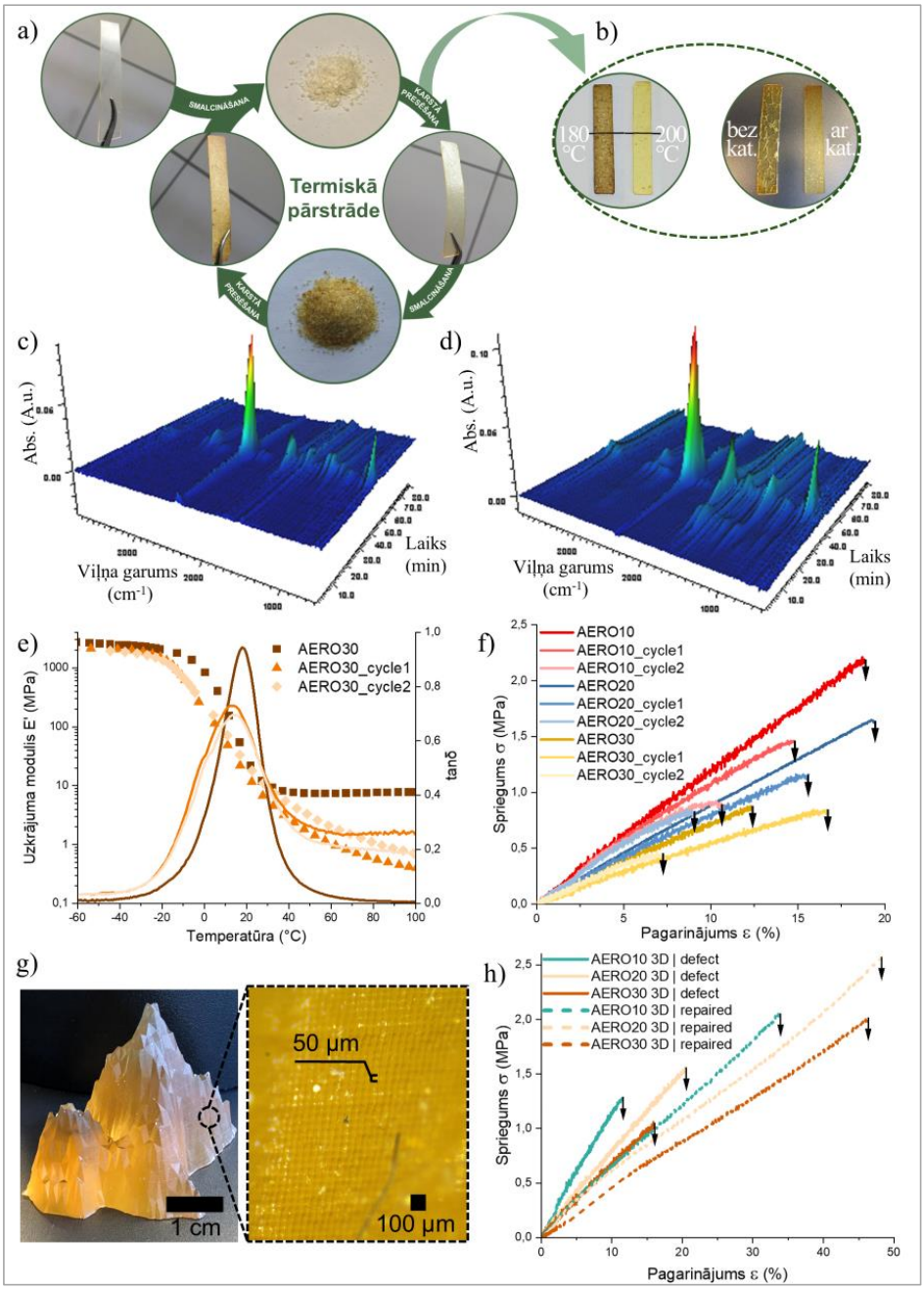

10. att. a) AERO vitrimēru termiskās pārstrādes shēma; b) temperatūras un katalizatora ietekme uz AERO vitrimēru karstās presēšanas laikā; c) un d) AERO30(n/c) un AERO30 izdalīto gāzu FTIR spektru 3D grafiki; UV cietināta un pārstrādāta AERO30 vitrimēra: e) uzglabāšanas moduļa un tanδ līknes, f) σ-ε līknes; g) AERO vitrimēra 3D drukas validācija, izmantojot DLP tehnoloģiju; h) σ-ε līknes 3D drukātiem paraugiem ar bojātu un atjaunotu struktūru.

Visbeidzot, vitrimēri tika 3D drukāti, lai demonstrētu izstrādāto materiālu pielietojumu aditīvajā ražošanā. Drukāšanai tika izvēlēts sastāvs ar augstāko AERO saturu, kas arī nodrošināja zemāko viskozitāti (η = apt. 663 mPa·s bīdes ātruma robežās no 1 s^{-1} līdz 1000 s^{-1}) un ir svarīgs parametrs vannas tipa 3D drukāšanā. 3D drukāšanas procesā tika novērota vienmērīga slāņu adhēzija ar slāņa biezumu 50 μm un pēc drukāšanas – augsta izšķirtspēja, dimensiju precizitāte un teicama virsmas kvalitāte (10. g att.).

Tālāk tika pētīta materiāla spēja atjaunot savu struktūru un īpašības pēc mehāniskiem bojājumiem, kas pagarina produktu kalpošanas laiku un var samazināt atkritumu daudzumu rašanos. Turklāt tas nodrošina efektīvāku resursu izmantošanu. Pēdējā darba daļā tas tika analizēts, veicot vitrimēru struktūras atjaunošanu. Tika 3D drukāti stienīši ar atvērumu, kura diametrs bija 5 mm, materiāla vidū (paraugu nosaukumā "*defect*"), simulējot mehānisku bojājumu. Sākotnējos eksperimentos simulētajā bojājumā tika ievietots 3D drukāts apļveida aizpildījums, kam sekoja termiskā apstrāde, lai aktivizētu dinamisko saišu apmaiņu. Tomēr šī pieeja nebija efektīva, jo stiepes testi uzrādīja, ka lūzums notika tieši saskares virsmā starp parauga materiālu un ievietoto 3D drukāto apļveida aizpildījumu, kas liecināja par nepietiekamu saskares laukumu un vāju adhēziju. Otrā pieeja izrādījās efektīvāka – simulētais bojājums pēc drukāšanas tika aizpildīts ar šķidriem sveķiem, UV cietināts un karsēts 200 °C 1 h (paraugu nosaukumā "*repaired*"), lai ierosinātu transesterifikācijas reakciju uz robežvirsmas. σ-ε līkņu rezultāti paraugiem ar atjaunotu struktūru uzrādīja līdz pat 2,0 reizes lielāku σ_B un līdz pat 2,9 reizes lielāku deformāciju sagraušanas brīdī (ε_B), salīdzinot ar bojātajiem paraugiem (10. h att.). Atšķirībā no sākotnējās pieejas šajos paraugos lūzums nenotika uz atjaunotās saskares robežvirsmas; tā vietā tas notika parauga nepārtrauktajā materiāla daļā, kas liecina par stipru saskares virsmas izveidošanos, ko nodrošina efektīva dinamisko saišu apmaiņa.

Apkopojot rezultātus, šajā darbā tika demonstrēta pieeja, kas apvieno dabas izcelsmes savienojumu izmantošanu, energoefektīvas tehnoloģijas izmantošanu un materiālu atkārtotu pārstrādi. Pētījumā izstrādātās vitrimēru formulācijas balstītas dinamisko saišu apmaiņas reakcijās, kas nodrošina sprieguma relaksāciju, pārstrādi un struktūras spēju atjaunoties pēc bojājumiem. Optimizējot katalizatora daudzumu, tostarp formulācijas bez katalizatora, iespējams panākt efektīvu tīkla pārkārtošanos, vienlaikus saglabājot labu strukturālo integritāti. Tas ļauj atjaunot vitrimēru mehānisko veiktspēju pat pēc vairākiem pārstrādes cikliem, nodrošinot termoreaktīvo polimēru atgriešanu apritē. Izstrādātie AERO vitrimēri uzrādīja lielisku piemērotību 3D drukas tehnoloģijai, turklāt nodrošinot struktūras atjaunošanu, kas paver plašākas iespējas UV cietējošu vitrimēru pielietojumam. Materiālu spēja atjaunot struktūru un stiepes īpašības pēc bojājumiem apliecina to ilgtspējības potenciālu.

SECINĀJUMI

1. Mērķtiecīgi pielāgojot akrilētu augu eļļu atvasinājumu sintēzes apstākļus un UV cietējošo sveķu formulācijas, ir iespējams kontrolēt fotopolimerizācijas kinētiku, makromolekulāro struktūru un galamateriālu mehāniskās īpašības.
   1.1. Optimizēta divpakāpju epoksidēšanas-akrilēšanas sintēzes metode ļauj mērķtiecīgi regulēt akrilgrupu saturu UV cietējošos linsēklu eļļas alkīdsveķos (ALO-A) (0,18 mol akrilgrupas/100 g sveķu vai 0,23 mol akrilgrupas/100 g sveķu). Reaktīvo atšķaidītāju pievienošana nodrošināja papildu iespējas viskozitātes, cietēšanas kinētikas (t_{gel} < 6,2 s) un polimēra tīkla struktūras pielāgošanai, sasniedzot vienlaicīgu pārklājuma cietības (104 s) un elastības (7,4 mm) pieaugumu.
   1.2. Reaktīvā atšķaidītāja glicerīna propoksitriakrilāta (GPT) pievienošana paātrināja fotopolimerizācijas procesu (< 70 s), palielināja šķērssaišu blīvumu (līdz $2{,}2 \cdot 10^3$ mol/m^3) un uzlaboja materiālu mehānisko veiktspēju (līdz 0,76 MPa). Izstrādātās akrilētu augu eļļu formulācijas demonstrēja pielietojumu kā UV cietējoši koksnes pārklājumi, uzrādot līdz 1,21 MPa adhēziju uz koksnes substrāta.
2. Dabas izcelsmes nepiesātināta furāna estera monomēra (UES) kā reaktīvā atšķaidītāja pievienošana samazināja UV cietējošo ARO sveķu viskozitāti (η = 291 mPa·s) un uzlaboja strukturālās īpašības (šķērssaišu blīvums = $1{,}65 \cdot 10^3$ mol/m^3), vienlaikus veicinot materiālu biodegradējamību (līdz pat 28 % masas zuduma 60 dienu laikā). Iegūtie rezultāti apliecina dabas izcelsmes monomēru potenciālu kā ilgtspējīgu alternatīvu naftas izcelsmes monomēriem.
3. UV cietējošas akrilētas augu eļļas ir piemērotas izmantošanai kā matricas saistviela dabisko šķiedru kompozītmateriālos. Efektīva matricas-šķiedru mijiedarbība, ko apliecina SEM analīze, nodrošināja uzlabotu spriegumu pārnesi un ekspluatācijas īpašības (σ_B = 35,6 MPa, E = 1,3 GPa), demonstrējot dabas izcelsmes kompozītmateriālu izstrādes potenciālu.
4. Kontrolējot akrilētas epoksidētas rapšu eļļas (AERO) makromolekulārajā režģa struktūrā dinamiski kovalento saišu saturu, iespējams izstrādāt UV cietējošus vitrimēru materiālus. Iegūtie vitrimēri demonstrēja termiski aktivētu transesterifikāciju, nodrošinot atkārtotu pārstrādi ar mehāniskās veiktspējas (σ_B = 1,46 MPa, E = 12,4 MPa) atgūšanu līdz pat 98 % pēc pirmā un 50 % pēc otrā cikla. Vitrimēru sveķi demonstrēja 3D drukājamību ar augstu izšķirtspēju un struktūras atjaunošanu, atjaunojot mehānisko izturību (σ_B pieaugums līdz 199 %) un pagarinājumu (ε_B pieaugums līdz 288 %) pēc imitēta mehāniska bojājuma.

DOCTORAL THESIS PROPOSED TO RIGA TECHNICAL UNIVERSITY FOR PROMOTION TO THE SCIENTIFIC DEGREE OF DOCTOR OF SCIENCE

To be granted the scientific degree of Doctor of Science (PhD), the present Doctoral Thesis has been submitted for defence at the open meeting of RTU Promotion Council on 25 May 2026 at 10.00 at the Faculty of Natural Sciences and Technology of Riga Technical University, Paula Valdena iela 3, Room 272.

OFFICIAL REVIEWERS

Associate Professor Dr. chem. Ingars Reinholds
University of Latvia, Latvia

Professor PhD Marco Sangermano
Polytechnic University of Turin, Italy

Professor PhD Minna Hakkarainen
KTH Royal Institute of Technology, Sweden

DECLARATION OF ACADEMIC INTEGRITY

I hereby declare that the Doctoral Thesis submitted for review to Riga Technical University for promotion to the scientific degree of Doctor of Science (PhD) is my own. I confirm that this Doctoral Thesis has not been submitted to any other university for promotion to a scientific degree.

Sabīne Greivule ……. (signature)

Date: ……

The Doctoral Thesis is prepared as a thematically unified collection of scientific publications. It includes a summary in Latvian and English and five SCI-indexed publications. The publications are written in English, with the total length of 67 pages.

ANNOTATION

This Doctoral Thesis addresses the problem of the excessive use of petroleum-based products in the polymer materials industry and their insufficient reprocessing. Such reliance contributes to resource depletion, environmental pollution, and increased challenges in waste management due to the limited recyclability of conventional thermosetting polymers. To demonstrate that a transition towards more sustainable solutions is possible, rapeseed, linseed, and grapeseed oils were used as renewable, bio-based resources for polymer material development. Vegetable oils and their polymer derivatives (fatty acid modified polyesters or alkyds) were converted into photoactive compounds by modification with acrylates and investigated under UV light-induced curing, which represents a faster, more energy-efficient, and environmentally friendly alternative to conventional thermal curing.

Photoactive vegetable oil acrylates were synthesized using one-step or two-step synthesis routes by optimizing reaction parameters and evaluating their influence on UV-curing kinetics. At the same time, the incorporation of photoactive acrylate groups was also adapted for linseed oil-based alkyds – materials of industrial importance in the coatings sector – via epoxy ring-opening reactions. This modification significantly accelerated alkyd curing, reduced the need for solvents, and preserved mechanical performance. UV-curable resin formulations containing various reactive diluents, including bio-based ones, were developed to reduce resin viscosity and improve the physical and (thermo)mechanical properties of the crosslinked polymer networks. The suitability of the developed resins for wood coating applications was evaluated by determining adhesion strength, pendulum hardness, and indentation depth. Furthermore, to enhance the mechanical performance of the crosslinked materials, cellulose-reinforced composites were developed while maintaining the renewable origin of the raw materials. Finally, this work demonstrates the development of UV-curable vitrimers based on acrylated epoxidized rapeseed oil, in which the content of dynamic covalent bonds within the network was controlled. The obtained materials were thermally reprocessed, 3D printed, and shown to exhibit structural recovery, significantly expanding their potential for reuse and reprocessing.

The results of this Doctoral Thesis demonstrate the potential of vegetable oil-based acrylates and their derivatives for the development of sustainable, functional, and reprocessable polymer materials, offering an environmentally friendly alternative to petroleum-derived polymers and broadening the practical application scope of UV-curable materials.

ABBREVIATIONS

3D	3-dimentional
A.u.	arbitrary units
AA	acrylic acid
AESO	acrylated epoxidized soybean oil
AERO	acrylated epoxidized rapeseed oil
AGO	acrylated grapeseed oil
ALO-A	acrylated linseed oil alkyd
ALO	acrylated linseed oil
ARO	acrylated rapeseed oil
AV	acid value
BHT	butylated hydroxytoluene
DBC	double bond conversion
DLP	digital light processing
DMA	dynamic mechanical analysis
DS	dielectric spectroscopy
DSC	differential scanning calorimetry
E	tensile modulus
E′	storage modulus (in DMA measurements)
E″	loss modulus (in DMA measurements)
EEW	epoxy equivalent weight
ELO-A	epoxidized linseed oil alkyd
ERO	epoxidized rapeseed oil
EtOAc	ethylacetate
EV	epoxy value
FTIR	Fourier transform infrared spectroscopy
G′	storage modulus (in photo-rheology measurements)
G″	loss modulus (in photo-rheology measurements)
$G_{(t)}/G_0$	normalized stress relaxation modulus
GDA	glycerol 1,3-diglycerolate diacrylate
GPT	glycerol propoxylate triacrylate
h	hours
HDDA	hexanediol diacrylate
HPPA	2-hydroxy-3-phenoxypropyl acrylate
HQ	hydroquinone
IBOA	isobornyl acrylate
MEHQ	4-methoxyphenol
NMR	nuclear magnetic resonance
NP	nanopaper
ppm	parts per million
Ref.	reference

RO	rapeseed oil
SEC	size exclusion chromatography
SEM	scanning electron microscopy
SLA	stereolithography
T	temperature
T_g	glass transition temperature
t_{gel}	gelpoint
Tanδ	loss factor
TEA	triethylamine
TGA	thermogravimetric analysis
TMPTMA	trimethylolpropane trimethacrylate
TPGDA	tripropylene glycol diacrylate
TPP	triphenylphosphine
UES	unsaturated ester
UV-Vis	ultraviolet-visible light spectroscopy
VOC	volatile organic compounds
wt%	weight percent
ε	strain
ε_B	elongation at break
η	viscosity
σ	tensile strength
σ_B	maximum strength
τ*	relaxation time

TABLE OF CONTENTS

Appendix IV Platnieks, O., Briede, S., Grase, L., Thakur, V., J., & Gaidukovs, S. (2023). Fully Bio-Based Thermoset Composites from UV Curable Prepregs: Vegetable Oil Acrylate Impregnated Hemp Nanopaper. *Polymer Composites*, 44(9), 5721-5733.

Appendix V Briede, S., Besprozvannaja I., Porcarello M., & Gaidukovs, S. (2026). Reprocessable and Repairable Bio-Based Vitrimers from Acrylated Epoxidized Rapeseed Oil for Additive Manufacturing. *Macromolecular Materials and Engineering*. doi: 10.1002/mame.70228. (Accepted).

GENERAL OVERVIEW OF THE THESIS

Introduction to State-of-the-Art

Nowadays, the polymer materials industry faces several challenges, primarily related to the excessive use of non-renewable resources and the relatively slow implementation of novel technological processes in industry. In 2019, global production of petroleum-based plastics reached nearly 370 million tons, of which only about 9 % was recycled, indicating significant limitations in the current circular system [1]. Considering the European Union's Green Deal goal to achieve climate neutrality by 2050, the transition to renewable feedstocks becomes crucial to reduce dependence on petroleum products and ensure materials' reprocessing. As a sustainable, renewable source of biopolymers, vegetable oils have been extensively studied in recent years. Interest in using vegetable oils in the polymer materials industry has grown rapidly, and since 2015, the number of publications on their application in biopolymer development has increased by more than 250 %. For example, rapeseed oil, which is suitable for the climate in Latvia, represents an important renewable resource and an available alternative feedstock for polymer material development.

Historically, vegetable oils such as linseed oil have been widely used in the polymer industry, primarily in the production of varnishes and coatings. Over the last few decades, interest in vegetable oils has significantly increased, driven by technological advances and the expansion of biomass applications [2], [3]. Vegetable oils are mainly composed of triglycerides (approximately 95 %); small amounts of mono- and diglycerides, free fatty acids, phospholipids, tocopherols, polyphenols, and other compounds are also present [4]. The reactive centers in the triglyceride molecules – double bonds, ester groups, allylic groups, and bis-allylic groups – provide opportunities for extensive structural modification. Furthermore, the viscosity (η) of vegetable oils makes them suitable for UV-curable resins, providing good flow properties.

To effectively use rapeseed and other vegetable oils in biopolymer production, particular attention is paid to their processing technologies. One of the modern solutions in polymer production is photoinduced or ultraviolet (UV) light-induced curing technology, which, as an alternative to thermal curing, provides faster reactions, lower energy consumption, and reduced volatile organic compound (VOC) emissions. UV curing of vegetable oils is possible after modifying the unsaturated double bonds remaining in the fatty acids by introducing photoactive acrylate groups.

Acrylation of vegetable oils can be achieved using several synthetic pathways, among which the conventional two-step epoxidation-acrylation route is the most widely applied. Alternative approaches, such as direct one-step acrylation of double bonds, have also been reported, although they are less extensively studied. The choice of synthesis method involves trade-offs between reaction conditions, control, and susceptibility to side reactions. The two-step method is well established and allows stepwise control over the formation of functional groups, although it requires precise optimization of both the epoxidation and the subsequent ring-opening reactions. In contrast, direct acrylation of double bonds represents a shorter and more atom-efficient route, but typically requires strong catalysts and may be more sensitive to reaction conditions.

The two-step acrylation of vegetable oils starts with the epoxidation of the double bonds in the triglyceride fatty acid residues, followed by the ring-opening of the oxirane with acrylic acid (AA) (Fig. 1a). Double bond epoxidation, also known as the Prilezhaev reaction via *in situ* generated peracid, has been widely used to obtain epoxidized soybean oil [5]. Under uncontrolled conditions, side reactions such as acid- or water-induced epoxide ring opening and other undesired reactions (e.g., H_2O_2 decomposition) may easily occur in the aqueous phase, oil phase, or at the interface [6]. Literature reports indicate that 60 °C is an optimal temperature for the epoxidation reaction [7]. Kousaalya *et al.* observed that increasing the reaction temperature from 40 °C to 60 °C increased the epoxidation yield from 58 % to 88 %. However, further increase in temperature led to an increase in undesired epoxide ring-opening reactions, as measured by *α*-glycol values [8]. Turco *et al.* noted that linseed oil should be epoxidized at lower temperatures to avoid epoxide ring-opening. Using a kinetic model, the authors calculated that due to the high linoleic acid content in the triglyceride structure, linseed oil is 1.5 times more reactive than soybean oil; therefore, during epoxidation, the reactivity toward ring-opening was approximately four times higher than for soybean oil [9]. The effect of H_2O_2 addition rate on reaction yield is not widely studied; typically, H_2O_2 is added over 30 minutes to 60 minutes. Santacesaria *et al.* demonstrated that the rate of H_2O_2 addition has a minor effect on double bond conversion and yield compared to the molar ratio of H_2O_2 to double bonds used in the reaction [10]. Formic or acetic acids are most commonly used catalysts. Some authors suggest using H_2SO_4 or adding a solvent, or even additional free fatty acids, to achieve higher epoxidation yields of vegetable oils [11], [12]. Interestingly, unlike most studies reporting that peracid formation is the rate-limiting step of epoxidation, the same author reported that the epoxidation reaction itself is five times slower than peracid formation [13]. Incomplete reaction, leaving unreacted double bonds in the fatty acid residues, can be caused by sterically hindered access to reactive centers, uncontrolled reaction conditions (temperature, time, reactant molar ratios), or, as reported by La Scala *et al.*, differences in fatty acid reactivity [14]. Epoxidation yield is usually reported as the epoxy value (EV, mol epoxy/100 g resin) or epoxy equivalent weight (EEW, g resin/mol epoxide), most commonly determined by titration with *in situ*-generated HBr [15]. Depending on the distribution of fatty acid residues in the triglyceride, the EV typically ranges from 0.250 mol epoxy/100 g resin to 0.613 mol epoxy/100 g resin. The relationship between these characteristic parameters is given by EV = 100/EEW. A comparison of epoxidation reactions for different vegetable oils, considering reactant molar ratios and reaction conditions, is summarized in Table 1.

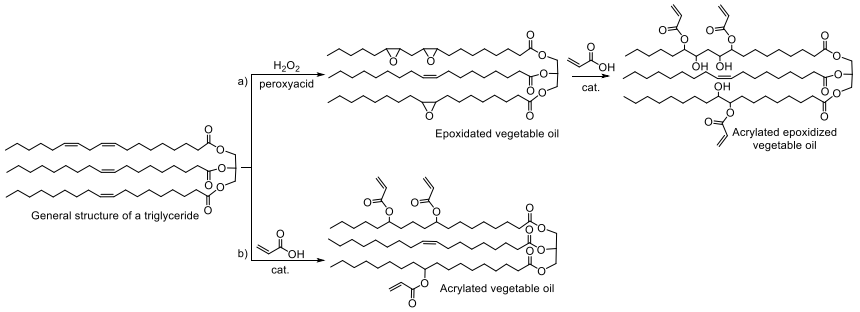

Fig. 1. Synthesis of acrylated vegetable oils: a) two-step route via epoxidation; b) one-step route using a catalyst.

Table 1

Comparison of epoxidation reactions of various vegetable oils based on reactant molar ratios and reaction conditions

Used vegetable oil	Reported iodine value (g I_2/100 g product)	Calculated C=C/fatty acid residue	Molar ratio, (mol/mol)		Time (h)	T (°C)	EV (mol epoxy/100 g resin)[a]	Yield, %	Ref.
			$n_{H2O2}/n_{C=C}$	$n_{HCOOH}/n_{C=C}$					
Linseed oil	174	2.01	1.4	0.2	5–9	45–60	0.375–0.531[b]	55–77	[9]
Jatropha oil	105	1.21	4.1	0.2	5–6	60–65	0.252[c]	61	[16]
Soybean oil	-	1.53[d]	2.0	0.6	1–7	45–55	0.288–0.481[e]	55–92	[17]
Soybean oil alkyd	57.63	0.96	3.0	2.9	6	0	0.298[f]	-	[18]
Soybean oil	-	-	1.8	0.8	7	50	0.383[g]	-	[19]
Perilla oil	196.9	2.27	10.3	3.4	8	40–60	0.610[h]	91	[8]

[a] For clarity and ease of comparison, the reaction yields are recalculated and presented in the table as EV, where the relationship between the characteristic parameters is as follows: EV = 100/EEW, and EV = Oxirane oxygen content/16.

[b] Reported value: Oxirane oxygen content is 6–8.5 g O/100 g resin.

[c] Reported value: EEW = 397 g resin/mol epoxide.

[d] Reported value: Number of starting double bonds is 4.60.

[e] Reported value: 2.4–4.6 epoxy groups/molecule.

[f] Reported value: EEW = 335.7 g resin/mol epoxide.

[g] Reported value: Oxirane oxygen content = 6.13 %.

[h] Reported value: EEW = 164 g resin/mol epoxide.

In 2011, the acrylation of epoxidized soybean oil with AA in the presence of triethylamine (TEA) was reported for the first time, aiming at the development of UV-curable wood coatings [19]. The acrylation reaction of epoxidized soybean oil was carried out at 80 °C for 15 h. The molar ratio of epoxidized vegetable oil to AA reported in the literature ranges from 1:0.165 up to 1:10, depending on the content of fatty acid residues in the triglyceride [20]. A large excess of AA increases the reaction probability; however, there is also a risk of polymerization to polyacrylic acid. Maassen *et al.* observed AA polymerization at 95 °C in three situations: 1) using more than two equivalents of AA (per equivalent of epoxide); 2) performing the reaction for longer than 7 h; 3) scaling the reaction to larger volumes [21]. Furthermore, unreacted AA after synthesis complicates the neutralization step, and its presence in the acrylated vegetable oil resin can affect the final properties of the UV-curable coating. In the literature, the acrylation reaction of epoxidized fatty acid residues is reported at temperatures ranging from 60 °C to 120 °C. It should be noted that 110 °C is considered the "upper limit" for acrylation, as higher temperatures may lead to AA polymerization [22]; conversely, Chu *et al.* reported 120 °C as the optimal temperature for the acrylation of epoxidized soybean oil [23]. Similarly, the reaction time for acrylation varies significantly in the literature, ranging from 2.3 h to 40 h [20]. The quantitative yield of epoxidized vegetable

oil acrylation is mostly not reported. Researchers usually evaluate the reaction progress based on the decrease in EV values or the amount of AA consumed, determined via titration of the acid value with ethanolic KOH solution [24]. Saithai *et al.* determined the quantitative yield of acrylated soybean oil (AESO) using ^{1}H-NMR spectroscopy, reporting 1.54–2.76 acryl groups per molecule depending on the epoxidation yield of the soybean oil [17]. A comparison of the acrylation reactions of different epoxidized vegetable oils, including both reactant molar ratios and reaction conditions, is summarized in Table 2.

Table 2

Comparison of acrylation reactions of various epoxidized vegetable oils based on reactants and reaction conditions

Used epoxidized vegetable oil	Calculated EV (mol epoxy/100 g resin)	Molar ratio $n_{AA}/n_{epoxide}$, (mol/mol)	Catalyst	Inhibitor	Time (h)	T (°C)	Reported end of the reaction/ yield	Ref.
Epoxidized soybean oil	0.250	1.41	TPP, 1 wt%	BHT, 0.03 wt%	6	90–95	AV = 1.15 mg KOH/g resin, Oxirane oxygen content = 0.012 g O/100 g resin	[24]
Epoxidized soybean oil	0.425	1.25	Triphenyl-phosphine oxide, 1.5 wt%	4-tert-butylcatechol, 0.15 wt%	6	120	AV = 5 mg KOH/g resin, 95 %	[23]
Epoxidized soybean oil	0.288	10	-	HQ	7	110	1.54–2.76 acrylic groups/ molecule	[17]
Epoxidized linseed oil	0.563	0.89	TPP, 0.059 wt%	HQ, 0.5 wt%	2.3	60–75	-	[25]
Epoxidized soybean oil	0.375	4	TEA, 1 wt%	MEHQ, 0.5 wt%	40	80–-110	AV = 10 mg KOH/g resin, Oxirane oxygen content = 0.15 %	[22]
Epoxidized soybean oil	0.383	0.6	TEA	HQ	15	80	AV = 6.2 mg KOH/g resin	[19]

In 2013, Zhang *et al.* reported a direct addition of AA to the double bonds present in the fatty acid residues of triglycerides in the presence of a $BF_3 \cdot OEt_2$ catalyst (Fig. 1b)) [26]. This synthesis approach offers advantages in terms of time and atom economy compared to the two-step synthesis via epoxidation. Moreover, after synthesis, it was possible to recover up to 86 % the starting materials (unreacted acrylic acid and catalyst). Using ^{1}H-NMR, the authors determined 3.09 acryl groups per molecule, corresponding to a 76 % yield assuming an average of 4.08 double bonds in the fatty acid residues of soybean oil. Subsequently, based on a literature analysis of catalysts for carbonyl and alkene double bond reactions, the same authors tested other catalysts for the direct acrylation of soybean oil [27]. They observed that, for both Brønsted and Lewis acids, the catalytic activity in soybean oil acrylation depended on acidity

in the following order: $BF_3 \cdot OEt_2$ > $FeCl_3$ > $SnCl_4$ > $TiCl_4$ and *p*TsOH > MsOH > Amberlyst 15. High catalyst concentrations not only accelerated the reaction but also ensured higher yields of up to 3.26 acryl groups per molecule. The authors further investigated the reaction conditions, concluding that temperatures above 80 °C led to side reactions, including AA polymerization. Later, another research group applied this synthesis method to produce acrylates from various vegetable oils, including palm, olive, peanut, rapeseed, corn, and grapeseed oils [28]. They observed that the number of acryl groups per molecule increased with the degree of unsaturation of the vegetable oil, while the reaction rate decreased due to steric hindrance, limiting further acryl group addition. After UV curing, vegetable oils with higher acryl group content exhibited higher crosslinking density, which is a quantitative measure describing the number of crosslinked nodes per unit volume of the polymer (mol/m^3). Higher crosslinking density influenced the thermomechanical and mechanical properties of the materials, resulting in increased glass transition temperature (T_g), maximum strength (σ_B) and tensile modulus (E). Among the oils studied, acrylated grapeseed oil exhibited the highest T_g (50 °C), E (8.94 MPa), and a yield of 2.17 acryl groups per molecule, as determined by ^{1}H-NMR spectroscopy.

Overall, the two-step epoxidation-acrylation synthesis route remains the most established over time and is more widely applied for the modification of various vegetable oils. However, it involves two reaction steps. One-step acrylation of vegetable oils provides a more straightforward synthetic route with reduced reaction time, although its efficiency and selectivity depend strongly on catalyst choice and reaction conditions. Consequently, the choice between these approaches depends on the desired balance between process simplicity and control over functional groups, as these factors influence the structure, reactivity, and suitability of the resulting materials for applications.

With the expansion of the sustainability concept, the development of resin formulations has become increasingly important, as modern materials must meet not only ecological criteria but also the requirements of advanced manufacturing technologies. The rapid development of industrial processes has led to the consolidation of the Fourth Industrial Revolution, or Industry 4.0, which is based on the integration of digital and automation technologies in manufacturing [29]. One of the most significant trends in this context is additive manufacturing, characterized by the layer-by-layer formation of three-dimensional (3D) objects from a digital model using digitally controlled equipment. Additive manufacturing technologies include material extrusion, binder jetting, powder layer fusion, sheet lamination, and vat photopolymerization [30]. Among vat photopolymerization methods, digital light processing (DLP) and stereolithography (SLA) 3D printing are widely used, in which UV-induced polymerization occurs layer by layer, either uniformly or pointwise, by irradiating a liquid resin layer with a laser [31]. UV-curable resins for 3D printing provide high resolution, excellent surface quality, and efficient use of raw materials, making them suitable for the production of complex parts [32]. Most UV-active resins are acrylate derivatives, which account for approximately half of the polymer materials used in 3D printing [33]. Several studies have already reported that 3D-printed materials containing acrylated vegetable oils can achieve mechanical properties comparable to commercially available 3D-printed materials based on petroleum-derived monomers. For example, 3D-printed soybean oil methacrylate with 78 % bio-based content exhibited a σ_B of 43.7 MPa [34]. Meanwhile, one-step synthesized AESO

oligomers showed excellent thermomechanical properties with T_g values of 128–130 °C. In addition, the UV light penetration depth reached 0.277 mm, which is higher than that of widely used commercial resins [35]. These examples clearly demonstrate the potential of vegetable oils for 3D printing. The development of such manufacturing technologies significantly increases the demands on the formulation of photoactive resins and the optimization of their parameters for specific applications, including viscosity, reactivity, and the mechanical properties of the final material.

Acrylated vegetable oils are characterized by high viscosity, which can exceed 17 000 mPa·s [36]. The high viscosity arises from the long alkyl chains of the molecules due to the possibility of entanglements, which increase the resistance to flow, as well as intermolecular interactions, including hydrogen bonding between hydroxyl, acrylate, and ester groups. High viscosity limits the processability of resins in both 3D printing and surface coating applications, as these processes require uniform material flow. To address these issues, UV-curable formulations typically incorporate reactive diluents – monomers and oligomers with low viscosity that not only reduce the system's viscosity but also participate in photoinitiated crosslinking reactions [19]. The use of reactive diluents eliminates the need for conventional solvents and ensures integration of all components into the polymer network. Common choices include mono-, di-, or multifunctional (meth)acrylates such as isobornyl acrylate (IBOA), tripropylene glycol diacrylate (TPGDA), trimethylolpropane tri(meth)acrylate (TMPT(M)A), and 1,6-hexanediol diacrylate (HDDA) [37]. The selection of reactive diluents is based on optimizing the balance between viscosity, reactivity, and the thermomechanical properties of the UV-cured material, tailoring the resin formulation for specific applications.

Unfortunately, most commercially available reactive diluents are derived from petroleum, raising sustainability and toxicity concerns. Consequently, recent research has increasingly focused on developing alternative bio-based reactive diluents. The literature describes the synthesis and application of reactive diluents in UV-curable systems from renewable feedstocks such as ricinoleic acid [38], cardanol [39], furan derivatives [40], castor oil [41], and eugenol [42], among others. There are also reports on the use of esters containing internal double bonds as reactive diluents in UV-curable resins, most commonly as maleate or fumarate derivatives [43], [44]. Although internal double bonds exhibit lower reactivity in UV curing compared to terminal double bonds – mainly due to steric hindrance, π-electron delocalization, and the presence of neighboring electron-withdrawing groups – they are widely used because they enable the incorporation of ester chains into the polymer network and influence the properties of the final product. An interesting study by Northrop *et al.* compared four compounds with internal double bonds in a free-radical thiol-ene "click" reaction, observing the following reactivity order: norbornene > fumarate > maleimide > crotonate [45]. The presence of internal double bonds in the macromolecule can impart flexibility or a plasticizing effect, and such esters are therefore often combined with other acrylates to enhance overall photopolymerization rates and the crosslinking density of the polymer [46]. Furthermore, the use of bio-based esters allows for a reduction in the proportion of petroleum-derived acrylates in the formulation. This approach, as well as its influence on the photopolymerization process and the properties of the crosslinked material, is discussed in detail in the third chapter of this Thesis.

Acrylates are also widely used as the main component in surface protective coatings, forming durable and aesthetically appealing polymer layers. Their functionality enables the tuning of coating properties such as adhesion, hardness, and flexibility. In the coatings industry, there is a growing demand for products with lower VOC content, including reduced solvent content, as solvent emissions are the second-largest source of air pollution after automobile emissions [47]. UV-curable coatings are typically formulated solvent-free, enabling rapid curing at room temperature, which increases production throughput and saves floor space in manufacturing facilities. Although the fastest growth of the UV-curable coatings market is observed in Asia, projected growth in Europe and North America is approximately 9 % per year, significantly higher than the average growth of the traditional coatings industry [48]. In response to increasingly stringent environmental regulations, the inclusion of biomass, including vegetable oils, in UV-curable coating formulations has become an increasingly popular topic in both scientific research and industry [49]. The literature has reported the potential of vegetable oil derivatives as sources for UV-curable coatings, including derivatives of castor oil [50], tung oil [51], jatropha oil, and palm oil [52]. These are used to protect wood, metal, plastic, and paper surfaces from corrosion, chemicals, and atmospheric exposure [53]. Using vegetable oils in UV-curable coatings enables a wide range of mechanical properties, including high hardness, adhesion, flexibility, and other physical parameters. Such coatings have been investigated for specialized applications such as antimicrobial [54], flame-retardant [55], high-performance [56], and nanocomposite coatings [57].

The potential of UV-curable materials is also being evaluated in structural material systems. Polymer matrices and fiber-reinforced composites represent a critical area of materials science, providing combinations of properties that cannot be achieved with individual components alone. Although commonly used composites exhibit high mechanical performance, their production relies on petroleum-based polymer matrices (epoxides, polyester resins) and glass or carbon fiber reinforcement, the production of which is energy-intensive [58]. The long-term use of such composites is contrary to the principles of a circular economy. The development of alternative composites based on renewable feedstocks has become an important field in materials science over the past decade. Hemp fibers are a promising natural fiber substitute for synthetic fibers. They are mechanically strong, have a high cellulose content, and require significantly less energy for production compared to glass or carbon fibers – literature reports indicate energy savings of up to 80 % [59].

It should be noted, however, that natural fibers are less homogeneous than synthetic ones, as their properties vary considerably depending on growth conditions, climate, and processing methods. This limitation can be mitigated by producing more uniform fiber structures, such as paper. Nanopaper (NP), obtained by fibrillating cellulose nanofibers, provides a uniform fiber distribution and a high surface area. Such a structure is well-suited for matrix impregnation, for example, with bio-based resins, as capillary effects and porosity enable efficient resin infiltration into the fiber network [60]. The preparation of NP is particularly economically advantageous when using various waste products containing natural fibers, as they can be easily processed (ground, pulped, pressed) using established and simple methods [61]. The development of composites using a UV-curable vegetable oil impregnation approach is discussed in the fourth chapter of this Thesis.

Despite advances in the development and application of bio-based resins, a significant challenge remains their reprocessability. Traditional UV-curable thermosetting materials form irreversible 3D crosslinked networks upon photopolymerization, which severely limit their flowability and reprocessing potential [62]. In recent years, increasing attention has been directed toward introducing dynamic covalent bonds into thermosetting polymers to develop reprocessable materials [63]. Such structures, known as vitrimers, combine the mechanical and thermal resistance of thermosets with the reprocessability of thermoplastics. In vitrimers, dynamic covalent bonds undergo exchange reactions at elevated temperatures, allowing topological rearrangement of the material. Transesterification is one of the most extensively studied exchange reactions due to the ease of incorporating ester and hydroxyl groups into thermosetting systems [64], [65]. Most reported vitrimers are developed via thermal curing, which is both energy-intensive and time-consuming, often requiring up to 12 h for complete curing [66]. The low energy consumption and short processing time characteristic of UV curing make it an efficient and sustainable method for vitrimer development [67]. Moreover, UV-curable vitrimers are particularly promising for modern manufacturing technologies, such as 3D printing, combining the ability to produce complex geometries with the possibility of reusing materials after end-of-life [68]. This approach is especially relevant for the development of bio-based polymer materials, as it enables the integration of sustainable feedstocks with reprocessability.

The present study aims to address the aforementioned challenges by synthesizing and formulating UV-curable resins from renewable feedstocks with deliberately tailored molecular structures. This approach enables the control of curing kinetics, the development of materials with tunable (thermo)mechanical properties, and the potential for material reprocessability. To achieve this, specific steps were followed in the development of UV-curable resins.

First, the selection of appropriate starting materials and their chemical functionality is crucial in designing UV-curable resins, as these factors determine resin reactivity during UV curing and the final material properties. Various vegetable oils – rapeseed, linseed, and grapeseed oils – were chosen as renewable feedstocks based on their availability, chemical structure, and potential for application in sustainable UV-curable materials. Rapeseed and linseed oils are readily available and suitable for cultivation under Latvian climatic conditions, whereas grapeseed oil, although less abundant, was selected due to its high content of double bonds per molecule. This selection allows the evaluation of how double-bond content influences acrylation efficiency and subsequent UV-curing reactivity. Unlike the widely studied and commercialized AESO, the acrylation of rapeseed oil and its application in UV-curable materials have so far been reported in only a few studies, making this work a novel contribution to the exploration of locally sourced vegetable oils.

Second, the introduction of photoactive groups into vegetable oil structures and the UV-curing concept was extended to the industrially established alkyd resins. Alkyds are traditionally used in coatings due to their good adhesion and flexibility, but their curing typically relies on metal-catalyzed oxidative drying, which is time- and energy-intensive. In this step, the alkyd structure was modified by incorporating a controlled number of acrylate groups, enabling a controllable UV-curing process. This approach combines the functional advantages of alkyds with the benefits of UV-curing technology.

Third, UV-curable resin formulations were developed and optimized by selecting and combining reactive diluents in various weight percentages (wt%) to achieve specific rheological and mechanical properties, including appropriate viscosity, curing rate, and mechanical strength. Monofunctional reactive diluents generally reduce the E and increase the plasticity of the crosslinked material, producing flexible materials. In contrast, di- and multifunctional reactive diluents increase E and reduce plasticity, yielding stiff but brittle materials. Higher functionality of reactive diluents accelerates curing and ensures higher crosslink density [69]. For example, HDDA and TPGDA significantly reduce the viscosity of UV-curable formulations, while trifunctional monomers such as TMPTA and TMPTMA considerably increase the polymer's crosslink density and, consequently, T_g. Similarly, bulky diluents such as IBOA raise T_g, whereas linear monomers like TPGDA and HDDA improve material flexibility [70], [71]. The careful selection and optimization of reactive diluents ensures resin suitability for 3D printing and coating applications. While most commercially available reactive diluents are petroleum-derived, there is growing interest in renewable alternatives. For example, photoactive furan derivatives have demonstrated higher hardness, E, and T_g in UV-cured coatings compared to petroleum-derived HDDA [40]. The third chapter of this Thesis analyzes a new furan derivative as a bio-based reactive diluent.

Fourth, the application of the synthesized photoactive vegetable oil derivatives was evaluated in three areas: (1) wood surface protective coatings, (2) nanocomposite development using acrylated vegetable oils as binders, and (3) DLP-type 3D printing. Resin and product curing rates, adhesion, hardness, thermal and (thermo)mechanical properties were analyzed, and the suitability of the materials for each application was assessed.

Fifth, the content of dynamic covalent bonds in the formulations was controlled to develop vitrimer materials based on thermally activated transesterification reactions. This approach enables the materials to retain mechanical and thermal stability while providing reprocessability and structural recovery after damage through covalent bond exchange at elevated temperatures. The introduction of the necessary functional groups into the vegetable oil structure is the first step toward obtaining UV-curable vitrimers. Consequently, the acrylated epoxidized rapeseed oil (AERO) used in this study was synthesized via epoxide ring opening, introducing additional -OH groups to enhance vitrimer reprocessability. The resulting vitrimer resin formulations were applied in 3D printing, demonstrating their utility in additive manufacturing. Key product development parameters, including catalyst influence and stress relaxation, were analyzed to ensure final material performance and reprocessability. The development of vitrimers using AERO allows assessment of the material's reprocessability potential, an essential aspect of environmentally friendly polymer materials.

The synthesized and formulated resins, as well as the crosslinked materials, were characterized for a wide range of properties using the following analyses and tests: Fourier-transform infrared spectroscopy (FTIR), nuclear magnetic resonance (NMR), size-exclusion chromatography (SEC), rheology, photorheology, photo-differential scanning calorimetry (photo-DSC), scanning electron microscopy (SEM), dynamic mechanical analysis (DMA), tensile testing, adhesion testing, microhardness testing, slip friction testing, pendulum hardness testing, indentation depth testing, ultraviolet-visible spectroscopy (UV-Vis), thermogravimetric analysis (TGA), biodegradation studies, density measurement, dielectric spectroscopy (DS),

TGA-FTIR coupled analysis, and optical microscopy. Detailed descriptions of these methods can be found in the respective publications.

The Doctoral Thesis combines the use of vegetable oils as renewable resources, modern energy-efficient UV-curing technology, and material structural functionality, resulting in innovative, environmentally friendly, and reprocessable materials. This approach not only reduces reliance on non-renewable resources but also promotes the implementation of circular economy principles in materials science.

Aim and Objectives

The Doctoral Thesis aims to develop polymer resins derived from vegetable oils with a controllable molecular structure for application in UV-curable thermosetting materials with tunable performance and reprocessing properties.

To achieve this aim, the following objectives were defined.

1. To synthesize acrylated derivatives of rapeseed, linseed, and grapeseed oils using one-step or two-step synthesis routes, and to optimize the synthesis reaction parameters in accordance with the chemical reaction mechanisms.
2. To develop UV-curable resin formulations with a deliberately tailored molecular structure using the synthesized vegetable oil acrylate derivatives, reactive diluents, and photoinitiators.
3. To investigate the influence of UV-curing kinetics and crosslinked polymer network structure on the physical-mechanical properties of thermosetting polymer materials, and to evaluate their application in wood coatings and 3D printing.
4. To control the content of dynamic covalent bonds within the crosslinked polymer network, to assess the reprocessability and structural recovery potential of the resulting vitrimer materials, and to investigate their applicability in 3D printing technologies.

Theses to Defend

1. By deliberately tailoring synthesis methods, reaction parameters, and formulation composition, it is possible to control the macromolecular structure of acrylated vegetable oil derivatives, UV-curing kinetics, and crosslinked polymer network density, thereby obtaining UV-curable resins with tunable final material properties.
2. UV-curable resin formulations can be developed with application-specific viscosity and physical-mechanical properties, making them suitable for the formation of highly crosslinked polymer coatings.
3. UV-curable acrylated vegetable oil-based polymer materials can be used as matrix binders for natural fiber composites, where incorporated cellulose reinforcement provides enhanced physical-mechanical properties.
4. By controlling the content of dynamic covalent bonds in the crosslinked polymer network, it is possible to obtain 3D-printable vitrimer materials which, based on a thermally activated transesterification reaction mechanism, enable reprocessability and structural recovery.

Scientific Novelty

1. Optimized one-step and two-step acrylation synthesis methods for rapeseed, linseed, and grapeseed oils were developed, enabling controlled tailoring of molecular structure to obtain materials with controlled photoactive group content and UV-curing kinetics.
2. It was demonstrated that the introduction of photoactive groups into alkyd structures, without the use of halogenated products, combines the characteristic performance properties of alkyds with the advantages of UV-curing technology, providing a fast and controllable curing process.
3. Relationships between molecular structure, reactive diluent content, curing kinetics, and physical-mechanical properties were established, allowing targeted regulation of crosslinking density in UV-curable resins and adaptation of materials for specific applications (wood coatings, 3D printing).
4. The use of UV-curable vegetable oil-based resins as matrix binders for natural fiber composites was demonstrated, showing effective matrix-fiber interaction and significant improvements in (thermo)mechanical properties.
5. Acrylated vegetable oil-based vitrimer materials with controlled dynamic covalent bond content were developed, where vitrimer stress relaxation behavior is governed by a thermally activated transesterification reaction, enabling reprocessability and structural recovery.
6. Overall, this Thesis provides a novel scientific contribution to the development of bio-based, UV-curable, and reprocessable polymer formulations by integrating synthesis, molecular design, and curing kinetics, and by demonstrating their application in coatings, 3D printing, and natural fiber composite materials.

Practical Significance

1. The synthesized photoactive acrylates of rapeseed, linseed, and grapeseed oils can be used for the production of highly crosslinked polymer coatings, providing rapid curing, a tunable profile of physical-mechanical properties, and demonstrating the potential of vegetable oils obtainable in Latvia to replace petroleum-based raw materials.
2. The results of this study demonstrate a halogen-free synthesis route for UV-curable alkyd resins derived from linseed oil, which enhances material sustainability, reduces environmental pollution, and complies with modern requirements for sustainable manufacturing.
3. UV-curable vegetable oil-based polymer materials used as matrix binders for natural fiber composites exhibit applicability in materials with improved (thermo)mechanical properties, making them suitable for composite material technologies.
4. Acrylated vegetable oil-based vitrimer materials with a controlled content of dynamic covalent bonds enable the development of reprocessable, reusable, and repairable thermosetting polymers suitable for 3D printing technologies.

Structure and Volume of the Thesis

The Doctoral Thesis is prepared as a summary of scientific publications dedicated to the synthesis and characterization of bio-based UV-curable resins, the investigation of their application in wood coatings, composite materials, and 3D printing, as well as the evaluation of their reprocessing potential. The Thesis includes five original scientific publications published in peer-reviewed scientific (SCI) journals. The overall structure of the Thesis is graphically illustrated in Fig. 2.

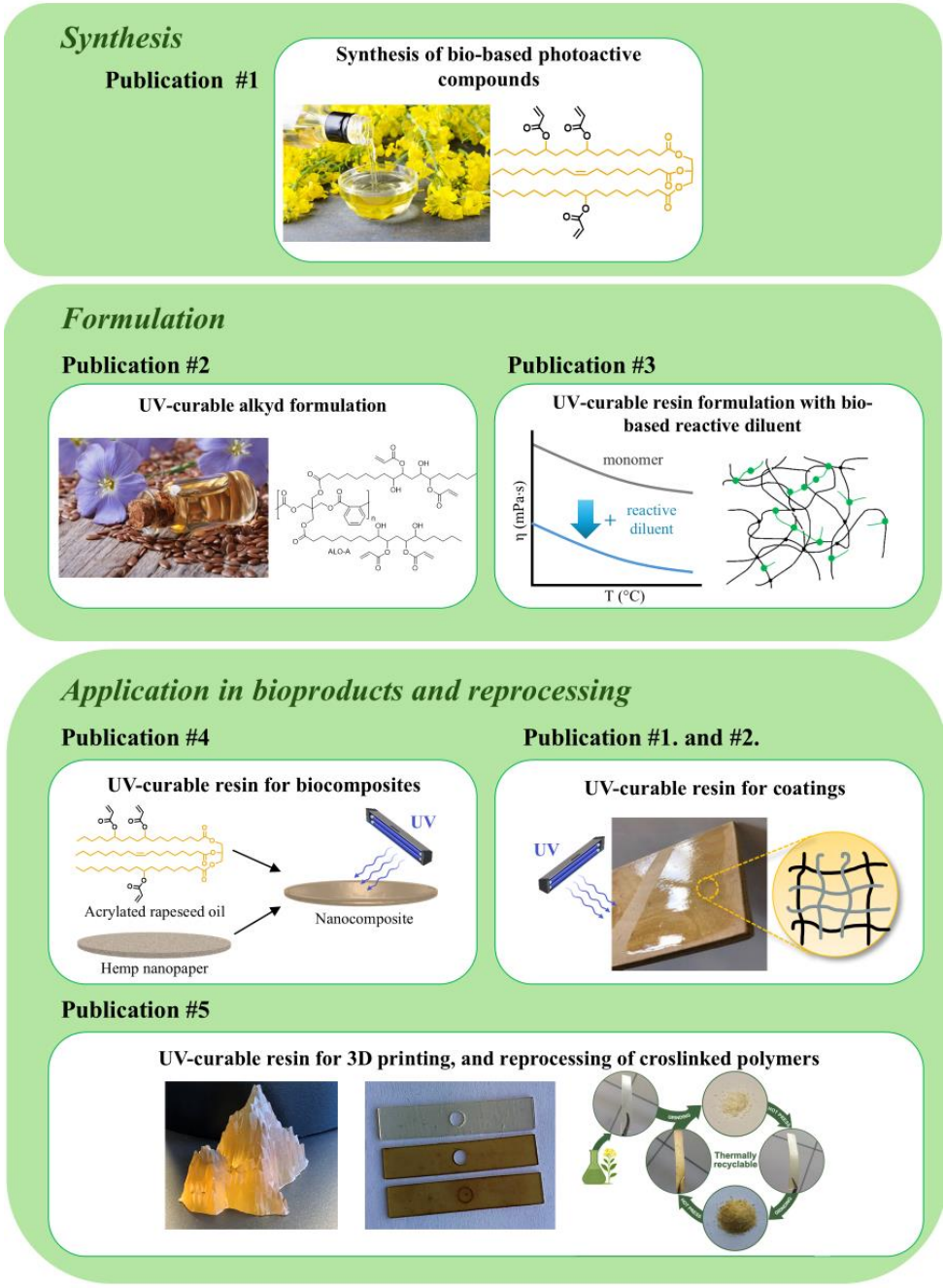

Fig. 2. General structure of the Thesis.

Publications and Approbation of the Thesis

The results and achievements obtained in the Doctoral Thesis have been published in five original scientific publications. During the development of the Doctoral Thesis, the main results were presented at five scientific conferences.

SCI publications

1. Briede, S., Platnieks, O., Barkane, A., Sivacovs, I., Leitans, A., Lungevics, J., & Gaidukovs, S. (2023). Tailored Biobased Resins from Acrylated Vegetable Oils for Application in Wood Coatings. *Coatings*, 13(3), 657. IF = 2.8, Q2.
2. Briede, S., Biemans, T., Platnieks, O., & Gaidukovs, S. (2025). Tailored UV-curable acrylated linseed oil-based alkyds: Optimizing crosslinking and coating performance through functionalization and reactive diluent design. *Polymer*, 323, 128227. IF = 4.5, Q1.
3. Briede, S., Platnieks, O., Darzina, M., Jirgensons, A., & Gaidukovs, S. (2023). Effect of novel furan-based ester reactive diluent on structure and properties of UV-crosslinked acrylated rapeseed oil. *Journal of Polymer Science*, 61(24), 3318–3328. IF = 3.6, Q1.
4. Platnieks, O., Briede, S., Grase, L., Thakur, V., J., & Gaidukovs, S. (2023). Fully Bio-Based Thermoset Composites from UV Curable Prepregs: Vegetable Oil Acrylate Impregnated Hemp Nanopaper. *Polymer Composites*, 44(9), 5721–5733. IF = 4.7, Q1.
5. Greivule, S., Besprozvannaja, I., Porcarello, M., & Gaidukovs, S. (2026). Reprocessable and Repairable Bio-Based Vitrimers from Acrylated Epoxidized Rapeseed Oil for Additive Manufacturing. *Macromolecular Materials and Engineering*. IF = 4.6, Q1, doi: 10.1002/mame.70228. (Accepted).

Scientific conferences

1. Briede, S., & Gaidukovs, S. 3D printing and reprocessing of rapeseed oil-based vitrimers. *European Polymer Congress*, Groningen, The Netherlands, June 22–27, 2025.
2. Briede, S., Biemans, T., & Gaidukovs, S. Synthesis of highly functional UV-curable alkyd resins for wood coating application. *European Regional Meeting of the Polymer Processing Society*, Ferrol, Spain, September 30 – October 3, 2024.
3. Briede, S., Jurinovs, M., & Gaidukovs, S. Rheological behavior of photoactive vegetable oil for extrusion-based UV-assisted 3D printing. *Nordic Rheology conference*, Aarhus, Denmark, May 31 – June 2, 2023.
4. Briede, S., Jurinovs, M., & Gaidukovs, S. Tailored biobased UV-curable resins from acrylated vegetable oils for application in wood coatings. *Renewable Resources & Biorefineries*, Riga, Latvia, April 12–14, 2023.
5. Briede, S., Jurinovs, M., & Gaidukovs, S. Photoactive vegetable oil synthesis for high-performance extrusion UV-light cured 3D printing. *Nordic Polymer Days*, Gothenburg, Sweden, June 1–3, 2022.

Other scientific publications produced during the preparation of the Doctoral Thesis

1. Platnieks O., Beluns S., Briede S., Jurinovs M., & Gaidukovs S. (2023). Cellulose synergetic interactions with biopolymers: Functionalization for sustainable and green material design. *Industrial Crops and Products*, 204, 117310.
2. Briede, S., Jurinovs, M., Nechausov, S., Platnieks, O., & Gaidukovs, S. (2022). State-of-the-art UV-assisted 3D printing via a rapid syringe-extrusion approach for photoactive vegetable oil acrylates produced in one-step synthesis. *Molecular Systems Design & Engineering*, 7(11), 1434–1448.
3. Briede, S., Barkane, A., Jurinovs, M., Thakur, V. K., & Gaidukovs, S. (2022). Acrylation of biomass: a review of synthesis process – know-how and future application directions. *Current Opinion in Green and Sustainable Chemistry*, 35, 100626.
4. Barkane, A., Jurinovs, M., Briede, S., Platnieks, O., Onufrijevs, P., Zelca, Z., & Gaidukovs, S. (2022). Biobased Resin for Sustainable Stereolithography: 3D Printed Vegetable Oil Acrylate Reinforced with Ultra-Low Content of Nanocellulose for Fossil Resin Substitution. *3D Printing and Additive Manufacturing*, 10(6), 1272–1286.
5. Jurinovs, M., Rukavisnikovs, N., Greivule, S., Starkova, O., Kovalovs, A., Brunāvs, J., Macutkevič, J., Juhnevica, I., Platnieks, O., & Gaidukovs, S. (2026). Nanostructure-reinforced epoxy-acrylate interpenetrated networks for UV-curable high-performance coatings. *Reactive and Functional Polymers*, 221, 106664.

MAIN RESULTS OF THE THESIS

Synthesis of acrylated vegetable oils, photopolymerization kinetics, and application in UV-curable wood coatings (Publication 1)

To investigate the application of vegetable oils in the development of UV-curable wood coating resins, three vegetable oils were initially acrylated: rapeseed oil, which is widely available in Latvia, and, for comparison, two oils rich in double bonds – linseed oil and grapeseed oil. The acrylated oils were obtained via an optimized one-step synthesis process using $BF_3 \cdot OEt_2$ as a catalyst (Fig. 3 a)), as described in the introduction and following a synthesis protocol similar to that published in 2013 [26]. After synthesis, the acrylated oils were named as ARO, ALO, and AGO, respectively.

The synthesis was optimized under laboratory conditions to a defined protocol: vegetable oil (1 mol C=C) was mixed with acrylic acid (AA) (2.1 mol) in a round-bottom flask, followed by the slow addition of the catalyst (0.21 mol). The reaction mixture was stirred and maintained at 80 °C for 5 h, after which it was left at room temperature overnight. At the end of the reaction, hexane was added to dissolve the organic phase, which was then washed with aqueous $NaHCO_3$ and NaCl solutions to neutralize and remove residual AA and catalyst. The organic phase was dried over Na_2SO_4, filtered, and the solvent was evaporated under reduced pressure. ARO, ALO, and AGO were obtained as viscous, dark yellow resins. The obtained resins were analyzed by ^{1}H-NMR spectroscopy; as a representative example, the spectra of rapeseed oil (RO) and ARO are shown in Fig. 3 b).

First, the key photopolymerization characteristics of the vegetable oils were determined and are summarized in Table 3 [72]. To study the double-bond conversion (DBC) of the terminal acrylate groups of the synthesized vegetable oils after UV curing, as well as the photopolymerization kinetics, viscosity was measured, Fourier transform infrared (FTIR) spectra were recorded at different irradiation times, and photo-differential scanning calorimetry (photo-DSC) measurements were performed. DBC represents the extent of conversion of reactive acrylate carbon double bonds into a covalently bonded structure during UV curing, reflecting the efficiency of network formation. The viscosity of the acrylated vegetable oils ranged from 430 mPa·s to 1305 mPa·s (ARO < AGO < ALO) at shear rates from 10 s^{-1} to 100 s^{-1}, ensuring optimal resin flowability and representing an important parameter for coating development [48], [72].

The DBC ranged from 69 % to 85 %, with ARO exhibiting the highest conversion, which correlates with the highest reaction yield (57 %, 2.14 acrylate groups per molecule). The maximum polymerization rate of AGO was reached at 9.5 s ($t_{max\ rate}$) at 5.1 % conversion and was the highest among the samples, indicating rapid initial reactivity but early diffusion-controlled (molecular mobility-controlled) polymerization, which hinders further reaction progress. In contrast, ARO polymerization proceeded slightly longer due to its higher acrylate functionality and lower viscosity.

Table 3

Characteristics of acrylated vegetable oils [72]

	Synthesis				UV curing		
Acrylated vegetable oils	Fatty acid residue double bonds (in the triglyceride)	Acryl groups in the molecule	Reaction yield (%)	η (mPa·s)	DBC (%)	$t_{max\ rate}$ (s)	DBC at max. rate (%)
ARO	3.74	2.14	57	430	85	9.8	4.5
ALO	5.99	1.62	28	1305	69	13.1	2.4
AGO	4.56	1.67	38	1140	76	9.5	5.1

To develop wood coatings from the synthesized oils, resin formulations were prepared. In this study, ARO, ALO, and AGO were mixed with a bio-based, low-viscosity glycerol propoxy triacrylate (GPT) (η = 91 mPa·s at shear rates from 10 s^{-1} to 100 s^{-1}), which serves as a reactive diluent and, being a trifunctional monomer, provides a high polymer crosslink density [73]. The polarity of GPT and its compatibility with acrylated vegetable oil resins were evaluated by dissolving it at room temperature in various substances and solvents of increasing polarity: rapeseed oil, acrylated vegetable oils, ethanol, methanol, and water. To initiate photopolymerization, the photoinitiator 2,4,6-trimethylbenzoyl diphenylphosphine oxide was added. In total, nine resin formulations were prepared, in which two acrylated vegetable oils were mixed in a one-to-one ratio: (1) three vegetable oil acrylate formulations (e.g., ARO/ALO); (2) three vegetable oil acrylate formulations with 5 wt% GPT (e.g., ARO/ALO_GPT5); and (3) three vegetable oil acrylate formulations with 20 wt% of GPT (e.g., ARO/ALO_GPT20). A simplified scheme of the preparation of UV-curable wood coatings is shown in Fig. 3 c).

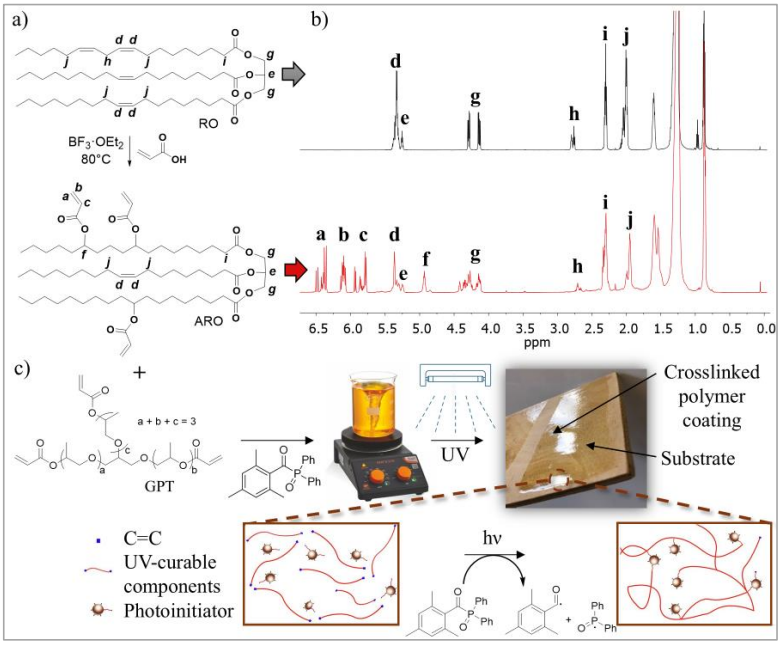

Fig. 3. a) One-step synthesis scheme of ARO; b) ^{1}H-NMR spectra of RO and ARO resins [72]; c) schematic illustration of the preparation of UV-curable coatings.

The (thermo)mechanical properties were determined for free-standing UV-cured resin films. Samples cured in this manner provide information on the performance of the crosslinked polymer network, which helps to better understand and predict the mechanical and thermomechanical behavior of the coating on a substrate (wood). For example, a higher elastic modulus (E) or glass transition temperature (T_g) in irradiated free-standing films often correlates with higher scratch resistance and improved chemical resistance, whereas more flexible films are associated with higher impact resistance and resistance to crack formation [74]. First, the storage modulus (E′) was determined using dynamic mechanical analysis (DMA), which characterizes how much energy the material can store under elastic deformation. The E′ curves of the irradiated samples within the investigated temperature range indicated a stable, thermally resistant crosslinked polymer network (Fig. 4 a)). At lower temperatures, for example, –30 °C, the addition of GPT increased the E′ value from 805.5 MPa for the ARO/ALO sample to 1182.3 MPa for the ARO/ALO_GPT20 sample. At room temperature (20 °C), the addition of GPT increased the E′ value from 13.7 MPa to 34.0 MPa for these samples, indicating a higher polymer crosslink density, increased stiffness, and lower molecular weight between crosslinks. The crosslink density calculated from DMA data for these samples increased from $1.5 \cdot 10^3$ mol/m^3 to $2.1 \cdot 10^3$ mol/m^3. The obtained E′ values are characteristic of crosslinked UV-curable polymers and indicate a balanced combination of stiffness and elasticity [75]. The loss modulus (E″) characterizes how much energy is dissipated as heat during deformation, i.e., the viscous or energy-dissipating component of the material. By dividing E″ values by E′ values, the loss factor (tanδ) curve is obtained, which shows how "mobile" or "relaxed" the polymer chains are at a given temperature. The peak of this curve reflects the onset of segmental mobility relaxation of polymer chains and is often associated with T_g. However, it should be noted that there is still debate as to whether T_g is more accurately determined from the peak of the E″ curve or from the peak of the tanδ curve, as both parameters provide similar but not identical information about polymer segmental motion [76]. In the tanδ plot (Fig. 4 b)), a shift of the peak toward higher temperatures is observed with increasing GPT content, indicating restricted chain mobility and increased polymer crosslink density. At the same time, the height of the tanδ peak decreased, reflecting a reduction in relaxation intensity, i.e., a smaller number of segments capable of moving during deformation, and indicating a stiffer polymer network. Finally, with the addition of GPT, a broadening of the tanδ curve was observed, reflecting heterogeneity in crosslink distribution. Unfortunately, this may also result in non-uniform mechanical behavior of the samples [77].

Next, the stress-strain (σ-ε) curves of the UV-curable materials and the calculated E values were analyzed (Fig. 4 c) and d)). The addition of GPT leads to nonlinear structure-property relationships. A certain correlation is observed between the shift of the tanδ peak to higher temperatures/lower tanδ peak intensity (from DMA) and higher E/maximum strength (σ_B) values; however, a contradiction is evident for samples with 5 wt% GPT, as their mechanical strength values decrease. This indicates network inhomogeneity and possible phase separation, with the GPT monomer forming domains. This was investigated using scanning electron microscopy (SEM) (Fig. 4 e)). In the representative SEM cross-sectional image (ii), a heterogeneous microstructure is observed, which likely results from phase separation between acrylated oils and GPT at an early stage of curing and may be one of the reasons for the decrease in σ_B [78]. The rough and heterogeneous microstructure observed in both ARO/ALO and

ARO/ALO_GPT5 samples indicates possible local stress concentration, where cracks mainly initiate at phase boundaries. This reduces the E values, which are similar for these samples (from 7.1 MPa to 10.5 MPa). In contrast, the homogeneous morphology of the ARO/ALO_GPT20 sample indicates that GPT is uniformly integrated into the polymer network, with no pronounced phase boundaries, and the applied tensile load is not localized. Stress is distributed uniformly throughout the material volume, and therefore, a higher stress is required to initiate fracture (E up to 20.3 MPa, σ_B up to 0.76 MPa).

To ensure effective coating performance, the adhesion of the formulations to birch plywood was evaluated. Considering that the influence of different formulations of ARO, ALO, and AGO on the (thermo)mechanical properties was less pronounced, for the sake of data clarity and simplicity, adhesion strength was determined only for ARO/ALO formulations. The liquid resin formulations were applied to plywood and irradiated, achieving 70–90 % DBC. The adhesion strength of the coatings gradually increased from 0.56 MPa to 1.21 MPa with increasing GPT content, which may be explained by improved interfacial adhesion. For comparison with literature, epoxy acrylate and tripropylene glycol diacrylate (TPGDA) coating formulations on wood have shown adhesion strength up to 1.12 MPa [79], while urethane acrylate, 1,6-hexanediol diacrylate (HDDA), TPGDA, and trimethylolpropane triacrylate (TMPTA) coating formulations on polycarbonate have shown values from 0.52 MPa to 2.25 MPa [80]. It should be noted that these are low-molecular-weight petroleum-derived products.

In summary, in the first chapter of the Thesis, rapeseed, linseed, and grapeseed oil acrylates were successfully obtained via one-step synthesis and can be used as bio-based precursors for the development of UV-curable polymer materials. The acryl groups introduced into the triglyceride structure provide a sufficient number of reactive centers (terminal double bonds), enabling control over the formation and properties of the crosslinked polymer network. In addition, the viscosity of the acrylated oils (η = 430–1305 mPa·s) ensures good flowability in coating formulations with the reactive diluent GPT, which at optimal concentration increases polymer crosslink density, raises T_g, and improves mechanical strength and stiffness. The obtained results in this section demonstrate the potential of acrylated vegetable oils for wood protection applications.

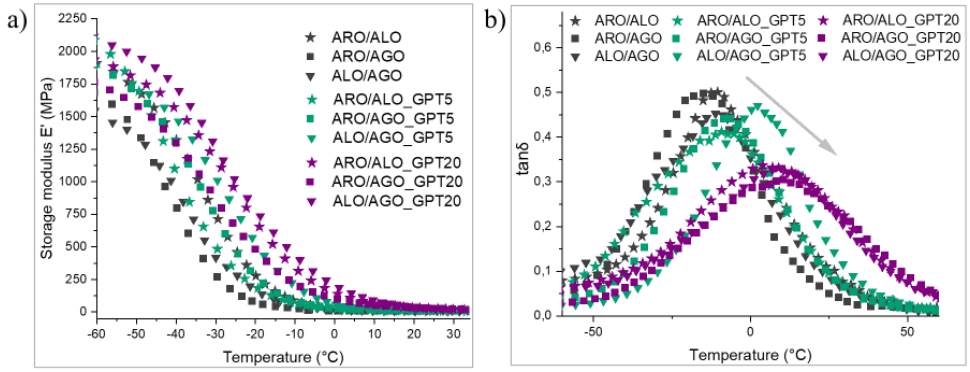

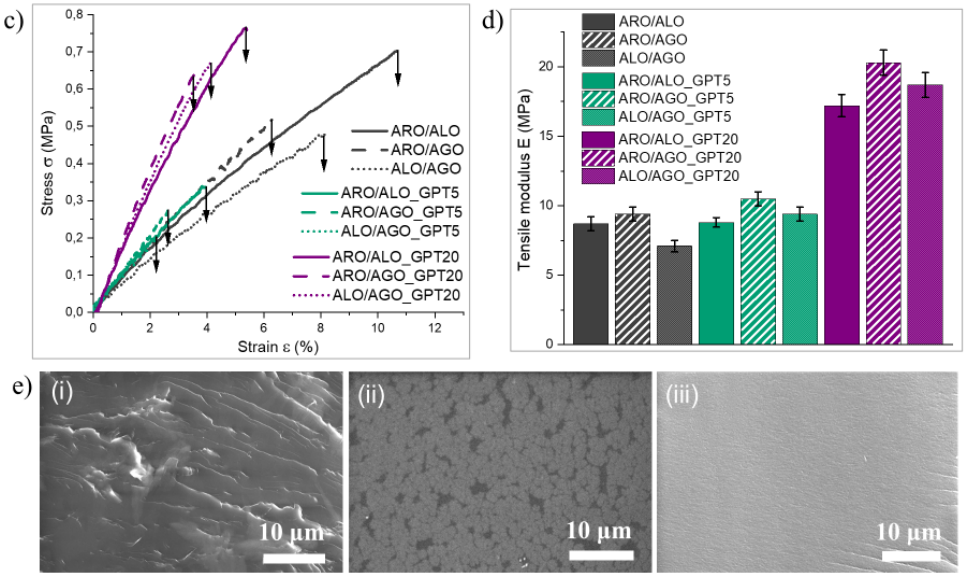

Fig. 4. Crosslinked materials: a) E′ curves; b) tanδ curves; c) σ-ε curves; d) E graph; e) fracture surface microstructure morphology – SEM images: (i) ARO/ALO, (ii) ARO/ALO_GPT5, (iii) ARO/ALO_GPT20.

Synthesis of linseed oil-based alkyd resins for the development of UV-curable wood coatings (Publication 2)

The synthesis of vegetable oil acrylates, their UV curing process, and the investigation of the properties of the developed coatings are essential steps in the use of renewable raw materials in wood coatings, and the results obtained in the previous chapter of the Thesis demonstrated a broad spectrum of material properties. The next step is to transfer this knowledge to an industrially significant class of wood coatings – alkyds. Alkyds are resins that, for many years, have been among the most widely used surface protective coatings due to their chemical and physical properties. However, alkyd resin coatings dry slowly; during the drying process, metal catalysts are required, and resins often contain organic solvents (xylene, dearomatized or aliphatic hydrocarbons, isoparafins, etc.), making them potentially hazardous to work with. These limitations can be overcome by UV-curing technology, which enables rapid curing without the need for metal-based drying catalysts or organic solvents. Instead, UV-curable systems rely on photoinitiators that generate reactive species upon irradiation to initiate crosslinking. Therefore, in the second step of the study, the double bonds of fatty acid residues present in the alkyd structure were acrylated, the UV curing kinetics of photoactive alkyd resins were studied, coating formulations were developed, and their properties were determined. To achieve this, linseed oil alkyd resins (LO-A) were first synthesized, containing 73 % linseed oil fatty acid residues, thus providing a sufficient number of modifiable internal double bonds. Acrylation was carried out in two steps via epoxidation, as described in the introductory chapter, in order to avoid the formation of halogenated products [18] and side reactions that could be possible in a one-step synthesis between functional fragments present in the alkyd structure and

the $BF_3 \cdot OEt_2$ catalyst. The epoxidation and subsequent acrylation reactions were performed under various conditions until the syntheses were optimized to the desired yields. The two-step acrylation reaction of LO-A is schematically shown in Fig. 5 a).

Epoxidation of LO-A resins was carried out in the presence of H_2O_2 and HCOOH. By varying the molar ratio of C=C and H_2O_2, two epoxidized linseed oil alkyd resins with different epoxy contents were synthesized – ELO-A (1) and ELO-A (2) – in order to subsequently study differences in the UV curing of the corresponding acrylates. After synthesis optimization, the molar ratio (mol) for ELO-A (1) was 1 : 0.4: 1.8 (fatty acid C=C : HCOOH : H_2O_2), whereas the molar ratio (mol) for ELO-A (2) was 1 : 0.4 : 0.9 (fatty acid C=C : HCOOH : H_2O_2). LO-A was mixed with HCOOH and heated to 60 °C in a round-bottom flask equipped with a condenser, dropping funnel, thermocouple, and mechanical stirrer. H_2O_2 was slowly added within 1 h, through the dropping funnel, to avoid side effects of an exothermic reaction. The reaction continued for 6.5 h, and its progress was monitored by titrating the epoxy value (EV), which gradually increased, and by recording FTIR spectra. In the FTIR spectra, vibrations of fatty acid residue double bonds at 3009 cm^{-1} and 1654 cm^{-1} disappeared after epoxidation, while a new absorption band appeared at 821 cm^{-1}, indicating the formation of an epoxy ring. After completion of the reaction, the mixture was dissolved in ethyl acetate (EtOAc), the organic phase was washed with aqueous $NaHCO_3$ and NaCl solutions, dried over Na_2SO_4, and filtered. EtOAc was removed by distillation under vacuum. The reaction yields, influenced by both the ratios of the used reagents and the reaction conditions, are shown in Table 4. ELO-A (1) and ELO-A (2) were used as starting materials to obtain the corresponding acrylated linseed oil alkyds ALO-A (1) and ALO-A (2).

Acrylation of ELO-A was carried out in the presence of AA and a catalyst (1 % by mass). The reaction progress was compared using two different molar ratios of AA relative to the epoxy ring, the catalytic activity of triethylamine (TEA) and triphenylphosphine (TPP), as well as the acrylation reaction progress of ELO-A (1) and ELO-A (2). To ensure a controlled reaction course [21], the epoxy to AA molar ratio (mol) of 1 : 1.3 was selected for further experiments. TEA was chosen as a catalyst because it provided a faster reaction rate than TPP. As expected, acrylation proceeded more slowly for the epoxy with lower EV (ELO-A (2)) and faster for the epoxy with higher EV (ELO-A (1)). ELO-A (1) and ELO-A (2) are precursors for obtaining ALO-A (1) and ALO-A (2), respectively. ELO-A, TEA, and free-radical inhibitors butylated hydroxytoluene (BHT, 600 ppm) and 4-methoxyphenol (MEHQ, 600 ppm) were mixed in a round-bottom flask equipped with a condenser, thermocouple, mechanical stirrer, and dropping funnel. The mixture was heated to 95 °C, followed by the addition of AA over 1 h. The reaction was monitored by titrating and calculating the acid value (AV). After 18.5 h, when AV was low or no longer changed, the mixture was dissolved in EtOAc, the organic phase was washed with aqueous $NaHCO_3$ and NaCl solutions, dried over Na_2SO_4, and filtered. EtOAc was removed by distillation under vacuum, leaving resins with an approximate solid content of 93 %. Acrylation yields are reported in Table 4. It should be noted that during acrylation, EV decreased slightly faster than AV, which could indicate an undesired side reaction – epoxy ring opening (hydrolysis).

Representative ^{1}H-NMR spectra of ELO-A (1) and ALO-A (1) are shown in Fig. 5 c). In the ELO-A (1) spectrum, the methylene protons located at the α-position of the epoxy ring (-**H**COC**H**-) appeared at $\delta = 3.11$ and 2.91 ppm. The methylene protons between two epoxy

groups (-COC-C**H₂**-COC-) appeared at δ = 1.66–1.83 ppm, while the protons at the *β*-position of the epoxy ring (-COC-C**H₂**-) were observed at δ = 1.47 ppm. After epoxidation, the proton signals corresponding to the double bonds of unsaturated fatty acid (-**H**C=C**H**-) residues in LO-A practically disappeared. In the ^{1}H-NMR spectrum of ALO-A (1), three new signals were observed in the chemical shift range δ = 5.80–6.50 ppm, corresponding to the acrylate group protons **H₂**C=C**H**-, while the epoxy-related signals disappeared.

Table 4

Characteristics of the synthesized LO-A, ELO-A, and ALO-A resins

Resins	AV (mg KOH/g resin)	OH value (mg KOH/g resin)	mol C=C/100 g resin	EV (mol epoxy/100 g resin)	mol acryl groups/100 g resin	Yield (%)
LO-A	2.3	69	0.49	-	-	-
ELO-A (1)	3.5	93	0.05	0.34	-	69
ELO-A (2)	4.7	90	0.23	0.27	-	55
ALO-A (1)	48.1	217	0.05	0.01	0.23	68
ALO-A (2)	34.9	183	0.23	0.02	0.18	67

Before UV curing, ALO-A (1) and ALO-A (2) resins were mixed with three different reactive diluents – monofunctional isobornyl acrylate (IBOA), bifunctional tripropylene glycol diacrylate (TPGDA), and trifunctional trimethylolpropane tri(meth)acrylate (TMPTMA) (Fig. 5 b)) at 10 wt%, 20 wt%, and 30 wt%, in order to reduce viscosity (η = 5700–60000 mPa·s) and improve mechanical performance. The name of each formulation was formed by indicating the wt% of the alkyd, the wt% of the reactive diluent, the name of the diluent, and the used alkyd – ALO-A (1) or (2). For example, 90_10 IBOA (1) corresponds to a formulation containing 90 wt% ALO-A (1) and 10 wt% IBOA.

The acrylated alkyd resins were characterized by photorheological parameters – storage modulus (G′), loss modulus (G″), and tanδ values – during UV curing (Fig. 5 f)). ALO-A (1) exhibited a higher polymer crosslink density and a faster formation of the crosslinked network than ALO-A (2), which is associated with a higher number of acrylate groups per molecule. At the end of curing (400 s), ALO-A (1) reached G′ = $3.9 \cdot 10^7$ Pa, whereas ALO-A (2) G′ = $0.6 \cdot 10^7$ Pa. For all formulations containing reactive diluents, both G′ and G″ increased after UV curing with increasing wt% of the reactive diluent in the formulation, indicating the formation of a denser and stiffer crosslinked polymer network (photorheological kinetic data for the formulations are summarized in a table and presented in Appendix 2). This trend is also reflected by tanδ, which decreased in most formulations. However, an excessive amount of reactive diluent can restrict radical diffusion and mobility, leading to premature termination of polymerization [81]. In addition, all formulations exhibited a general trend whereby a higher content of reactive diluent resulted in a shorter time to reach the gel point (t_{gel}). At the gel point (G′ = G″, i.e., tanδ = 1), the liquid resin transforms into a continuous, elastic network; the material ceases to behave as a viscous liquid and begins to behave as an elastic solid.

After evaluating the behavior of the alkyd resins under photopolymerization conditions, the formulations were applied onto a wooden substrate and cured under UV light using a conveyor-type UV lamp (Fig. 5 e)). In visual comparison with commercially available UV-curable resins, the synthesized acrylated alkyd resins ALO-A (1) demonstrated significantly

better penetration into the wood, enhancing the wood tone while preserving the visibility of the wood grain (Fig. 5 d)). Alkyd resins are chemically compatible with cellulose and lignin, which improves their ability to interact with the wood structure and enables deeper penetration. This enhances the protective performance of the coating and reduces the risk of deformation and cracking under the influence of temperature and humidity, thereby ensuring a longer service life [82].

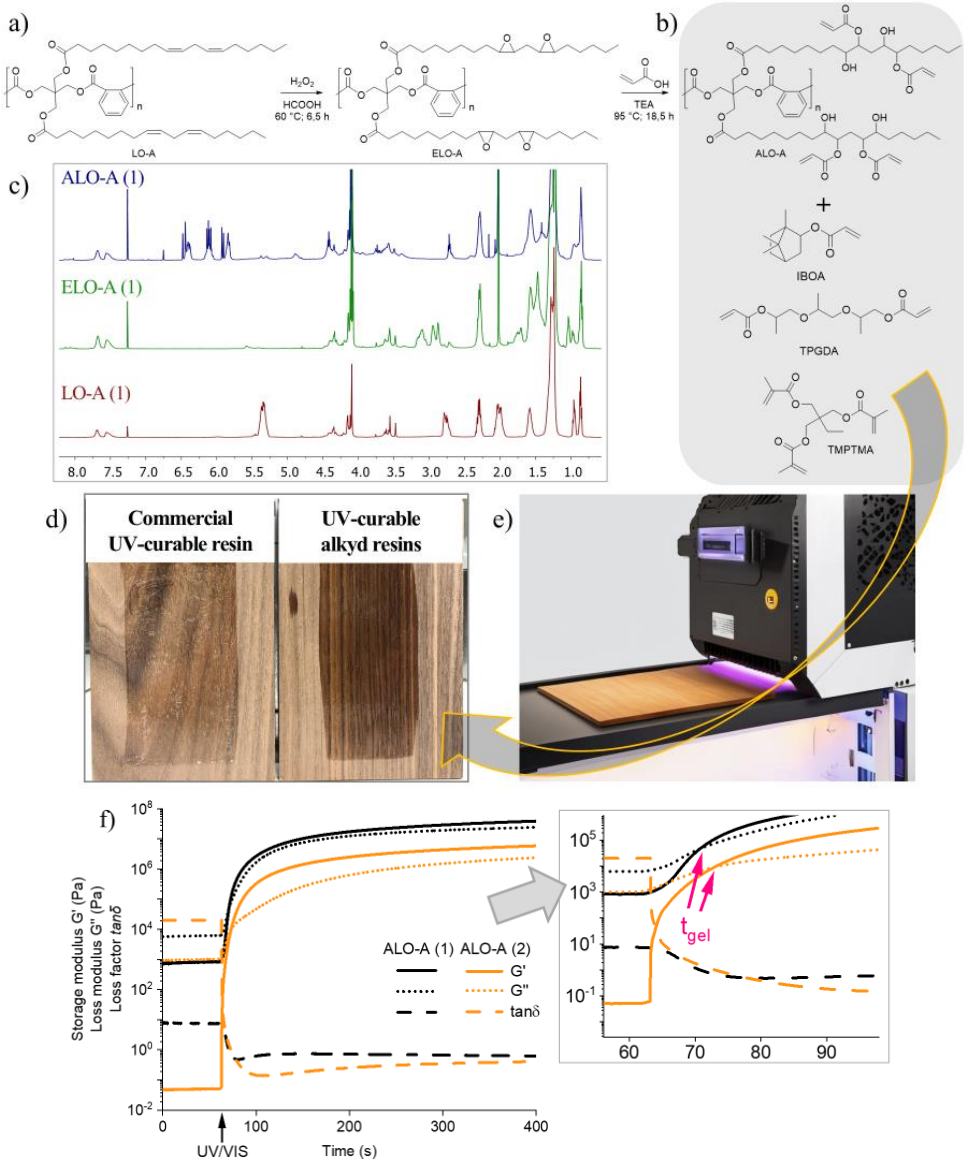

Fig. 5. a) Synthesis of ALO-A via epoxidation reaction; b) used reactive diluents; c) ^{1}H-NMR spectra of LO-A, ELO-A, and ALO-A; d) comparison of the wood tone enhancement effect; e) visualized UV curing process; f) photorheological kinetic curves of ALO-A (1) and (2) with an enlarged graph for identification of t_{gel}.

After UV irradiation, the pendulum hardness of the coatings was determined (Fig. 6 a) (i) and (ii)), which depends on molecular structure, acrylate group concentration, and polymer crosslink density [75]. Acrylated alkyd resins with different acrylate group contents exhibited a 2.2-fold difference in hardness, with ALO-A (1) reaching a high hardness value of 103 s. The hardness was further increased by adding reactive diluents with different molecular structures and acrylate group contents. Thus, the functionality of the acrylated alkyd resins and the choice of reactive diluents enabled tuning of hardness values in the range from 47 s to 174 s.

In addition to increasing hardness, reactive diluents also influenced elasticity, which was evaluated using the Erichsen cupping test by measuring indentation depth (mm) of coatings applied to an aluminum metal substrate (Fig. 6 b) (i) and (ii)). ALO-A (2), with a lower crosslink density than ALO-A (1), provided higher polymer network mobility and consequently exhibited higher elasticity, with an indentation depth of 7.0 mm. The effect of reactive diluents on indentation depth depended on both their functionality and molecular structure. The bulky isobornyl group present in the monofunctional IBOA structure enables free chain movement and reduces internal stresses in the polymer matrix, thereby increasing elasticity. The maximum indentation depth (7.4 mm) was observed for the 70_30 IBOA sample, which simultaneously exhibited high pendulum hardness (104 s). This demonstrates that it is possible to obtain coatings with both high hardness and high elasticity without a compromise between these properties. In contrast, TPGDA, as a bifunctional monomer, provides a higher polymer crosslink density than IBOA, while the propyl groups in its structure allow retention of some chain mobility and thus moderate elasticity (6.4–7.1 mm) [71]. When TMPTMA was used as the reactive diluent, the indentation depth decreased to 2.5 mm, because as a trifunctional monomer, it promotes the formation of a dense crosslinked polymer network, significantly limiting the material's ability to deform. The obtained coating characteristics indicate that by tailoring the functionality of ALO-A and selecting appropriate reactive diluents, it is possible to simultaneously increase hardness and elasticity, thereby reducing the traditionally existing trade-off between mechanical strength and flexibility [83].

In summary, this study demonstrates a systematic approach from the synthesis of renewable raw materials to the optimization of final coating properties, highlighting the possibility to tailor the structure of UV-curable acrylated alkyd resins according to the desired mechanical properties. The investigation of formulations enables the combination of high functionality, a tunable range of mechanical properties, and environmentally friendly technology, offering a solution for the industrially significant wood coating sector.

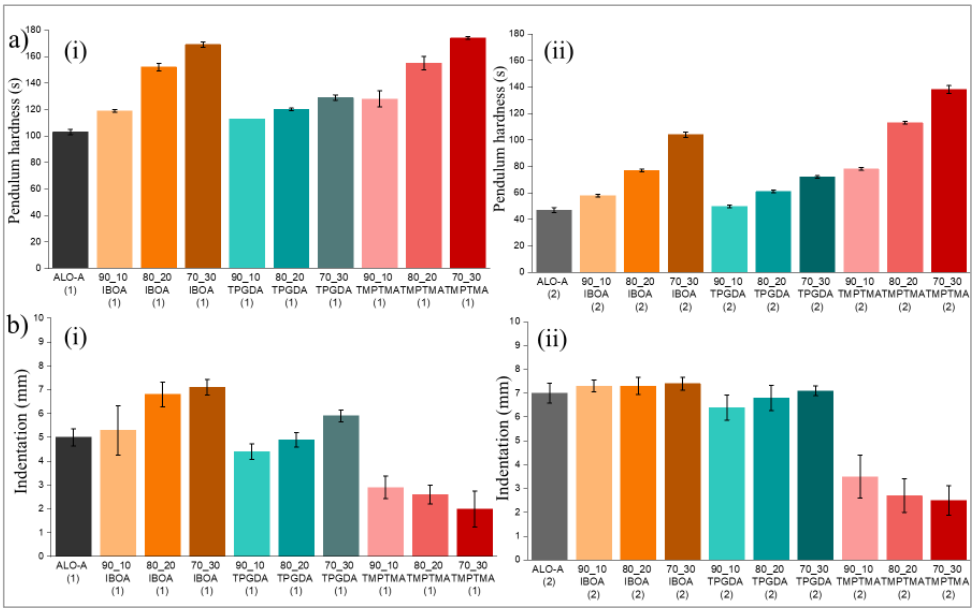

Fig. 6. UV-curable alkyd coatings: a) pendulum hardness values for (i) ALO-A (1) and (ii) ALO-A (2); b) indentation depth values for (i) ALO-A (1) and (ii) ALO-A (2).

Characterization of a new bio-based UV-curable reactive diluent in a crosslinked acrylated rapeseed oil polymer network (Publication 3)

In the first two chapters of this Thesis, UV-curable formulations were developed and characterized, containing acrylated vegetable oils and acrylated alkyd resins with various reactive diluents. These studies highlight the potential of the resins as environmentally friendly coating materials. However, most commercial reactive diluents are petroleum-derived acrylates, which reduce the content of bio-based compounds in formulations and can potentially affect the safety and ecological impact of the coatings. Consequently, there is a growing interest in bio-based reactive diluents. In the third chapter of the Thesis, this issue was addressed by investigating and characterizing a new internal double bond containing unsaturated ester (UES) derived from furan.

UES was obtained in two steps via an electrosynthesis process from furfurylated ethylene glycol: first, by electrochemically converting it to a spirocycle, and then subjecting it to electrochemically induced rearrangement to form UES. ARO was obtained via a $BF_3 \cdot OEt_2$-catalyzed one-step synthesis reaction, as described in the first chapter of the Thesis. UES was added to ARO as a reactive diluent at 5 wt% and 20 wt% (ARO/UES5 and ARO/UES20, respectively), reducing the resin viscosity up to 1.6 times. A further effect on photopolymerization and crosslinked materials was analyzed using FTIR and UV-visible (UV-Vis) light spectroscopy, mechanical analysis, SEM, DMA, and thermogravimetric analysis (TGA). Finally, the biodegradability of the material was evaluated.

Three potential reaction pathways can be considered: (1) crosslinking between ARO and UES, (2) homopolymerization of UES, and (3) homopolymerization of ARO (Fig. 7 a)).

Considering the reactivity of acryl groups and their mass fraction in the formulations, reactions involving ARO ((1) and (3)) are expected to dominate, whereas UES homopolymerization (2) is less likely. The incorporation of UES into the ARO polymer network was confirmed by FTIR spectroscopy, where the characteristic C=C double bond absorption band of UES at 1659 cm^{-1} almost completely disappeared after UV curing (Fig. 7 b)). This is further supported by the increase in optical transmittance up to 90 % in the UV-Vis region for the developed crosslinked materials (Fig. 7 c) and d)), which can be explained by the dilution of UV-absorbing chromophores and improved optical homogeneity.

In the macromolecular network structure, the triglyceride alkyl chains act as plasticizers, reducing the E and σ of the crosslinked material, whereas the short pendant UES chains at higher wt% rather increase the free volume of the material and promote relaxation (Fig. 7 e)) [84]. The polymer crosslink density increased from $1.07 \cdot 10^3$ mol/m^3 to $1.65 \cdot 10^3$ mol/m^3 upon the addition of 5 wt% UES. The increased polymer crosslink density enhanced the mechanical strength of the polymer material (σ_B increased from 0.49 MPa to 0.55 MPa) and E′ across all temperature range (at room temperature, 20 °C: from 7.98 MPa to 11.8 MPa). Increasing the UES concentration to 20 wt% led to a decrease in mechanical strength, indicating excessive reactive diluent concentration; the network becomes too diluted, thus reducing mechanical strength.

In addition to the advantage that both ARO and UES are bio-based, the biodegradation of the materials under controlled conditions was also determined. Photographs of the samples after removal from the soil are shown in Fig. 7 f). After 30 days of biodegradation, the ARO, ARO/UES5, and ARO/UES20 materials exhibited 13–15 % material mass loss, showing a relatively stable degradation rate. Over the next 30 days, the biodegradation rate decreased more rapidly for the ARO crosslinked polymer network, resulting in a total material mass loss of 18–28 %, assuming hydrolysis of fatty acid esters as the main ongoing reaction. The biodegradation data show very good results, based on similar systems reported in the literature, which observed approximately 14–16 % mass loss over 90 days [85]. Moreover, most commonly used reactive diluents in UV-curable coatings are petroleum-derived, which do not exhibit biodegradation [86].

(Thermo)mechanical tests indicated the possibility of further tailoring the mechanical properties of bio-based materials. Several strategies could be employed to optimize the mechanical performance of the materials. For example, increasing T_g and polymer crosslink density using multifunctional reactive diluents, improving the acrylation degree of vegetable oils, or optimizing post-curing conditions [87]. Additionally, the mechanical properties of the materials could be enhanced by introducing reinforcement and developing composite materials, which is discussed in the next section of the Thesis.

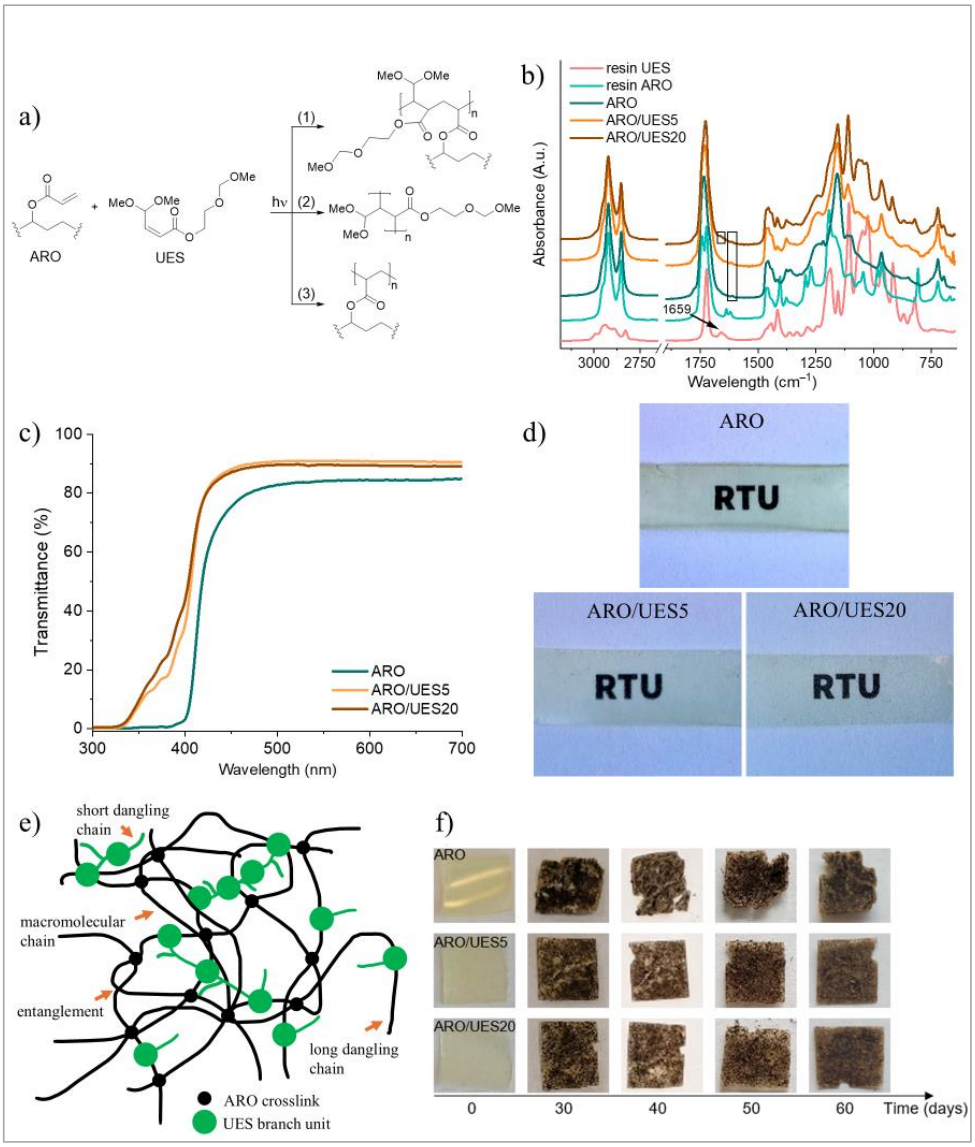

Fig. 7. a) Possible reactions between ARO and UES; b) FTIR spectra of ARO, UES and their formulations before and after UV curing; c) UV-Vis transmittance spectra of crosslinked ARO and UES materials; d) photographs of the materials; e) visualization of the crosslinked network of ARO and UES; f) photographs of crosslinked ARO and UES materials during biodegradation.

Development and characterization of UV-curable nanocomposite materials impregnated with acrylated vegetable oils (Publication 4)

In this study, bio-based nanopaper (NP) composites were developed using hemp stalks (an agricultural waste product) and compared with two vegetable oil acrylates as binders: commercially available acrylated soybean oil (AESO) and ARO obtained via one-step synthesis, as characterized in the first section of the study. Hemp fiber NP was prepared by mechanically grinding the hemp stalks to form a homogeneous fiber suspension, which was then fibrillated to obtain a nanofibrillated cellulose suspension (diameter 86 ± 41 nm). The nanofibrillated suspension was subsequently poured into molds, dried under controlled conditions, and pressed to form a dense and uniform NP layer (80 μm). During NP formation, the fibrils agglomerated with each other, forming a continuous structure. A schematic representation of the nanocomposite preparation, illustrating the interaction between cellulose and ARO or AESO via hydrogen bonding, as well as the physical confinement of cellulose fibers within the polymer matrix, is shown in Fig. 8 a). A photograph of the obtained nanocomposite is presented in Fig. 8 d).

The NP impregnation process with ARO and AESO was analyzed by determining the resin viscosity, wetting on the NP surface, and the influence of temperature and vacuum. The composite composition was governed by resin uptake during impregnation, resulting in 35/65 wt% NP/AESO and 50/50 wt% NP/ARO due to differences in viscosity and wetting behavior. The abbreviation N was used for impregnated NP samples; for ARO- or AESO-impregnated samples – R or S; for samples impregnated at room temperature – R; vacuum-impregnated samples – V; and samples impregnated at elevated temperature – T. ARO exhibited more than 20 times lower viscosity both at room temperature (20 °C) and elevated temperature (50 °C) within shear rate ranging from 1 s^{-1} to 100 s^{-1}, as well as better wetting ability on the hemp NP surface than AESO, as evidenced by measured contact angles. The ARO contact angle on NP decreased from 48.2° (5 s) to 39.3° (90 s) at 20 °C and from 46.5° (5 s) to 33.3° (90 s) at 50 °C, while the AESO contact angles under the same conditions decreased from 98.6° to 43.7° and from 83.5° to 41.1°, respectively. This ensured deeper and more uniform filling of NP pores with ARO resin, reducing the risk of air entrapment in the composite structure and improving matrix-fiber interaction.

After oil impregnation into the NP structure, the samples were UV-cured to obtain composites, whose structure and physical properties were characterized. The impregnation depth and the resulting composite microstructure were evaluated using SEM at fracture cross-sections by analyzing the residual resin layer above the substrate and the degree of pore filling. In the case of AESO, a resin layer (up to 188 μm at room temperature) indicated limited penetration into the NP structure, whereas ARO exhibited significantly deeper penetration, with a minimal residual surface layer and a high degree of filling of the porous structure, further enhanced by impregnation at elevated temperature (50 °C) and under vacuum.

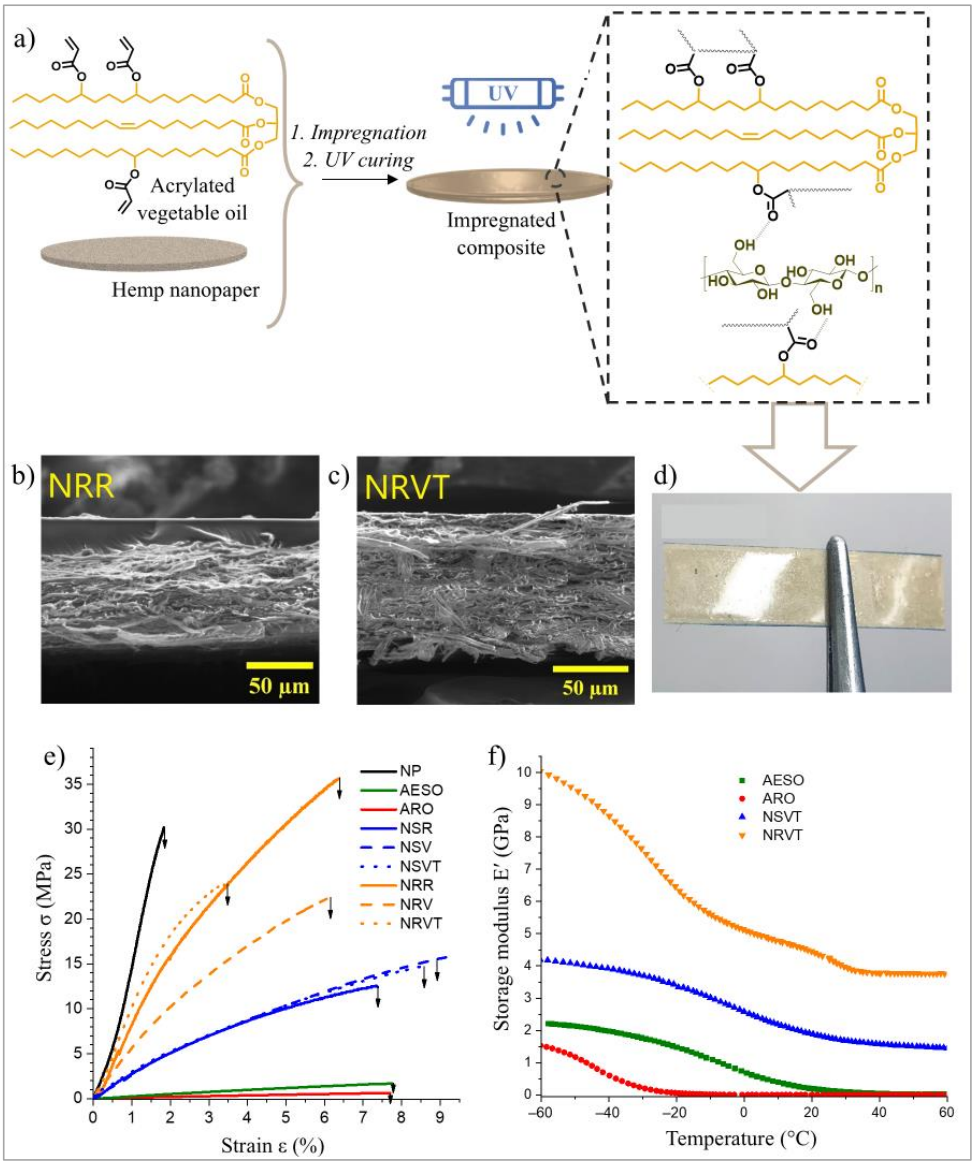

Fig. 8. a) Representative scheme for the preparation of bio-based UV-curable nanocomposites; SEM images of NP impregnated with ARO: b) at room temperature, c) at 50 °C under vacuum; d) photograph of the obtained nanocomposite; e) σ-ε curves of NP, crosslinked ARO and AESO, and their nanocomposites; f) E′ curves of crosslinked ARO and AESO and their nanocomposites impregnated at elevated temperature under vacuum.

Figure 8 b) and c) demonstrate SEM image comparisons of NP impregnated with ARO: b) at room temperature (NRR) and c) at 50 °C under vacuum (NRVT). Temperature increase and vacuum impregnation also enhanced the mechanical and thermomechanical properties (Fig. 8 e) and f)). The impregnated NP with ARO in vacuum and at 50 °C (NRVT) exhibited an E of 1.3 GPa, σ_B of 26.1 MPa, and E′ of 4.4 GPa at 20 °C. Considering that ARO and AESO are relatively soft materials, the cyclic load-bearing capacity in the viscoelastic state was almost fully ensured by NP reinforcement. Additionally, dielectric spectroscopy (DS) was performed, revealing the potential of the developed bio-based composites for electrical insulator applications, where epoxy-paper systems dominate.

In summary, this study demonstrates the compatibility of NP obtained from hemp waste with acrylated vegetable oils using UV curing. The research highlights a promising direction for the development of bio-based thermosetting composites and the enhancement of the mechanical performance of acrylated vegetable oils, achieving a balance between process simplicity and sustainability.

Development of UV-curable acrylated rapeseed oil vitrimers for thermoset reprocessing and 3D printing application (Publication 5)

Based on the results obtained in the previous chapters of this Thesis on UV-curable bio-based formulations, it is evident that such materials offer broad application possibilities with a diverse property spectrum. The research directions considered outline a unified materials development pathway – from the chemical modification of renewable feedstocks to functional UV-curable coatings and composites. As the final step, the possibilities for material reprocessing and reuse were investigated through the development of vitrimers. Expanding the application of UV-curing technology, three-dimensional (3D) printing of the developed vitrimers was also performed.

To introduce additional -OH groups into the vitrimer structure and ensure rapid transesterification reactions, rapeseed oil was acrylated via epoxide ring opening, forming *β*-hydroxyester groups (Fig. 9 a)). The epoxidation was carried out in a round-bottom flask equipped with a mechanical stirrer, thermometer, and dropping funnel. Rapeseed oil (1 mol C=C) was mixed with HCOOH (0.3 mol), and the reaction mixture was heated to 60 °C, followed by slow addition of H_2O_2 (1.8 mol). The reaction proceeded for 7 h. At the end of the reaction, the mixture was cooled to room temperature and dissolved in EtOAc to extract the organic fraction. The organic layer was then washed with $NaHCO_3$ and NaCl aqueous solutions to remove acids. Subsequently, the organic phase was dried over Na_2SO_4, filtered, and the solvent was evaporated under reduced pressure. Epoxidized rapeseed oil (ERO) was obtained as a pale yellow resin.

Acrylation of ERO was performed in a round-bottom flask equipped with a mechanical stirrer, thermometer, and dropping funnel. ERO (1 mol epoxy) was mixed with hydroquinone (HQ, 300 ppm of AA) as a polymerization inhibitor and TEA (1 wt% of total reactant mass) as a catalyst, and the mixture was heated to 90–95 °C. Then AA (2 mol) was slowly added, and the reaction mixture was left for 18.5 h. Afterwards, it was cooled to room temperature, dissolved in EtOAc, and washed with $NaHCO_3$ and NaCl aqueous solutions. The organic phase was dried over Na_2SO_4, filtered, and the solvent was evaporated under reduced pressure.

Acrylated epoxidized rapeseed oil (AERO) was obtained as dark yellow, viscous resin. The ^{1}H-NMR spectra are shown in Fig. 9 b).

Formulations were prepared using 10 wt%, 20 wt%, or 30 wt% AERO, 2-hydroxy-3-phenoxypropyl acrylate (HPPA), and glycerol 1,3-diglycerolate diacrylate (GDA) to ensure an optimal -COOR to -OH group ratio and transesterification reaction (Fig. 9 f)). Two sample series were prepared – with (10 wt% of total acrylate mass) and without $Zn(acac)_2$ as the transesterification catalyst – to evaluate the effect of the catalyst on material properties and to assess the reprocessing potential of vitrimers without a catalyst.

A total of six formulations were prepared, containing 70 wt % HPPA and 10 wt%, 20 wt%, or 30 wt % AERO, while the GDA content was 10 wt% or 20 wt %. GDA was not included in the formulation with 70 wt % HPPA and 30 wt % AERO. The sample series without a catalyst are named with the abbreviation (n/c). Sample names indicate the AERO content in wt% and the presence of the catalyst. For example, AERO20(n/c) contains 70 wt% HPPA, 20 wt% AERO, and 10 wt % GDA, but no $Zn(acac)_2$ catalyst.

The UV-curing kinetics of the formulations were studied by photo-DSC, showing a faster and more complete photopolymerization reaction for formulations without the transesterification catalyst (Fig. 9 c)). Vitrimers without the catalyst exhibited photopolymerization enthalpy values of 235–241 J/g and an exothermic maximum around 5 s. In contrast, catalyst-containing vitrimers showed photopolymerization enthalpies of 167–203 J/g and an exothermic maximum around 12 s. The reduced photopolymerization enthalpy observed in the presence of $Zn(acac)_2$ may be attributed to optical effects due to scattering in the opaque formulation, which reduces light penetration and radical generation. This was also confirmed by lower gel fractions, indicating a less crosslinked polymer network. Gel fraction values for catalyst-containing vitrimers ranged from 73 % to 79 %, whereas vitrimers without a catalyst had gel fractions between 85 % and 96 %.

Stress relaxation of the UV-curable vitrimers was performed to investigate how efficiently the polymer network can release accumulated internal stress and adapt to thermal conditions. The stress relaxation rate in vitrimers is influenced by temperature, type and concentration of catalyst, polymer network structure, and crosslink density. The relaxation time (τ^*) is defined as the time required for the sample to relax to 1/e (~ 37 %) of the initial modulus. It was observed that the stress relaxation rate increased with temperature due to thermally activated dynamic bond exchange reactions. For example, the relaxation time of a vitrimer containing $Zn(acac)_2$ and 30 wt% AERO decreased from 20 min at 180 °C to 14 min at 200 °C. Vitrimers without a catalyst exhibited 2–3 times slower stress relaxation at the respective temperatures. Stress relaxation curves for samples with and without a catalyst at 200 °C are compared in Fig. 9 d).

Figure 9 e) illustrates the dynamic -COOR and -OH exchange reactions in the polymer network, showing that i) at higher crosslink density without catalyst, stress relaxation occurs more slowly, and ii) at lower crosslink density, $Zn(acac)_2$ accelerates the transesterification reaction. Literature reports also indicate the effect of -COOR and -OH group excess on the stress relaxation time. Differences in relaxation times between samples with varying AERO content were less pronounced, consistent with gel fraction data, indicating minimal differences in polymer crosslink density within a series of vitrimers.

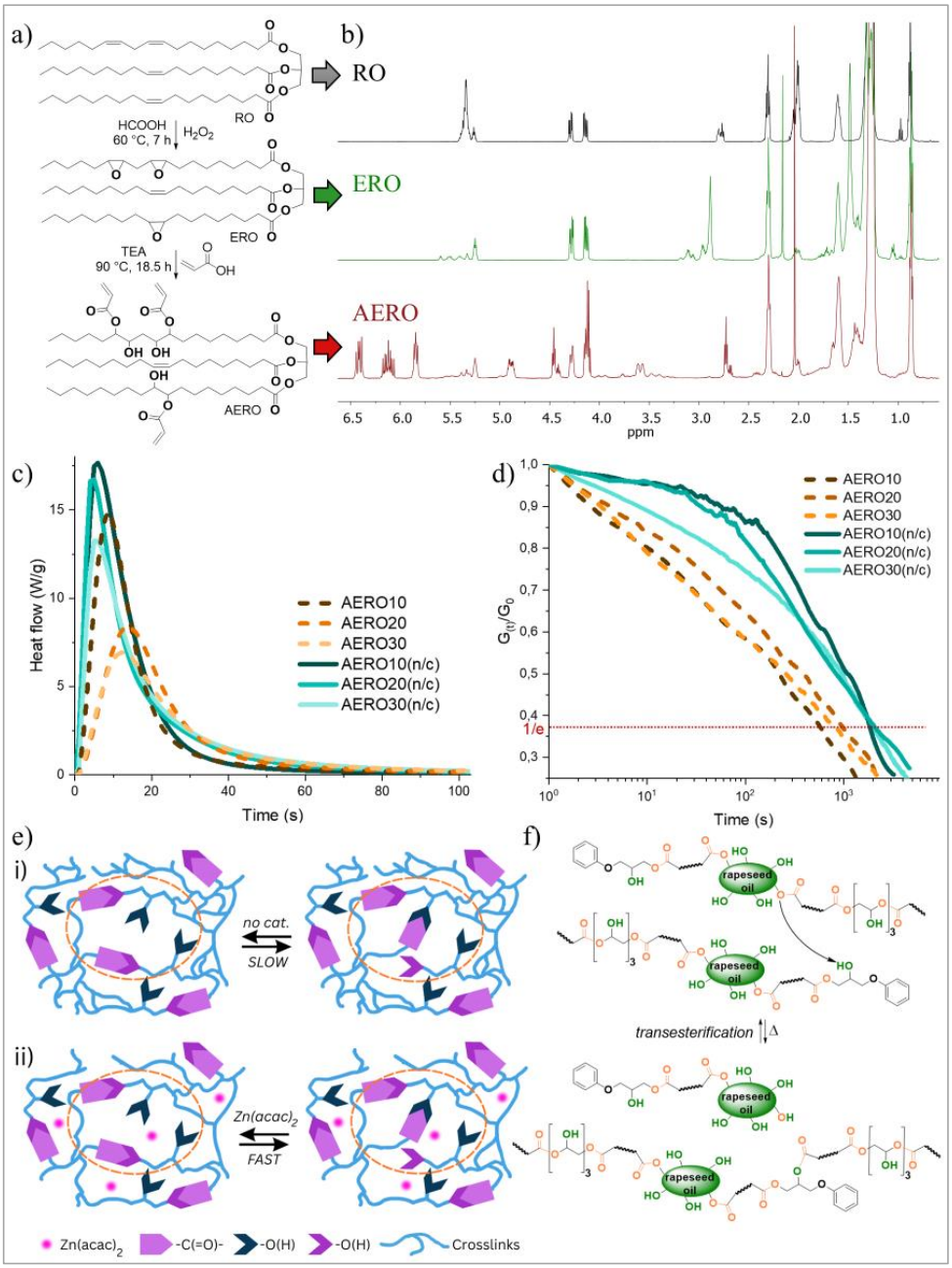

Fig. 9. a) Synthesis of AERO via epoxy ring-opening reaction; b) ^{1}H-NMR spectra of RO, ERO, and AERO; c) photo-DSC curves; d) stress relaxation curves; e) stress relaxation visualization: i) at higher polymer crosslink density without a catalyst, and i) at lower polymer crosslink density in the presence of $Zn(acac)_2$; f) a possible thermally activated dynamic bond exchange reaction in vitrimers.

To evaluate the reprocessability of UV-curable vitrimers, both sample series were ground and hot-pressed in a metal mold (Fig. 10 a)). By optimizing the processing conditions, it was determined that the most efficient reprocessing occurred at 200 °C for 2 h (Fig. 10 b)). Under these conditions, two consecutive reprocessing cycles were performed, after which the vitrimer performance was evaluated. During reprocessing, the vitrimers maintained a high degree of crosslinking, as evidenced by sol-gel fraction values of up to 90 %. However, after thermal reprocessing, cracks were observed in vitrimers without the added catalyst, whereas no cracks formed in catalyst-containing samples, confirming the catalyst's ability to rearrange the crosslinked network and restore the material structure (Fig. 10 b)). Crack formation under similar conditions has also been reported in studies by other authors [92]. After thermal reprocessing, the vitrimer samples were named, including the reprocessing cycle number; for example, AERO30_cycle2 denotes an AERO30 vitrimer obtained after the second thermal reprocessing cycle.

UV-curable vitrimers were further analyzed using combined TGA-FTIR, which simultaneously determines mass loss during heating and identifies evolved gaseous products. The obtained data indicated enhanced release of gaseous products from catalyst-containing vitrimers, confirming different polymer network rearrangement pathways for samples without (Fig. 10 c)) and with (Fig. 10 d)) catalyst. In catalyst-containing vitrimers, volatile fragments formed significantly faster due to dynamic bond exchange and exhibited higher absorption band intensities, particularly in the CO_2 and C=O regions [90]. Consequently, catalyst-containing vitrimers exhibited lower thermal stability, with the maximum decomposition rate occurring at 370 °C, compared to vitrimers without a catalyst, which showed a maximum decomposition rate at 410 °C. It should be noted that the thermal stability of both vitrimer series increased with each reprocessing cycle, most likely due to the evaporation of low-molecular-weight or unreacted components during thermal reprocessing, leaving a material composed predominantly of a stable crosslinked network.

Subsequent experiments were conducted on catalyst-containing vitrimers. The effect of reprocessing on the (thermo)mechanical properties of the materials was evaluated (Fig. 10 e) and f)). As shown in Fig. 10 e), E′ values decreased over the entire temperature range after reprocessing, reflecting a loss of stiffness, most likely due to network rearrangement, observed degradation, and chain scission [93]. The reduction in tanδ peak intensity indicated lower molecular mobility at T_g. At the same time, slight broadening of the tanδ curve suggested increased macromolecular network heterogeneity and a wider distribution of relaxation times, as regions with different crosslink densities may form after dynamic bond exchange reactions [94]. Nevertheless, overall, the prepared vitrimers exhibited similar thermomechanical behavior before and after reprocessing, indicating that the material retains its key characteristic properties. Fig. 10 f) shows that mechanical strength was not fully restored after reprocessing; however, significant recovery of σ_B was observed: 67–98 % after the first cycle and 41–50 % after the second cycle relative to the initial values. One of the reasons for the reduction in mechanical strength after reprocessing is damage to the covalent network caused by intensive grinding during vitrimer reprocessing [95], [96].

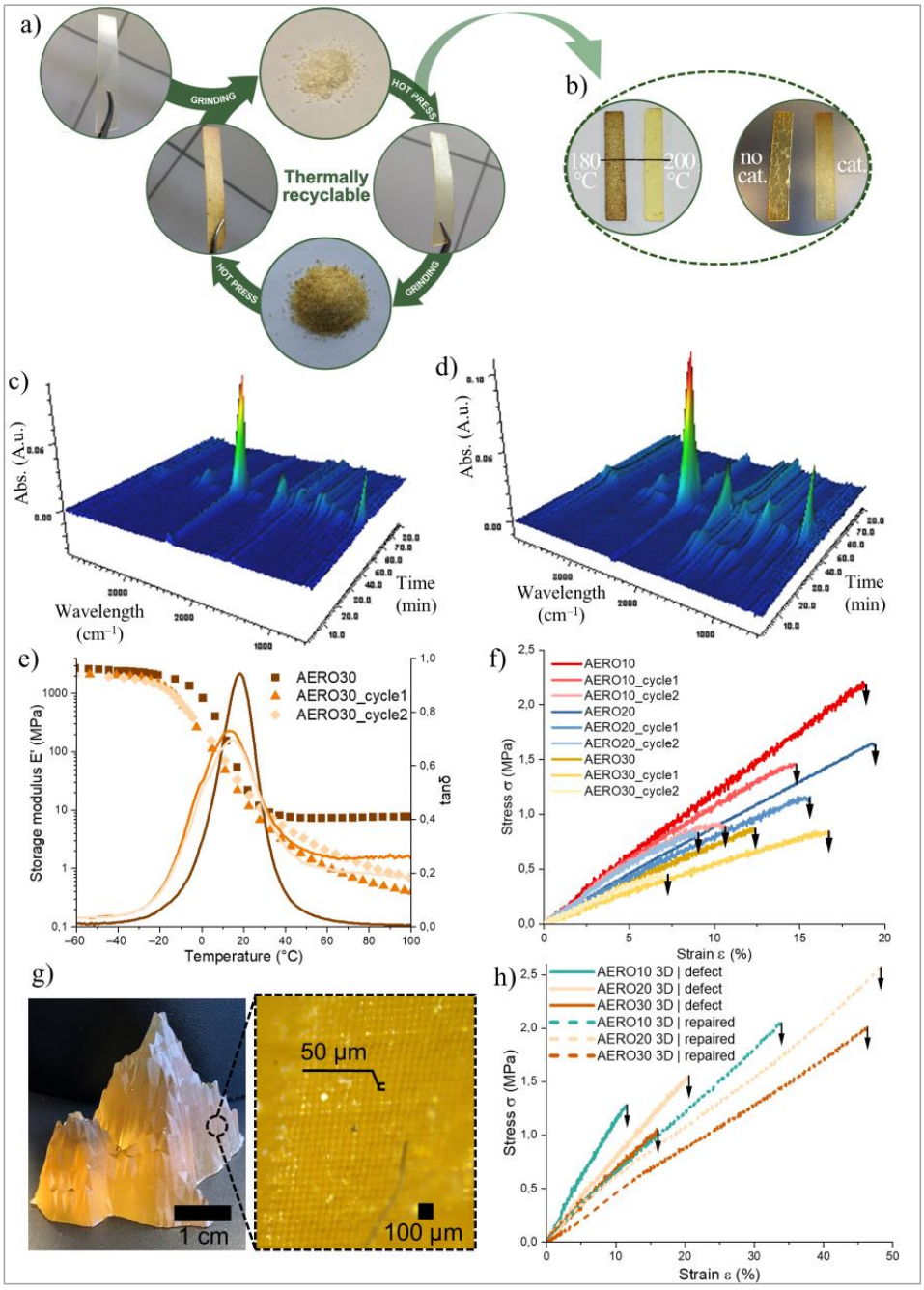

Fig. 10. a) Scheme of thermal reprocessing of AERO vitrimers; b) effect of temperature and catalyst on AERO vitrimer hot pressing; c) and d) 3D FTIR spectra of gases released from AERO30(n/c) and AERO30; e) storage modulus and tanδ curves; f) σ-ε curves of UV-cured and reprocessed AERO30 vitrimer; g) validation of AERO vitrimer 3D printing using DLP technology; h) σ-ε curves of 3D printed defected and repaired samples.

Finally, vitrimer resins were 3D printed to demonstrate their applicability in additive manufacturing. The formulation with the highest AERO content was selected for printing, as it also exhibited the lowest viscosity ($\eta \approx 663$ mPa·s at shear rates from 1 s^{-1} to 1000 s^{-1}), which is a critical parameter for vat-based 3D printing. During the printing process, uniform layer adhesion was observed with a layer thickness of 50 μm, while the printed objects exhibited high resolution, dimensional accuracy, and excellent surface quality (Fig. 10 g)).

Subsequently, the material's ability to restore its structure and properties after mechanical damage was investigated, as this can extend product lifetime and reduce waste generation while enabling more efficient resource utilization. In the final chapter of the Thesis, vitrimer repairability was analyzed. 3D-printed rods containing a 5 mm diameter opening in the center of the material (denoted as "defect" in the sample name) were fabricated to simulate mechanical damage.

In early repair trials, a 3D printed circular insert was placed into the opening, followed by thermal treatment to activate the dynamic bond exchange. However, this approach was not effective, as tensile testing showed that fracture occurred at the interface between the original material and the inserted part, indicating insufficient interfacial contact and weak adhesion. A second approach proved more effective – fresh liquid resin was poured into the opening, then UV-cured and heated at 200 °C for 1 h to activate transesterification reactions at the interface (denoted as "repaired" in the sample name). The σ-ε curves of samples with restored structure showed up to 2.0-fold increase in σ_B and up to 2.9-fold increase in strain at break (ε_B) compared to damaged samples (Fig. 10 h)). In contrast to the insert-based repair, these samples did not fail at the repaired interface; instead, fracture occurred in the adjacent bulk material, indicating the formation of a strong interfacial bond, which is attributed to efficient dynamic bond exchange.

In summary, this study demonstrates an approach that combines the use of bio-based compounds, energy-efficient technologies, and material reprocessing. The vitrimer formulations developed in this study are based on dynamic bond exchange reactions, which enable stress relaxation, reprocessing, and structural recovery after damage. By optimizing catalyst content, including catalyst-free formulations, effective network rearrangement can be achieved while maintaining good structural integrity. This allows recovery of vitrimer mechanical performance even after multiple reprocessing cycles, enabling thermoset polymers to be returned to the materials life cycle. The developed AERO vitrimers exhibited excellent suitability for 3D printing technology while also providing structural repairability, opening broader application opportunities for UV-curable vitrimers. The ability of these materials to restore structure and tensile properties after damage confirms their strong sustainability potential.

CONCLUSIONS

1. By deliberately adjusting the synthesis conditions of acrylated vegetable oil derivatives and UV-curable resin formulations, it is possible to control photopolymerization kinetics, macromolecular structure, and the mechanical properties of the final materials.
   1.1. An optimized two-step epoxidation-acrylation synthesis method enables targeted regulation of the acryl group content in UV-curable linseed oil alkyd resins (ALO-A) (0.18 mol or 0.23 mol acryl groups/100 g resin). The addition of reactive diluents provided additional possibilities for adjusting viscosity, curing kinetics (t_{gel} < 6.2 s), and polymer network structure, achieving a simultaneous increase in coating hardness (104 s) and flexibility (7.4 mm).
   1.2. The addition of the reactive diluent glyceryl propoxy triacrylate (GPT) accelerated the photopolymerization process (< 70 s), increased crosslink density (up to $2.2 \cdot 10^3$ mol/m^3), and improved the mechanical performance of the materials (up to 0.76 MPa). The developed acrylated vegetable oils formulations demonstrated applicability as UV-curable wood coatings, exhibiting adhesion to wood substrates of up to 1.21 MPa.
2. The addition of a bio-based unsaturated furan ester monomer (UES) as a reactive diluent reduced the viscosity (η = 291 mPa·s) and improved structural properties (crosslink density = $1.65 \cdot 10^3$ mol/m^3) of UV-curable ARO resins, while simultaneously promoting material biodegradability (up to 28 % mass loss over 60 days). The obtained results confirm the potential of bio-based monomers as sustainable alternatives to petroleum-based monomers.
3. UV-curable acrylated vegetable oils are suitable for use as matrix binders in natural fiber composite materials. Effective matrix-fiber interaction, confirmed by SEM analysis, ensured improved stress transfer and mechanical performance (σ_B = 35.6 MPa, E = 1.3 GPa), demonstrating the potential for the development of bio-based composite materials.
4. By controlling the content of dynamic covalent bonds in acrylated epoxidized rapeseed oil (AERO) macromolecular network structure, it is possible to develop UV-curable vitrimer materials. The obtained vitrimers demonstrated thermally activated transesterification, enabling reprocessing with recovery of mechanical performance (σ_B = 1.46 MPa, E = 12.4 MPa) of up to 98 % after the first and 50 % after the second cycle. The vitrimer resins demonstrated 3D printability with high resolution and structural repairability, restoring mechanical strength (σ_B increase up to 199 %) and elongation (ε_B increase up to 288 %) after simulated mechanical damage.

ATSAUCES / REFERENCES

[1] L. E. P. Real, “Plastics Statistics: Production, Recycling, and Market Data,” in *Recycled Materials for Construction Applications*, no. PlasticsEurope 2020, Cham: Springer International Publishing, 2023, pp. 103–113.

[2] R. Saraswat, A. Dhir, A. S. S. Balan, S. Powar, and M. Doddamani, “Synthesis and application of sustainable vegetable oil-based polymers in 3D printing,” *RSC Sustain.*, vol. 2, no. 6, pp. 1708–1737, 2024.

[3] S. Kumar, S. Krishnan, and K. Prabakaran, “Renewable resource-based epoxy vitrimer composites for future application: A comprehensive review,” *ACS Sustain. Resour. Manag.*, vol. 1, no. 9, pp. 2086–2107, 2024.

[4] F. D. Gunstone, “Vegetable oils,” *Bailey’s Ind. Oil Fat Prod.*, 2005.

[5] K. Saremi, T. Tabarsa, A. Shakeri, and A. Babanalbandi, “Epoxidation of Soybean Oil,” *Scholars Research Library Annals of Biological Research*, vol. 3, no. 9. pp. 4254–4258, 2012, [Online]. Available: http://scholarsresearchlibrary.com/archive.html.

[6] Z. Wu *et al.*, “Mass transfer and reaction kinetics of soybean oil epoxidation in a formic acid-autocatalyzed reaction system,” *Can. J. Chem. Eng.*, vol. 94, no. 8, pp. 1576–1582, 2016, doi: 10.1002/cjce.22526.

[7] C. Song, D. Gao, S. Li, L. Liu, X. Chen, and Y. Jiang, “Determination and quantification of fatty acid C=C isomers by epoxidation reaction and liquid chromatography-mass spectrometry,” *Anal. Chim. Acta*, vol. 1086, pp. 82–89, 2019, doi: 10.1016/j.aca.2019.08.023.

[8] A. B. Kousaalya, S. D. Beyene, V. Gopal, B. Ayalew, and S. Pilla, “Green epoxy synthesized from Perilla frutescens: A study on epoxidation and oxirane cleavage kinetics of high-linolenic oil,” *Ind. Crops Prod.*, vol. 123, no. June, pp. 25–34, 2018, doi: 10.1016/j.indcrop.2018.06.047.

[9] R. Turco, R. Tesser, V. Russo, T. Cogliano, M. Di Serio, and E. Santacesaria, “Epoxidation of Linseed Oil by Performic Acid Produced in Situ,” *Ind. Eng. Chem. Res.*, vol. 60, no. 46, pp. 16607–16618, 2021, doi: 10.1021/acs.iecr.1c02212.

[10] E. Santacesaria, A. Renken, V. Russo, R. Turco, R. Tesser, and M. Di Serio, “Biphasic model describing soybean oil epoxidation with H 2O 2 in continuous reactors,” *Ind. Eng. Chem. Res.*, vol. 51, no. 26, pp. 8760–8767, 2012, doi: 10.1021/ie2016174.

[11] X. Zhang, J. Burchell, and N. S. Mosier, “Enzymatic Epoxidation of High Oleic Soybean Oil,” *ACS Sustain. Chem. Eng.*, vol. 6, no. 7, pp. 8578–8583, Jul. 2018, doi: 10.1021/acssuschemeng.8b00884.

[12] V. V. Goud, N. C. Pradhan, and A. V. Patwardhan, “Epoxidation of karanja (Pongamia glabra) oil by H 2 O 2,” *J. Am. Oil Chem. Soc.*, vol. 83, no. 7, pp. 635–640, Jul. 2006, doi: 10.1007/s11746-006-1250-7.

[13] E. Santacesaria, R. Tesser, M. Di Serio, R. Turco, V. Russo, and D. Verde, “A biphasic model describing soybean oil epoxidation with H2O2 in a fed-batch reactor,” *Chem. Eng. J.*, vol. 173, no. 1, pp. 198–209, 2011, doi: 10.1016/j.cej.2011.05.018.

[14] J. La Scala and R. P. Wool, “Effect of FA composition on epoxidation kinetics of TAG,” *J. Am. Oil Chem. Soc.*, vol. 79, no. 4, pp. 373–378, Apr. 2002,

doi: 10.1007/s11746-002-0491-9.

[15] W. Gong, X. Liu, X. G. Zhao, H. Lv, and X. X. Yao, “Epoxy Value Measurement of Epoxy Resin TDE-85 by Nuclear Magnetic Resonance Spectroscopy and Titration Methods,” *J. Phys. Conf. Ser.*, vol. 2460, no. 1, 2023, doi: 10.1088/1742-6596/2460/1/012127.

[16] P. Gogoi, M. Boruah, S. Sharma, and S. K. Dolui, “Blends of epoxidized alkyd resins based on jatropha oil and the epoxidized oil cured with aqueous citric acid solution: A green technology approach,” *ACS Sustain. Chem. Eng.*, vol. 3, no. 2, pp. 261–268, 2015, doi: 10.1021/sc500627u.

[17] P. Saithai, J. Lecomte, E. Dubreucq, and V. Tanrattanakul, “Effects of different epoxidation methods of soybean oil on the characteristics of acrylated epoxidized soybean oil-co-poly(methyl methacrylate) copolymer,” *Express Polym. Lett.*, vol. 7, no. 11, pp. 910–924, 2013, doi: 10.3144/expresspolymlett.2013.89.

[18] S. Walther, B. Strehmel, and V. Strehmel, “Functionalization of an alkyd resin with (meth)acrylate groups for photoinitiated polymerization,” *Prog. Org. Coatings*, vol. 125, no. April, pp. 316–324, 2018, doi: 10.1016/j.porgcoat.2018.08.028.

[19] F. Habib and M. Bajpai, “Synthesis and Characterization of Acrylated Epoxidized Soybean Oil for UV-Cured Coatings,” *Chem. Chem. Technol.*, vol. 5, no. 3, pp. 317–326, 2011, doi: 10.23939/chcht05.03.317.

[20] Y. H. Ho, A. Parthiban, M. C. Thian, Z. H. Ban, and P. Siwayanan, “Acrylated Biopolymers Derived via Epoxidation and Subsequent Acrylation of Vegetable Oils,” *Int. J. Polym. Sci.*, vol. 2022, 2022, doi: 10.1155/2022/6210128.

[21] W. Maaßen, S. Oelmann, D. Peter, W. Oswald, N. Willenbacher, and M. A. R. Meier, “Novel Insights into Pressure-Sensitive Adhesives Based on Plant Oils,” *Macromol. Chem. Phys.*, vol. 216, no. 15, pp. 1609–1618, 2015, doi: 10.1002/macp.201500136.

[22] M. S. Ibrahim, N. G. Kandile, H. M. Said, and I. M. Moussa, “Development of radiation curable surface coating based on soybean oil. Part II. Evaluation of the prepared acrylated resin as surface coatings by using EB or UV sources for radiation curing applications,” no. November, pp. 1–16, 2005.

[23] X. M. Chu, S. J. Liu, and Z. Feng-Qing, “Preparation of acrylated epoxidized soybean oil with excellent properties,” *Appl. Mech. Mater.*, vol. 662, pp. 7–10, 2014, doi: 10.4028/www.scientific.net/AMM.662.7.

[24] D. Behera and A. K. Banthia, “Synthesis, characterization, and kinetics study of thermal decomposition of epoxidized soybean oil acrylate,” *J. Appl. Polym. Sci.*, vol. 109, no. 4, pp. 2583–2590, Aug. 2008, doi: 10.1002/app.28350.

[25] A. R. Mahendran, G. Wuzella, N. Aust, A. Kandelbauer, and U. Müller, “Photocrosslinkable modified vegetable oil-based resin for wood surface coating application,” *Prog. Org. Coatings*, vol. 74, no. 4, pp. 697–704, 2012, doi: 10.1016/j.porgcoat.2011.09.027.

[26] P. Zhang and J. Zhang, “One-step acrylation of soybean oil (SO) for the preparation of SO-based macromonomers,” *Green Chem.*, vol. 15, no. 3, pp. 641–645, 2013, doi: 10.1039/c3gc36961g.

[27] P. Zhang, J. Xin, and J. Zhang, “Effects of Catalyst Type and Reaction Parameters on One-Step Acrylation of Soybean Oil,” 2014.

[28] Y. Su, S. Zhang, Y. Chen, T. Yuan, and Z. Yang, “One-step synthesis of novel renewable multi-functional linseed oil-based acrylate prepolymers and its application in UV-curable coatings,” vol. 148, no. June 2020, doi: 10.1016/j.jclepro.2019.119869.

[29] M. Ghobakhloo, “Industry 4.0, digitization, and opportunities for sustainability,” *J. Clean. Prod.*, vol. 252, p. 119869, 2020.

[30] W. Piedra-Cascón, V. R. Krishnamurthy, W. Att, and M. Revilla-León, “3D printing parameters, supporting structures, slicing, and post-processing procedures of vat-polymerization additive manufacturing technologies: A narrative review,” *J. Dent.*, vol. 109, p. 103630, 2021.

[31] H. Quan, T. Zhang, H. Xu, S. Luo, J. Nie, and X. Zhu, “Photo-curing 3D printing technique and its challenges,” *Bioact. Mater.*, vol. 5, no. 1, pp. 110–115, 2020.

[32] C. Mendes-Felipe, J. Oliveira, I. Etxebarria, J. L. Vilas-Vilela, and S. Lanceros-Mendez, “State-of-the-art and future challenges of UV curable polymer-based smart materials for printing technologies,” *Adv. Mater. Technol.*, vol. 4, no. 3, p. 1800618, 2019.

[33] V. S. D. Voet, J. Guit, and K. Loos, “Sustainable photopolymers in 3D printing: a review on biobased, biodegradable, and recyclable alternatives,” *Macromol. Rapid Commun.*, vol. 42, no. 3, p. 2000475, 2021.

[34] J. Guit *et al.*, “Photopolymer resins with biobased methacrylates based on soybean oil for stereolithography,” *ACS Appl. Polym. Mater.*, vol. 2, no. 2, pp. 949–957, 2020.

[35] G. Zhu *et al.*, “High-performance 3D printing UV-curable resins derived from soybean oil and gallic acid,” *Green Chem.*, vol. 23, no. 16, pp. 5911–5923, 2021.

[36] L. Feng, G. Ma, R. Li, J. Luo, and J. Qu, “Preparation of high-performance modified acrylated epoxy soybean oil for 3D printing,” *Mater. Today Commun.*, vol. 44, p. 111865, 2025.

[37] A. Barkane *et al.*, “UV-Light Curing of 3D Printing Inks from Vegetable Oils for Stereolithography,” *Polymers (Basel).*, vol. 13, no. 8, p. 1195, Apr. 2021, doi: 10.3390/polym13081195.

[38] G. Phalak, D. Patil, V. Vignesh, and S. Mhaske, “Development of tri-functional biobased reactive diluent from ricinoleic acid for UV curable coating application,” *Ind. Crops Prod.*, vol. 119, pp. 9–21, 2018.

[39] Y. Su, S. Zhang, X. Zhou, Z. Yang, and T. Yuan, “A novel multi-functional bio-based reactive diluent derived from cardanol for high bio-content UV-curable coatings application,” *Prog. Org. Coatings*, vol. 148, p. 105880, 2020.

[40] J. Wu, Y. Qian, C. A. Sutton, J. J. La Scala, D. C. Webster, and M. P. Sibi, “Bio-based furanic di (meth) acrylates as reactive diluents for UV curable coatings: synthesis and coating evaluation,” *ACS Sustain. Chem. Eng.*, vol. 9, no. 46, pp. 15537–15544, 2021.

[41] Y. Hu *et al.*, “Low volume shrinkage, high bio-based, and UV-curable coatings from castor oil-based reactive diluent via a one-step reaction,” *Ind. Crops Prod.*, vol. 209, p. 117951, 2024.

[42] Q. He *et al.*, “Eugenol-based multi-functional monomer as reactive diluent for high bio-content UV-curable coatings,” *Prog. Org. Coatings*, vol. 200, p. 109079, 2025.

[43] B. T. White, V. Meenakshisundaram, K. D. Feller, C. B. Williams, and T. E. Long, “Vat photopolymerization of unsaturated polyesters utilizing a polymerizable ionic

liquid as a non-volatile reactive diluent," *Polymer (Guildf).*, vol. 223, p. 123727, 2021.

[44] H. Wei *et al.*, "Characterization and photopolymerization of divinyl fumarate," *Macromolecules*, vol. 40, no. 17, pp. 6172–6180, 2007.

[45] B. H. Northrop and R. N. Coffey, "Thiol–ene click chemistry: computational and kinetic analysis of the influence of alkene functionality," *J. Am. Chem. Soc.*, vol. 134, no. 33, pp. 13804–13817, 2012.

[46] H. Esen, S. Küsefoğlu, and R. Wool, "Photolytic and free-radical polymerization of monomethyl maleate esters of epoxidized plant oil triglycerides," *J. Appl. Polym. Sci.*, vol. 103, no. 1, pp. 626–633, 2007.

[47] F. N. Jones, M. E. Nichols, and S. P. Pappas, *Organic coatings: science and technology*. John Wiley & Sons, 2017.

[48] R. Schwalm, *UV coatings: basics, recent developments and new applications*. Elsevier, 2006.

[49] Q. Wu *et al.*, "High-performance soybean-oil-based epoxy acrylate resins:'Green' synthesis and application in UV-curable coatings," *ACS Sustain. Chem. Eng.*, vol. 6, no. 7, pp. 8340–8349, 2018.

[50] M. Black and J. W. Rawlins, "Thiol–ene UV-curable coatings using vegetable oil macromonomers," *Eur. Polym. J.*, vol. 45, no. 5, pp. 1433–1441, 2009.

[51] N. Thanamongkollit, K. R. Miller, and M. D. Soucek, "Synthesis of UV-curable tung oil and UV-curable tung oil-based alkyd," *Prog. Org. Coatings*, vol. 73, no. 4, pp. 425–434, 2012, doi: 10.1016/j.porgcoat.2011.02.003.

[52] M. M. Aung, Z. Yaakob, L. C. Abdullah, M. Rayung, and W. J. Li, "A comparative study of acrylate oligomer on Jatropha and Palm oil-based UV-curable surface coating," *Ind. Crops Prod.*, vol. 77, pp. 1047–1052, 2015.

[53] C. Decker, "New developments in UV radiation curing of protective coatings," *Surf. Coatings Int. Part B Coatings Trans.*, vol. 88, no. 1, pp. 9–17, 2005.

[54] P. Bednarczyk *et al.*, "UV curable coatings based on urethane acrylates containing eugenol and evaluation of their antimicrobial activity," *Coatings*, vol. 11, no. 12, p. 1556, 2021.

[55] X. Yang *et al.*, "Highly transparent acrylate epoxidized soybean oil based UV–curable silicone–modified coatings with good thermal stability and flame retardancy," *Prog. Org. Coatings*, vol. 165, p. 106769, 2022.

[56] Y. Hu *et al.*, "Synthesis and application of UV-curable phosphorous-containing acrylated epoxidized soybean oil-based resins," *J. Bioresour. Bioprod.*, vol. 4, no. 3, pp. 183–191, 2019.

[57] B. Dong, Y. Yuan, J. Luo, L. Dong, R. Liu, and X. Liu, "Acryloyl-group functionalized graphene for enhancing thermal and mechanical properties of acrylated epoxidized soybean oil UV-curable based coatings," *Prog. Org. Coatings*, vol. 118, pp. 57–65, 2018.

[58] M. Rani, P. Choudhary, V. Krishnan, and S. Zafar, "A review on recycling and reuse methods for carbon fiber/glass fiber composites waste from wind turbine blades," *Compos. part B Eng.*, vol. 215, p. 108768, 2021.

[59] Y. S. Song, J. R. Youn, and T. G. Gutowski, "Life cycle energy analysis of fiber-

reinforced composites," *Compos. Part A Appl. Sci. Manuf.*, vol. 40, no. 8, pp. 1257–1265, 2009.

[60] A. Mautner, W. M. F. W. Nawawi, K.-Y. Lee, and A. Bismarck, "High porosity cellulose nanopapers as reinforcement in multi-layer epoxy laminates," *Compos. Part A Appl. Sci. Manuf.*, vol. 131, p. 105779, 2020.

[61] P. Khawas, A. J. Das, and S. C. Deka, "Production of renewable cellulose nanopaper from culinary banana (Musa ABB) peel and its characterization," *Ind. Crops Prod.*, vol. 86, pp. 102–112, 2016.

[62] W. Post, A. Susa, R. Blaauw, K. Molenveld, and R. J. I. Knoop, "A review on the potential and limitations of recyclable thermosets for structural applications," *Polym. Rev.*, vol. 60, no. 2, pp. 359–388, 2020.

[63] T. Maeda, H. Otsuka, and A. Takahara, "Dynamic covalent polymers: Reorganizable polymers with dynamic covalent bonds," *Prog. Polym. Sci.*, vol. 34, no. 7, pp. 581–604, 2009.

[64] A. Adjaoud, A. Trejo-Machin, L. Puchot, and P. Verge, "Polybenzoxazines: a sustainable platform for the design of fast responsive and catalyst-free vitrimers based on trans-esterification exchanges," *Polym. Chem.*, vol. 12, no. 22, pp. 3276–3289, 2021, doi: 10.1039/D1PY00324K.

[65] S. Lemouzy *et al.*, "Understanding the Reshaping of Fluorinated Polyester Vitrimers by Kinetic and DFT Studies of the Transesterification Reaction," *Chemistry – A European Journal*, vol. 28, no. 48. 2022, doi: 10.1002/chem.202201135.

[66] Y. Yang *et al.*, "Green and ultrastrong polyphenol lignin-based vitrimer adhesive with photothermal conversion property, wide temperature adaptability, and solvent resistance," *Chem. Eng. J.*, vol. 477, p. 147216, Dec. 2023, doi: 10.1016/j.cej.2023.147216.

[67] D. Ahn, L. M. Stevens, K. Zhou, and Z. A. Page, "Rapid High-Resolution Visible Light 3D Printing," *ACS Cent. Sci.*, vol. 6, no. 9, pp. 1555–1563, Sep. 2020, doi: 10.1021/acscentsci.0c00929.

[68] H. Li *et al.*, "Solvent-Free Upcycling Vitrimers through Digital Light Processing-Based 3D Printing and Bond Exchange Reaction," *Adv. Funct. Mater.*, vol. 32, no. 28, pp. 1–11, 2022, doi: 10.1002/adfm.202111030.

[69] S. Kaewpirom and D. Kunwong, "Curing behavior and cured film performance of easy-to-clean UV-curable coatings based on hybrid urethane acrylate oligomers," *J. Polym. Res.*, vol. 19, no. 11, p. 9995, 2012.

[70] P. Kardar, M. Ebrahimi, S. Bastani, and M. Jalili, "Using mixture experimental design to study the effect of multifunctional acrylate monomers on UV cured epoxy acrylate resins," *Prog. Org. coatings*, vol. 64, no. 1, pp. 74–80, 2009.

[71] P. Chittavanich, K. Miller, and M. D. Soucek, "A photo-curing study of a pigmented UV-curable alkyd," *Prog. Org. Coatings*, vol. 73, no. 4, pp. 392–400, 2012, doi: 10.1016/j.porgcoat.2011.02.005.

[72] S. Briede, M. Jurinovs, S. Nechausov, O. Platnieks, and S. Gaidukovs, "State-of-the-art UV-assisted 3D printing via a rapid syringe-extrusion approach for photoactive vegetable oil acrylates produced in one-step synthesis," *Mol. Syst. Des. Eng.*, vol. 7, no. 11, pp. 1434–1448, 2022, doi: 10.1039/D2ME00085G.

[73] A. Olivier *et al.*, “Static and Dynamic Mechanical Behavior of Electron Beam-Cured Monomer and Monomer/Liquid Crystal Systems,” *Macromol. Mater. Eng.*, vol. 289, no. 12, pp. 1047–1052, 2004.

[74] A. Hermann *et al.*, “Understanding indentation, scratch and wear behavior of UV-cured wood finishing products,” *Prog. Org. Coatings*, vol. 161, p. 106504, 2021.

[75] S. Tasic, B. Bozic, and B. Dunjic, “Synthesis of new hyperbranched urethane-acrylates and their evaluation in UV-curable coatings,” *Prog. Org. Coatings*, vol. 51, no. 4, pp. 320–327, 2004, doi: 10.1016/j.porgcoat.2004.07.021.

[76] D. Dunson, “Characterization of polymers using dynamic mechanical analysis (DMA),” *EAG Appl Note*, pp. 1–8, 2017.

[77] V. A. Kong, T. A. Staunton, and J. E. Laaser, “Effect of cross-link homogeneity on the high-strain behavior of elastic polymer networks,” *Macromolecules*, vol. 57, no. 10, pp. 4670–4679, 2024.

[78] K. S. Worthington, C. Baguenard, B. S. Forney, and C. A. Guymon, “Photopolymerization kinetics in and of self-assembling lyotropic liquid crystal templates,” *J. Polym. Sci. Part B Polym. Phys.*, vol. 55, no. 6, pp. 471–489, 2017, doi: /10.1002/polb.24296.

[79] S. Pellerin, F. Samyn, S. Duquesne, and V. Landry, “Preparation and characterisation of UV-curable flame retardant wood coating containing a phosphorus acrylate monomer,” *Coatings*, vol. 12, no. 12, p. 1850, 2022.

[80] G. Mashouf, M. Ebrahimi, and S. Bastani, “UV curable urethane acrylate coatings formulation: experimental design approach,” *Pigment Resin Technol.*, vol. 43, no. 2, pp. 61–68, 2014.

[81] K. S. Anseth, C. M. Wang, and C. N. Bowman, “Kinetic evidence of reaction diffusion during the polymerization of multi(meth)acrylate monomers,” *Macromolecules*, vol. 27, no. 3, pp. 650–655, Jan. 1994, doi: 10.1021/ma00081a004.

[82] R. S. Williams, “Finishing of Wood,” *Wood as an Eng. Mater.*, vol. 1, pp. 15–37, 1999.

[83] R. Schwalm, L. Häußling, W. Reich, E. Beck, P. Enenkel, and K. Menzel, “Tuning the mechanical properties of UV coatings towards hard and flexible systems,” *Prog. Org. Coatings*, vol. 32, no. 1–4, pp. 191–196, 1997, doi: 10.1016/S0300-9440(97)00060-X.

[84] D. P. Pfister, Y. Xia, and R. C. Larock, “Recent advances in vegetable oil-based polyurethanes,” *ChemSusChem*, vol. 4, no. 6, pp. 703–717, 2011.

[85] J. Chen, H. Liu, W. Zhang, L. Lv, and Z. Liu, “Thermosets resins prepared from soybean oil and lignin derivatives with high biocontent, superior thermal properties, and biodegradability,” *J. Appl. Polym. Sci.*, vol. 137, no. 26, p. 48827, 2020.

[86] Y. Bao, N. Paunović, and J. Leroux, “Challenges and opportunities in 3D printing of biodegradable medical devices by emerging photopolymerization techniques,” *Adv. Funct. Mater.*, vol. 32, no. 15, p. 2109864, 2022.

[87] M. Lebedevaite, V. Talacka, and J. Ostrauskaite, “High biorenewable content acrylate photocurable resins for DLP 3D printing,” *J. Appl. Polym. Sci.*, vol. 138, no. 16, p. 50233, 2021.

[88] N. S. Jyothi, T. S. Ramu, and M. Mandlik, “Temperature distribution in resin impregnated paper insulation for transformer bushings,” *IEEE Trans. Dielectr. Electr.*

Insul., vol. 17, no. 3, pp. 931–938, 2010.

[89] H. Matsubara, A. Yoshida, H. Ohtani, and S. Tsuge, "Compositional analysis of UV-cured acrylic ester resins by pyrolysis-gas chromatography in the presence of organic alkali," *Journal of Analytical and Applied Pyrolysis*, vol. 64, no. 2. pp. 159–175, 2002, doi: 10.1016/S0165-2370(02)00028-1.

[90] M. Capelot, D. Montarnal, F. Tournilhac, and L. Leibler, "Metal-catalyzed transesterification for healing and assembling of thermosets," *J. Am. Chem. Soc.*, vol. 134, no. 18, pp. 7664–7667, 2012, doi: 10.1021/ja302894k.

[91] U. Shaukat, E. Rossegger, and S. Schlögl, "Thiol–acrylate based vitrimers: From their structure–property relationship to the additive manufacturing of self-healable soft active devices," *Polymer (Guildf).*, vol. 231, p. 124110, Sep. 2021, doi: 10.1016/j.polymer.2021.124110.

[92] P. Wu, L. Liu, and Z. Wu, "A transesterification-based epoxy vitrimer synthesis enabled high crack self-healing efficiency to fibrous composites," *Compos. Part A Appl. Sci. Manuf.*, vol. 162, no. May, 2022, doi: 10.1016/j.compositesa.2022.107170.

[93] L. Li, X. Chen, K. Jin, and J. M. Torkelson, "Vitrimers Designed Both to Strongly Suppress Creep and to Recover Original Cross-Link Density after Reprocessing: Quantitative Theory and Experiments," *Macromolecules*, vol. 51, no. 15. pp. 5537–5546, 2018, doi: 10.1021/acs.macromol.8b00922.

[94] G. Capiel, E. Hernández, N. E. Marcovich, and M. A. Mosiewicki, "Stress relaxation behavior of weldable crosslinked polymers based on methacrylated oleic and lauric acids," *Eur. Polym. J.*, vol. 132, no. March, p. 109740, 2020, doi: 10.1016/j.eurpolymj.2020.109740.

[95] Y. You, W. L. Peng, P. Xie, M. Z. Rong, M. Q. Zhang, and D. Liu, "Topological rearrangement-derived homogeneous polymer networks capable of reversibly interlocking: From phantom to reality and beyond," *Mater. Today*, vol. 33, pp. 45–55, Mar. 2020, doi: 10.1016/j.mattod.2019.09.005.

[96] H. Hinsken, S. Moss, J. R. Pauquet, and H. Zweifel, "Degradation of polyolefins during melt processing," *Polymer Degradation and Stability*, vol. 34, no. 1–3. pp. 279–293, 1991, doi: 10.1016/0141-3910(91)90123-9.

Pielikumi
Appendices

Pielikums I

Appendix I

Briede, S., Platnieks, O., Barkane, A., Sivacovs, I., Leitans, A., Lungevics, J., & Gaidukovs, S.

Tailored Biobased Resins from Acrylated Vegetable Oils for Application in Wood Coatings

Coatings, **2023**, 13(3), 657.

doi: 10.3390/coatings13030657

coatings

MDPI

Article

Tailored Biobased Resins from Acrylated Vegetable Oils for Application in Wood Coatings

Sabine Briede [1], Oskars Platnieks [1,*], Anda Barkane [1], Igors Sivacovs [2], Armands Leitans [3], Janis Lungevics [3] and Sergejs Gaidukovs [1,*]

[1] Institute of Polymer Materials, Faculty of Materials Science and Applied Chemistry, Riga Technical University, P. Valdena 3/7, LV-1048 Riga, Latvia; sabine.briede@rtu.lv (S.B.); anda.barkane@rtu.lv (A.B.)
[2] JSC Olaine Chemical Plant BIOLAR, Rupnicu 3, LV-2114 Olaine, Latvia; igors.sivacovs@biolar.lv
[3] Department of Mechanical Engineering and Mechatronics, Faculty of Mechanical Engineering, Transport and Aeronautics, Riga Technical University, Kipsalas 6B, LV-1048 Riga, Latvia; armands.leitans@rtu.lv (A.L.); janis.lungevics@rtu.lv (J.L.)
* Correspondence: oskars.platnieks_1@rtu.lv (O.P.); sergejs.gaidukovs@rtu.lv (S.G.)

Abstract: The modern coating market is dominated by acrylic, polyurethane, and polyester polymer resins produced from unsustainable fossil resources. Herein, we propose the preparation of resins from biobased components to produce functional and solvent-free wood coatings with enhanced performance properties. Acrylated rapeseed, linseed, and grapeseed oils were prepared via a one-step synthesis and used as a basis for the control of resin viscosity and fatty acid content. A combination of vegetable oil acrylates was used as a matrix and the biobased monomer propoxylated glycerol triacrylate (GPT) was selected to tailor the properties of the UV crosslinked network. During polymerization, the GPT monomer induced a two-phase microstructure as indicated by an SEM analysis. The possibility of generating a tailored microstructure in the final material was examined in this study. The addition of GPT increased the storage modulus by up to five-fold, crosslink density by up to two-fold at 20 °C, and glass transition temperature by up to 10.2 °C. Pull-off adhesion tests showed a strength of 1.21 MPa. In addition, the photo-oxidation effect on samples, i.e., aging, was assessed with microhardness, sliding friction, and optical microscopy. Coatings showed a microhardness value up to 250 MPa, while a coefficient of friction (μ) was in the range of 0.21 to 0.88.

Keywords: UV photopolymerization; photo-oxidative degradation; microhardness; adhesion; sliding friction

Citation: Briede, S.; Platnieks, O.; Barkane, A.; Sivacovs, I.; Leitans, A.; Lungevics, J.; Gaidukovs, S. Tailored Biobased Resins from Acrylated Vegetable Oils for Application in Wood Coatings. *Coatings* **2023**, *13*, 657. https://doi.org/10.3390/coatings13030657

Academic Editors: Rafael L. Quirino and Thomas Garrison

Received: 27 February 2023
Revised: 15 March 2023
Accepted: 18 March 2023
Published: 20 March 2023

1. Introduction

Coatings contribute significantly to material protection and preservation. With the current global sustainability issues, wood is the material of choice for modern engineering solutions and functional and decorative applications. Recent trends show that sustainability is being incorporated into the coatings industry [1]. So far, the sustainability approach has targeted reduced energy consumption by utilizing ultraviolet (UV)-curable coatings that use high solid content or solvent-free technology. The UV approach has proven to be more efficient than thermal curing [2]. The next step is switching to UV-curable monomers and oligomers sourced from renewable resources. This research undertakes the challenge of formulating biobased coating resins by incorporating the energy-saving aspects of UV-curing technology.

Vegetable oils are characterized by biodegradability, low toxicity, high flash points (>300 °C), and low flammability and are considered sustainable [3]. These excellent properties play a role in their selection as wood-coating materials. However, some drawbacks to vegetable oils (VOs) and their derivatives (susceptibility to oxidative polymerization

reactions, low mechanical strength, and low toughness due to long aliphatic chains) [4] must be addressed. Nevertheless, these properties can be improved by adding additives, selecting a modification route for vegetable oils, and controlling the fatty acid composition [5]. In our previous research, we demonstrated that one-step acrylation is suitable for preparing relatively low-viscosity resin for UV-assisted 3D printing [6]. Therefore, the modification route of choice was the optimized acrylation route for coating preparation.

VO has been demonstrated as a perspective source for UV-curable coatings, including linseed [7], castor [8], tung [9], jatropha, and palm oils [10]. Likewise, various properties are intentionally designed from oil derivatives. The production, quality, and processing of polymer coatings depend highly on rheological behavior [11]. UV-curable coatings are characterized mainly by high viscosity, which is one of the major challenges in broadening their application. Therefore, non-reactive or, most often, reactive diluents, i.e., monomers, are used to reduce viscosity and improve fluidity [12,13]. Relatively low-viscosity soybean oil acrylate (5406 mPa·s) was synthesized using 2-hydroxyethyl acrylate as an acrylic agent to obtain acrylic ethers instead of esters [14]. The authors concluded that, compared to ester linkages, ethers have a greater free volume due to their freedom of rotation, meaning lower viscosity can be obtained. Hongjie et al. created another biobased acrylate by reacting soybean oil polyol with acryloyl chloride at low temperatures and without using a catalyst or inhibitor [15]. By changing the molar ratio, the obtained products had a lower viscosity of 208 and 192 mPa·s compared to acrylated epoxidized soybean oil (AESO) with a reported viscosity of 1225 mPa·s. The authors observed that introducing unsaturated bonds reduced the product's viscosity. Fei et al. reported the addition of three reactive diluents for AESO: styrene, 1,4-butanediol dimethacrylate (BDDMA), and trimethylolpropane trimethacrylate (TMPTMA) [16]. The viscosity for these resins decreased from 3352 mPa·s for pure AESO to 44, 165, and 624 mPa·s for the AESO/diluent system at 30 °C, respectively. Thus, according to the literature, frequently used reactive diluents for the acrylated vegetable oil (AVO) matrix are primarily derived from petroleum feedstocks and are often volatile and harmful. Some studies reported using AVOs as reactive diluents [17], or other renewable feedstocks such as eugenol [18], methacrylated isosorbide [19], etc. Dai et al. developed a high-performance UV-curable coating from AESO, fossil-based additives, and the crosslinking agent IG synthesized from itaconic acid and glycidyl methacrylate with a biobased content of 31.4% [20]. The rigid coating showed an increase in mechanical strength from 1.6 MPa (pure AESO) to 6.0 and 10.1 MPa (20 and 40 wt% IG added), while the tensile modulus rose significantly by 670% and 1932%, respectively. Despite all the success of reducing the resin viscosity, the lack of commercially available biobased coatings shows that more research is still required. Emphasis should also be placed on biobased solutions' mechanical and aging performance.

In our work, phase separation was induced as a strategy to create an enhanced microstructure. The stability and low viscosity of the initial homogeneous solution are benefits of the phase separation process in terms of toughening thermosetting networks [21]. The possibility of generating a tailored microstructure in the final material was examined in this study. Distinct polymeric microstructures were produced by the addition of 5 and 20 wt% of propoxylated glycerol triacrylate (GPT) in the AVO matrix and studied by SEM. This work expanded on the plant oil derivatives by introducing acrylated rapeseed, linseed, and grapeseed oils as value-added monomers. The resin formulations focused on the use of biobased components. Furthermore, extensive mechanical and photo-oxidation (aging) studies explored the feasibility of actual biobased wood coatings, not just the concept.

2. Materials and Methods

2.1. Materials

Unrefined rapeseed and linseed oils were purchased from a local producer "Iecavnieks" (Latvia) and the grapeseed oil used in this study was "Monini" (Italy). The synthesis of acrylated rapeseed, linseed, and grapeseed oil (R, L, and G, respectively) was described in our previous work [6]. Briefly, the selected oil, acrylic acid, and $BF_3{\cdot}OEt_2$ were mixed in a round-bottom flask and stirred for 5 h at 80 °C before being left overnight at room temperature (22 ± 1 °C). In the work-up, the organic phase was dissolved in hexane, washed with the $NaHCO_3$ solution, dried, filtered, and evaporated under reduced pressure. $BF_3{\cdot}OEt_2$, hexane, $NaHCO_3$, and photoinitiator diphenyl(2,4,6-trimethylbenzoyl)phosphine oxide (TPO) were supplied by Sigma Aldrich. In addition, propoxylated glycerol triacrylate (GPT) was added as a reactive diluent and was supplied by Arkema. The biobased content of GPT was 15%. The chemical structures of the investigated components and their application are illustrated in Figure 1.

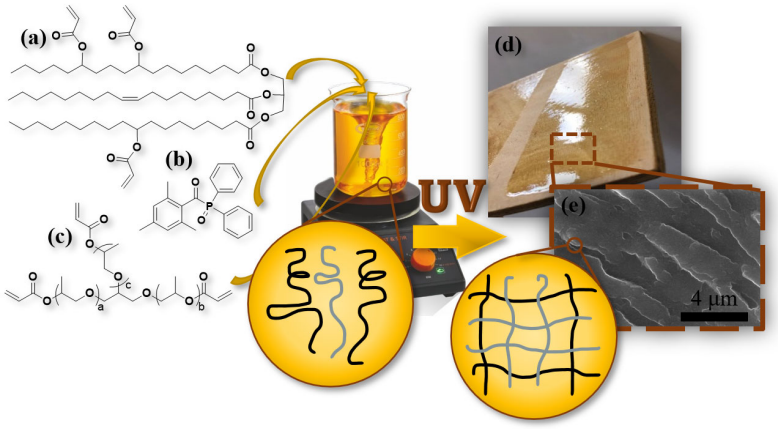

Figure 1. Scheme for this study: (**a**) acrylated vegetable oil (generalized structure); (**b**) TPO photoinitiator; (**c**) GPT monomer; (**d**) ultraviolet (UV)-cured acrylated vegetable oil coating on plywood; (**e**) formation of microstructure, SEM image.

2.2. UV-Curing Process of Coatings

Acrylated R, L, and G oils—a series of yellowish oily products—were mixed in a mass ratio of 50/50 to obtain a viscosity that was approximately the same for all compositions, as well as fatty acid residues in a similar ratio. The representative fatty acid residues in R were oleic acid (~58.8%), L—linolenic acid (~48.8%), and G—linoleic acid (~74.7%) [22–24]. GPT was used as an additional monomer in the UV-curable system and acted as a reactive diluent. In addition, GPT can considerably enhance mechanical strength since the trifunctional monomer leads to higher crosslinking density [25]. Nine resin compositions were prepared to study acrylated vegetable oils' (AVOs') application for wood coatings: three acrylated vegetable oil resins, three resins with 5 wt% GPT (named G5), and three with 20 wt% GPT (named G20) (Table 1). At the same time, 3 wt% of the TPO photoinitiator was dissolved in less than one milliliter of acetone and added to the compositions of acrylated oils. Finally, liquid coatings were applied on 130 mm × 130 mm × 6.2 mm 5-layer birch plywood substrate using an applicator with a wet film thickness of 5 mils (127 microns). One coating specimen occupied an area of approximately 100 cm^2 of plywood. Samples were then cured under monochromatic conditions (λ = 405 nm) at a UV intensity of 0.13 $\mu W/cm^2$ at a distance of 3 cm. The optimal curing, i.e., crosslinking,

time of coatings was 70 s, determined by FT-IR spectroscopy, as described in our previous work [6]. The conversion of vegetable oil acrylic double bonds ranged from 70 to 90%, which can be seen in Supplementary Materials Figure S1. Acrylates subjected to radical polymerization are vulnerable to inhibition by molecular oxygen, leading to incomplete curing, particularly manifested by a tacky upper surface or even complete non-curing [26]. For this reason, samples were washed with acetone to remove the unreacted resin. In addition, free-standing coating films were obtained by applying resin on the glass substrate before they were peeled off. Properties such as storage modulus and tensile strength were measured from the prepared free-standing films.

Table 1. Resin composition of biobased acrylates for wood coating application.

Biobased Resins	Resin Composition	Monomers (wt%)			
		R	L	G	GPT
RL	R/L (50/50)	50	50	0	0
RG	R/G (50/50)	50	0	50	0
LG	L/G (50/50)	0	50	50	0
RL_G5	R/L (50/50) 95 wt%, GPT 5 wt%	47.5	47.5	0	5
RG_G5	R/G (50/50) 95 wt%, GPT 5 wt%	47.5	0	47.5	5
LG_G5	L/G (50/50) 95 wt%, GPT 5 wt%	0	47.5	47.5	5
RL_G20	R/L (50/50) 80 wt%, GPT 20 wt%	40	40	0	20
RG_G20	R/G (50/50) 80 wt%, GPT 20 wt%	40	0	40	20
LG_G20	L/G (50/50) 80 wt%, GPT 20 wt%	0	40	40	20

2.3. Viscosity

The viscosity of liquid coating resin was measured using an MCR102 rheometer from Anton Paar (Graz, Austria). The instrument was equipped with a 25 mm diameter spindle with plate-plate geometry, and the measurement gap was set to 0.1 mm. The changes in the viscosities with temperature were calculated using the Arrhenius relationship:

$$\eta = \eta_0 e^{\frac{E_a}{RT}} \quad (1)$$

where η (Pa·s)—viscosity, η_0—pre-factor, E_a (J/mol)—activation energy for the viscous flow, R = 8.31 (J/K·mol)—ideal gas constant, and T (K)—absolute temperature.

2.4. Scanning Electron Microscopy

Scanning electron microscopy (SEM) was used for the surface morphology studies of coated plywood using a NovaNano SEM 650 (Hillsboro, OR, USA). The fracture surface was prepared with liquid nitrogen, and images were taken of the cross-sections of the coatings. The samples were attached to standard aluminum pin stubs with electrically conductive double-sided carbon tape, and the image was generated with 10 kV acceleration voltage coatings.

2.5. Dynamic Mechanical Analysis

The storage modulus, loss modulus, and loss factor of the cured free-standing coating films were recorded using a dynamic mechanical analysis (DMA) Mettler DMA/SDTA861e (Mettler Toledo, Columbus, OH, USA) analyzer. An experiment was carried out in tension mode from −70 to 100 °C with a 3 °C/min heating rate, the applied force of 10 N and 10 μm elongation, and a frequency of 1 Hz. The glass transition temperature (T_g) was defined by the maximum of the loss modulus curve. The photopolymerized coating films were prepared with dimensions of 20 mm × 4 mm and a thickness of approximately 0.2 mm. The crosslink density (ν_e) was calculated according to an equation from the literature [27]:

$$\nu_e = \frac{E'}{3RT'} \quad (2)$$

where ν_e (mol/m³)—molar concentration of crosslinks, E' (Pa)—represents the storage modulus of the samples at the rubbery plateau, R = 8.31 (J/K·mol)—universal gas constant, and T' (K)—temperature corresponding to the storage modulus value.

2.6. Tensile Tests

Tensile tests were performed on cured free-standing coating films with dimensions of 40 × 10 and a thickness of approximately 0.2 mm to study the tensile behavior of coatings. Elongation at break, tensile strength, and Young's modulus were recorded on Tinius Olsen model 25ST (Horsham, PA, USA). All tensile tests were conducted at a strain rate of 1 mm/min and were repeated at least five times. The average results were reported.

2.7. Pull-Off Adhesion Test

Pull-off adhesion tests were adopted to observe the interfacial bonding between AVO coatings and birch plywood substrate based on modified LVS EN ISO 4624:2003. First, the AVO coatings were applied on the plywood substrate using an applicator before it was treated with sandpaper (medium grit), providing a smooth plywood surface. The coatings were then cured under UV light. Next, 20 mm metal dollies were sanded with 80- and 180-grit sandpapers and cleaned with isopropanol. Then, 2K Bison epoxy resin glue was used as an adhesive. Dollies were glued to the coating surface at least 25 mm apart, and the adhesive was allowed to cure for 24 h. After that, the cut along the circumferences of the dollies was performed and the dollies were pulled off using a PoliTest AT-M adhesion tester at 0.25 MPa/s load intensity. The measurements were repeated six times, and the average result was reported. After the removal of the dolly, a visual examination of the surface was performed to determine the nature of joint failure (cohesive, adhesive, or mixed).

2.8. Photo-Oxidation

Photo-oxidation of the coated plywood was carried out under an Hg-UV lamp with an intensity of 9400 mW/cm², at a distance of 30 cm.

2.9. Microhardness

Microhardness testing of photo-oxidized wood coatings was performed with Vickers, Vickers Instruments (York, UK). The Vickers microhardness (in MPa) was determined according to the equation:

$$Microhardness = \frac{2 \cdot P \cdot 9.807 \cdot \sin\left(\frac{\alpha}{2}\right)}{\left(d \cdot k \cdot \frac{n}{1000}\right)^2} = 1.854 \cdot \frac{P \cdot 9.807}{\left(d \cdot k \cdot \frac{n}{1000}\right)^2} \quad (3)$$

where P—load (kg); α—angle between opposite faces of the diamond = 136°; n—interval; d—mean diagonal of the indentation (mm); k—equipment coefficient that depends on applied load.

The typical Vickers diamond pyramid was used as an indenter (apex angle of 136°), which was forced onto the surface of the specimens. Then, the 0.2 kg load was selected with an indentation time of 30 s. The area of the remaining indentation after the retraction of the diamond pyramid was calculated from the remaining imprint's diagonals visible in the microscope. Indentation diagonals were measured under a magnification of 4×. The test was repeated three times, and an average result was reported.

2.10. Sliding Friction Test

Sliding friction measurements were performed on coated plywood using a pin-on-disc tribometer *TRB*³ (CSM Instruments, Peseux, CH) under dry friction conditions according to ASTM G99-05 ("Standard test method for wear testing with a pin-on-disk machine"). Investigated coatings were tested against a standardized 100Cr6 (EN 683-17 "Heat-treated steels, alloy steels and free-cutting steels—Part 17: Ball and roller bearing steels") steel ball (Ø 6 mm) as a stationary counter body or triboindenter. All the tribotests were performed for a 25 m sliding distance applying the indenter load of 0.5, 1.5, and 3.0 N; the tribotrack radius was set to 3 mm, and there was a linear sliding speed of 0.03 m/s. All tests took place at room temperature.

3. Results and Discussion

3.1. Physical Properties

Viscosity is affected by the fatty acid chain length and degree of unsaturation [28]. The viscosity of liquid vegetable oil-based coating resins decreased with reactive diluents (Figure 2a). Acrylated vegetable oils (AVOs) were mixed with propoxylated glycerol triacrylate (GPT), which acts as a reactive diluent during resin formulation and becomes an integral part of the coating during curing [29]. The addition of GPT monomer to the AVO reduced the viscosity by an average of 550 mPa·s for all three resins. Viscosity affects molecular mobility when exposed to UV irradiation. Low viscosity affects the diffusion of the reactive species and therefore increases the mobility of the monomers. Zong et al. concluded that relative reactivity is proportional to viscosity [30]. The authors added vinyl ether that reduced the viscosity of the resin and led to higher diffusion rates for the propagating cationic species, resulting in the acceleration of linseed oil derivative polymerization. The increased mobility of the molecules increases the lifespan of free radicals, thus reducing disproportionation and termination reactions [31].

The Arrhenius relationship (Equation (1)) was used to assess how viscosities changed with temperature. Calculating the pre-factor η_0 requires extrapolating to infinite temperature; therefore, it is very challenging to measure it accurately. Viscosity decreased exponentially with temperature (Supplementary Materials Figure S2). As a result, a slight increase in the temperature of the acrylated resins can reduce their viscosities significantly, which makes them easier to process. The viscosities of resins that include GPT varied only slightly compared with AVOs; nevertheless, that influenced the activation energy (E_a). For RG samples, we observed a linear decrease in E_a with an increase in GPT content (Figure 2b). The GPT molecule is smaller than AVOs' molecules, decreasing and disrupting the intermolecular interactions among the larger AVO monomers [32]. Thus, monomer molecules can slide past one another, reducing the activation energy for viscous flow [33].

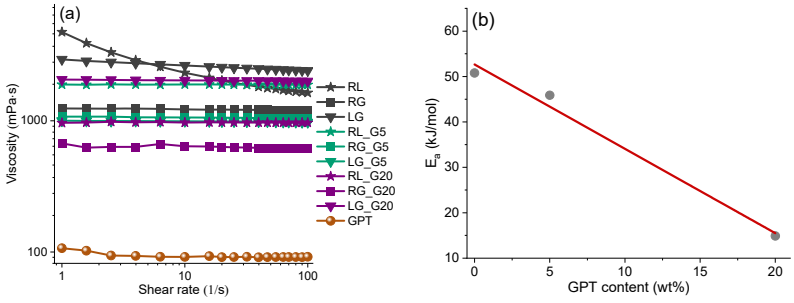

Figure 2. (**a**) Viscosity of acrylated vegetable oil resins with GPT; (**b**) activation energy (E_a) drop with an increasing GPT content in RG coating.

AVOs and GPT are mutually soluble when in the form of monomers (Table 2). To determine the polarity of GPT, its solubility was tested in four different solvents with an increasing polarity. As expected, GPT dissolved in ethanol and methanol, confirming the polar characteristic of the molecule. This was also supported by the fact that GPT was insoluble in non-polar rapeseed oil. The polarity of the GPT molecule is most similar to that of alcohol, while water is too polar for GPT.

Table 2. Solubility of GPT monomer in different solvents at room temperature.

	Liquid	GPT Solubility
Increased polarity ↓	Rapeseed oil	Insoluble
	AVOs	Soluble
	Ethanol	Soluble
	Methanol	Soluble
	Water	Insoluble

3.2. SEM Structure Studies

The cross-section images of RL, RL_G5, and RL_G20 coatings were obtained with SEM (Figure 3). SEM revealed the formation of two phases in the microstructure when GPT was added. Induced microstructure directly relates to the separation behavior and local order of reactive groups [34]. Two distinctly different types of microstructures can be observed. GPT as a photocurable polar monomer segregated in domains, creating cavities in the AVO-rich microphase. Likewise, more hydrophobic AVOs will preferentially segregate in the oil-soluble domains because of the existing long alkyl chains [34]. Large local inclusions can be observed in sample RL_G5 (Figure 3a). It is assumed that one phase was formed by the AVO matrix, while the other phase was formed by the AVO regions that were saturated with GPT. This type of microstructure should result in lowered mechanical properties as this type of morphology promotes local stress concentrations. The addition of 20 wt% GPT resulted in a much finer microstructure with the mixed phase of AVOs and GPT dominating, while regions of saturated GPT became almost invisible in the same magnification (Figure 3b). In addition, the cross-section of RL_20 was much rougher than RL_G5 and RL in 10,000× magnification, indicating that a toughened microstructure was formed, which should result in enhanced mechanical properties (Supplementary Materials Figure S3).

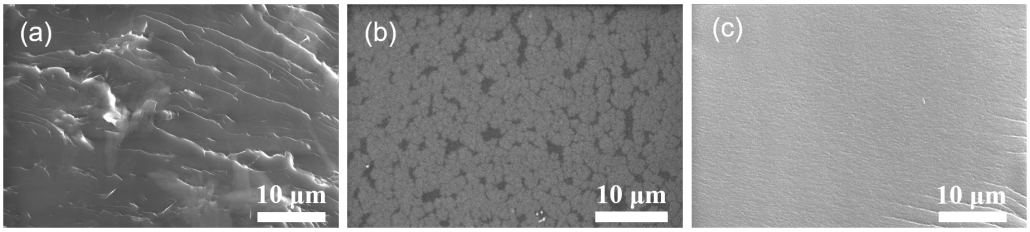

Figure 3. Cross-section SEM micrographs of the fracture surface morphology of (**a**) RL, (**b**) RL_G5, and (**c**) RL_G20 in 2500× magnification.

3.3. Dynamic Mechanical Properties

A dynamic mechanical analysis (DMA) was conducted on free-standing coating films. The DMA graphs are shown in Figure 4, and some defining characteristics are given in Table 3. Glass transition temperatures (T_g) were determined from the maximum of loss modulus (E″), which was described as a more precise method rather than determination from tanδ peaks (Figure 4b) [35]. The storage modulus for all coatings was very high at low temperatures when the material was in a glassy state, especially for coatings with 20

wt% GPT. It decreased rapidly with the temperature rise until the rubbery plateau was reached. As the GPT content increased from 0 wt% to 20 wt%, the E′ of coatings increased by 15 MPa at room temperature.

Table 3. Mechanical properties of coatings.

Coatings	T_g (°C) [1]	E′ at Rubbery Plateau (MPa)	ν_e (mol/m^3)	Tensile Strength (MPa)	Elongation at Break (%)
RL	−34.0	13	1.5	0.70 ± 0.10	10.7 ± 1.5
RG	−40.6	8	1.1	0.52 ± 0.08	6.3 ± 1.0
LG	−37.6	7	0.7	0.48 ± 0.02	8.1 ± 1.1
RL_G5	−42.3	7	1.0	0.27 ± 0.06	2.7 ± 0.5
RG_G5	−31.2	13	1.7	0.34 ± 0.05	3.8 ± 0.4
LG_G5	−24.7	11	1.4	0.20 ± 0.04	2.2 ± 0.2
RL_G20	−31.3	17	2.1	0.76 ± 0.10	5.3 ± 0.6
RG_G20	−30.4	17	2.2	0.64 ± 0.16	3.5 ± 0.1
LG_G20	−32.1	13	1.9	0.67 ± 0.12	4.1 ± 0.1

[1] Obtained from loss modulus curve.

The loss modulus characterizes the dissipated energy and thus signifies the viscous response of the sample. The loss modulus curves reached a maximum with a temperature rise and then decreased due to the maximum energy dissipation brought on by the free movement of the polymeric chains [36]. A correlation between the added GPT content and T_g can be seen. RL_G20, RG_G20, and LG_G20 had T_g 2.7, 10.2, and 5.5 °C higher than their corresponding RL, RG, and LG coatings. T_g shifted to the right due to a decrease in chain mobility and a loss of free volume, which were also the effects of increased crosslinking [37]. However, the T_g values of RL_G5, RG_G5, and LG_G5 were fluctuating due to the local inhomogeneities. The fatty acids in vegetable oils act as plasticizers, allowing more flexibility between the chains and resulting in relatively low T_g values [38]. The fatty acids enlarge the linear chains; therefore, the energy required to cause rotations around molecular bonds is reduced. As a result, the glass transition temperature shifts to relatively low temperatures [37].

As the GPT concentration increased, the tanδ maximum shifted to the right, while the decrease in the height of the tanδ curve for coatings with 20 wt% GPT confirmed the reduced polymer chain mobility and, therefore, higher crosslink density. However, the limited concentration of crosslinked polymers must always be considered. For example, the effect of styrene was examined in soybean oil-based thermosets, where the crosslinking density increased with the styrene content up to 20 wt% but decreased beyond that with an increasing styrene concentration [39]. The change in shape and width of the tanδ peak of the coatings with GPT suggested that the crosslinked network became more complex. Here, the broad peaks indicated the formation of two phases which were prominently seen in compositions with 20 wt% GPT. More time was needed for the relaxation of molecules due to the lower polymeric chain movement resulting from the formation of higher crosslinking densities [36]. Yin et al. compared interpenetrating polymer networks (IPN) prepared from polyurethanes and cottonseed, tung, and castor oil derivatives [40]. Different tanδ peak widths were observed and explained by the competition between two processes in the IPN formation: firstly, polymer chain migration which causes phase separation; and secondly, the interpenetration (chain entanglement) between the two networks, which prevents phase separation. The proposed processes that occur in IPN could apply to the AVO/GPT system, while the presence of the acrylate group in both components suggests that the existence of two fully independent networks is unlikely.

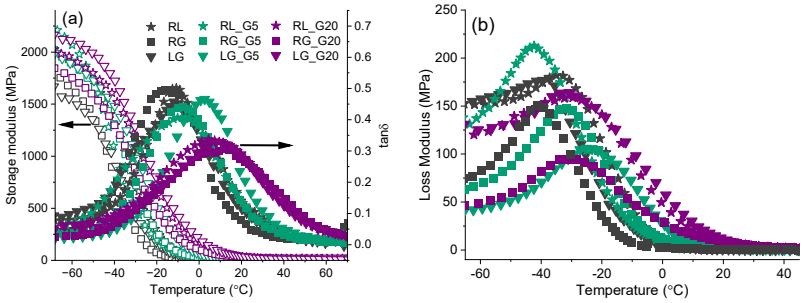

Figure 4. DMA plots for photopolymerized AVO coating films: (**a**) storage modulus and tanδ; (**b**) loss modulus.

3.4. Tensile Properties

The tensile properties of free-standing coating films are shown in Figure 5 and the results are displayed in Table 3. The addition of GPT to AVOs significantly changed the tensile curves (Figure 5a). The addition of 5 wt% GPT yielded overall reduced properties, while samples with 20 wt% GPT increased the stiffness and enhanced the tensile strength of AVOs. Tensile strength depended on crosslink density, the rigidity of the formed crosslinks, the uniformity of the crosslink distribution, and crosslinking agent penetration. Increasing the concentration of GPT in the polymer system provided a higher crosslink density (ν_e in Table 3) and thus a higher Young's modulus (E) (Figure 5b), which correlates with higher hardness [41]. Coating films with 5 wt% GPT showed lower tensile properties, which could be attributed to the formation of stress concentration promoting local inclusions described in the SEM analysis. A non-uniform crosslinking distribution and boundary regions between phases reduce the tensile strength [42]. In addition, the limited orientation of the long triglyceride molecules can cause high tensile strength loss [43]. The slight increase in Young's modulus for samples with 5 wt% GPT could be explained by the reduced content of oils, which contain saturated fatty acid moieties.

Propylene glycol units present in GPT may influence Young's modulus [44]. The addition of GPT increased the modulus up to 20.3 MPa, achieving a 2.0- to 2.6-fold increase compared to coating films without GPT. It can be seen that the most considerable contribution to the elongation of coatings came from linseed oil. This can be explained by the amount of saturated fatty acids in linseed oil (approx. 11.3%). As saturated fatty acids cannot be acrylated, they act as plasticizers [23]. Elongation at break for samples with GPT was below 6%, confirming structural changes induced by the enhanced crosslink density [20].

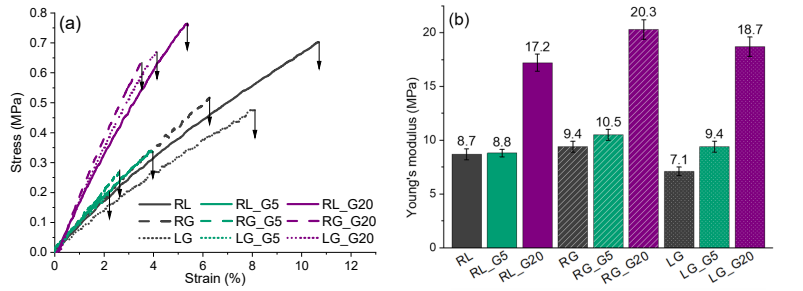

Figure 5. Tensile strength of vegetable oil-based coatings; (**a**) stress–strain curves; (**b**) Young's modulus.

3.5. Adhesion Strength

The coating can only effectively achieve other functions when the interface between it and the substrate is reliable and robust. The pull-off adhesion test was used to evaluate the coating's adhesion to birch plywood. The way the wood substrate is treated and prepared is essential. Surface energy and associated morphology play a crucial role in determining the interfacial parameters, regardless of polymer-coating properties.

The adhesion of coatings presents the combined performance of the two-phase interface between AVO and plywood, which directly affects the lifespan of the substrate. To demonstrate the adhesion strength, we conducted the test only for RL coatings. As shown in Table 4, the force required to remove the AVO coating from the substrate increased with increasing GPT content. The pull-off strength increased from 0.56 MPa for RL to 1.21 MPa for RL_G20. Hence, GPT contributed to a 0.65 MPa increase, which was more than half of the adhesion strength of the RL_G20. In comparison, the interfacial adhesion between the AESO coating and the starch membrane was reported to be around 2 MPa and was improved after surface treatment with (3-aminopropyl) triethoxysilane (APTES) [45].

After the test, a visual approach was used to determine the type of failure of the coating materials (Figure 6). In both cases with GPT, the failure pattern was mixed (Figure 6b,c). We could observe a failure of the bond between the applied coating and substrate as well as a cohesive failure of the coating itself. In the case of RL (Figure 6a), a glue failure between the applied coating and epoxy resin predominated. In all cases, there were no visible wood fibers remaining on the samples, which means that the substrate failure did not occur. The reason could be the non-sufficient penetrating of resin into the wood substrate, as well as the lack of intramolecular bonds between the coating and wooden substrate. There is potential room for improvement and a future investigation is needed. The RL coating remained tacky, even after the treatment with acetone. The adhesive was practically applied to the surface's unpolymerized part and did not stick properly. Therefore, the coating itself should be able to withstand more stress. This was due to the presence of oxygen as a free radical scavenger during photopolymerization, thus competing with acrylic radicals formed during UV-curing. In some cases, amines are used as oxygen scavengers and function as an efficient sacrificial site for hydrogen and electron abstraction reactions, protecting the material structure [46].

Table 4. Coatings' pull-off strength with the evaluation of the type of failure.

Coatings	Average Adhesion Strength (MPa)	Type of Failure
RL	0.56 ± 0.12	Glue failure
RL_G5	0.87 ± 0.15	Mixed (adhesive + cohesive failure)
RL_G20	1.21 ± 0.14	Mixed (adhesive + cohesive failure)

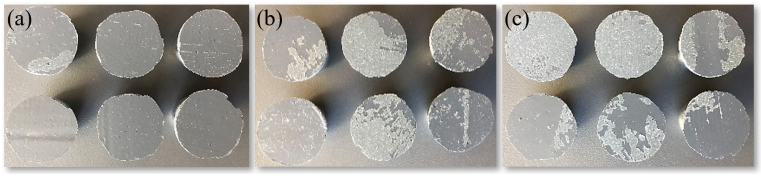

Figure 6. Failure patterns of coating materials (**a**) RL; (**b**) RL_G5; (**c**) RL_G20.

3.6. Photo-Oxidation Effect on Coatings' Properties

Photo-oxidation of coated plywood was conducted under an Hg-UV lamp for up to 9 h. Microhardness measurements were performed at the surface of photo-oxidized coatings, calculated according to Equation (3), and presented as a function of irradiation time (Figure 7a). The microhardness test was not applicable for AVOs without a GPT monomer

because of the observed self-healing effect (the samples were too soft to detect the indentation). Figure 7a reveals a significant increase in microhardness during the irradiation for coatings with added GPT. The microhardness of coatings with 5 wt% of GPT remained constant after about the first hour of exposure, but for coatings with 20 wt% of GPT, the microhardness continued to increase and continuously harden. Local inclusions in coatings with 5 wt% of GPT reflected the relatively lower microhardness, reaching values below 100 MPa. In the case of coatings with 20 wt% GPT, microhardness increased up to 250 MPa, showing the effect of tri-functional acrylic groups on coating strength. During photo-oxidation, crosslinked structures can be produced by any bimolecular combination of radicals. It is essential to know that in the early stages of photo-oxidation, chain scission reactions are less common than oxidative crosslinking coupling. For this reason, there is an increase in the stiffness of the oxidized layer. Dupuis et al. concluded that at short irradiation times, the crosslinking reactions regulate changes in the top surface's mechanical properties, whereas at longer irradiation times, the β scission reactions become more competitive and reduce the surface stiffness. They measured an increase in crosslink density upon aging by analyzing the T_g of the upper layer of the sample and the bulk material. An increase of 7 °C was detected for the upper layer, while T_g of the bulk material remained unchanged, confirming that new crosslinks were formed mainly in the upper layer of the coating [47].

Microhardness as a micromechanical characteristic plays a role as a connecting link between the structure and micromechanical properties. In recent studies, microhardness was reported for different vegetable oil derivatives. Linseed oil epoxide together with epoxidized glycerol, methyl-tetrahydrophtalic anhydride as a curing agent, and 2-methylimidazole as an initiator reached a microhardness of approximately 160 MPa after 100 h of irradiation [47]. For epoxidized soybean oil, the microhardness was reported to be around 58 MPa [48]. Compared to epoxidized soybean oil, acrylated epoxidized soybean oil had a higher microhardness by more than 50%, and a slightly higher indentation elastic modulus [49]. The polyurethane derivative synthesized from rapeseed oil polyol showed a microhardness of 178 MPa [50]. However, in a dicyclopentadiene-based tetrapolymer system, linseed oil lowered the hardness [51]. Hence, it can be seen from the comparison that the obtained coatings RL_G20 and LG_G20 showed competitive microhardness or even higher values than the ones reported in the reviewed literature.

A direct relationship was observed between Vickers microhardness and Young's modulus, or tensile strength for the cured acrylate coatings with GPT. Acrylate systems showed an excellent linear relationship ($R^2 = 0.9732$) when plotting microhardness vs. E as depicted in Figure 7b. The equation is as follows: microhardness = aE^b [48]. The relationship between microhardness and Young's modulus relates to materials' stiffness because both depend on the material's structure and the corresponding intra- and intermolecular interactions. This proportional dependence has been developed for many systems, such as ultrahigh molecular weight polyethylene, copolymers of ethylene-α-olefins, and highly oriented polyethylene [52]. It is proposed that microhardness could be used as an indicator of Young's modulus in some specimens that do not easily lend themselves to routine testing procedures [53]. A slightly poorer relationship was observed between tensile strength and microhardness ($R^2 = 0.8317$). The plywood color shifted to darker during UV exposure (Figure 7c), while coatings retained good clarity and transparency.

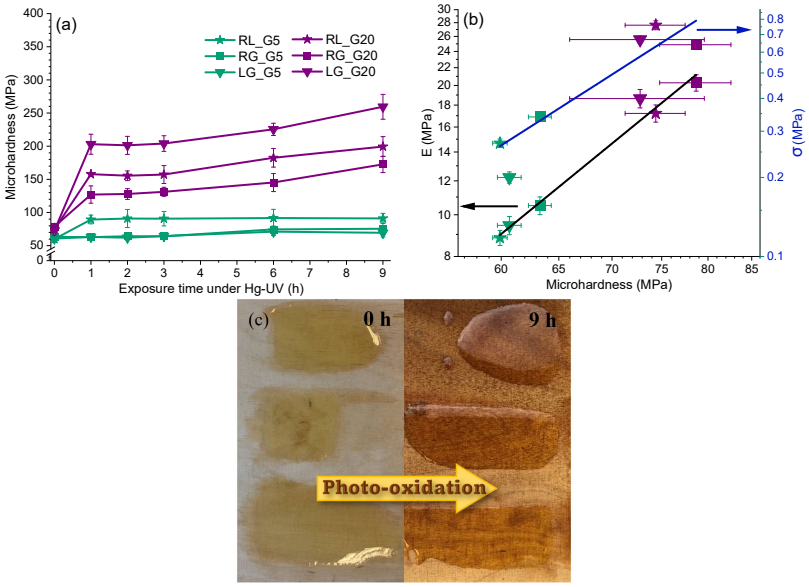

Figure 7. (**a**) Change of microhardness of coatings with GPT during Hg-UV exposure; (**b**) linear relationship between microhardness (0 h) and Young's modulus or tensile strength for coatings with GPT (log-log scale); (**c**) plywood and coatings after 9 h of photo-oxidation.

3.7. Sliding Friction

The coefficient of friction (μ) between two solids is defined as F/N where F denotes the friction force and N the load or the force normal to the surface, and it is independent of the apparent area of contact [54]. To determine the performance and durability of the wood coatings after 9 h of photo-oxidation, which serves as degradation, sliding friction was measured. RL, RL_G5, and RL_G20 were selected as representative photo-oxidized coating samples for the test. Experiments were conducted under three indenter loads: 0.5, 1.5, and 3.0 N. The coefficient of friction values is displayed in Table 5 as an average of the constant plateau zone of the measurement, where the friction pair adjustment process ("run-in") and final part ("run-off") are not considered. Figure S4 in Supplementary Materials demonstrates μ vs. sliding distance or time, or laps, in which the μ at the plateau is plotted. The RL_G5 sample at load 1.5 N and 3.0 N displayed a stable μ value, increasing to a high steady-state value ($0.6 < \mu < 0.9$) and reaching a plateau. In contrast, the sample at 0.5 N load reached the plateau gradually. When the applied load was increased from 0.5 N to 1.5 N, an increase of μ was observed. When the load was increased further up to 3N, the μ decreased for RL and RL_G20 but increased for RL_G5. A similar trend was reported with linseed oil as the metal coating. μ ranged from ~1.0 up to ~1.5 for linseed oil cured under different UV radiation intensities (100 and 300 mJ/cm^2), but μ decreased below 0.2 when the sample was additionally cured thermally at 80 °C after the UV irradiation [55]. Wang et al. investigated the lubricating properties of palm oil-based nanofluids. The authors reported that carbon nanotubes (CNTs) could reduce the sliding friction force due to their high strength and hardness, as CNTs will not be ground into a hard film under heavy loads [56]. Another study measured μ for epoxidized soybean oil, which was around 0.11 under dry conditions [48].

Resistance to sliding depends on the surface morphology of the polymer, and, in many instances, this morphology is affected by sliding [57]. Optical microscopy images in

Figure 8 represent the wear of coating after the test. When a hard slider is pressed into a soft polymer, the surface is extended [57]. Thereby, indentations were formed in the RL and RL_G5 coatings. Indentations for the RL and RL_G5 samples occurred when the 1.5 N load was added. However, RL_G20 remained smooth and showed only the path formed by the sliding ball. The width of the wear track increased as the applied load increased. For RL_G20, it rose from 0.242 to 0.372 and up to 0.544 mm for 0.5, 1.5, and 3.0 N, respectively. This was due to the depth of penetration of the metal ball in coating.

Table 5. Coefficient of friction values for photo-oxidized samples.

Photo-Oxidized (9 h) Coatings	μ (in Plateau Zone)		
	0.5 (N)	1.5 (N)	3.0 (N)
RL	0.24	0.88	0.79
RL_G5	0.42	0.65	0.80
RL_G20	0.21	0.47	0.31

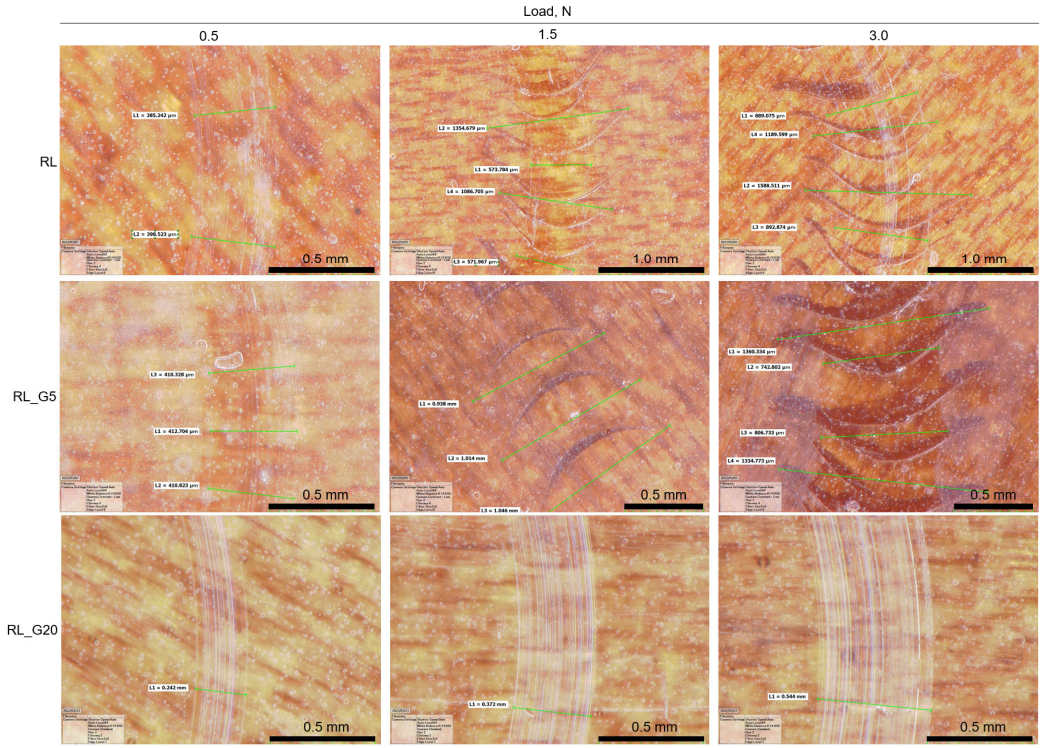

Figure 8. Optical microscopy photos of photo-oxidized (9 h) wood coating samples after sliding friction test at different loads.

4. Conclusions

The present study explored biobased resins that introduced two-phase microstructures after UV-curing. The testing was limited to potential applications for wood surfaces but was not limited to this purpose. The viscosity of AVOs decreased by an average of 550

mPa·s with the addition of a propoxylated glycerol triacrylate (GPT) monomer. The addition of the GPT monomer to acrylated vegetable oils (AVOs) resulted in two distinct effects based on the added loading: 5 or 20 wt%. The addition of 5 wt% resulted in the partial formation of the GPT network, which contributed to a pronounced two-phase separation in the microstructure and relatively large boundaries between phases. As a result, the tensile properties saw a significant decrease, and the glass transition temperature was inconsistent. Increasing GPT content yielded a much finer and well-dispersed microstructure. The addition of 20 wt% of GPT resulted in an enhanced tensile performance, dynamic mechanical properties, and increased glass transition temperature. The addition of GPT increased the storage modulus by up to five-fold, Young's modulus by up to two-fold at 20 °C, and the crosslink density by up to two-fold. Exposure to photo-oxidation enhanced the microhardness, which reached the maximum value of 250 MPa for LG_G20. The coatings remained clear and transparent after the photo-oxidation induced aging.

Supplementary Materials: The following supporting information can be downloaded at: https://www.mdpi.com/article/10.3390/coatings13030657/s1, Figure S1: Conversion of acrylic double bonds in coating samples; Figure S2: Viscosity and temperature relation for coating samples; Figure S3: Cross-section SEM micrographs of the fracture surface morphology; Figure S4: Photo-oxidized (9 h) coating friction coefficient dependance on applied indenter load, time, distance, and number of laps.

Author Contributions: Conceptualization, S.G.; methodology, S.G.; software, S.B.; validation, S.G.; formal analysis, S.B.; investigation, S.B., I.S., A.L., J.L.; resources, S.G.; writing—original draft preparation, S.B., S.G.; writing—review and editing, O.P., A.B., S.G.; visualization, S.B., S.G.; supervision, S.G.; project administration, S.G.; funding acquisition, S.G. All authors have read and agreed to the published version of the manuscript.

Funding: Sabine Briede was funded by the European Social Fund within the Project No 8.2.2.0/20/I/008 «Strengthening of PhD students and academic personnel of Riga Technical University and BA School of Business and Finance in the strategic fields of specialization» of the Specific Objective 8.2.2 «To Strengthen Academic Staff of Higher Education Institutions in Strategic Specialization Areas» of the Operational Programme «Growth and Employment». Sabine Briede was supported by Riga Technical University's Doctoral Grant programme.

Institutional Review Board Statement: Not applicable.

Informed Consent Statement: Not applicable.

Data Availability Statement: Data will be made available on request.

Acknowledgments: The authors wish to thank their parental institute for providing the necessary facilities to accomplish this work.

Conflicts of Interest: The authors declare no conflict of interest.

References

1. Cunningham, M.F.; Campbell, J.D.; Fu, Z.; Bohling, J.; Leroux, J.G.; Mabee, W.; Robert, T. Future green chemistry and sustainability needs in polymeric coatings. *Green Chem.* **2019**, *21*, 4919–4926.
2. Valet, A. Outdoor applications of UV curable clearcoats-a real alternative to thermally cured clearcoats. *Prog. Org. Coat.* **1999**, *35*, 223–233.
3. Rafiq, M.; Lv, Y.Z.; Zhou, Y.; Ma, K.B.; Wang, W.; Li, C.R.; Wang, Q. Use of vegetable oils as transformer oils–a review. *Renew. Sustain. Energy Rev.* **2015**, *52*, 308–324.
4. Wang, R.; Schuman, T.P. Vegetable oil-derived epoxy monomers and polymer blends: A comparative study with review. *Express Polym. Lett.* **2013**, *7*, 272–292.
5. Mendoza, G.; Igartua, A.; Fernandez-Diaz, B.; Urquiola, F.; Vivanco, S.; Arguizoniz, R. Vegetable oils as hydraulic fluids for agricultural applications. *Grasas Y Aceites* **2011**, *62*, 29–38.
6. Briede, S.; Jurinovs, M.; Nechausov, S.; Platnieks, O.; Gaidukovs, S. State-of-the-art UV-assisted 3D printing via a rapid syringe-extrusion approach for photoactive vegetable oil acrylates produced in one-step synthesis. *Mol. Syst. Des. Eng.* **2022**, *7*, 1434–1448.
7. Wuzella, G.; Mahendran, A.R.; Müller, U.; Kandelbauer, A.; Teischinger, A. Photocrosslinking of an Acrylated Epoxidized Linseed Oil: Kinetics and its Application for Optimized Wood Coatings. *J. Polym. Environ.* **2012**, *20*, 1063–1074.

8. Black, M.; Rawlins, J.W. Thiol–ene UV-curable coatings using vegetable oil macromonomers. *Eur. Polym. J.* **2009**, *45*, 1433–1441.
9. Thanamongkollit, N.; Miller, K.R.; Soucek, M.D. Synthesis of UV-curable tung oil and UV-curable tung oil based alkyd. *Prog. Org. Coat.* **2012**, *73*, 425–434.
10. Aung, M.M.; Yaakob, Z.; Abdullah, L.C.; Rayung, M.; Li, W.J. A comparative study of acrylate oligomer on Jatropha and Palm oil-based UV-curable surface coating. *Ind. Crops Prod.* **2015**, *77*, 1047–1052.
11. Grüneberger, F.; Künniger, T.; Zimmermann, T.; Arnold, M. Rheology of nanofibrillated cellulose/acrylate systems for coating applications. *Cellulose* **2014**, *21*, 1313–1326.
12. Wang, X.; Soucek, M.D. Investigation of non-isocyanate urethane dimethacrylate reactive diluents for UV-curable polyurethane coatings. *Prog. Org. Coat.* **2013**, *76*, 1057–1067.
13. Ma, Q.; Liu, X.; Zhang, R.; Zhu, J.; Jiang, Y. Synthesis and properties of full bio-based thermosetting resins from rosin acid and soybean oil: The role of rosin acid derivatives. *Green Chem.* **2013**, *15*, 1300–1310.
14. Rengasamy, S.; Mannari, V. Development of soy-based UV-curable acrylate oligomers and study of their film properties. *Prog. Org. Coat.* **2013**, *76*, 78–85.
15. Liu, H.; Lu, W.; Liu, S. Development of acrylated soybean oil-based UV-curable coatings with high impact strength from low viscosity oligomer. *J. Appl. Polym. Sci.* **2018**, *135*, 45698.
16. Fei, M.-E.; Liu, W.; Jia, A.; Ban, Y.; Qiu, R. Bamboo fibers composites based on styrene-free soybean-oil thermosets using meth-acrylates as reactive diluents. *Compos. Part A Appl. Sci. Manuf.* **2018**, *114*, 40–48.
17. Chu, Z.; Feng, Y.; Xie, B.; Yang, Y.; Hu, Y.; Zhou, X.; Yuan, T.; Yang, Z. Bio-based polyfunctional reactive diluent derived from tung oil by thiol-ene click reaction for high bio-content UV-LED curable coatings. *Ind. Crops Prod.* **2021**, *160*, 113117.
18. Zhang, Y.; Li, Y.; Wang, L.; Gao, Z.; Kessler, M.R. Synthesis and Characterization of Methacrylated Eugenol as a Sustainable Reactive Diluent for a Maleinated Acrylated Epoxidized Soybean Oil Resin. *ACS Sustain. Chem. Eng.* **2017**, *5*, 8876–8883.
19. Liu, W.; Xie, T.; Qiu, R. Biobased Thermosets Prepared from Rigid Isosorbide and Flexible Soybean Oil Derivatives. *ACS Sustain. Chem. Eng.* **2017**, *5*, 774–783.
20. Dai, J.; Liu, X.; Ma, S.; Wang, J.; Shen, X.; You, S.; Zhu, J. Soybean oil-based UV-curable coatings strengthened by crosslink agent derived from itaconic acid together with 2-hydroxyethyl methacrylate phosphate. *Prog. Org. Coat.* **2016**, *97*, 210–215.
21. Williams, R.J.J.; Rozenberg, B.A.; Pascault, J.-P. Reaction-induced phase separation in modified thermosetting polymers. In *Advances in Polymer Science*; Springer: Berlin/Heidelberg, Germany, 2005; pp. 95–156.
22. Mirzaee Ghazani, S.; Garcia-Llatas, G.; Marangoni, A. Micronutrient content of cold-pressed, hot-pressed, solvent extracted and RBD canola oil: Implications for nutrition and quality. *Eur. J. Lipid Sci. Technol.* **2014**, *116*, 380–387.
23. Taherkhani, M.; Hashemzadeh Gargari, M.; Sadrameli, S.M. Investigating the Batch and Continuous Biodiesel Production from Linseed Oil in the Presence of a Heterogeneous Based Catalyst in a Packed Bed Reactor. *J. Renew. Energy Environ.* **2018**, *148*, 888–895.
24. Garavaglia, J.; Markoski, M.M.; Oliveira, A.; Marcadenti, A. Grape Seed Oil Compounds: Biological and Chemical Actions for Health. *Nutr. Metab. Insights* **2016**, *2016*, 59.
25. Olivier, A.; Benkhaled, L.; Pakula, T.; Ewen, B.; Best, A.; Benmouna, M.; Maschke, U. Static and Dynamic Mechanical Behavior of Electron Beam-Cured Monomer and Monomer/Liquid Crystal Systems. *Macromol. Mater. Eng.* **2004**, *289*, 1047–1052.
26. Taki, K.; Watanabe, Y.; Ito, H.; Ohshima, M. Effect of oxygen inhibition on the kinetic constants of the UV-radical photopoly-merization of diurethane dimethacrylate/photoinitiator systems. *Macromolecules* **2014**, *47*, 1906–1913.
27. Hill, L.W. Calculation of crosslink density in short chain networks. *Prog. Org. Coat.* **1997**, *31*, 235–243.
28. Wardana, I.; Widodo, A.; Wijayanti, W. Improving vegetable oil properties by transforming fatty acid chain length in jatropha oil and coconut oil blends. *Energies* **2018**, *11*, 394.
29. Sharmin, E.; Zafar, F.; Akram, D.; Alam, M.; Ahmad, S. Recent advances in vegetable oils based environment friendly coatings: A review. *Ind. Crops Prod.* **2015**, *76*, 215–229.
30. Zong, Z.; Soucek, M.D.; Liu, Y.; Hu, J. Cationic photopolymerization of epoxynorbornane linseed oils: The effect of diluents. *J. Polym. Sci. Part A Polym. Chem.* **2003**, *41*, 3440–3456.
31. Anastasio, R.; Cardinaels, R.; Peters, G.W.M.; Breemen, L.C.A. Structure–mechanical property relationships in acrylate networks. *J. Appl. Polym. Sci.* **2019**, *137*, 48498.
32. Campanella, A.; La Scala, J.J.; Wool, R.P. The use of acrylated fatty acid methyl esters as styrene replacements in triglyceride-based thermosetting polymers. *Polym. Eng. Sci.* **2009**, *49*, 2384–2392.
33. LaScala, J.J.; Jeyarajasingam, A.; Winston, C.; Sand, J.M.; Palmese, G.R. *Predicting the Viscosity of Low VOC Vinyl Ester and Fatty Acid-Based Resins*; U.S. Army Research Laboratory, Aberdeen Proving Ground: Aberdeen Proving Ground, MD, USA, 2005.
34. Worthington, K.S.; Baguenard, C.; Forney, B.S.; Guymon, C.A. Photopolymerization kinetics in and of self-assembling lyotropic liquid crystal templates. *J. Polym. Sci. Part B Polym. Phys.* **2017**, *55*, 471–489.
35. Sun, Y.; Zhang, Z.; Moon, K.-S.; Wong, C.P. Glass transition and relaxation behavior of epoxy nanocomposites. *J. Polym. Sci. Part B: Polym. Phys.* **2004**, *42*, 3849–3858.
36. Hazarika, A.; Mandal, M.; Maji, T.K. Dynamic mechanical analysis, biodegradability and thermal stability of wood polymer nanocomposites. *Compos. Part B Eng.* **2014**, *60*, 568–576.
37. Núñez-Regueira, L.; Villanueva, M.; Fraga-Rivas, I. Effect of a reactive diluent on the curing and dynamomechanical properties of an epoxy-diamine system. *J. Therm. Anal. Calorim.* **2006**, *86*, 463–468.

38. Henna, P.H.; Andjelkovic, D.D.; Kundu, P.P.; Larock, R.C. Biobased thermosets from the free-radical copolymerization of conjugated linseed oil. *J. Appl. Polym. Sci.* **2007**, *104*, 979–985.
39. Lu, J.; Khot, S.; Wool, R.P. New sheet molding compound resins from soybean oil. I. Synthesis and characterization. *Polymer* **2005**, *46*, 71–80. https://doi.org/10.1016/j.polymer.2004.10.060.
40. Yin, Y.; Yao, S.; Zhou, X. Synthesis and dynamic mechanical behavior of crosslinked copolymers and IPNs from vegetable oils. *J. Appl. Polym. Sci.* **2003**, *88*, 1840–1842.
41. Coran, A.Y. Chapter 7–Vulcanization. In *The Science and Technology of Rubber*, 4th ed.; Mark, J.E., Erman, B., Roland, C.M., Eds.; Academic Press: Boston, MA, USA, 2013; pp. 337–381.
42. Li, F.; Larock, R.C. New soybean oil-styrene-divinylbenzene thermosetting copolymers. III. Tensile stress-strain behavior. *J. Polym. Sci. Part B Polym. Phys.* **2001**, *39*, 60–77.
43. Zhou, L.M.; Yeung, K.W.; Yuen, C.W.M.; Zhou, X. Tensile Strength Loss of Mercerized and Crosslinked Ramie Fabric. *Text. Res. J.* **2003**, *74*, 367–372.
44. De Godoy Fróes-Salgado, N.R.; Gajewski, V.; Ornaghi, B.P.; Pfeifer, C.S.C.; Meier, M.M.; Xavier, T.A.; Braga, R.R. Influence of the base and diluent monomer on network characteristics and mechanical properties of neat resin and composite materials. *Odontology* **2014**, *103*, 160–168.
45. Chen, Y.; Duan, Q.; Zhu, J.; Liu, H.; Chen, L.; Yu, L. Anchor and bridge functions of APTES layer on interface between hydrophilic starch films and hydrophobic soyabean oil coating. *Carbohydr. Polym.* **2021**, *272*, 118450.
46. Allen, N.S.; Robinson, P.J.; White, N.J.; Swales, D.W. Photo-oxidative stability of electron-beam and UV cured triacrylate resin films: Influence of the structure of the multifunctional monomer. *Polym. Degrad. Stab.* **1989**, *23*, 245–255.
47. Dupuis, A.; Perrin, F.-X.; Ulloa Torres, A.; Habas, J.-P.; Belec, L.; Chailan, J.-F. Photo-oxidative degradation behavior of linseed oil based epoxy resin. *Polym. Degrad. Stab.* **2017**, *135*, 73–84.
48. Diez-Pascual, A.M.; Diez-Vicente, A.L. Epoxidized soybean oil/ZnO biocomposites for soft tissue applications: Preparation and characterization. *ACS Appl. Mater. Interfaces* **2014**, *6*, 17277–17288.
49. Rahman, M.S.B.A.; Shaktur, K.M.; Mohammad, R.; Zalikha, W.A.; Nawi, N.; Mohd, A.F. Optical properties and indentation hardness of thin-film acrylated epoxidized oil. *Opt. Eng.* **2012**, *51*, 025002.
50. Ivakina, K.; Skadins, E.; Kiyanitsa, A.; Gaidukov, S.; Tupureina, V.; Cabulis, U.; Maksimov, R.D. Influence of nanoclay additive on mechanical properties of bio-based polyurethane nanocomposites. *Proc. Key Eng. Mater.* **2013**, *559*, 37–42.
51. Smith, J.A.; Green, S.J.; Petcher, S.; Parker, D.J.; Zhang, B.; Worthington, M.J.; Wu, X.; Kelly, C.A.; Baker, T.; Gibson, C.T. Cross-linker copolymerization for property control in inverse vulcanization. *Chem.–A Eur. J.* **2019**, *25*, 10433–10440.
52. Zamfirova, G.; Lorenzo, V.; Benavente, R.; Pereña, J.M. On the relationship between modulus of elasticity and microhardness. *J. Appl. Polym. Sci.* **2003**, *88*, 1794–1798.
53. Evans, G.; Behiri, J.; Currey, J.; Bonfield, W. Microhardness and Young's modulus in cortical bone exhibiting a wide range of mineral volume fractions, and in a bone analogue. *J. Mater. Sci. : Mater. Med.* **1990**, *1*, 38–43.
54. Persson, B.N.J. *Sliding Friction: Physical Principles and Applications*; Springer Science & Business Media: Berlin/Heidelberg, Germany, 2013.
55. Bexell, U.; Olsson, M.; Johansson, M.; Samuelsson, J.; Sundell, P.-E. A tribological study of a novel pre-treatment with linseed oil bonded to mercaptosilane treated aluminium. *Surf. Coat. Technol.* **2003**, *166*, 141–152.
56. Wang, Y.; Li, C.; Zhang, Y.; Li, B.; Yang, M.; Zhang, X.; Guo, S.; Liu, G.; Zhai, M. Comparative evaluation of the lubricating properties of vegetable-oil-based nanofluids between frictional test and grinding experiment. *J. Manuf. Process.* **2017**, *26*, 94–104.
57. Bikerman, J.J. Sliding friction of polymers. *J. Macromol. Sci. Part C Polym. Rev.* **1974**, *11*, 1–44.

Pielikums II

Appendix II

Briede, S., Biemans, T., Platnieks, O., & Gaidukovs, S.

Tailored UV-curable acrylated linseed oil-based alkyds: Optimizing crosslinking and coating performance through functionalization and reactive diluent design

Polymer, **2025**, 323, 128227.

doi: 10.1016/j.polymer. 2025.128227

Polymer 323 (2025) 128227

Contents lists available at ScienceDirect

Polymer

journal homepage: www.elsevier.com/locate/polymer

Tailored UV-curable acrylated linseed oil-based alkyds: Optimizing crosslinking and coating performance through functionalization and reactive diluent design

Sabine Briede [a,*], Toine Biemans [b], Oskars Platnieks [a], Sergejs Gaidukovs [a,**]

[a] Institute of Chemistry and Chemical Technology, Faculty of Natural Sciences and Technology, Riga Technical University, P. Valdena 3/7, Riga LV-1048, Latvia
[b] Worlée Chemie GmbH, Worléestraße 1, Lauenburg, 21481, Germany

ARTICLE INFO

Keywords:
Alkyds
UV-Curing
Epoxidation
Acrylation
Bio-based wood coatings
Erichsen cupping
Pendulum hardness

ABSTRACT

This study outlines a safer and greener pathway for the synthesis of UV-curable acrylated linseed oil-based alkyds (ALO-A), introducing enhancement in bio-based coating performance while addressing environmental and industrial challenges. Building upon conventional methods, our optimized process integrates acrylic functionality directly into the alkyd backbone through an improved reaction pathway, offering a significant advancement in resin synthesis. This method eliminates halogenated reagents, reduces the need for excess acrylic acid, and supports rapid, VOC-free UV curing. To investigate the impact of acrylate functionality on coating properties, two strategies were employed: adjusting the number of acrylic groups integrated into the alkyd backbone and incorporating reactive diluents. Two ALO-A resins with 2.3 and 1.8 mmol of acrylic groups/g resin, determined by ^{1}H NMR, were synthesized. ALO-A resins were mixed with bio-based isobornyl acrylate (IBOA), tripropylene glycol diacrylate (TPGDA), or trimethylolpropane trimethacrylate (TMPTMA) in various ratios. Real-time photorheology demonstrated that higher acrylate functionality in ALO-A together with reactive diluents lowered the gel point to 3.0 s. The acrylate functionality led to a 2.2-fold difference in coating hardness, reaching a maximum pendulum hardness of 103 s. The incorporation of reactive diluents further enhanced hardness, achieving up to 2.9-fold with lower-functionality ALO-A and 1.7-fold with higher-functionality ALO-A (max. 174 s). Indentation tests revealed exceptional flexibility, showing up to 7.4 mm in Erichsen cupping. Adjusting the reagent ratio during ALO-A synthesis and incorporating reactive diluents offer two effective strategies for precise control over the mechanical performance of coatings. The comparison of these approaches highlights advancements in UV-curable coating design.

1. Introduction

Traditional alkyd resins cure via an oxidative-drying process that requires metal-based catalysts (containing, e.g., cobalt, manganese, and iron as primary driers) and can last several hours to achieve the "touch dry" stage to days or weeks to achieve full through drying and final hardness. Ultraviolet (UV)-curable alkyds have been of broad interest due to the advantage of being free of metal-containing catalysts and providing a fast curing process. Moreover, transporting traditional alkyd resins often means transporting significant amounts of non-solid material – a carrier such as water or solvent. In contrast, UV-curable alkyds are 100 % solid, enhancing transport efficiency and reducing unnecessary weight [1].

To obtain UV-curable alkyd resins, most researchers simply combine alkyd resins with compatible or soluble acrylates, epoxides, or siloxane compounds by mixing them [2–5]. A recent study explored an acrylation of the alkyd end groups using (meth)acryloyl chloride [6]. Some researchers incorporate additional unsaturation, for example, by adding maleic or fumaric acid into the alkyd structure [7–9]. A less studied approach to synthesizing UV-curable alkyd resins is to modify the less reactive fatty acid double bonds by incorporating acrylic groups. Unsaturated double-bond bromoacrylation with *N*-bromosuccinimide (NBS) requires only one step. The drawback of this method is the considerable excess of acrylic acid (AA). Eren et al. used 254 and 554

* Corresponding author.
** Corresponding author.
E-mail addresses: Sabine.Briede@rtu.lv (S. Briede), Sergejs.Gaidukovs@rtu.lv (S. Gaidukovs).

https://doi.org/10.1016/j.polymer.2025.128227
Received 20 December 2024; Received in revised form 20 February 2025; Accepted 2 March 2025
Available online 3 March 2025

times more mols of AA to acrylate methyl oleate and soybean oil, respectively. When authors used a lower excess of AA, they observed dibromination [10]. Moreover, halogenated reagents (such as NBS) are industrially undesirable due to their harmful environmental impact, potential health risks, and the challenges and costs associated with disposing of halogenated by-products.

Diels–Alder cycloaddition is another approach to obtain UV-curable fatty acid acrylates but requires a conjugated diene [11–13]. Thanamongkollit et al. demonstrated that the Diels–Alder adduct of TMPTMA with tung oil-based alkyd exhibited faster curing speed than the adduct with tung oil [14]. In another study, Chittavanich et al. mixed the same tung oil-based alkyd adduct with ten different reactive diluents. The authors obtained UV-curable alkyd paint films with excellent impact resistance (>40 lb/in.), flexibility (>32 % elongation by conical mandrel test), and adhesion (cross-cut adhesion of 5B) to the metal substrate when using isodecyl methacrylate – a long chain linear structure diluent. When using isobornyl acrylate (IBOA), films showed better gloss (99.6 at 60 °C) and hardness (pencil hardness of 2H) [15].

Regarding fatty acid double bond acrylation, Maaβen et al. compared three different acrylation pathways for fatty acid esters via one-, two-, and three-step routes. The one-step route comprised the bromoacrylation with NBS, as described before. Interestingly, the authors reduced the AA amount to ten equivalents and reached 89 % conversion and 66 % yield after purification. The two-step route comprised enzymatic epoxidation followed by ring-opening with AA. Authors reached up to 88 % conversion after acrylation and 64 % yield after purification. The three-step route comprised enzymatic epoxidation, ring-opening with methanol or ethanol, and acrylation (esterification) with acryloyl chloride. The authors achieved 72 % conversion after acrylation and 49 % yield after purification [16].

Although the acrylation of fatty acid esters and vegetable oils via epoxy ring-opening is well-documented, a significant gap remains in the realm of UV-curable alkyds—particularly concerning the development of green synthesis routes, how resin functionality influences the curing process and the associated mechanical property characterization. To address this, our synthesis strategy eliminates halogenated reagents (like NBS), significantly reduces the need for excess acrylic acid, and enables rapid, VOC-free UV curing. We began by synthesizing linseed oil-based alkyd resins (LO-A) through a one-step fatty acid process, followed by epoxidation and halogen-free acrylation using only 0.3 equivalents of excess acrylic acid (AA). This process yielded two alkyd resins with different epoxy values (EV), which allowed for varying acrylate functionalization. UV-curable formulations were then prepared by mixing acrylated linseed oil alkyds (ALO-A) of different functionalities with reactive diluents. The resins were applied to a wood substrate, UV-cured, and the coating properties were evaluated. To establish the relationship between mechanical performance and flexibility, we employed two industry-standard tests: pendulum hardness and Erichsen cupping. By systematically exploring the relationship between alkyd functionality, reactive diluent content, and coating performance, our study establishes a foundation for designing tailored UV-curable formulations. This enables the design of tailored formulations to meet specific performance demands, advancing the precision of UV-curable coating technologies.

2. Experimental

2.1. Materials

Linseed oil fatty acids (LOFA) were purchased from Oleon NV (Nouracid LE 80). Phthalic anhydride, triphenyl phosphite, acrylic acid (AA), and ethyl acetate (EtOAc) were purchased from Penpet. Formic acid (78 wt%) was purchased from Reher & Ramsden. Triphenylphosphine (TPP) and H_2O_2 (30 wt%) were purchased from Carl Roth. 4-Methoxyphenol (MEHQ) was purchased from Th. Geyer (Merck). Butylated hydroxytoluene (BHT) was purchased from Aldrich. Pentaerythritol was purchased from Perstorp. Xylene was purchased from BCD Chemie. Triethylamine (TEA) was purchased from Möller Chemie. Isobornyl acrylate (IBOA) was purchased from ECEM. Tripropylene glycol diacrylate (TPGDA; Miramer M220) and trimethylolpropane trimethacrylate (TMPTMA; Miramer 3130) was kindly supplied by Miwon. Ethyl (2,4,6-trimethylbenzoyl) phenylphosphinate (TPOL) was kindly supplied by BCH Brühl (Chemikalien Handel GmbH).

2.2. Linseed oil-based alkyd (LO-A) synthesis

LO-A was synthesized using the fatty acid process. The molar ratio of LOFA: phthalic acid anhydride: pentaerythritol was 4 : 1: 2. LOFA (1935.7 g), phthalic acid anhydride (255.8 g), pentaerythritol (470.1 g), triphenyl phosphite (6.2 g) and xylene (30 ml) were charged into a 4 L four-necked round-bottom flask equipped with a mechanical stirrer, Dean-Stark trap and reflux condenser. The reaction flask was thoroughly flushed with nitrogen gas and the system was heated to 200 °C and left for 1 h for water to form, which was azeotropically removed with xylene. After this initial stage, the reaction was heated to 240 °C. Reaction progress was monitored by measuring the acid value (AV), and it reached 3.7 mg KOH/g after about 4 h. Then, the reaction was cooled to 200 °C, and xylene was removed by distillation under vacuum. The structure of LO-A and concentration of fatty acid double bonds was determined using ^{1}H NMR spectroscopy and resulted in 4.9 mmol of double bonds/g resin (Fig. S1, Table 2). The end AV and OH value of LO-A is summarized in Table 2.

2.3. Epoxidation of LO-A (ELO-A)

The LO-A resin epoxidation was carried out in the presence of hydrogen peroxide and formic acid (Fig. 1a). By varying the molar ratio of H_2O_2, we synthesized two batches ((1) and (2)) of epoxidized linseed oil-based alkyd (ELO-A) with different amounts of epoxy groups (Table 2). For ELO-A (1) the molar ratio was as follows: 1 : 0.4: 1.8 (mole of fatty acid double bonds: mols of HCOOH: mols of H_2O_2). Formic acid (78 wt%) (31.69 g) was added to LO-based alkyd (300 g), stirred and heated up to 60 °C in a four-necked round-bottom flask equipped with a condenser, dropping funnel, thermocouple and mechanical stirrer. Then H_2O_2 (30 wt%) (304.7 g) was added dropwise through a dropping funnel within 1 h. Since the epoxidation process is exothermic, proper precaution was taken to avoid overheating the reaction mixture. The reaction continued for 6.5 h, and the progress was monitored with epoxy titration. After completion of the reaction, the mixture was dissolved in 600 ml EtOAc, washed with a slightly basic water solution and brine, then dried over Na_2SO_4 and filtered. EtOAc was removed by distillation under a vacuum. For ELO-A (2) the molar ratio was as follows: 1 : 0.4: 0.9 (mole of fatty acid double bonds: mols of HCOOH: mols of H_2O_2). The rest of the procedure remained the same.

Table 1
ALO-A resin formulations.

Sample name	ALO-A, wt%	Reactive diluents, wt%		
		IBOA	TPGDA	TMPTMA
ALO-A[a]	100			
90_10 IBOA	90	10		
80_20 IBOA	80	20		
70_30 IBOA	70	30		
90_10 TPGDA	90		10	
80_20 TPGDA	80		20	
70_30 TPGDA	70		30	
90_10 TMPTMA	90			10
80_20 TMPTMA	80			20
70_30 TMPTMA	70			30

[a] In the work samples are divided between (1) and (2), which denotes resins that are formulated with either ALO-A (1) and ALO-A (2).

Table 2
Characteristics of synthesized LO-A, ELO-A, and ALO-A.

Resins	AV, mg KOH/g resin	OH value, mg KOH/g resin	mmol of fatty acid C=C/g resin	EV, mmol epoxy/g resin	mmol acrylic groups/g resin	Yield, %	GPC		
							M_n (g/mol)	M_w (g/mol)	PDI
LO-A	2.3	69	4.9	–	–	–	1182	3373	2.9
ELO-A (1)	3.5	93	0.5	3.4	–	69	1509	11604	7.7
ELO-A (2)	4.7	90	2.3	2.7	–	55	1526	7063	4.6
ALO-A (1)[a]	48.1	217	0.5	0.1	2.3	68	1740	46645	26.8
ALO-A (2)[a]	34.9	183	2.3	0.2	1.8	67	1771	25318	14.3

[a] Acrylated alkyds ALO-A (1) and ALO-A (2) were synthesized from the respective epoxides ELO-A (1) and ELO-A (2).

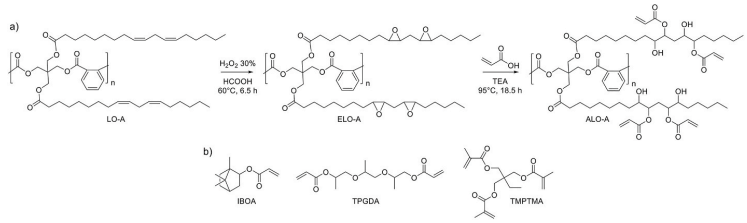

Fig. 1. a) Synthesis steps to obtain acrylated linseed oil-based alkyd (ALO-A); b) Structures of the used reactive diluents.

2.4. Acrylation of ELO-A (ALO-A)

Acrylation of epoxidized alkyd (45 g) was carried out in the presence of AA (14 g) and TEA (1 wt%) (0.81 ml) as catalyst (Fig. 1a). BTH (0.06 wt% = 600 ppm) (0.0354 g) and MEHQ (0.06 wt% = 600 ppm) (0.0354 g) were used as free radical inhibitors. The molar ratio was 1 : 1.3 (mole of epoxy: mols of AA). Epoxidized alkyd, TEA, BHT, and MEHQ were mixed in a 500 ml four-necked round-bottom flask equipped with a condenser, thermocouple, mechanical stirrer, and dropping funnel. The mixture was stirred and heated to 95 °C. Then AA was added slowly through the dropping funnel within 1 h. The reaction conversion was monitored by measuring the AV of the mixture periodically. The reaction was stopped after 18.5 h when there was little to no change in the AV. After synthesis, the acrylated linseed oil-based alkyd (ALO-A) product was dissolved in EtOAc, and the unreacted AA and catalyst were removed through water extraction. The product was dried over Na_2SO_4 and filtered. EtOAc was removed by vacuum, leaving resins with an approximate solid content of 93 %. ELO-A (1) and ELO-A (2) were precursors to yield ALO-A (1) and ALO-A (2), respectively. The acrylation yields were 68 % for ALO-A (1) and 67 % for ALO-A (2) as calculated by ^{1}H NMR (Table 2).

2.5. Preparation of UV-curable coatings

ALO-A resins were mixed with reactive diluents to lower the application viscosity and increase the final mechanical performance (Table 1). Three different reactive diluents in concentrations of 10, 20, and 30 wt% were chosen – monofunctional IBOA, difunctional TPGDA, and trifunctional TMPTMA (Fig. 1b). 5 wt% of photoinitiator TPOL was added to each formulation to initiate crosslinking upon UV irradiation. Two sets of formulations were prepared – one with ALO-A (1) and the other with ALO-A (2), resulting in 20 samples in total (including ALO-A (1) and ALO-A (2) without reactive diluent). For better visualization, only one set is shown in Table 1.

Liquid resins were applied on cleaned glass and aluminum (when testing deformation by indentation) substrates using a film applicator of a wet film thickness of 100 μm. The applied resins were cured under a UV-Hg lamp (IST-Metz, type I-250-NA-3-40 with a UV range of 180–450 nm with max. 200 W/cm^2) at a distance of 3–4 cm and with a conveyor speed of 5 m/min (simulated industrial production line). The samples were run under the lamp up to 5 times (one curing cycle corresponded to 9 s of UV exposure). We should note that a significant amount of heat is generated during curing with a UV-Hg lamp. The heat may facilitate the curing process; however, it was out of our scope to determine this extent.

2.6. Characterization

Acid value (AV) was determined by titration with 0.1 M KOH in EtOH [17]. Epoxy value (EV) was determined according to ASTM D1652 by titrating with 0.1 M $HClO_4$ in glacial acetic acid and using crystal violet as an indicator. Hydroxyl (OH) value was determined according to DIN EN ISO 4629-2 by titrating with 0.1 M KOH in EtOH. Fourier-transform infrared (FTIR) spectra of the specimens were recorded on a Brucker Alpha FTIR spectrometer over a 4000- 600 cm^{-1} frequency range. The ^{1}H NMR spectra for the samples were recorded on Bruker Avance 500 spectrometer (Bruker BioSpin, Switzerland) at 500 MHz, using the residual peak of $CDCl_3$ (^{1}H: $\delta = 7.26$ ppm) as an internal standard. The acrylic group content (mmol of acrylic groups/g resin) was determined using 3,4,5-trimethoxybenzaldehyde as an internal standard. The molar masses of synthesized alkyd derivatives were determined by gel permeation chromatography (GPC) using Shimadzu Prominence-i LC 2030 3D equipped with Agilent PLGEL 5-μm Mixed-C (200–2000000 g/mol) and Agilent PLGEL 5-μm Mixed-D (200–400000 g/mol) columns protected by an upstream GuardColumn. Tetrahydrofuran (HPLC Quality, unstabilized) from Biosolve) 1.0 ml/min was used as the mobile phase. Linear polystyrene standards were used for the calibration. The viscosity of resins was measured with an Anton Paar rheometer MCR102 (Graz, Austria) with a parallel-plate measuring system (25 mm diameter). The results are presented at a shear rate of 50 1/s at 22 °C. The measurement gap was set to 0.1 mm. To study the behavior of the resins during UV curing, the rheometer was equipped with a Peltier-controlled temperature chamber with a glass plate (38 mm diameter) and PP08 metal spindle (8 mm diameter). The resins were exposed to radiation using a UV/VIS spot curing system,

OmniCure S1500 (Excelitas Technologies Corp., USA). Radiation was applied at wavelengths between 250 and 450 nm with an intensity of 2 mW/cm^2 at 22 °C. The measurement gap was set to 0.1 mm. The measurements were performed with an angular frequency of 10 rad/s and 0.3 % shear strain. The UV/VIS onset was 60 s after the start of the experiment. Storage modulus (G′), loss modulus (G″), and loss factor tanδ (G″/G′) were recorded during real-time measurement. The crossover point where G′ equals G″ is defined as the gel point (t_{gel}) calculated from the onset of UV/VIS irradiation. Coatings properties were determined for all samples according to standards. Hardness was evaluated by subjecting coatings to Konig pendulum hardness (ASTM D4366). Coating resistance to cracking and deformation was measured by the Erichsen ball indentation (cupping) test according to DIN 53156, ISO 20482, by applying and curing the coatings on aluminum plates.

3. Results and discussion

3.1. Synthesis of epoxidized alkyd resins (ELO-A)

Linseed oil-based alkyd resins (LO-A) were prepared to investigate the feasibility of synthesized UV-curable alkyds using two steps: epoxidation and acrylation. Epoxidation was carried out via Prilezhaev reaction using *in situ* generated performic acid [18]. The reaction was monitored by titration to determine the epoxy value (EV) (Fig. 2a). We conducted the epoxidation at 60 °C as it has been found to be an optimal temperature for unsaturated fatty acid epoxidation [19]. In the FTIR spectrum of LO-A, the fatty acid double bond vibrations attributed to absorption bands at 3009 and 1654 cm^{-1} disappeared after the epoxidation (Fig. 2b). In the meantime, a new absorption band at 821 cm^{-1} indicated the formation of epoxy groups in ELO-A. A slight increase in the absorption band around 3460 cm^{-1} responsible for the –OH group can be evidence of epoxy ring-opening (hydrolysis) [20]. This is also confirmed by increased OH value after epoxidation (Table 2).

The ^{1}H NMR spectra after epoxidation (Fig. 2c) revealed that the methylene protons in the α-position of the epoxy ring (-**H**COC**H**-) appeared at δ = 3.11 and 2.91 ppm. Methylene protons between two epoxy groups (-COC-C**H$_2$**-COC-) appeared at δ = 1.66–1.83 ppm, and protons in the β-position of the epoxy ring (-COC-C**H$_2$**-) appeared at δ = 1.47 ppm. Meanwhile, the proton signals corresponding to unsaturated fatty acid double bonds disappeared (Fig. S1). However, as the conversion is not complete, small peaks remained visible in ELO-A (1) and ELO-A (2), corresponding to 0.4 and 2.1 mmol of internal fatty acid double bonds, respectively (Table 2). ELO-A spectra also revealed increased integrals at δ = 3.43–4.48 ppm, indicating the undesirable epoxy ring-opening (hydrolysis) where -**H**C**O**H- protons resonate.

Table 2 summarizes the epoxidation reaction overview. The maximum EV obtained was 3.4 mmol epoxy/g resin with a molar ratio of 1 : 1.8 (mole of fatty acid double bonds: mols of H_2O_2). This gave the first epoxidized product ELO-A (1). The yield after epoxidation was 69 %, making it incomplete. Some fatty acid double bonds remained unreacted due to steric hindrance, different fatty acid reactivities [21], or inefficient reaction conditions (temperature, time, molar ratio of reagents). Increasing H_2O_2 (up to 2.1 mol) or changing the H_2O_2 feed rate (from 1.9 to 9.2 ml 30 % H_2O_2/min) did not affect the reaction progress and conversion. Walther et al. reported a similar EV of 3.0 mmol epoxy/g resin after alkyd resin epoxidation at 0 °C [22]. We suggest that complete conversion might require better mixing or more HCOOH. However, HCOOH can also protonate the epoxy ring, leading to undesirable ring-opening (hydrolysis) via an S_N1 mechanism. Due to traces of HCOOH that remain in the resins after washing, we also observed a slight increase in AV. Some researchers suggest H_2SO_4 as a catalyst, a solvent, or additional free fatty acids to achieve high unsaturated double-bond epoxidation yields [23,24]. The increase in M_n indicates the addition of epoxy groups, leading to a moderate rise in the average molecular weight of individual alkyd chains. However, the significant rise in M_w reflects the presence of a few much larger alkyd species, likely caused by side reactions like oligomerization.

As this study focuses on evaluating the effects of different functionalities on the product properties, we performed the second epoxidation using half of the amount of H_2O_2 under the same conditions: 1 : 0.9 (mole of fatty acid double bonds: mols of H_2O_2). This gave the second epoxidized product ELO-A (2) with EV = 2.7 mmol epoxy/g resin (^{1}H

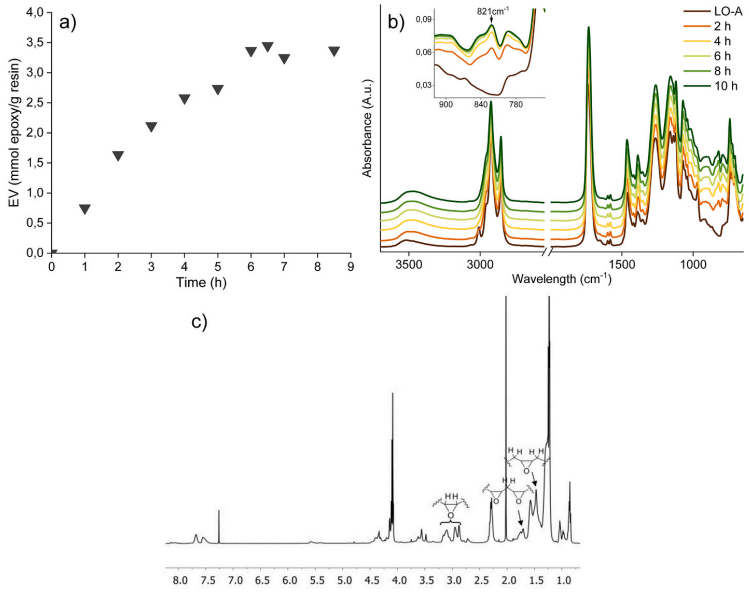

Fig. 2. LO-A epoxidation reaction progress a) by titration; b) by FTIR analysis (the inset plot shows zoomed-in spectra corresponding to the formed epoxy ring at 821 cm^{-1}); c) ^{1}H NMR spectra of ELO-A (1).

NMR spectrum of ELO-A (2) can be seen in Fig. S2.). Since we used a lower amount of H_2O_2, the epoxidation yield reduced to 55 % and the number of remaining fatty acid double bonds increased nearly fivefold (Table 2). Both epoxidized products ELO-A (1) and ELO-A (2) were used as starting materials to obtain respective acrylated alkyds ALO-A (1) and ALO-A (2).

3.2. Synthesis of acrylated alkyd resins (ALO-A)

Acrylic acid (AA) was employed as the acrylation agent to modify ELO-A without using halogen compounds, such as the frequently reported NBS [22,25,26]. First, we compared reaction progress using 1.3 or 1.7 mol of AA (Fig. 3a). The decrease of AV at higher AA concentrations (1.7) is faster than at lower AA concentrations (1.3), which is evident from the decreasing distance between the dotted lines. This indicates faster acrylation at higher AA concentrations. However, a higher concentration of AA can lead to a higher chance for the reaction to gel [16] and can make the workup phase challenging, leading to AA residue traces in resins, thus influencing the UV-cured coating properties. Therefore, a ratio of 1 : 1.3 (mole of epoxy group to moles of AA) was selected for the acrylation process.

Using ELO-A (1) or ELO-A (2) as a starting epoxide, we obtained ALO-A (1) or ALO-A (2), respectively. We did not change the epoxy: AA molar ratio when using ELO-A (1) or ELO-A (2) as a starting material; instead, we compared the acrylation reaction progress (Fig. 3b). From AA consumption, we calculated that acrylation proceeds slower for epoxide with lower EV (ELO-A (2)). That is due to the lower number of epoxy groups and, thus, their reduced availability during the reaction, which aligns with our expectations.

We conducted two acrylation reactions under the same conditions but using two different catalysts: triphenylphosphine (TPP) and triethylamine (TEA). Fig. 3a and b present the reaction progress for each catalyst. There is a slight difference in the reaction progress where TEA catalyzes the reaction faster (comparing yellow and red dotted lines from Fig. 3a and b, respectively). The catalytic mechanism of TEA in the acrylation reaction is proposed, while the catalytic mechanism of TPP has not been reported [27]. It could be that the lone pair of electrons in the phosphorus atom (in TPP) acts similarly to the lone pair of electrons in the nitrogen atom (in TEA), withdrawing the hydrogen from AA and creating a negative charge on oxygen, which can act as a nucleophile to open the epoxy ring. We chose to examine and use TEA-catalyzed ALO-A resins. Saithai et al. acrylated soybean oil epoxide without catalyst but used a high excess of AA – molar ratio of 1 : 10 (epoxidized soybean oil: AA) and high temperatures (110 °C) [28]. We performed the acrylation at 95 °C. Increasing the temperature to 120 °C led to gelation after 1.5 h, even with a four times higher inhibitor concentration. The acylation reaction was stopped after 18.5 h when there was little to no change in the AV.

Again, Table 2 facilitates several key conclusions. During acrylation, the EV decreased slightly faster than the AV, with an end EV of 0.1 and 0.2 for ALO-A (1) and ALO-A (2), respectively. This could indicate the undesirable epoxy ring-opening reaction (hydrolysis). Another factor that suggests this is the increased OH value of ALO-A and the increased OH absorption band around 3460 cm^{-1} in the FTIR spectrum (Fig. 3c). Successful addition of AA was confirmed by the characteristic acrylic C═C absorption bands at 1637, 1618, and 810 cm^{-1}. At the same time, the absorption band of the epoxy group at 821 cm^{-1} disappeared. A small amount of epoxy rings remained unreacted, probably due to steric hindrance caused by the bulky alkyd structure. In the ^{1}H NMR spectrum, three signals appeared at δ = 5.80–6.50 ppm, corresponding to **H_2C═CH-** of an acrylic group, while the epoxy peaks disappeared (Fig. 3d). The ^{1}H NMR spectrum of ALO-A (2) can be seen in Fig. S3). The acrylation yield was 67 and 68 % (2.3 and 1.8 mmol acrylic groups/g resin for ALO-A (1) and ALO-A (2), respectively), which is mainly due to competitive hydrolysis. The reported yield of a one-step bromoacrylated alkyd using NBS was 55 % [22]. As GPC indicates, the broader molecular weight distribution after acrylation could indicate possible crosslinking involving C═C of acrylic moiety during ALO-A synthesis. Acrylation has introduced molecular weight heterogeneity, leading to broader molecular weight distribution and higher polydispersity index (PDI). GPC curves are represented in Fig. S4 and Fig. S5.

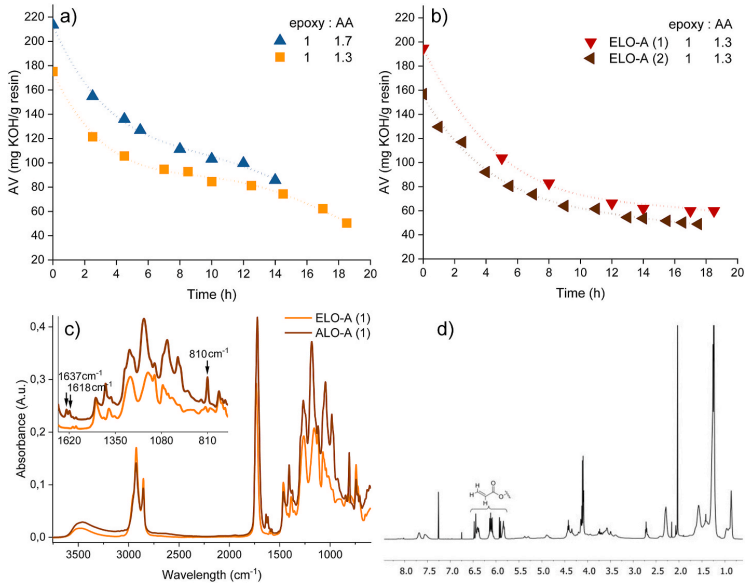

Fig. 3. a) TPP catalyzed acrylation reaction progress; b) TEA catalyzed acrylation reaction progress; c) ELO-A (1) and ALO-A (1) FTIR spectra (ALO-A (1) synthesized using TEA as catalyst), (the inset plot shows a zoomed-in spectra); d) ^{1}H NMR spectra of ALO-A (1).

3.3. Viscosity

The synthesized ALO-A (1) resin has a viscosity of 120210 mPa s, which is tremendously viscous compared to other alkyd resins for coating applications (Fig. 4a, the viscosity of ALO-A (1) is presented as a pink dashed line). As we decreased the functionality for ALO-A (2), the viscosity decreased to 27815 mPa s (Fig. 4b, the viscosity of ALO-A (2) is presented as a pink dashed line). That is expected to be due to the lower amount of hydrogen bonds. Viscosity dependence on functionality can also be explained by the electronic double-layer theory and the effects of steric hindrance, as described by Zhang et al. [29] Some studies show different results. For example, acrylated epoxidized soybean oil (AESO) with a functionality of 2.6 demonstrated lower viscosity compared to AESO with a functionality of 1.3 [30]. Viscosity also increases as the polymer molecular weight increases [31]. The increasing PDI after acrylation (Table 2) could indicate possible crosslinking involving C═C of acrylic moiety during ALO-A synthesis, leading to higher viscosity. An exciting synthesis was performed by Arvin et al., in which the authors reduced the methacrylated resin viscosity by further substituting the formed hydroxyl groups. After opening the epoxy ring with methacrylic acid, the authors added additional methacrylic anhydride and a second anhydride (acetic, propionic, or butyric anhydride). However, either of the anhydrides could react with hydroxyl groups, forming a mixture of dimethacrylate and methacrylate-acetate, -propionate, or -butyrate products. After synthesis, the viscosity of the dimethacrylated product was 67300 and dropped to 7800 mPa s for the formed non-functional esters due to their role as internal plasticizers [32].

All reactive diluents considerably reduced the viscosity. The viscosity of each formulation was in the range of 5700–60000 mPa s. Formulations containing TPGDA reduced viscosity the most. However, these resins remain too viscous, which is the limiting factor for their use in industry. Further studies are necessary to optimize the synthesis and viscosity of resins.

3.4. Photocuring kinetics by real-time photorheology

Resins were tested under low shear strain (0.3 %) to keep the material in a linear viscoelastic region, providing intrinsic material properties. Increasing the strain caused scattered, inaccurate results during UV curing, indicating material yielding (irreversible deformation). The changes in storage modulus (G′), loss modulus (G″), and loss factor (tanδ) for ALO-A during irradiation are presented in Fig. 5. For the rest of the samples, photorheological data is presented in Table 3.

Storage modulus characterizes the rigidity of materials and demonstrates how crosslinking density evolves during UV exposure. Meanwhile, the loss modulus characterizes viscous behavior. ALO-A (1) shows higher G′ than ALO-A (2), indicating higher crosslinking density. ALO-A (1) also shows a steeper G’ curve after UV exposure than ALO-A (2), indicating faster crosslinking network formation.

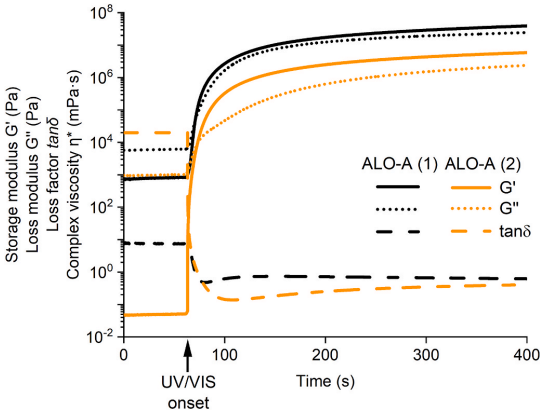

Fig. 5. Storage modulus G′, loss modulus G″, and loss factor tanδ versus irradiation time for ALO-A (1) and ALO-A (2).

Table 3
Real-time photocuring data of all formulations.

Resins	Storage modulus G′ x10^7, Pa[b]		Loss modulus G″ x10^7, Pa[b]		Loss factor tanδ[b]		t_{gel}, s	
	(1)[a]	(2)	(1)	(2)	(1)	(2)	(1)	(2)
ALO-A	3.9	0.6	2.4	0.2	0.62	0.41	10.8	13.0
90_10 IBOA	3.7	0.6	2.1	0.4	0.56	0.55	4.9	8.0
80_20 IBOA	6.6	1.0	3.4	0.8	0.51	0.86	3.7	5.9
70_30 IBOA	9.6	2.0	4.2	1.8	0.44	0.88	3.4	4.6
90_10 TPGDA	3.9	0.8	2.1	0.3	0.54	0.45	4.4	6.2
80_20 TPGDA	4.8	1.2	2.4	0.8	0.51	0.63	3.4	4.8
70_30 TPGDA	5.8	2.0	2.8	1.2	0.48	0.60	3.0	3.6
90_10 TMPTMA	8.2	2.1	2.9	0.9	0.36	0.42	6.2	7.2
80_20 TMPTMA	12.9	6.7	3.3	2.5	0.25	0.37	5.6	6.6
70_30 TMPTMA	18.8	9.7	3.6	3.0	0.19	0.31	5.2	6.1

[a] (1) and (2) denotes resins that are formulated with either ALO-A (1) and ALO-A (2).
[b] at an irradiation time of 400 s.

In most cases, tanδ decreased with the addition of reactive diluents. Meaning that more elastic deformation occurs since G′ rises more than G’’. However, tanδ increased for ALO-A (2) formulations with IBOA or TPGDA. Too much reactive diluent can restrict radicals’ diffusion and motion, leading to premature termination [33]. If the reactive diluent polymerizes more rapidly, the network may crosslink at a rate that limits the reactivity of the alkyd-modified chains. Due to reduced mobility, alkyd chains may remain partially unreacted within the final network.

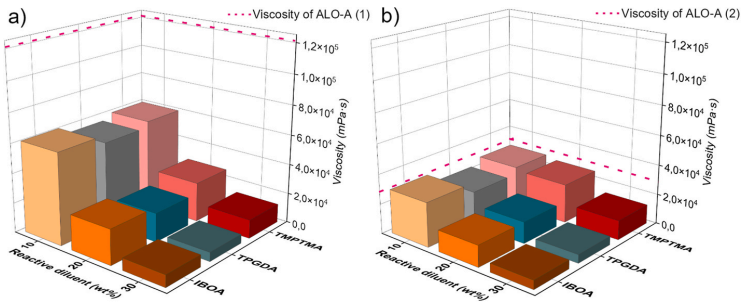

Fig. 4. Viscosity of a) ALO-A (1) and b) ALO-A (2) and their formulations with reactive diluents in different weight ratios.

The presence of these softer, longer alkyd chain segments could then act as plasticizers, thereby increasing G″ more than G' and eventually increasing tanδ.

Gel point (t_{gel}) indicates the formation of a polymeric network where material turns from a viscous liquid to a viscoelastic gel. T_{gel} for ALO-A (1) and ALO-A (2) was 10.8 s and 13.0 s, respectively. T_{gel} appears faster for ALO-A (1) due to higher acrylic group density and, thus, faster crosslinking. All formulations showed the same trend - the higher the amount of reactive diluent, the faster resins reached t_{gel}. T_{gel} for 70_30 TPGDA (1) was only 3.0 s. T_{gel} of formulations with TMPTMA occurred later than for other reactive diluents, demonstrating lower reactivity of the methacrylic group than the acrylic group. The higher stability of tertiary radicals formed on methacrylate, compared to the secondary radicals formed on acrylates, reduces their reactivity [34]. Besides, methacrylates are more sterically hindered, limiting segmental mobility for growing free radicals [35].

3.5. Coating properties: pendulum hardness and indentation

Table 4 summarizes the pendulum hardness values for the coatings, illustrating the effects of resin functionality and reactive diluents. All samples showed a considerable increase in pendulum hardness up to the 3rd curing cycle (equivalent to 27 s of UV exposure). Beyond this point (the 4th and 5th cycles), further hardness gains were minimal, accounting for only a 2–4% increase (Fig. S6). From an industrial perspective, this slight improvement does not justify the additional energy expenditure. The limited increase in hardness after multiple UV exposures may be attributed to the bulky structure of ALO-A, which restricts the diffusion of free radicals and thus impedes further double bond conversion. Interestingly, Cheong et al. observed a decrease in pendulum hardness after 8–10 curing cycles when using 46 wt% reactive diluent (1,6-hexanediol diacrylate or trimethylolpropane triacrylate), which they attributed to degradation at higher UV doses [36]. Excessive radiation can lead to degradation in acrylic coatings, diminishing crosslinking density and gel content [37].

Notably, our design approach produced two distinct resins with markedly different hardness: ALO-A (2) reached a pendulum hardness of 47 s, whereas ALO-A (1) achieved 103 s, corresponding to a 2.2-fold difference. Incorporating reactive diluents further enhanced hardness, with up to a 2.9-fold increase for lower-functionality ALO-A (2) and 1.7-fold for higher-functionality ALO-A (1), attaining a maximum hardness of 174 s. Hence, the choice of resin and reactive diluent enabled a scalable hardness range from 47 to 174 s. Hardness in acrylate-based coatings primarily depends on the molecular structure and crosslink density, which is a function of the concentration of acrylate functionalities [38]. Consistent with this principle, all formulations exhibited higher hardness with the addition of reactive diluents (Table 4). Coatings with IBOA and TMPTMA displayed higher hardness than those formulated with TPGDA. In the case of IBOA, the bulky bicyclo[2.2.1] heptane unit derived from camphor contributes to the observed hardness increase. In contrast, TMPTMA imparts high crosslinking density by virtue of its trifunctional acrylate groups, leading to increased hardness but reduced flexibility [36]. By comparison, the linear molecular backbone of mono- and difunctional monomers (e.g., IBOA and TPGDA) tends to yield softer or more flexible coatings than trifunctional monomers [36]; this effect is especially evident in formulations based on ALO-A (2), where those containing TMPTMA stand out significantly.

Table 4
UV-cured coating properties.

Resins	Pendulum hardness, s		Flexibility (Erichsen), mm	
	(1)[a]	(2)	(1)	(2)
ALO-A	103 ± 2	47 ± 2	5.0 ± 0.4	7.0 ± 0.4
90_10 IBOA	119 ± 1	58 ± 1	5.3 ± 1.0	7.3 ± 0.3
80_20 IBOA	152 ± 3	77 ± 1	6.8 ± 0.5	7.3 ± 0.4
70_30 IBOA	169 ± 2	104 ± 2	7.1 ± 0.3	7.4 ± 0.3
90_10 TPGDA	113 ± 0	50 ± 1	4.4 ± 0.3	6.4 ± 0.5
80_20 TPGDA	120 ± 1	61 ± 1	4.9 ± 0.3	6.8 ± 0.5
70_30 TPGDA	129 ± 2	72 ± 1	5.9 ± 0.3	7.1 ± 0.2
90_10 TMPTMA	128 ± 6	78 ± 1	2.9 ± 0.5	3.5 ± 0.9
80_20 TMPTMA	155 ± 5	113 ± 1	2.6 ± 0.4	2.7 ± 0.7
70_30 TMPTMA	174 ± 1	138 ± 3	2.0 ± 0.8	7.0 ± 0.6

[a] (1) and (2) denotes resins that are formulated with either ALO-A (1) and ALO-A (2).

In addition to enhance hardness, the selected reactive diluents also promoted adhesion and imparted significant flexibility. This synergy is particularly evident in the Erichsen indentation tests (Table 4), which demonstrate that higher hardness can be achieved without sacrificing flexibility. By carefully tuning the functionality of ALO-A and incorporating diluents such as IBOA or TPGDA, we achieved a concurrent increase in hardness and flexibility, thus mitigating the conventional trade-off between mechanical strength and flexibility.

The chosen diluent modulates the coating's mechanical response in distinct ways. IBOA (monofunctional) features a bulky isobornyl moiety that accommodates free chain movement and relieves internal stresses in the polymer matrix, thereby increasing flexibility. As a result, all compositions with IBOA exhibited not only an increase in hardness but also higher indentation depths. For example, 70_30 IBOA (1) and 70_30 IBOA (2) attained the highest indentation depths among their respective ALO-A resin groups (7.1 and 7.4 mm), highlighting IBOA's capacity to enhance flexibility. Notably, 70_30 IBOA (1) produced the second-highest pendulum hardness value (169 s) while also exhibiting a 42 % improvement in indentation depth (before cracking occurs).

TPGDA (bifunctional) confers a higher crosslink density than IBOA, yet its propyl groups allow some degree of chain mobility, preserving moderate flexibility [15]. Similar to IBOA, TPGDA displayed the greatest compatibility with ALO-A at 30 wt% loading, yielding enhanced indentation depths (5.9 and 7.1 mm, respectively), whereas lower loadings led to a moderate reduction in indentation values. Interestingly, Gan et al. observed a comparable phenomenon when studying the impact of melamine on palm stearin alkyd enamels [39]. Although higher melamine content typically elevates crosslink density, it can paradoxically increase flexibility at sufficiently high concentrations—possibly because excess melamine may form fewer crosslinks per alkyd chain, thereby reducing the effective crosslink density. This rationale may apply equally to our IBOA- and TPGDA-based formulations, where certain diluent levels introduce enough free volume to permit greater deformation before cracking. In contrast, TMPTMA's trifunctional methacrylate structure, coupled with the absence of flexible alkyl chains, produces highly dense crosslinked networks. Consequently, TMPTMA formulations display substantially reduced deformation capacities and earlier crack onset.

Schwalma et al. summarized Erichsen indentation values for a range of fossil-based UV-curable systems, including epoxy, polyester, polyether, urethane acrylates, and waterborne systems [40]. Among these, urethane acrylates were the most flexible (though relatively soft), with aliphatic urethane acrylates reaching up to 8 mm in indentation depth. By contrast, epoxy acrylates exhibited the poorest performance (1–4.1 mm). The average flexibility for all tested UV-curable acrylate coatings was 4.4 mm. Plotting pendulum hardness against Erichsen indentation, the authors noted that hardness values of 170–190 s typically correlated with low indentations of only 1–2 mm. They further remarked that high hardness and a flexible network can be achieved simultaneously using appropriate reactive monomers.

Wang et al. investigated four bio-based UV-curable alkyd resins—methacrylated medium linseed oil alkyd, methacrylated long linseed oil alkyd, acrylated medium linseed oil alkyd, and acrylated long linseed oil alkyd—along with glycerol trimethacrylate and glycerol triacrylate [6]. Their pendulum hardness values ranged from 21 to 101 s, but the hardest coatings suffered relatively poor adhesion, while those optimized for adhesion were comparatively soft. Similarly, Oktay et al. reported bio-based epoxy coatings derived from soybean oil-based epoxy

resin cured with a hempseed oil-based curing agent, yielding pendulum hardness values of 28–42 s and Erichsen indentations of 8–8.8 mm [41]. Although these results were obtained using a different pendulum hardness standard, they align with the relatively soft ALO-A (2) coating.

Although the literature increasingly reports various bio-based coating formulations, many do not include industry-standard measurements such as pendulum hardness and Erichsen indentation. Instead, studies often present Vickers hardness, pencil hardness, or other tests that are difficult to compare across different publications. Furthermore, comprehensive evaluations of both flexibility and hardness are frequently lacking. By using pendulum hardness and Erichsen indentation, we have demonstrated that our formulations are not only tunable in hardness but also capable of retaining remarkable flexibility – an important factor for prolonging the service life of coatings.

3.6. Coating properties: wood staining

The initial assessment of coating properties often involves visual inspection or subjective judgment, especially regarding appearance. In Fig. 6 we have visually compared commercial UV-curable resins (diacrylate ester of a bisphenol A epoxy resin) and our synthesized alkyd-based UV-curable resins ALO-A (1). Both resins were mixed with a photoinitiator, applied to wood (walnut wood), and cured under UV light. We can see that ALO-A coating has penetrated the wood, providing a darker color while allowing features of the wood, such as grain, to remain visible. The alkyd resin penetration is mainly determined by its flow into the wood capillaries [42]. Alkyd resins are chemically compatible with cellulose and lignin, enhancing their ability to bond with and penetrate the wood structure. Ratajczak et al. studied an organosilane binding to wood substance through an alkyd resin. The authors found that alkyd resin significantly reduced organosilane leaching and improved its bonding to the wood matrix [43]. The commercial coating only formed a thin film on the surface of the wood. Coating penetration into wood provides more protection, and because of the better bonding to the wood, it prevents the wood and the coating from warping, cracking, or splitting when temperature and humidity fluctuations occur. Penetrating coatings typically last longer than surface coatings because they are less prone to wear away [44]. Next to that, the penetration of the coating into the wood provides a visual aspect that accentuates the wood's natural grain and is generally considered more pleasing and desired.

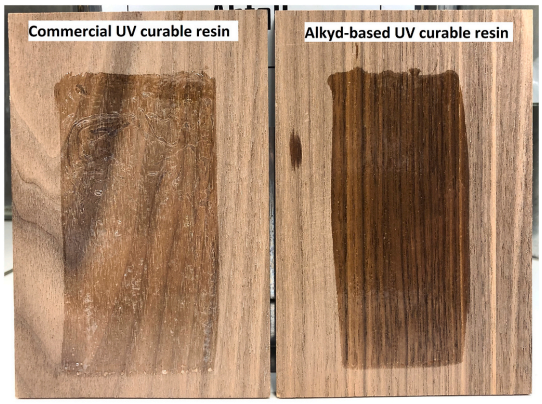

Fig. 6. Wood staining effect on alkyd-based UV-curable resins ALO-A (1).

4. Conclusions

This study presents an optimized synthesis route for UV-curable acrylated linseed oil-based alkyds (ALO-A), demonstrating a sustainable, high-performance alternative for bio-based coatings. By integrating acrylic functionality directly into the alkyd backbone through a halogen-free epoxidation and acrylation approach, we achieved precise control over resin properties while eliminating the need for environmentally hazardous reagents.

The resulting bio-based resins exhibit outstanding coating performance, balancing high mechanical strength with remarkable flexibility. Real-time photorheology confirmed rapid UV curing, with ALO-A's gel point (t_{gel}) ranging from 10.8 to 13.0 s and as low as 3.0 s for optimized formulations, supporting efficient, VOC-free industrial applications. The incorporation of reactive diluents, particularly IBOA and TPGDA, further enhanced the mechanical properties of coatings, enabling up to a 2.9-fold increase in hardness while maintaining exceptional flexibility. Notably, the highest-performing formulation reached a pendulum hardness of 174 s, with indentation depths up to 7.4 mm (before crack formation). These bio-based coatings offer competitive performance comparable to conventional fossil-based UV-curable coatings.

Beyond mechanical improvements, the bio-based ALO-A resins demonstrated superior adhesion and wood penetration, enhancing durability and aesthetic appeal in wood coating applications. The coating application process was conducted using a simulated industrial process via a conveyor belt system, ensuring practical relevance for large-scale production. These results establish a pathway for the development of next-generation, sustainable coatings that meet stringent industrial performance criteria while reducing environmental impact. Future work will focus on refining synthesis parameters, creating full formulations with more functional additives, and conducting environmental durability tests to enhance the coatings' longevity and resilience across diverse conditions.

CRediT authorship contribution statement

Sabine Briede: Writing – review & editing, Writing – original draft, Methodology, Investigation, Formal analysis, Data curation, Conceptualization. **Toine Biemans:** Writing – review & editing, Validation, Supervision, Methodology, Investigation, Data curation, Conceptualization. **Oskars Platnieks:** Formal analysis, Writing – review & editing. **Sergejs Gaidukovs:** Writing – review & editing, Validation, Funding acquisition.

Declaration of competing interest

The authors declare that they have no known competing financial interests or personal relationships that could have appeared to influence the work reported in this paper.

Acknowledgment

This work has been supported by the EU Recovery and Resilience Facility within the Project No 5.2.1.1.i.0/2/24/I/CFLA/003 "Implementation of consolidation and management changes at Riga Technical University, Liepaja University, Rezekne Academy of Technology, Latvian Maritime Academy and Liepaja Maritime College for the progress towards excellence in higher education, science and innovation" academic career doctoral grant (ID 1097). This work has been supported by DBU (Deutsche Bundesstiftung Umwelt, Federal German Foundation for the Environment) MOE-Fellowship for university graduates from Central and Eastern Europe. The authors would like to thank Worlée Chemie GmbH for their support. The authors would like to thank Dr. Lüttke from Hobum Oleochemicals GmbH for valuable discussions regarding the determination of epoxy values.

Appendix A. Supplementary data

Supplementary data to this article can be found online at https://doi.

org/10.1016/j.polymer.2025.128227.

Data availability

Data will be made available on request.

References

[1] A. Sheel Wali, S. Kumar, D. Khan, A review on recent development and application of radiation curing, Mater. Today Proc. 82 (2023) 68–74, https://doi.org/10.1016/j.matpr.2022.11.342.

[2] M.Y. Yong, W.J. Basirun, N.M. Sarih, M. Shalauddin, S.Y. Lee, D.T.C. Ang, Utilization of liquid epoxidized natural rubber as prepolymer and crosslinker in development of UV-curable palm oil-based alkyd coating, React. Funct. Polym. 191 (July) (2023) 105658, https://doi.org/10.1016/j.reactfunctpolym.2023.105658.

[3] N.M. Saman, D.T.C. Ang, N. Shahabudin, S.N. Gan, W.J. Basirun, UV-curable alkyd coating with self-healing ability, J. Coating Technol. Res. 16 (2) (2019) 465–476, https://doi.org/10.1007/s11998-018-0124-x.

[4] D.T.C. Ang, S.N. Gan, Environment friendly UV-curable resins from palm stearin alkyds, J. Appl. Polym. Sci. 125 (S2) (Sep. 2012), https://doi.org/10.1002/app.36858.

[5] A.A. Golubev, K.S. Baranova, D.A. Bazhanov, R.R. Khasbiullin, A.A. Shcherbina, M. A. Soldatov, Preparation and study of novel UV-curable alkyd-siloxane coating materials, J. Appl. Polym. Sci. 141 (33) (Sep. 2024), https://doi.org/10.1002/app.55838.

[6] Q. Wang, J. Thomas, M.D. Soucek, Investigation of UV-curable alkyd coating properties, J. Coating Technol. Res. 20 (2) (2023) 545–557, https://doi.org/10.1007/s11998-022-00697-9.

[7] D.T.C. Ang, S.N. Gan, Development of palm oil-based alkyds as UV curable coatings, Pigment Resin Technol. 41 (5) (2012) 302–310, https://doi.org/10.1108/03699421211264866.

[8] D.T.C. Ang, S.N. Gan, Novel approach to convert non-self drying palm stearin alkyds into environmental friendly UV curable resins, Prog. Org. Coating 73 (4) (2012) 409–414, https://doi.org/10.1016/j.porgcoat.2011.11.013.

[9] D.T.C. Ang, Y.K. Khong, S.N. Gan, Novel approach to enhance film properties of environmentally friendly UV-curable alkyd coating using epoxidised natural rubber, Prog. Org. Coating 76 (4) (2013) 705–711, https://doi.org/10.1016/j.porgcoat.2012.12.013.

[10] T. Eren, S.H. Küsefoğlu, Synthesis and polymerization of the bromoacrylated plant oil triglycerides to rigid, flame-retardant polymers, J. Appl. Polym. Sci. 91 (4) (2004) 2700–2710, https://doi.org/10.1002/app.13471.

[11] T.M. Lacerda, A.J.F. Carvalho, A. Gandini, Two alternative approaches to the Diels-Alder polymerization of tung oil, RSC Adv. 4 (51) (2014) 26829–26837, https://doi.org/10.1039/c4ra03416c.

[12] Y. Huang, L. Pang, H. Wang, R. Zhong, Z. Zeng, J. Yang, Synthesis and properties of UV-curable tung oil based resins via modification of Diels-Alder reaction, nonisocyanate polyurethane and acrylates, Prog. Org. Coating 76 (4) (2013) 654–661, https://doi.org/10.1016/j.porgcoat.2012.12.005.

[13] J. Wu, T. Zhang, G. Ma, P. Li, L. Ling, B. Wang, Synthesis of a tung oil-rosin adduct via the diels-alder reaction: its reaction mechanism and properties in an ultraviolet-curable adhesive, J. Appl. Polym. Sci. 130 (6) (2013) 4201–4208, https://doi.org/10.1002/app.39495.

[14] N. Thanamongkollit, K.R. Miller, M.D. Soucek, Synthesis of UV-curable tung oil and UV-curable tung oil based alkyd, Prog. Org. Coating 73 (4) (2012) 425–434, https://doi.org/10.1016/j.porgcoat.2011.02.003.

[15] P. Chittavanich, K. Miller, M.D. Soucek, A photo-curing study of a pigmented UV-curable alkyd, Prog. Org. Coating 73 (4) (2012) 392–400, https://doi.org/10.1016/j.porgcoat.2011.02.005.

[16] W. Maaßen, S. Oelmann, D. Peter, W. Oswald, N. Willenbacher, M.A.R. Meier, Novel insights into pressure-sensitive adhesives based on plant oils, Macromol. Chem. Phys. 216 (15) (2015) 1609–1618, https://doi.org/10.1002/macp.201500136.

[17] J. Hulsbosch, L. Claes, D. Jonckheere, D. Mestach, D.E. De Vos, Synthesis and characterisation of alkyd resins with glutamic acid-based monomers, RSC Adv. 8 (15) (2018) 8220–8227, https://doi.org/10.1039/c8ra00060c.

[18] D. Swern, Organic peracids, Chem. Rev. 45 (1) (Aug. 1949) 1–68, https://doi.org/10.1021/cr60140a001.

[19] C. Song, D. Gao, S. Li, L. Liu, X. Chen, Y. Jiang, Determination and quantification of fatty acid C=C isomers by epoxidation reaction and liquid chromatography-mass spectrometry, Anal. Chim. Acta 1086 (2019) 82–89, https://doi.org/10.1016/j.aca.2019.08.023.

[20] P. Gogoi, M. Boruah, S. Sharma, S.K. Dolui, Blends of epoxidized alkyd resins based on jatropha oil and the epoxidized oil cured with aqueous citric acid solution: a green technology approach, ACS Sustain. Chem. Eng. 3 (2) (2015) 261–268, https://doi.org/10.1021/sc500627u.

[21] J. La Scala, R.P. Wool, Effect of FA composition on epoxidation kinetics of TAG, J. Am. Oil Chem. Soc. 79 (4) (Apr. 2002) 373–378, https://doi.org/10.1007/s11746-002-0491-9.

[22] S. Walther, B. Strehmel, V. Strehmel, Functionalization of an alkyd resin with (meth)acrylate groups for photoinitiated polymerization, Prog. Org. Coating 125 (April) (2018) 316–324, https://doi.org/10.1016/j.porgcoat.2018.08.028.

[23] X. Zhang, J. Burchell, N.S. Mosier, Enzymatic epoxidation of high oleic soybean oil, ACS Sustain. Chem. Eng. 6 (7) (Jul. 2018) 8578–8583, https://doi.org/10.1021/acssuschemeng.8b00884.

[24] V.V. Goud, N.C. Pradhan, A.V. Patwardhan, Epoxidation of karanja (Pongamia glabra) oil by H 2 O 2, J. Am. Oil Chem. Soc. 83 (7) (Jul. 2006) 635–640, https://doi.org/10.1007/s11746-006-1250-7.

[25] T. Eren, S.H. Küsefoğlu, Synthesis and characterization of copolymers of bromoacrylated methyl oleate, J. Appl. Polym. Sci. 94 (6) (2004) 2475–2488, https://doi.org/10.1002/app.21207.

[26] T. Eren, S.H. Küsefoğlu, One step hydroxybromination of fatty acid derivatives, Eur. J. Lipid Sci. Technol. 106 (1) (2004) 27–34, https://doi.org/10.1002/ejlt.200300869.

[27] E.R. Jusoh Taib, et al., Physico-chemical characterisation of epoxy acrylate resin from jatropha seed oil, Pigment Resin Technol. 46 (6) (Nov. 2017) 485–495, https://doi.org/10.1108/PRT-11-2016-0116.

[28] P. Saithai, J. Lecomte, E. Dubreucq, V. Tanrattanakul, Effects of different epoxidation methods of soybean oil on the characteristics of acrylated epoxidized soybean oil-co-poly(methyl methacrylate) copolymer, Express Polym. Lett. 7 (11) (2013) 910–924, https://doi.org/10.3144/expresspolymlett.2013.89.

[29] T. Zhang, W. Wu, X. Wang, Y. Mu, Effect of average functionality on properties of UV-curable waterborne polyurethane-acrylate, Prog. Org. Coating 68 (3) (Jul. 2010) 201–207, https://doi.org/10.1016/j.porgcoat.2010.02.004.

[30] C. Chen, J.H. Podolsky, R.C. Williams, E.W. Cochran, Laboratory investigation of using acrylated epoxidized soybean oil (AESO) for asphalt modification, Constr. Build. Mater. 187 (2018) 267–279, https://doi.org/10.1016/j.conbuildmat.2018.07.204.

[31] B. Liang, J. Zhao, G. Li, Y. Huang, Z. Yang, T. Yuan, Facile synthesis and characterization of novel multi-functional bio-based acrylate prepolymers derived from tung oil and its application in UV-curable coatings, Ind. Crops Prod. 138 (April) (2019), https://doi.org/10.1016/j.indcrop.2019.111585.

[32] A.Z. Yu, J.M. Sahouani, R.A. Setien, D.C. Webster, Effect of nature and extent of functional group modification on properties of thermosets from methacrylated epoxidized sucrose soyate, React. Funct. Polym. 128 (May) (2018) 29–39, https://doi.org/10.1016/j.reactfunctpolym.2018.05.003.

[33] K.S. Anseth, C.M. Wang, C.N. Bowman, Kinetic evidence of reaction diffusion during the polymerization of multi(meth)acrylate monomers, Macromolecules 27 (3) (Jan. 1994) 650–655, https://doi.org/10.1021/ma00081a004.

[34] J. Hioe, H. Zipse, Radical stability and its role in synthesis and catalysis, Org. Biomol. Chem. 8 (16) (2010) 3609, https://doi.org/10.1039/c004166a.

[35] D. Watts, A.A. Hindi, Intrinsic 'soft-start' polymerisation shrinkage-kinetics in an acrylate-based resin-composite, Dent. Mater. 15 (1) (Jan. 1999) 39–45, https://doi.org/10.1016/S0109-5641(99)00012-3.

[36] M.Y. Cheong, T. Lye Ooi, S. Ahmad, W.M.Z.W. Yunus, D. Kuang, Synthesis and characterization of palm-based resin for UV coating, J. Appl. Polym. Sci. 111 (5) (Mar. 2009) 2353–2361, https://doi.org/10.1002/app.29257.

[37] J.-F. Larché, P.-O. Bussière, J.-L. Gardette, How to reveal latent degradation of coatings provoked by UV-light, Polym. Degrad. Stabil. 95 (9) (Sep. 2010) 1810–1817, https://doi.org/10.1016/j.polymdegradstab.2010.05.005.

[38] S. Tasic, B. Bozic, B. Dunjic, Synthesis of new hyperbranched urethane-acrylates and their evaluation in UV-curable coatings, Prog. Org. Coating 51 (4) (2004) 320–327, https://doi.org/10.1016/j.porgcoat.2004.07.021.

[39] S.N. Gan, K.T. Teo, Curing and film properties of palm stearin alkyds, Pigment Resin Technol. 28 (5) (1999) 283–292, https://doi.org/10.1108/03699429910294337.

[40] R. Schwalm, L. Häußling, W. Reich, E. Beck, P. Enenkel, K. Menzel, Tuning the mechanical properties of UV coatings towards hard and flexible systems, Prog. Org. Coating 32 (1–4) (1997) 191–196, https://doi.org/10.1016/S0300-9440(97)00060-X.

[41] B. Oktay, J.H. Türkcan, O.K. Özdemir, N. Kayaman-Apohan, Vegetable oil-based epoxy coating materials for self-healing and anticorrosive applications, Macromol. Res. 31 (11) (Nov. 2023) 1077–1086, https://doi.org/10.1007/s13233-023-00190-1.

[42] M. de Meijer, K. Thurich, H. Militz, Comparative study on penetration characteristics of modern wood coatings, Wood Sci. Technol. 32 (5) (Oct. 1998) 347–365, https://doi.org/10.1007/BF00702791.

[43] I. Ratajczak, M. Woźniak, K. Szentner, M. Babicka, J. Jenczyk, B. Mazela, Aminosilane binding to wood substance through an alkyd resin, J. Wood Chem. Technol. 40 (1) (Jan. 2020) 73–79, https://doi.org/10.1080/02773813.2019.1697292.

[44] R.S. Williams, Finishing of wood, Wood as an Eng. Mater 1 (1999) 15–37.

Pielikums III

Appendix III

Briede, S., Platnieks, O., Darzina, M., Jirgensons, A., & Gaidukovs, S.

Effect of novel furan-based ester reactive diluent on structure and properties of UV-crosslinked acrylated rapeseed oil

Journal of Polymer Science, **2023**, 61(24), 3318-3328.

doi: 10.1002/pol.20230451

Received: 1 July 2023 | Revised: 9 September 2023 | Accepted: 18 September 2023

DOI: 10.1002/pol.20230451

RESEARCH ARTICLE

JOURNAL OF POLYMER SCIENCE WILEY

Effect of novel furan-based ester reactive diluent on structure and properties of UV-crosslinked acrylated rapeseed oil

Sabine Briede[1] | **Oskars Platnieks**[1] | **Madara Darzina**[2] | **Aigars Jirgensons**[2] | **Sergejs Gaidukovs**[1]

[1]Institute of Polymer Materials, Faculty of Materials Science and Applied Chemistry, Riga Technical University, Riga, Latvia

[2]Latvian Institute of Organic Synthesis, Riga, Latvia

Correspondence
Sergejs Gaidukovs, Institute of Polymer Materials, Faculty of Materials Science and Applied Chemistry, Riga Technical University, P. Valdena 3/7, Riga LV-1048, Latvia.
Email: sergejs.gaidukovs@rtu.lv

Funding information
European Social Fund, Grant/Award Number: 8.2.2.0/20/I/008; Latvian Institute of Organic Synthesis, Grant/Award Number: IG-2023-07; Latvijas Zinātnes Padome, Grant/Award Number: lzp-2022/1-0485; Rīgas Tehniskā Universitāte.Doctoral Grant Programme

Abstract

Unsaturated furan-based ester (UES) was prepared by green electrosynthesis using a single-cell setup and inexpensive graphite electrodes. The UES was validated as a reactive diluent for a bio-based acrylated rapeseed oil (ARO). UV-light photopolymerization of the bio-based resin was initiated using a diphenyl (2,4,6-trimethylbenzoyl)phosphine oxide (TPO) radical photoinitiator. The addition of 20 wt% UES to ARO dropped the resin viscosity by 1.6-fold. Incorporating 5 wt% UES into the ARO resin increased crosslinking density ν_e from 1.07 to 1.65 mol/m^3. Fourier-transform infrared spectroscopy (FT-IR) spectra revealed that ARO has been grafted with UES. The UES functional moieties promote the formation of soft mobile dangling chain end segments in the developed macromolecular network. UV-cured thermoset polymer reveals distinct morphologies in SEM micrographs, indicating notable structural changes with the addition of UES. A total of 5 wt% UES increased tensile strength from 0.49 to 0.55 MPa and storage modulus from 7.9 to 12.0 MPa at room temperature (22 ± 1 °C). The biodegradability in composting conditions was investigated, and up to 28% of the initial mass was lost after 60 days. UES was shown as to be efficient reactive diluent that can successfully replace fossil-based acrylate monomers in vegetable oil-based thermoset polymer synthesis.

KEYWORDS

bio-based, biodegradation, mechanical properties, Photopolymerization, vegetable oil

1 | INTRODUCTION

Unsaturated polyester (UPE) oligomers are used in photopolymerization because of their ability to cure upon UV irradiation.[1] UPEs can form a crosslinked network through intramolecular and intermolecular reactions. Often, monomers are combined with UPEs to increase the reactivity.[2] Styrene is the most common reactive diluent used in UPE systems to reduce viscosity, increase crosslink density, and reduce cost, but its use comes with known drawbacks, such as toxicity.[3] Nebioglu et al. synthesized UPE acrylates to evaluate the internal and terminal double bond position effects in UV-curable network formation.[4] The authors reported that the final conversion of the internal double bonds was not much lower than that of the terminal double bond. Thus, monomer structures are not limited by double bond location. With new sustainability goals set by European Union, the search for alternatives requires the integration of bio-based monomers.[5] For this purpose, we

explored bio-based monomers obtained from furan-based derivatives in a green manner via electrosynthesis as a possible reactive diluent for enhancement of UV-curable thermosets prepared from unsaturated polyester (UPE) oligomers.

White et al. reported a nonvolatile and "green" ionic liquid 4-vinylbenzyl trioctyl phosphonium bis(trifluoromethanesulfonyl)imide (VBTOP Tf_2N) as a reactive diluent for UPE oligomers containing internal double bonds from maleic acid anhydride.[6] In combination with dimethoxyethane as an unreactive diluent, they produced resins suitable for stereolithography, where 3D printed networks reached an ionic conductivity of 1×10^{-5} S cm^{-1} at 150 °C. Another grafting using maleate esters with an internal double bond was done by Esen et al.[7] First, epoxidized soybean oil was reacted with monomethyl maleate. Afterward, monomethyl maleate was treated with maleic anhydride, yielding a high unsaturation of 4.9 maleates per triglyceride. Finally, the synthesized maleates were copolymerized with styrene, vinyl acetate, and methyl methacrylate as reactive diluents. Superior properties were observed after treatment with maleic anhydride compared to monomethyl maleate due to the increased number of internal double bonds. As a result, the glass transition temperature increased from 55 °C to 90 °C for produced styrene copolymers. Bonneaud et al. observed only partial homopolymerization of synthesized maleate ester, whereas the copolymerization with oligo(hexafluoropropylene) vinyl ether was much faster.[8] The complete conversion was achieved in less than 40 s, and highly hydrophobic polymers were obtained. Wei et al. studied fumarates instead of maleates.[9] Fumarates have lower reactivity than acrylates and methacrylates, and their kinetics depend on the UV initiator, monomer molecule size, and monomer concentrations. The authors investigated electron density distribution and its influence on the copolymerization behavior of fumarate esters. The vinyl ester double bonds of divinyl fumarate are electron more affluent, and the fumarate double bonds are electron poorer compared to nonconjugated analogues; therefore, for example, thiol addition to the internal fumarate double bond of divinyl fumarate was much faster than that of diethyl fumarate. Thus, the polymerization rate of vinyl ester groups was faster than that of fumarate groups.

Recently, interest has grown in plant and vegetable oil-based UV-curable monomers with various unsaturated pendant moieties or groups synthesized and researched.[10,11] Yang et al. used the Diels-Alder process to synthesize tung oil monomer (TOA) with cyclic internal unsaturation moieties using acrylic acid.[12] The subsequent step involved a glycidylation reaction and ring-opening esterification producing a liquid monomer (TOA-GMA) with both internal and terminal unsaturation. Next, TOA-GMA was mixed with myrcene and modified with acrylic acid yielding the monomer (ADMM). High TOA-GMA content in a mixture with ADMM resulted in a strong preference for homopolymerization. In addition, TOA-GMA viscosity and branching were higher than ADMM, limiting the monomer from free movement. Despite low rates of copolymerization, the double bond conversion of copolymers was up to 95%. In another study, vegetable oil-derived dimer acid was combined with glycidyl methacrylate to create monoesters with a methacrylate group.[13] The distance between the two methacrylate groups was adjusted using a diepoxy extender. The final dimethacrylate was UV cross-linked for 10 s, reaching a double bond conversion of 82%. Meng et al. obtained castor oil-derived acrylate in a transesterification reaction with *N*-hydroxyethylacrylamide, which, after polymerization with acrylic acid, methyl methacrylic acid, and butyl acrylate, formed a multifunctional substituted polyacrylate.[14] The authors evaluated the material's performance as a wood coating with pencil hardness up to 3H, tensile strength up to 12.2 MPa and elongation up to 301.5%. Wei et al. reported castor oil-based hyperbranched acrylate (C20AA) synthesis.[15] The authors studied the potential of replacing polyurethane acrylate with bio-based C20AA and achieved the best results with 40 wt% of C20AA, which showed the highest double bond conversion of 83.7% after UV-curing. Chen et al. revealed an efficient photoredox catalytic method for radical-mediated functionalization of internal alkenes.[16] Four alkenes with internal double bonds were investigated in free-radical thiol-ene click reaction. The predicted order of reactivity of these internal alkenes was: norbornene > fumarate > maleimide > crotonate.[17]

Despite the growing research into environmentally friendly UV-curable materials, most commercial solutions rely on fossil-based monomers because of their high reactivity.[18] Our previous study showed the feasibility of the commercially available biobased components as a modifier for vegetable oil acrylate coatings.[19] In this study, we propose a novel biobased unsaturated furan-based ester (UES), which can successfully replace fossil-based reactive diluents like trimethylolpropane triacrylate (TMPTA),[20] broadly commercially available nowadays. Herein, furan-based unsaturated ester as a reactive diluent for vegetable oil acrylate is explored with 5 and 20 wt% loadings.

Vegetable oils have been used for the synthesis of polymer materials for decades. The current study focuses on the use of rapeseed oil as one of the most popular plant oils in Europe, consisting of more than 90% unsaturated acids.[21] Moreover, acrylated rapeseed oil (ARO) has

displayed much promise for developing new effective formulations used as resins for coatings, composites, foams, and 3D printing.[22–24] Herein, ARO has been grafted with UES through a UV-light-initiated photopolymerization crosslinking approach. UV curing was chosen due to its sustainability, versatility, and significant energy-saving aspects. The current research is focused on the reactivity and compatibility investigation of the lab-synthesized bio-based monomers, obtained resin properties, and light-cured thermoset biopolymer structural performance.

2 | EXPERIMENTAL SECTION

2.1 | Materials

Unrefined rapeseed oil was purchased from a local producer, "Iecavnieks" (Latvia). Acrylic acid, $BF_3{\cdot}Et_2O$, hexane, $NaHCO_3$, Na_2SO_4, acetone, and photoinitiator diphenyl(2,4,6-trimethylbenzoyl) phosphine oxide (TPO) were supplied by Sigma Aldrich. $LiClO_4$, MeOH, AcOH, and triethylamine (TEA) were supplied by Acros and Sigma-Aldrich. All chemicals were used as received unless otherwise stated.

2.2 | Synthesis of photoactive components

As described in our previous work, the furan-based unsaturated ester (UES) monomer was obtained in two electrochemical steps from furfurylated ethylene glycol X (Figure 1A).[25] First, it was electrochemically transformed to a spirocycle, which was then subjected to electrochemically induced rearrangement to form UES. Electrolysis was performed using the commercially available potentiostat Electrasyn 2.0.

The procedure is as follows: In the first electrolysis, furfurylated ethylene glycol, the supporting electrolyte $TBABF_4$, and the additive PPTS were transferred to an undivided cell, and dissolved in dry MeOH. Graphite electrodes were fitted to the cell and electrolysis was performed in constant current conditions until 2.3 F/mol of charge was passed through the cell. Afterward, the solvent was evaporated, and the product was purified using column chromatography (74% yield). During the second electrolysis, the spirocycle and supporting electrolyte $LiClO_4$ were transferred to an undivided electrochemical cell and dissolved in distilled MeOH. Then the additive AcOH was added. Graphite electrodes were fitted to the cell, and electrolysis was performed under constant current conditions. A total of 4.0 F/mol of charge was passed through the cell until all the starting material was consumed. After electrolysis, TEA was added, and the reaction mixture was filtered through a silica plug. The solvent was evaporated, and the product UES was purified using column chromatography (63% yield). The formation of UES with a *Z*-configuration double bond was observed, while *E*-isomer formation was not detected. The full synthesis procedure starting with furfuryl alcohol is available in supplementary file.

The acrylation reaction of rapeseed oil is shown in Figure 1B. Rapeseed oil, acrylic acid, and $BF_3{\cdot}Et_2O$ as catalyst were mixed in a round-bottom flask and stirred for 5 h at 80 °C before being left overnight at room

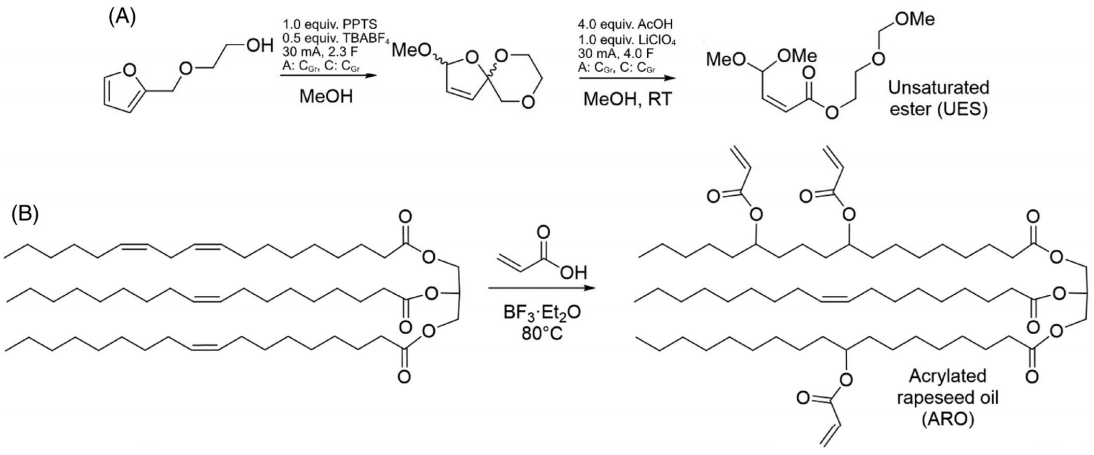

FIGURE 1 Synthesis of used materials (A) Unsaturated furan-based ester (UES) and (B) acrylated rapeseed oil (ARO).

temperature (22 ± 1 °C). In the work-up, the organic phase was dissolved in hexane, washed with a $NaHCO_3$ solution, dried over Na_2SO_4, and filtered. The solvent was removed via a rotary evaporator to obtain liquid acrylated rapeseed oil (ARO).

2.3 | Resin preparation

The UV-curable resins were prepared by mixing liquid ARO resin with 5 and 20 wt% liquid UES (approximately 1 mol ARO double bond equivalent was mixed with 0.1 and 0.4 mol UES double bond equivalent). Next, 3 wt% TPO dissolved in a small amount of acetone was added to each resin, mixed, and left overnight under the hood to allow the acetone to evaporate, yielding compositions ARO/UES5 and ARO/UES20, respectively.

2.4 | UV-curing and sample film preparation

Liquid resins were applied on a glass substrate using an applicator with a wet film thickness of 20 mils (508 μm). Then samples were cured under monochromatic conditions ($\lambda = 405$ nm) at a UV intensity of 400 μW cm^{-2} at a distance of 3 cm. The curing time was set to 70 s. After treating the samples' surfaces with acetone to remove the unreacted resins, they were peeled off and free-standing polymer films were obtained.

2.5 | Characterization

2.5.1 | Viscosity

The viscosity of liquid resins was measured on an Anton Paar MCR102 rheometer (Graz, Austria). The instrument was equipped with a 25 mm diameter spindle with plate-plate geometry. The measurement gap was set to 0.1 mm, and the shear rate range was set from 0.01 1 to 1000 s^{-1}.

2.5.2 | Fourier-transform infrared spectroscopy

Fourier-transform infrared spectroscopy (FT-IR) performed in attenuated total reflectance mode was used for the investigation. FT-IR Nicolet 6700 (ThermoScientific, Germany) was used to analyze the prepared samples. With 16 measurements, of which the average spectrum is displayed, a measurement error of 1% was achieved.

2.5.3 | UV–Vis spectroscopy

UV–Vis spectra of UV-cured samples were measured on a Shimadzu SolidSpec3700 UV–VIS–NIR spectrophotometer (Kyoto, Japan) with a 60 mm diameter integration sphere and a wavelength precision of 0.5 nm in the wavelength range of 300–700 nm. Tests were performed on UV-cured samples with a width of 250 μm in transmittance mode.

2.5.4 | Tensile tests

Tensile tests were performed on cured free-standing films to study the tensile behavior. Elongation at break, tensile strength, and tensile modulus were recorded on Tinius Olsen model 25ST (Horsham, PA, USA). All tensile tests were conducted at room temperature (22 ± 1 °C) at a 1 mm min^{-1} strain rate and repeated thrice. The average results are reported. Before measurements, samples were preconditioned for 24 h at room temperature with a RH of 40%.

2.5.5 | Scanning electron microscopy

A field emission scanning electron microscope (FE-SEM) Nova NanoSEM 650 (the Netherlands) was used to characterize the cross-sectional morphology of the cured samples. The samples were submerged in liquid nitrogen, cooled for about 60 s, removed from liquid nitrogen, and fractured with a light stroke of a hammer. Images were taken of the fractured cross-sections of the films. The samples were attached to standard 45°/90° angled aluminium pin stubs with electrically conductive double-sided carbon tape. The image was acquired with a 10 kV electron acceleration voltage in low vacuum conditions.

2.5.6 | Dynamic mechanical analysis

The cured free-standing films' storage modulus, loss modulus, and loss factor (tanδ) were recorded using a dynamic mechanical analyzer Mettler DMA/SDTA861e (Mettler Toledo, Columbus, OH, USA). The experiment was carried out in tension mode from −70 °C to 100 °C with a 3 °C min^{-1} heating rate, the applied force of 10 N and 10 μm elongation, and a frequency of 1 Hz. The photopolymerized films were prepared with dimensions of 8.5 mm (length) × 4 mm (width) × 0.2 mm (thickness).

2.5.7 | Thermogravimetric analysis

The thermal properties of cured samples were obtained using a thermogravimetric analyzer Mettler TG50 (Mettler Toledo, USA). About 10 mg of each cured sample was heated from 25 °C to 750 °C at a heating rate of 10 °C min^{-1} under an inert (N_2) atmosphere.

2.5.8 | Biodegradation

To measure the density (d) Sartorius KB BA 100 electronic scales with a Sartorius YDK 01 hydrostatic density measuring kit were set up. The following equation was used to determine the composite densities:

$$d = \frac{m_a(d_{EtOH} - d_{air})}{d_{water}(m_a - m_s)} + d_{air},$$

where m_a is the sample's measured mass in the air; m_s is the sample's measured mass when the sample is submerged in ethanol; d_{EtOH} is the density of ethanol (0.805 g/cm^3), which was measured with the aerometer; d_{air} is the density of the air (0.00120 g/cm^3), and d_{water} is the density of the water (0.99983 g/cm^3). For measurements, 10 replicates of each sample were utilized.

Soil burial tests evaluated the biodegradation of films. The weight loss of the films was studied under aerobic simulated composting conditions at 58 °C, soil humidity above 50% and a pH range between 5.7 and 6.5. Thin films were cut into rectangular shapes (10 mm × 10 mm × 0.1 mm) and sandwiched between sieves. Specimens were submerged in a commercial compost soil of local Latvian swamp peat (Formoss, Latvia) and packed in plastic containers. Recovered samples were cleaned with a brush and washed with distilled water. Before the measurements, specimens were vacuum dried for 4–6 h at 37 °C. The specimen's weight was measured before the test (reference abbreviated as 0 days) and on days 30, 40, 50, and 60. The remaining mass in percentage was calculated after measurements.

3 | RESULTS AND DISCUSSION

3.1 | Chemical structure, reaction analysis, and physical properties

The radical photopolymerization crosslinking between ARO and UES is shown in Figure 2A. Reaction (1) occurs between ARO and UES vinyl groups, forming dangling chains. The free radical generation is mainly restricted to a terminal double bond, whereas the conversion of internal double bonds usually remains challenging because the increased steric congestion hampers the intermolecular addition of radicals.[16] UES contains an internal double bond; therefore, reaction (2) between two unsaturated bonds of UES should be the slowest and occurs with a low probability. Internal alkenes are linked to more carbons along the chain, where the surrounding carbons stabilize their π bonds. This makes them more stable and less reactive than terminal alkenes.[26] The third crosslinking reaction (3) is between two ARO molecules and is likely to be favored and occur faster than other reactions. This could be explained by the terminal double bonds in the ARO structure. Since the terminal double bond is located at the end of the chain, it is only connected to primary carbon, which is the least stable. In addition, more rotational energy and higher steric freedom enable the terminal double bond to react more efficiently.[27]

Figure 2B visualizes the possible macromolecular chain network structure. The formation of the resulting macromolecular chain network with incorporated mobile pendant dangling chain ends may be explained by the many factors that affect crosslinking polymerization reactions.[28] The fatty acid composition, the nature of the oil, and the number of carbon–carbon double bonds, and dangling chains strongly impact the developed macromolecular structure and crosslinking quality. The long dangling chains present in the triglyceride structures have been reported to act as plasticizers, which can lower the mechanical properties (e.g., elastic modulus and tensile strength) of the polymer-based material. While the short dangling chains, resulting from furan-based unsaturated ester, cannot be counted as elastically effective chains but contribute to the free volume of the material and chain relaxation phenomena.[29] In turn, the observed dangling chains account for the crosslinking network degree and decrease in the glass transition temperature of the developed polymer. The crosslinking density ν_e, calculated by the Flory–Rehner equation as reported elsewhere,[30,31] increased significantly from $1.07 \cdot 10^3$ to $1.65 \cdot 10^3$ mol/m^3 for ARO and ARO/UES5 (ARO with 5 wt% UES), respectively. The improved crosslinking density after incorporating 5 wt% of UES enhances the polymer materials' tensile strength, storage modulus and glass transition temperature (discussed in the following sections). The materials' measured density is 1.009 ± 0.0029, 1.013 ± 0.0017, and 1.003 ± 0.0056 g/cm^3 for ARO, ARO/UES5, and ARO/UES20, respectively. The proposed reactive diluent UES facilitates the crosslinking of chains; it also significantly decreases the resin viscosity, as shown in Figure 2C. With 20 wt% UES, the resin viscosity drops approximately 1.6 times. A biobased diluent, cardanyl acrylate, was used as a reactive diluent for UV-curable castor oil-based polyfunctional

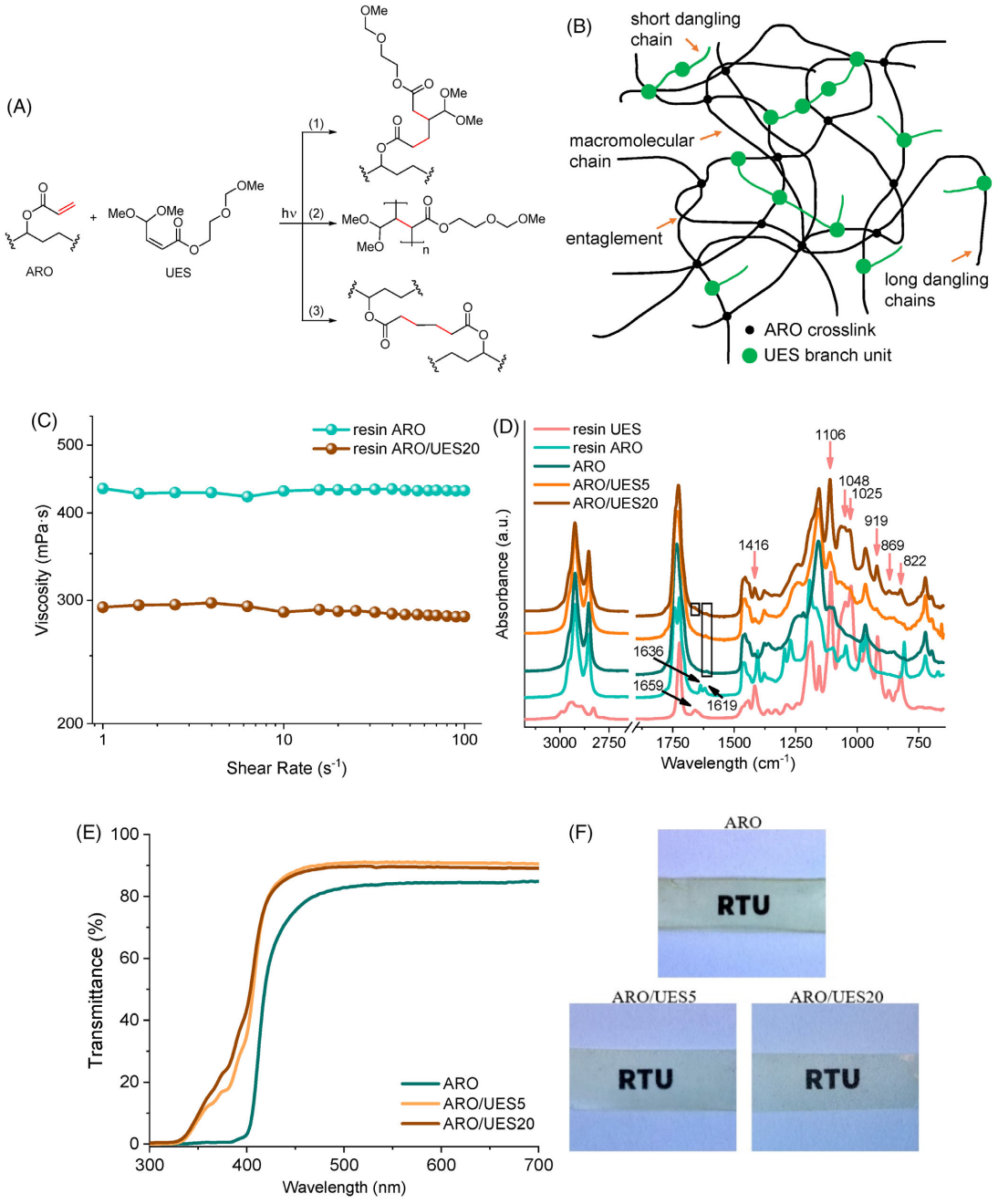

FIGURE 2 (A) Possible reactions between ARO and UES; (B) schematic illustration of ARO and UES crosslinked network; (C) viscosity dependence on shear rate; (D) FT-IR spectra of UES and ARO liquid resins and polymerized samples; (E) UV–VIS transmittance spectra of sample films; (F) Optical images of sample films.

polyurethane acrylate resin.[32] With the addition of 20 wt% cardanyl acrylate, viscosity dropped from 1360 to 340 mPa s. Dipak et al. used a bio-based castor oil-based reactive diluent as an additive to lower the viscosity of UV-curable urethane acrylate oligomer.[33] The authors showed that viscosity dropped from about 1070 mPa·s (neat) to about 560 mPa·s for resin that contained 20 wt% reactive diluent. Zhang et al. reported the successful use of bio-based of methacrylated eugenol as a reactive diluent for maleinated acrylated epoxidized soybean oil.[34] While viscosities between matrices vary significantly, it can be noted that methacrylated eugenol has a viscosity of about 110 mPa s (shear rate up to 100 s^{-1}). Hence, UES acts as an effective reactive diluent, achieving viscosity values comparable to those presented in the literature.

Figure 2D reveals the FT-IR spectra of liquid resins ARO and UES (resin ARO, and resin UES, respectively) and respective UV-cured polymers (ARO, ARO/UES5, and ARO/UES20). The characteristic UES vibrational type peaks can be seen in ARO/UES5 and ARO/UES20 samples (marked with pink arrows). Characteristic peaks of ARO are described in detail elsewhere.[23] We are interested in the internal double bond peak for UES and ARO's terminal double bond peak. Double bond peaks at 1636 and 1619 cm^{-1} in ARO resin spectra and 1659 cm^{-1} in UES resin spectra (black arrows) almost fully disappear after UV curing.[23] From two ARO peaks, only a minimal peak remains at 1619 cm^{-1}, while in the ARO/UES20 spectra at 1659 cm^{-1} some traces of unreacted UES double bonds can be observed. Thus, FTIR serves as an indication of the high conversion rate of double bonds. It is also testified by boosting up to 90% optical transmittance in the UV–VIS region of the developed polymer film when the UES monomer is incorporated (Figure 2E). The excellent optical transparency of the obtained films can be seen in the optical images in Figure 2F. Some reactive groups remain in the polymer after complete photopolymerization and absorb in specific regions (i.e., below 400 nm).[35] At the same time, UES enhances the polymer's overall optical transparency, which could also be related to the observations that reactive diluent increases the crosslinking density of the developed polymer network.

3.2 | Tensile properties

Tensile test stress–strain curves are shown in Figure 3. With the addition of UES, tensile strength increased from 0.49 to 0.55 MPa for ARO/UES5, while a decrease was observed for ARO/UES20 showing a value of 0.31 MPa. Two distinct stress–strain patterns are visible, with ARO/UES20 following the curve of ARO, while ARO/UES5 becomes noticeably stiffer. This observation is complemented by tensile modulus values of 9.2, 16.2, and 7.9 MPa for ARO, ARO/UES5, and ARO/UES20, respectively. This can be explained by an increased crosslink density in ARO/UES5. The content of long fatty acid aliphatic chains is lowered by adding UES. Small molecules of UES can find the optimal placements in the structure and provide strong intermolecular bonding. It should be noted that the ARO double bond reactivity is limited by steric interference; thus, ARO cannot reach 100% of double bond conversion. However, smaller UES molecules can overcome these limitations and add denser intermolecular bonding on top of chemical crosslinking; as such, a material's tensile strength and tensile modulus increase.

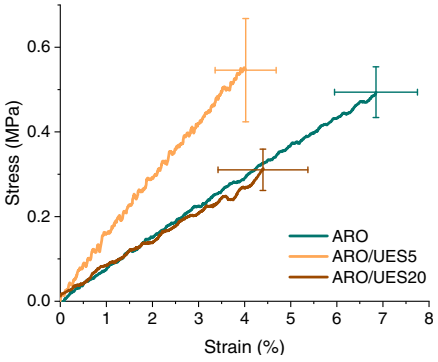

FIGURE 3 Stress–strain curves of UV-cured polymers.

Adding 20 wt% of UES introduces a notable amount of the second component. This opens several routes of possible interactions. As a smaller molecule, UES can more easily find double bonds to react with, hindering the formation of a strong crosslinked network of ARO, resulting in lower chemical cross-linking. Thus, reducing crosslinking between ARO and adding too many dangling chains and a plasticizing effect.[29] While a notable amount of the second component can also yield the formation of an additional phase in the thermoset structure.[36] If the material's phase interface is weak, then a drop in mechanical properties is observed.[37] The decreased elongation (strain) values for ARO/UES5 match the observed increase in tensile modulus, thus clearly indicating structural changes attributed to enhanced crosslinking. While for ARO/UES20, the decrease in strain is assigned to disrupted ARO network, which cannot achieve the conformation changes required for elongation due to interference of the second phase or dangling chains.

3.3 | Morphology of sample films

The morphology of the UV-cured films was examined with SEM. The micrographs of cured samples are shown in Figure 4. The incorporation of UES increased the

overall roughness of the fracture surface. No visible phase separation can be observed, indicating that both components are cross-linked. The enhanced fracture roughness indicates structural changes related to increased crosslinked network complexity. Thus, fracture forms and finds a route that spreads through the weakest structural links. The pronounced cracks of ARO/UES5 indicate elongation of the fracture route, which matches the observed increase in tensile strength. In the case of ARO/UES20, the uneven fracture surface could be explained by stress concentrations and very loosely connected regions in the thermoset structure, which serves as multiple failure points that connect during fracture. The complex nature of the observable surface for ARO/UES20 also indicates that components did not react in balanced proportions, creating local defects, which explain the decrease in tensile properties.

3.4 | Dynamic mechanical analysis

Storage modulus, loss modulus, and loss factor (tanδ) graphs for ARO and ARO/UES5 are shown in Figure 5. Tensile test results showed that adding 5 wt% UES increased storage modulus. Given the similarities between the storage modulus and tensile modulus, the increase observed for ARO/UES5 matches the abovementioned observations. ARO showed 7.9 MPa and ARO/UES5 12.0 MPa at 22 °C (Figure 5A). The difference in storage modulus values reached as high as 583 MPa at −60 °C. The loss modulus shows the materials dissipated energy, which peaks at the glass transition, where large segmental motions start to occur.[38,39] The ARO/UES5 saw an increase of the glass transition temperature by 2 °C and had an increased peak maximum and broader overall shape compared to ARO. This indicates that crosslinking between ARO molecules was enhanced, while UES chains restricted segmental rearrangements, as indicated by increased loss modulus value. In the tanδ graph, the narrower peak of ARO/UES5 indicates the structural changes in the ARO network as molecular relaxations take place at slightly lower temperatures. Also, a slightly lower tanδ peak maximum of ARO indicates a more rigid structure of the macromolecular network. Still, in a viscoelastic state, the material proved to have higher resistance to deformation, as indicated by increased storage modulus and

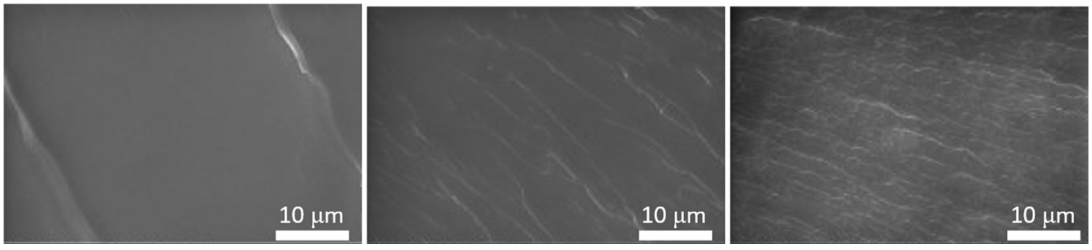

FIGURE 4 Fracture surface SEM images at 2500× magnification: (A) ARO; (B) ARO/UES5; and (C) ARO/UES20.

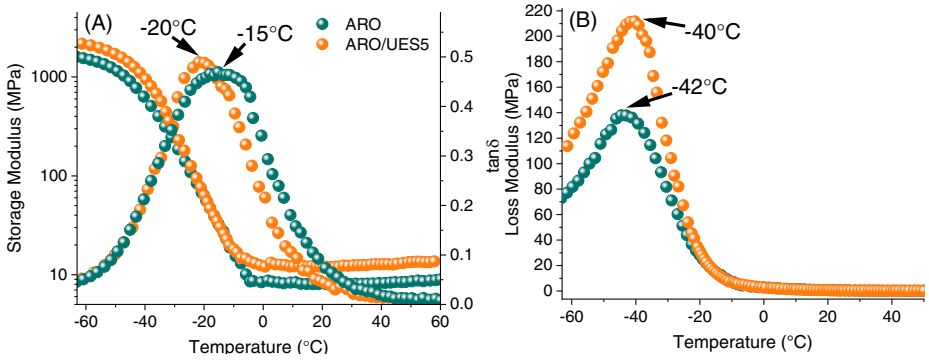

FIGURE 5 Dynamic mechanical analysis (DMA) curves for cured samples: (A) Storage modulus and tanδ and (B) Loss modulus.

crosslinking degree. This could be explained by changes in chain structural packing, augmented chain intermolecular entanglements and enhanced crosslinking degree.

Tensile tests and dynamic mechanical analysis (DMA) both indicate that ARO-based polymers in this study yield relatively soft materials. At the same time, if more rigid properties are desired, several modification strategies can be applied. First, aimed at increased glass transition, which can be achieved by increasing crosslinking density, for example, by the use of additional polyfunctional reactive diluents, additional steps to enhance acrylation degree of vegetable oil, and improve post-curing processes.[40] Second, the use of reinforcement via the preparation of biocomposites could be considered. This can be achieved with the use of nanofillers like nanocellulose.[41]

3.5 | Thermogravimetric analysis

Thermogravimetric analysis (TGA) and derivative thermogravimetric (DTG) curves for the samples are shown in Figure 6. The initial thermal decomposition temperature of crosslinked ARO/UES was lower than that of neat ARO. With the addition of UES, the $T_{5\%}$, which indicates the weight loss at 5 wt%, decreased from 289 to 271 and 204 °C for ARO/UES5 and ARO/UES20, respectively (Figure 6A). TGA revealed a linear decrease in $T_{5\%}$ temperature, proportional to UES content (Figure 6A inset plot).

A three-step degradation pattern is observed for all samples in Figure 6B. The first peak is attributed to the degradation of the crosslinked ester-ether moieties in the UES side chain.[42] The maximum rate of ester decomposition is reached at around 205 °C. While the first notable weight drop in ARO is attributed to more loosely connected sections of the network. The second visible peak with a maximum of around 350 °C is assigned to the degradation of acrylic moieties and the polymer backbone. The maximum degradation rate (T_{max}) is achieved between 370 and 430 °C, resulting from chain scission in the oil-based ester groups.[43] The remaining degradation products are further carbonized at a higher temperature. Over 600 °C, pyrolysis occurs with little weight loss.[42]

3.6 | Biodegradation studies in the composting conditions

Reactive diluents are typically fossil vinyl monomers, and their addition into the formulation increases the non-degradable component of the product.[44] In the literature, there is no evidence for the commonly used crosslinked reactive diluents like (2-hydroxyethyl methacrylate (HEMA) to be biodegradable.[45]

The percentage weight loss in composting conditions for ARO and ARO/UES films is presented in Figure 7A. Furthermore, Figure 7B visualizes the samples after removal from the soil. Although ARO showed 28% weight loss after 2 months, the degradation rate remained relatively stable but slightly decreased over time. The compositions with UES showed a similar degradation rate during the initial 30 days compared to ARO but afterwards saw a significant drop in degradation speed. We assume that fatty acid hydrolysis is the primary reaction that occurs during biodegradation, and the presence of UES obstructs microbial activity and limits access to ester bonds. The ARO/UES20 degraded slightly faster than ARO/UES5. This could be explained by the looser structure that lacks

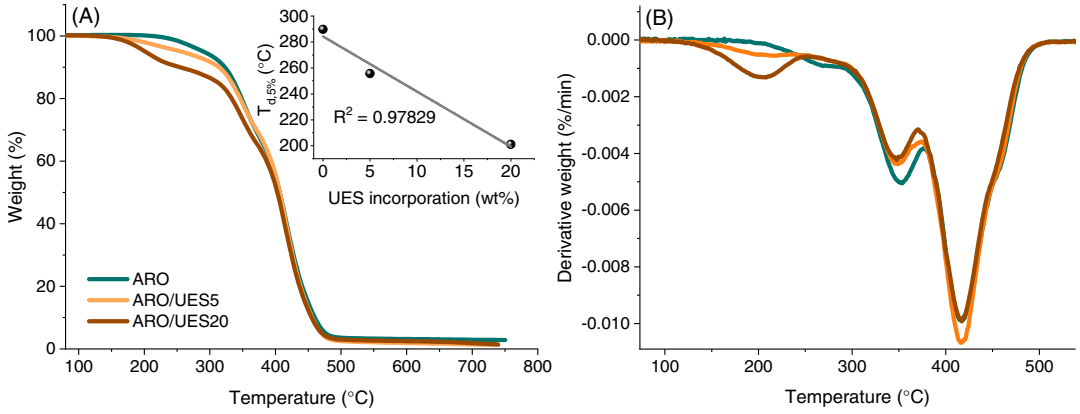

FIGURE 6 TGA of photocured polymers containing varied amounts of UES: (A) TGA thermogram (the inset plot reveals the trend in $T_{d,5\%}$ with increasing UES content); (B) Derivative thermogram (DTG).

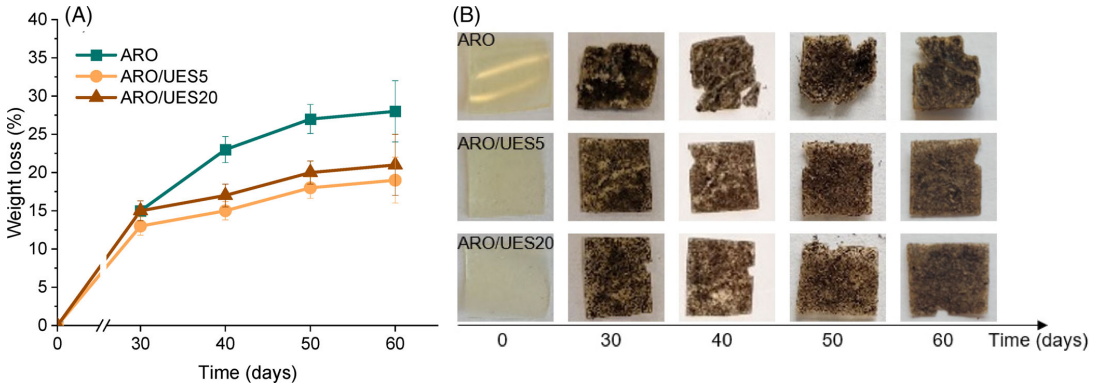

FIGURE 7 (A)) Weight loss of ARO and ARO/UES during soil burial test and (B) Optical images of samples before and after biodegradation.

the dense crosslinking in the ARO/UES5 structure, making the water migration easier, exposing more surface, and losing the structural integrity faster.

It has been reported before that the increase in double bond content does not significantly affect the biodegradability of acrylated epoxidized soybean oil (AESO).[46] After a 3-month biodegradation test in the garden soil, AESO showed a weight loss of approximately 16%. Adding a co-monomer lowered the degradation by about 2%. In another study, 3D printed objects from waste cooking oil collected from McDonald's restaurant demonstrated a weight loss of around 20% in only 2 weeks when buried in soil and kept at 25 °C and 30% relative humidity.[47]

4 | CONCLUSIONS

This work focuses on a polymer material made from two bio-based photoactive components, presenting the influence of UES as a reactive diluent on the ARO matrix. Three proposed reactions can occur during photopolymerization between the two components.

A correlation between tensile and DMA results showed a notable performance increase with the addition of 5 wt% UES. With the addition of relatively low loadings, UES can potentially tune the mechanical properties of ARO towards stiffer structures. Furthermore, the thermal degradation temperature of UES is notably lower than ARO's. Still, this should not limit most applications and uses.

The biodegradability of compositions was explored, and a maximum mass loss of 28 wt% was achieved in 60 days for ARO. The addition of UES slightly reduced the biodegradation rate. Follow-up studies with evolved carbon dioxide measurements are needed to evaluate the degradation rate further.

ACKNOWLEDGMENTS

This work was supported by Latvian Council of Science in the framework of FLPP "Printed biopolymer 4D TENG device for mechanical energy harvesting" (lzp-2022/1-0485). Sabine Briede was funded by the European Social Fund within the Project No 8.2.2.0/20/I/008 «Strengthening of PhD students and academic personnel of Riga Technical University and BA School of Business and Finance in the strategic fields of specialization» of the Specific Objective 8.2.2 «To Strengthen Academic Staff of Higher Education Institutions in Strategic Specialization Areas» of the Operational Programme «Growth and Employment». Sabine Briede was supported by Riga Technical University's Doctoral Grant programme. The authors would like to thank their parental institutions for their support. Madara Darzina was supported by Latvian Institute of Organic Synthesis student grant no. IG-2023-07.

CONFLICT OF INTEREST STATEMENT

The authors declare that they have no conflict of interest.

DATA AVAILABILITY STATEMENT

Data is available upon request from corresponding author as it is part of larger ongoing study.

ORCID

Oskars Platnieks https://orcid.org/0000-0001-5529-0912
Aigars Jirgensons https://orcid.org/0000-0002-8937-8792
Sergejs Gaidukovs https://orcid.org/0000-0001-8638-5009

REFERENCES

[1] W. Shi, B. Rånby, *UV J. Appl. Polym. Sci.* **1994**, *51*, 1129.

[2] Z. Dai, Q. Li, Z. Chen, R. K. Shawon, Y. Zhu, H. Lv, F. Fu, Y. Zhu, Y. Fu, X. Liu, *ACS Sustain. Chem. Eng.* **2020**, *8*, 17379.
[3] S. Cousinet, A. Ghadban, E. Fleury, F. Lortie, J.-P. Pascault, D. Portinha, *Eur. Polym. J.* **2015**, *67*, 539.
[4] A. Nebioglu, M. D. J. Soucek, *Polym. Sci., Part A: Polym. Chem.* **2006**, *44*, 6544.
[5] S. RameshKumar, P. Shaiju, K. E. O'Connor, *Curr. Opin. Green Sustain. Chem.* **2020**, *21*, 75.
[6] B. T. White, V. Meenakshisundaram, K. D. Feller, C. B. Williams, T. E. Long, *Polymer* **2021**, *223*, 123727. https://doi.org/10.1016/j.polymer.2021.123727
[7] H. Esen, S. Küsefoğlu, R. Wool, *J. Appl. Polym. Sci.* **2007**, *103*, 626.
[8] C. Bonneaud, M. Decostanzi, J. Burgess, G. Trusiano, T. Burgess, R. Bongiovanni, C. Joly-Duhamel, C. M. Friesen, *RSC Adv.* **2018**, *8*, 32664.
[9] H. Wei, T. Y. Lee, W. Miao, R. Fortenberry, D. H. Magers, S. Hait, A. C. Guymon, S. E. Jönsson, C. E. Hoyle, *Macromolecules* **2007**, *40*, 6172.
[10] S. K. Yadav, K. M. Schmalbach, E. Kinaci, J. F. Stanzione, G. R. Palmese, *Eur. Polym. J.* **2018**, *98*, 199.
[11] S. Briede, A. Barkane, M. Jurinovs, V. K. Thakur, S. Gaidukovs, *Curr. Opin. Green Sustain. Chem.* **2022**, *35*, 100626.
[12] X. Yang, S. Li, J. Xia, J. Song, K. Huang, M. Li, *Ind. Crop. Prod.* **2015**, *63*, 17.
[13] M. Fei, T. Liu, B. Zhao, A. Otero, Y.-C. Chang, J. Zhang, *ACS Appl. Polym. Mater.* **2021**, *3*, 2470.
[14] L. Meng, H. Qiu, D. Wang, B. Feng, M. Di, J. Shi, S. Wei, *Prog. Org. Coat.* **2020**, *140*, 105492.
[15] D. Wei, X. Huang, J. Zeng, S. Deng, J. Xu, *J. Appl. Polym. Sci.* **2020**, *137*, e49054.
[16] Y. Chen, J. Wang, X. Wu, C. Zhu, *ACS Org. Inorg. Au* **2022**, *2*, 392.
[17] B. H. Northrop, R. N. Coffey, *J. Am. Chem. Soc.* **2012**, *134*, 13804.
[18] L. Dall Agnol, F. T. G. Dias, H. L. Ornaghi, M. Sangermano, O. Bianchi, *Prog. Org. Coat.* **2021**, *154*, 106156.
[19] S. Briede, O. Platnieks, A. Barkane, I. Sivacovs, A. Leitans, J. Lungevics, S. Gaidukovs, *Coatings* **2023**, *13*, 657.
[20] A. Barkane, O. Platnieks, M. Jurinovs, S. Kasetaite, J. Ostrauskaite, S. Gaidukovs, Y. Habibi, *Polymer* **2021**, *13*, 1195.
[21] E. Woźniak, E. Waszkowska, T. Zimny, S. Sowa, T. Twardowski, *Front. Plant Sci.* **2019**, *10*, 1423.
[22] Y. Su, H. Lin, S. Zhang, Z. Yang, T. Yuan, *Polymer* **2020**, *12*(5), 1165.
[23] S. Briede, M. Jurinovs, S. Nechausov, O. Platnieks, S. Gaidukovs, *Mol. Syst. Des. Eng.* **2022**, *7*, 1434.
[24] M. Kolář, J. Machotová, M. Hájek, J. Honzíček, T. Hájek, Š. Podzimek, *Coatings* **2023**, *13*(2), 262.
[25] M. Darzina, A. Lielpetere, A. Jirgensons, *Eur. J. Org. Chem.* **2021**, *2021*, 4224.
[26] Y. Li, H. Liu, Z. Huang, H. Wang, Z. Yu, *Tetrahedron Lett.* **2021**, *82*, 153396.
[27] Z. P. Vang, A. Reyes, R. E. Sonstrom, M. S. Holdren, S. E. Sloane, I. Y. Alansari, J. L. Neill, B. H. Pate, J. R. Clark, *J. Am. Chem. Soc.* **2021**, *143*, 7707.
[28] T. S. Omonov, V. Patel, J. M. Curtis, *J. Am. Oil Chem. Soc.* **2019**, *96*, 1389.
[29] D. P. Pfister, Y. Xia, R. C. Larock, *ChemSusChem* **2011**, *4*, 703.
[30] P. J. Flory, J. Rehner, *J. Chem. Phys.* **1943**, *11*, 512.
[31] S. Gaidukovs, A. Medvids, P. Onufrijevs, L. Grase, *Express Polym Lett* **2018**, *12*, 918.
[32] Y. Hu, Q. Shang, J. Tang, C. Wang, F. Zhang, P. Jia, G. Feng, Q. Wu, C. Liu, L. Hu, W. Lei, Y. Zhou, *Ind. Crop. Prod.* **2018**, *117*, 295.
[33] D. S. Tathe, R. N. Jagtap, *J. Coat. Technol. Res.* **2015**, *12*(1), 187.
[34] Y. Zhang, Y. Li, L. Wang, Z. Gao, M. R. Kessler, *ACS Sustain. Chem. Eng.* **2017**, *5*(10), 8876.
[35] F. Masson, C. Decker, S. Andre, X. Andrieu, *Prog. Org. Coat.* **2004**, *49*(1), 1.
[36] M. J. Stevens, *J. Chem. Phys.* **2021**, *155*, 054905.
[37] D. A. Jesson, J. F. Watts, *Polym. Rev.* **2012**, *52*, 321.
[38] P. Lall, M. Kasturi, H. Wu, E. Davis, Proceedings of 2020 19th IEEE Intersociety Conference on Thermal and Thermomechanical Phenomena in Electronic Systems (ITherm), pp. 1389–1394. **2020** https://doi.org/10.1109/ITherm45881.2020.9190482
[39] Y. Sun, Z. Zhang, K.-S. Moon, C. P. J. Wong, *Polym. Sci. B: Polym. Phys.* **2004**, *42*, 3849.
[40] M. Lebedevaite, V. Talacka, J. Ostrauskaite, *J. Appl. Polym. Sci.* **2021**, *138*(16), 50233.
[41] A. Barkane, M. Jurinovs, S. Briede, O. Platnieks, P. Onufrijevs, Z. Zelca, S. Gaidukovs, *3D Print. Addit. Manuf.* **2022**. https://doi.org/10.1089/3dp.2021.0294
[42] X. Yang, Y. Li, W. Lei, X. Liu, Q. Zeng, Q. Liu, W. Feng, K. Li, P. Wang, *Polym. Degrad. Stab.* **2021**, *191*, 109668.
[43] S. K. Sahoo, V. Khandelwal, G. Manik, *Polym. Adv. Technol.* **2018**, *29*, 2080.
[44] Y. Bao, N. Paunović, J. C. Leroux, *Adv. Funct. Mater.* **2022**, *32*(15), 2109864.
[45] G. Mabilleau, M. Moreau, R. Filmon, M. Baslé, D. Chappard, *Biomaterials* **2004**, *25*(21), 5155.
[46] J. Chen, H. Liu, W. Zhang, L. Lv, Z. Liu, *J. Appl. Polym. Sci.* **2020**, *137*, 48827.
[47] B. Wu, A. Sufi, R. Ghosh Biswas, A. Hisatsune, V. Moxley-Paquette, P. Ning, R. Soong, A. P. Dicks, A. J. Simpson, *ACS Sustain. Chem. Eng.* **2019**, *8*, 1171.

SUPPORTING INFORMATION

Additional supporting information can be found online in the Supporting Information section at the end of this article.

How to cite this article: S. Briede, O. Platnieks, M. Darzina, A. Jirgensons, S. Gaidukovs, *J. Polym. Sci.* **2023**, *61*(24), 3318. https://doi.org/10.1002/pol.20230451

Pielikums IV

Appendix IV

Platnieks, O., Briede, S., Grase, L., Thakur, V., J., & Gaidukovs, S.

Fully Bio-Based Thermoset Composites from UV Curable Prepregs: Vegetable Oil Acrylate Impregnated Hemp Nanopaper

Polymer Composites, **2023**, 44(9), 5721-5733.

doi: 10.1002/pc.27521

Received: 8 March 2023 | Revised: 17 May 2023 | Accepted: 13 June 2023

DOI: 10.1002/pc.27521

RESEARCH ARTICLE

Polymer COMPOSITES WILEY

Fully bio-based thermoset composites from UV curable prepregs: Vegetable oil acrylate impregnated hemp nanopaper

Oskars Platnieks[1] | **Sabine Briede**[1] | **Liga Grase**[2] | **Vijay Kumar Thakur**[3] | **Sergejs Gaidukovs**[1]

[1]Institute of Polymer Materials, Faculty of Materials Science and Applied Chemistry, Riga Technical University, Riga, Latvia

[2]Institute of Materials and Surface Engineering, Faculty of Materials Science and Applied Chemistry, Riga Technical University, Riga, Latvia

[3]Biorefining and Advanced Materials Research Center, Scotland's Rural College (SRUC), Edinburgh, UK

Correspondence
Oskars Platnieks and Sergejs Gaidukovs, Institute of Polymer Materials, Faculty of Materials Science and Applied Chemistry, Riga Technical University, P. Valdena 3/7, Riga LV-1048, Latvia.
Email: oskars.platnieks_1@rtu.lv and sergejs.gaidukovs@rtu.lv

Funding information
Latvijas Zinātnes Padome, Grant/Award Number: lzp-2019/1-0390

Abstract

Modern thermoset composite matrices are primarily prepared from petroleum-based plastics, while reinforcements commonly consist of non-renewable and energy-demanding glass and carbon fibers. Herein, a non-chemically treated hemp fiber-reinforced composite was prepared from bio-based components: hemp nanopaper (NP) and acrylated epoxidized soybean oil (AESO) or acrylated rapeseed oil (ARO). A commercial-grade AESO was selected as a reference and compared to ARO prepared in a one-step synthesis. The impregnation process was examined in detail by studying the impact of surface wetting, temperature, and vacuum on the composite structure. ARO has excellent fiber surface wettability, showing initial contact angles between 46.5° and 48.2° on hemp NP. A more than 10-fold difference in viscosity between AESO and ARO was observed. ARO composite with 50 wt% hemp loading achieved a Young's modulus of 1.3 GPa, a tensile strength of 26 MPa, and a storage modulus of 4.4 GPa (at 20°C). The results are supplemented by scanning electron microscope analysis of composite morphology via liquid nitrogen fracture and tensile failure analysis, that is, fractography. Dielectric spectroscopy analysis shows that composites have the potential to replace epoxy/paper composite insulators.

KEYWORDS

biofibers, dielectric properties, mechanical properties, photopolymerization, renewable resources

1 | INTRODUCTION

Modern reinforced thermoset composites have become an integral part of various cutting-edge technologies. Since their introduction, fiber-reinforced composites have become increasingly widespread across various sectors, from electronics to aerospace. However, from a modern perspective, their long-term production cannot meet sustainability goals, especially considering the energy required to manufacture synthetic fibers such as glass and carbon fibers.[1] Song et al. reviewed the potential of hemp fiber, indicating that up to 80% of energy could be saved by introducing hemp fiber-based materials as replacements for various conventional materials.[2] The second aspect is the non-renewable nature of polymer resins, which require appropriate replacements from bio-based sources.[3] Thus, a fully bio-based thermoset composite consisting of bio-based resins combined with plant fiber reinforcement can be devised.

In the last decade, the cultivation of natural fiber-rich plants such as hemp, jute, kenaf, flax, and sisal has risen tremendously.[4] Various plant parts, such as coir from coconuts and hemp stalks, have found practical applications, while previously they were often regarded as agricultural waste.[5,6] Hemp stands out as a multifunctional crop that can be applied in several fields depending on the part of the crop, including bioenergy production, oil extraction, pharmaceuticals, and fibers.[7] In addition, hemp is compatible with cold climates and produces relatively large yields, of which hemp stalks are still underutilized but full of exceptionally durable cellulose fibers.[8,9]

Triglycerides (vegetable oils) have shown great potential for polymer production and have even yielded commercial products such as acrylated epoxidized soybean oil (AESO).[10] While direct application of oils is challenging, relatively simple modification methods are very efficient in turning them into reactive monomers. However, the commercial bio-based monomer field is relatively small now, and AESO is one of the leading products with a relatively high viscosity (up to 37,500 mPa·s[11]), which limits its applications.[12] Epoxides and epoxidized oil acrylates have been shown to impact viscosity more than acrylates.[13–15] Our previous research showed that direct acrylation of vegetable oils results in better processing properties (due to reduced viscosity), which enable 3D printing without diluents.[16]

Hemp and other natural fibers have been explored for their potential as replacements for glass and carbon fibers in various composite materials. These primarily include the use of spun fibers or fabrics that are impregnated with thermoset polymers such as epoxy. Lebrun et al. prepared epoxy-impregnated unidirectional hemp fiber composites as an alternative to fiberglass composites.[17] The authors reported that adding a paper layer to composites reduced the variation in their mechanical properties, which stem from the growing conditions of plants. Åkesson et al. used a combination of spray impregnation and hot compression molding to produce flax fiber mats and AESO composites.[18] The authors reported that viscosity was reduced by increasing the AESO temperature to 50°C, and composites with fiber loadings up to 70 wt% were produced. Various other authors have reported that using natural fibers leads to inconsistent composite properties.[19] Paper, fabrics, or mats can be prepared from natural fibers to reduce property variability. Paper preparation is especially beneficial in the case of various waste products that contain natural fibers. They can be ground, cast, and compressed by applying methods that have been historically used for hundreds of years and are relatively simple in terms of technology.

Fossil-derived chemicals such as mineral oil and epoxides are widely used for paper impregnation in electric insulation systems.[20] Kolcunova et al. demonstrated mineral oil replacement with a sustainable alternative, that is, sunflower oil, which yields similar performance after a long thermal aging process.[21] Miao et al. applied epoxidized soybean oil as a coating on the paper and characterized the obtained composites as potential water-resistant materials.[22] A hemp fabric/bio-epoxy sandwich structure was tested for sound transmission loss, thus expanding the potential application field.[23] Aitomäki et al. studied cellulose nanofiber networks impregnated with low-viscosity epoxy.[24] The authors reported that impregnated composites' properties depended more on the fiber network's properties than the nanofibrils' properties. Thus, rather than obtaining high-quality nanocellulose, other parameters, such as porosity, should be optimized for the impregnation process.

We propose using hemp stalks (agricultural waste) to produce cheap, low-environmental-impact papers. Hemp nanopaper (NP) is impregnated with modified vegetable oil-based monomers to prepare fully bio-based composites. Commercially sourced AESO was selected as a reference and compared with acrylated rapeseed oil (ARO) prepared in one-step synthesis to prepare impregnated composites. Samples were prepared from cast and compressed papers by grinding and fibrillating hemp stalks without any chemical treatment. Hemp NP was impregnated in a controlled environment to produce UV-curable prepregs. The penetration depth of impregnated oil and surface adsorption were analyzed with scanning electron microscope (SEM). In addition, tensile, dynamic mechanical, and dielectric properties were measured and compared. The obtained biobased thermoset composites can be applied as decorative or structural panels in construction, electrical insulation, composites in the automotive industry, furniture, thermal insulators for indoor environments, and surfaces that are occasionally exposed to humid or wet environments. Figure 1 shows the proposed steps for preparing hemp/vegetable oil composites.

2 | EXPERIMENTAL

2.1 | Materials

AESO, hexane, boron trifluoride diethyl etherate, sodium hydroxide (NaOH), sodium hydrogen carbonate ($NaHCO_3$), acrylic acid, and photoinitiator diphenyl (2,4,6-trimethyl benzoyl) phosphine oxide (TPO) were supplied by Sigma Aldrich. Unrefined rapeseed oil was purchased from a local market. Hemp stalks (Santhica 27) were obtained from a farm in Latvia and are locally grown. The chemical composition of the hemp stalks showed 68.5% cellulose, 11.1% hemicellulose, and 6%

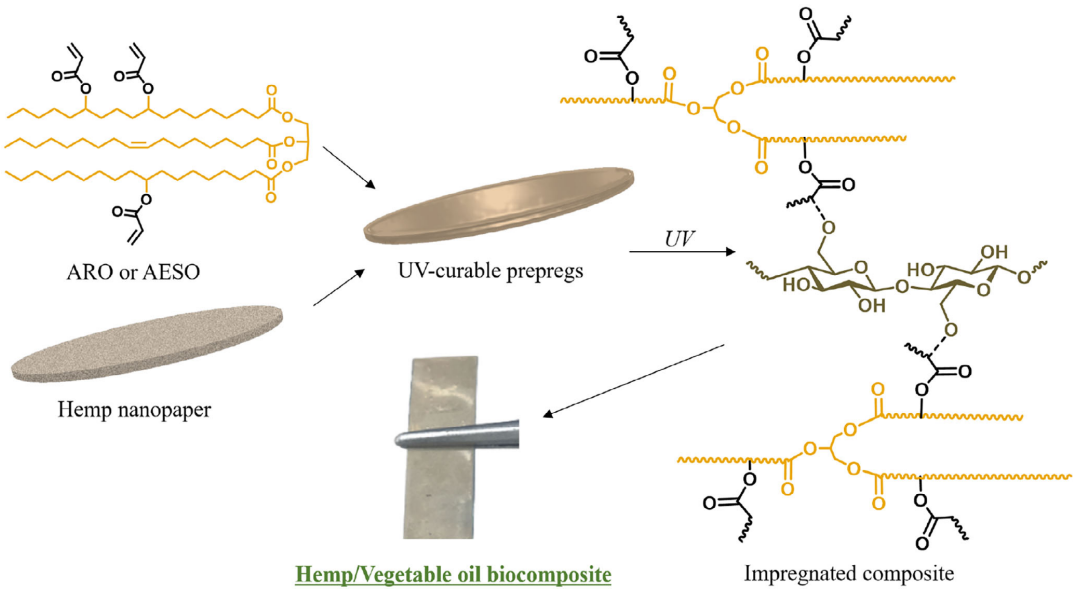

FIGURE 1 Schematic representation of the composite preparation.

lignin; a full analysis is presented in our previous research.[25] A laboratory-grade filtering system was used to prepare deionized (DI) water.

2.2 | Material processing and synthesis

ARO was synthesized via a one-step synthesis as described in our previous work.[16] Briefly, rapeseed oil, acrylic acid, and $BF_3{\cdot}OEt_2$ were mixed in a round-bottom flask. Next, the mixture was stirred for 5 h at 80°C before being left overnight at a room temperature of 20°C. In the work-up, the organic phase was dissolved in hexane, washed with a $NaHCO_3$ solution, dried, filtered, and evaporated under reduced pressure.

Hemp stalks were ground using a Retsch SM300 cutting mill. Two pass-troughs were used, and the mill was equipped with a sieve size of 4.00 and 0.25 mm, respectively. An additional milling step was performed on a Retsch ZM200 with sieve sizes of 0.12 mm. The obtained hemp powder was dispersed in DI water to prepare a 1.00 wt% suspension. For 5 cycles, the obtained suspension was passed through a microfluidizer (LM20, Microfluidic, United States) with chamber H210Z (200 m) and pressure set to 30,000 psi. As a result, a nanofibrillated hemp suspension was produced with a diameter of 86 ± 41 nm. Figure 2 shows a transmission electron microscopy (TEM) micrograph of the produced hemp nanofibers. Hemp NP was produced by casting the

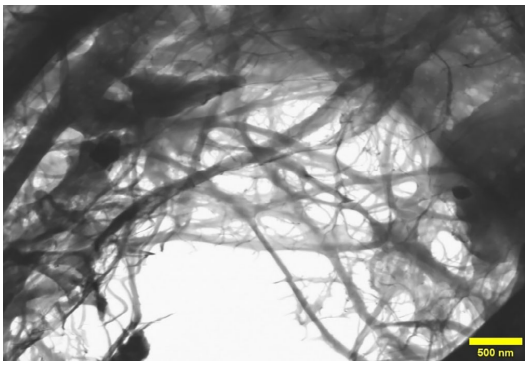

FIGURE 2 Transmission electron microscopy (TEM) micrograph of hemp nanofibers.

nanofibrillated suspension onto polystyrene (PS) Petri dishes with a diameter of 14.5 cm. Films were dried at room temperature (relative humidity 30%) for 4 days and one additional day with the thermostat set to 60°C.

2.3 | Preparation of impregnated UV-curable NP prepregs

The hemp NP was left overnight in a vacuum chamber at 70°C. After removal from the vacuum, it was pressed under 3 metric tons of pressure at 80°C (Carver CH 4386)

TABLE 1 Composition and processing condition for impregnated NP.

Sample	NP (wt%)	AESO (wt%)	ARO (wt%)	Temperature (°C)	Pressure (bar)
NSR	35	65	-	20	1.01
NSV	35	65	-	20	0.02
NSVT	35	65	-	50	0.02
NRR	50	-	50	20	1.01
NRV	50	-	50	20	0.02
NRVT	50	-	50	50	0.02

Abbreviations: AESO, acrylated epoxidized soybean oil; ARO, acrylated rapeseed oil; NP, nanopaper.

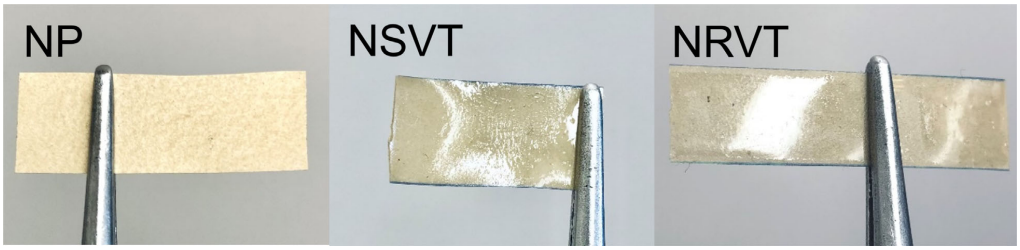

FIGURE 3 Photos of nanopaper (NP), hemp nanopaper impregated with AESO in a vacuum at 50°C (NSVT), and hemp nanopaper impregated with ARO in a vacuum at 50°C (NRVT) samples.

for 2 min and cooled rapidly between steel plates (20 kg). The thickness of the NP was reduced from around 150 μm to about 80 μm after processing through a press.

Using a 15 mils (381 μm) applicator, a single layer was applied on one side of the hemp NP. The thickness of the applicator was tested experimentally until an even layer of AESO was achieved, but ARO's lower viscosity contributed to initial spreading and a lower thickness of the applied layer. After coating application, samples were left for 30 min in a controlled environment to let the oil penetrate and impregnate hemp NP. The conditions were optimized between room temperature (20°C), elevated temperature (50°C), and a vacuum chamber. Sample abbreviations and preparation conditions are listed in Table 1 (N——NP, S——AESO or R——ARO, R——room temperature or V——vacuum, T——50°C temperature). After oil absorption into the NP, prepreg samples were cured under a UV lamp (405 nm, 0.13 mW cm^{-2}) for 90 s, and free-standing composites were obtained. Finally, the top layer was cleaned with filter paper. Photos of NP and composites are shown in Figure 3.

2.4 | Characterization

Viscosity measurements were performed with an MCR102 rheometer from Anton Paar (Graz, Austria). The instrument was equipped with a 25 mm diameter spindle with plate–plate geometry. The measurement gap was set to 0.1 mm. The viscosity was determined at 0.05–2500 s^{-1} shear rate.

The densities of ARO and AESO were determined using the hydrostatic displacement method by measuring sample weight in air and ethanol on analytical scales (Sartorius KBBA 100) equipped with a hydrostatic density measurement kit (Sartorius YDK 01). Five parallel measurements were used for each sample. Density (d) equation:

$$d = \frac{m_a(d_{EtOH} - 0.0012)}{0.99983(m_a - m_s)} + 0.0012 \quad (1)$$

where m_a (g) is the sample's mass in air, m_s is the sample's apparent mass measured submerged in ethanol (g), d_{EtOH} is the density of ethanol (0.805 g cm^{-3}), which was determined with a hydrometer.

The densities (d) of NP and composites were determined using geometrical dimensions and weight. Five parallel measurements were used for each sample. For the calculation of the void percentage (V_p) the following equation was used:

$$V_p = \left(1 - \frac{d_e}{d_t}\right) \times 100 \quad (2)$$

where d_e is the experimental density of composites and d_t is the theoretical density of composites. It was assumed that theoretical hemp density (d_h) is 1.5 g cm^{-3}, while for

ARO and AESO, measured density was used as the basis for the calculation of theoretical composite density.

Hemp fiber volume percentage (vol%) in composites was determined using the following equation:

$$\text{Hemp(vol\%)} = \left(\frac{m_h}{d_h} \div \frac{m_c}{d_e}\right) \times 100 \quad (3)$$

where m_h is the mass of hemp fibers in the composite and m_c is the mass of the composite.

Storage modulus, loss modulus, and loss factor were recorded using a dynamic mechanical analysis (DMA) Mettler DMA/SDTA861e (Mettler Toledo, United States) device. Measurements were carried out in tension mode from −60 to 60°C with a 3°C min^{-1} heating rate, an applied force of 10 N, 10 μm elongation, and a frequency of 1 Hz.

Tensile tests were performed on the Tinius Olsen model 25ST (Horsham, PA, United States). Cut sample strips with a 10 mm width and 60 mm length were used with a fixed distance of 30 mm between grips. The experiment used a 5 kN load cell with a testing crosshead speed of 1 mm/min. Five parallel measurements were recorded for each sample at 20°C and 40% relative humidity.

The dielectric properties of impregnated nanocellulose were obtained using a dielectric spectrometer (DS) from Novocontrol Alpha Broadband (Novocontrol Technologies, Germany). Samples with a diameter of 30 mm were placed between plate electrodes and tested using a frequency range of 0.01–10 MHz at 20°C.

The contact angle of the samples was recorded with a Theta Lite optical tensiometer (Attension®, China) using the static sessile drop method. Five parallel measurements with drops (9 μL) of modified oil were deposited on the sample's surface, and the measurements were recorded with a fixed 12 frames per second for 90 s at 20°C.

A SEM model NovaNano SEM 650 (Hillsboro, OR, United States) was used to record sample micrographs. The fracture surface was prepared with liquid nitrogen for morphology and with a tensile test for fractography. The samples were attached to standard aluminum pin stubs with electrically conductive double-sided carbon tape, and the image was generated with a 5 kV acceleration voltage for NP and 10 kV for composites. Hemp nanofiber images were obtained using TEM mode with a 15 kV acceleration voltage.

3 | RESULTS AND DISCUSSION

3.1 | Prepreg impregnation

The viscosity of the used oils (uncured) is provided in Figure 4. There is more than a 10-fold difference in viscosity between AESO and ARO. Some resins exhibited Newtonian behavior in the investigated shear rate region, whereas some deviation from the law corresponds to shear thinning and pseudoplastic fluid properties, which are common in many polymeric resins used in industrial and everyday applications.[26] Vegetable oil acrylate's viscosity is determined by the number of acryl groups present in each triglyceride. The presence of ester groups increases viscosity due to their polar interaction. Low-viscosity resins are desirable because they require minimal or no reactive diluents and other additives. Reduced viscosity also prevents air from being trapped in the composite structure.

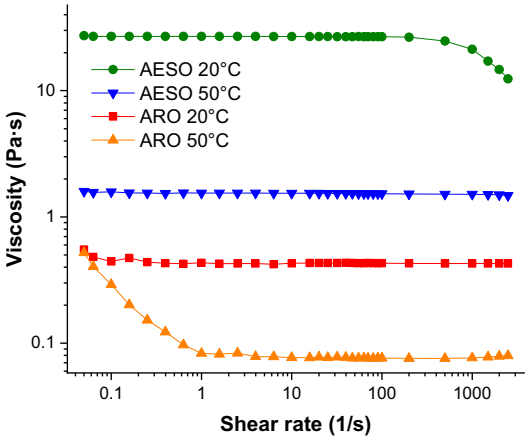

FIGURE 4 Acrylated epoxidized soybean oil (AESO) and acrylated rapeseed oil (ARO) viscosity at 20 and 50°C.

The contact angle of oil drops was determined on the NP to understand modified oil impregnation potential and processes. Figure 5 shows the contact angles of ARO and AESO after 5 and 90 s with two different oil temperatures of 20 and 50°C. For the 50°C measurements, preheated oil was used and deposited on a room-temperature NP surface. For the initial values (after 5 s) of ARO and AESO, there was an almost twofold difference, which matches well with the viscosity values shown in Figure 4. After 90 s, the AESO value drops significantly, achieving a value of 43.7°, which is almost 2.3 times lower than the value after 5 s. At the same time, ARO values dropped slightly from the initial ones, showing only an 8.9° difference from the initial 48.2°. The introduction of heated oils on NP showed a significant change; the initial value of AESO and the 90 s value of ARO had the highest drops in contact angle values. The ARO shows overall a much better ability to wet NP surfaces.

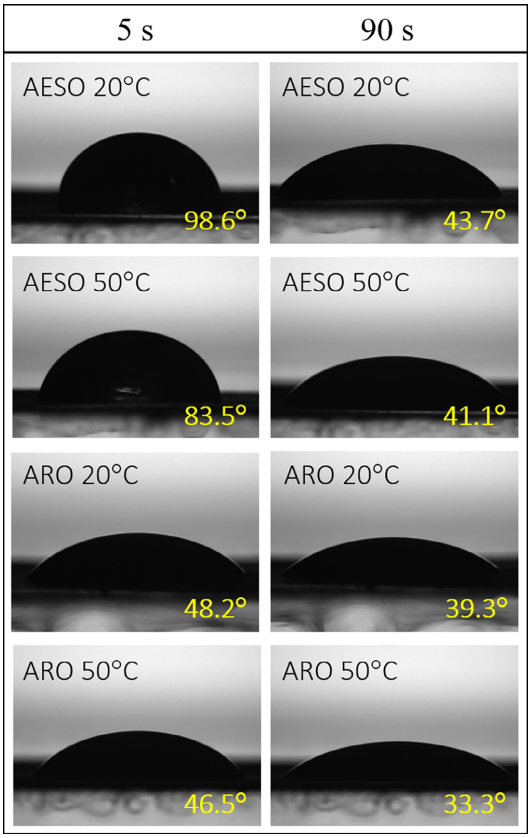

FIGURE 5 Contact angle values for acrylated epoxidized soybean oil (AESO) and acrylated rapeseed oil (ARO) drops applied on nanopaper (NP).

3.2 | Structure of composites

Vegetable oil impregnation depth and the resulting composite structure were evaluated with SEM, and the obtained fractures of the cross-section are visible in Figure 6. Compressed NP had a thickness of around 80 μm, and even after impregnation, the thickness of the NP remained almost unchanged, with values up to 85 μm. In contrast, above the NP, a layer of oil remained with a varied thickness. The only notable exception was the NRVT sample, with an increase in size to around 90 μm and complete ARO impregnation (only a single layer). This indicates that NP provides a reinforcing substrate with enough porosity (18.3%, Table 2) for the resin to permeate and adhere to the fibers. At room temperature, the NSR sample shows almost no impregnation of AESO, and a thick layer of around 188 μm remains above NP. In the NSR sample, the hemp substrate clearly shows unoccupied voids. In the case of NRR, the penetration of ARO is visible throughout the reinforcing substrate, and around 10 μm layer above the substrate is visible. Increasing temperature increases the viscosity of oils, and the removal of air allows them to fill the substrate better. In the NSVT sample cross-section, it is visible that AESO penetrated the hemp substrate fully and even formed a layer below it. The AESO layer above NP was reduced to 100 μm, yielding an almost twofold improvement compared to NSR. Unfortunately, phase segregation is visible in impregnated NSVT samples; layers of AESO have been formed between hemp fibers, and there is even a layer below the hemp substrate. At the same time, the NRVT cross-section image demonstrates excellent impregnation performance; low-viscosity ARO wetted the surface of hemp fibers sufficiently, and no layer of clear ARO was visible above the substrate. There is a notable improvement over NRR, where only some fibers have adsorbed ARO on the surface.

Some similar studies have been performed. For example, epoxidized soybean oil was applied to paper, and SEM images revealed that partial impregnation happened at room temperature during the curing process.[22] However, the authors did not examine impregnation in detail or specify curing conditions.

3.3 | Tensile properties

Fractography is a versatile method to understand the failure of composite structures.[27] To compare the failure of AESO and ARO composites, composites with the best impregnation from each oil were selected. Figure 7 shows SEM micrographs of composite fracture surfaces obtained via the tensile test procedure. NSVT shows pronounced fiber pull-outs, unlike NRVT, which shows mixed failure from both pull-outs and fiber failure. The NSVT fracture shows that AESO formed separate layers between hemp fibers, forming more of a layered structure, which can also be seen by the pulled-out sections (large voids) in the crosscut. But in the case of NRVT, a much more evenly distributed polymer matrix with fibers enclosed is visible.

The representative stress–strain curves of all impregnated samples are shown in Figure 8. Young's modulus, tensile strength, and elongation at break values are presented in Table 2. The temperature elevation to 50°C and impregnation in vacuum increased modulus values for both AESO and ARO composites, yielding the best results of 347 and 1331 MPa for NSVT and NRVT, respectively. The results are complemented by the void percentage

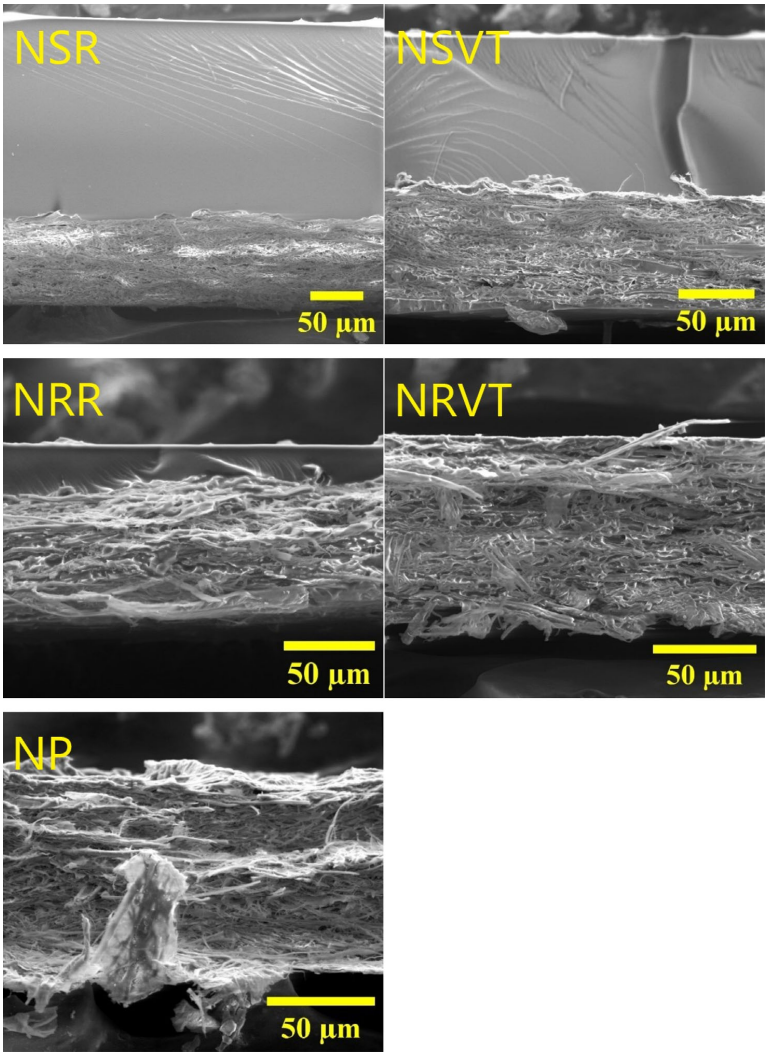

FIGURE 6 Scanning electron microscope (SEM) cross-section micrographs for selected impregnated compositions and neat nanopaper (NP).

calculation shown in Table 2. For NP, this value can also be referred to as porosity, which is essential and shows that structure can be impregnated. In the case of AESO-impregnated NP, the void percentage in the material increases by about 25%, but for ARO-impregnated NP, a drop in void percentage of ∼50% is observed. As it is assumed that NP contributes most of the voids (porosity) in the composite, the values should drop significantly with the impregnation of oil. Thus, even ARO composites' values could be further improved with the addition of viscosity-lowering additives. This matches well with SEM observations, where AESO composites yielded a more laminate-like structure, and the obtained modulus values for NSVT are relatively low, reaching only about 16% of the reinforcing substrate value (NP) while containing about 24 vol% (Table 2) of reinforcement. On the other hand, NRVT achieved 61% of NP's modulus value with about 38 vol% reinforcement.

The results from modulus correlate well with tensile strength values, which decreased by 52% and 14% for NSVT and NRVT compared to NP. This indicates that ARO adsorption on the cellulose fiber surface occurred during the composite formation process. The NRR composition stands out with an increased tensile modulus

TABLE 2 Tensile properties, density, and void percentage of impregnated composites, NP and cured vegetable oils.

Sample	Young's modulus (MPa)	Tensile strength (MPa)	Elongation at break (%)	Density (g cm^{-3})	Void percentage (%)	NP (vol%)
NP	2186 ± 260	31.1 ± 3.4	1.8 ± 0.2	1.226 ± 0.050	18.3[a]	-
AESO	10 ± 1	1.67 ± 0.2	7.8 ± 1.6	1.119 ± 0.001	-	-
ARO	16 ± 2	0.64 ± 0.1	7.4 ± 1.2	1.008 ± 0.003	-	-
NSR	147 ± 21	12.5 ± 1.2	7.5 ± 1.3	1.056 ± 0.072	22.7	24.6
NSV	264 ± 35	15.7 ± 1.7	9.1 ± 1.6	1.062 ± 0.054	22.3	24.8
NSVT	347 ± 56	14.7 ± 1.6	8.6 ± 1.1	1.029 ± 0.015	24.7	24.0
NRR	812 ± 144	35.6 ± 3.8	6.3 ± 1.3	1.093 ± 0.008	12.8	36.4
NRV	954 ± 155	24.6 ± 1.9	6.9 ± 0.9	1.162 ± 0.031	7.3	38.7
NRVT	1331 ± 172	26.1 ± 2.1	3.4 ± 0.5	1.138 ± 0.035	9.3	37.9

Abbreviations: AESO, acrylated epoxidized soybean oil; ARO, acrylated rapeseed oil; NP, nanopaper.
[a]Porosity of nanopaper.

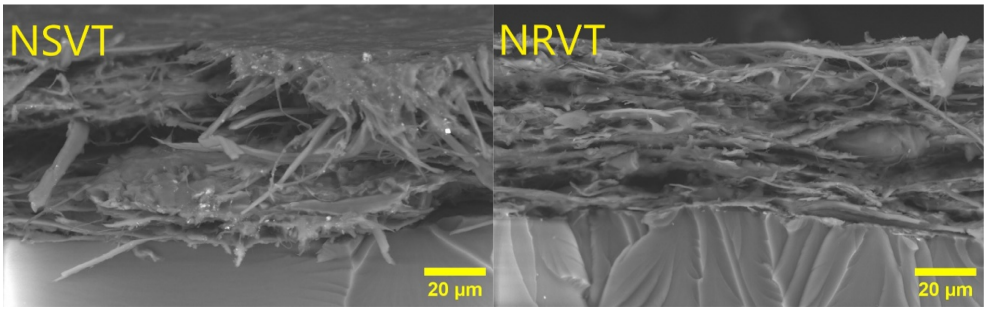

FIGURE 7 Scanning electron microscope (SEM) cross-section micrographs for NSVT and NRVT, which show sample failure in tensile testing mode.

value compared to NP; this indicates that NP structure disruption during ARO impregnation was limited. The NRV stress–strain curve does not position itself between NRR and NRVT, indicating that different processes occurred. This could be explained by enhanced impregnation but limited ability to wet hemp fibers. A significant drop in tensile strength testifies to this. In the case of NRVT, the increase in temperature reduces intermolecular bonding between hemp fibers, thus contributing to lower tensile strength, but enhanced interaction with the ARO matrix can be achieved.

The vegetable oil matrix influenced strain values. Two different behaviors were observed. For AESO composites, there is an increase in elongation at break values; this could be explained by phase separation observed in SEM, which could promote layer slippage. ARO-impregnated composites showed typical performance of impregnated composites, that is, a decrease in elongation value compared to the polymer matrix and an increase in Young's modulus that is approaching reinforcement values. Both vegetable oils can act as

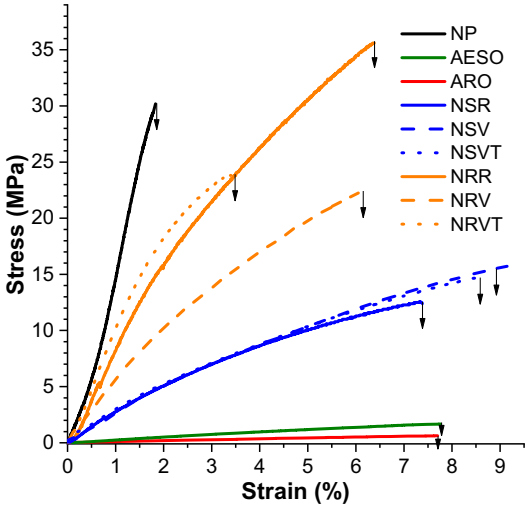

FIGURE 8 Tensile test stress–strain curves of impregnated composites, nanopaper (NP), and cured vegetable oils.

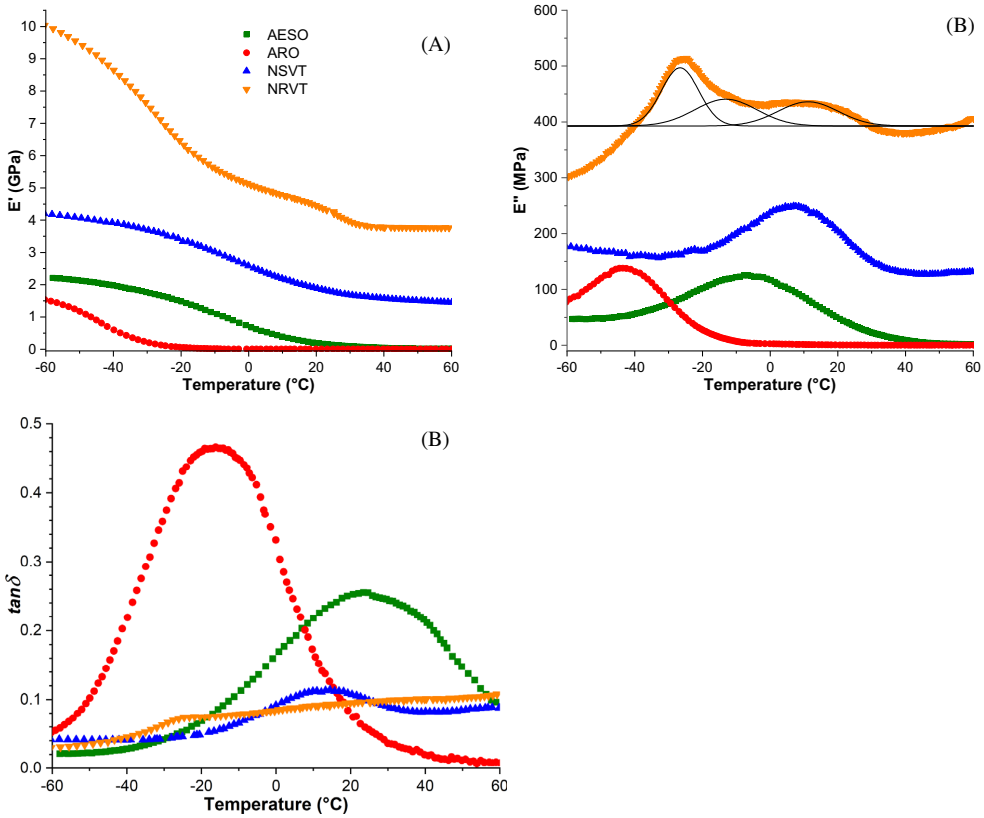

FIGURE 9 Dynamic mechanical analysis (DMA) curves for selected impregnated composites and cured vegetable oils: (A) storage modulus (E'), (B) loss modulus (E''), and (C) loss tangent (tanδ) dependence on temperature.

elastomeric components due to their chemical structure of long —(CH_2)— chains. These chains can originate from saturated fatty acids and unreacted modified fatty acid moieties.

Existing works with natural fibers are relatively different and commonly use a fossil-based matrix. Examples include fossil-based epoxy composites with woven fiber mats,[28] delignified wood pulp fibers,[29] or alkali and silane-treated hemp fibers.[30] These fibers often involve special processing and are not sourced as waste. As a result of the excellent fiber parameters, they can achieve a Young's modulus in the range of 2–6 GPa and a tensile strength of around 30–100 MPa. Furthermore, industrial high-performance, multi-component epoxy resin cannot be directly compared with single-component acrylated vegetable oil. On the other hand, the highest results achieved in this work, that is, a Young's modulus of 1.3 GPa and a tensile strength of 35.6 MPa, indicate tremendous potential for bio-based alternatives.

3.4 | Dynamic mechanical analysis

Thermo-mechanical properties of the vegetable oil-impregnated NP films were investigated via DMA. The storage modulus (E'), loss modulus (E''), and loss factor (tanδ) are recorded as a function of temperature and are displayed in Figure 9. Storage modulus shows the decreased elastic response of materials as the glass transition occurs from a glassy to a rubbery state. AESO and ARO are relatively soft materials in a rubbery state as fatty acid chains become more mobile and only show around 195 and 8 MPa at 20°C, respectively. This indicates that the cyclic load bearing is almost entirely achieved by reinforcing NP in the rubbery state. While a direct comparison of NRVT and NSVT cannot be made due to different ratios of reinforcement and polymer matrix, there is a 2.4-fold difference at 20°C for storage modulus values and only a 1.6-fold difference in NP vol% content.

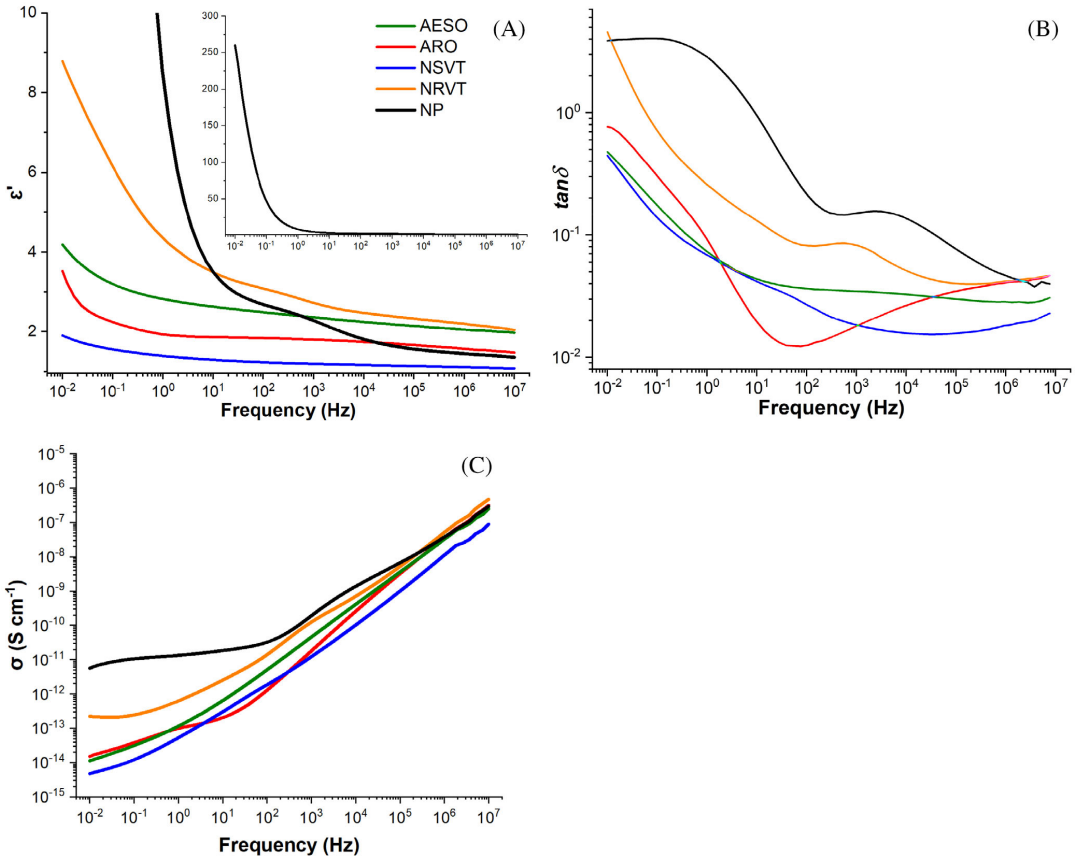

FIGURE 10 Dielectric properties of selected impregnated composites, nanopaper (NP), and cure vegetable oils: (A) dielectric permittivity (ε'), (B) dielectric loss tangent (tanδ), and (C) electric conductivity (σ) dependence on frequency.

Loss modulus can be used to determine precise glass transition temperatures (T_g). The difference in T_g between −44°C for ARO and −6°C for AESO indicates that the AESO structure is more crosslinked. For both composites, T_g increases, indicating that molecular motions are restricted. The difference between the T_g of ASEO and NSVT is 13°C, but between ARO and NRVT, it is 18°C. This matches well with the observed structure, where AESO interface with NP is much more limited, thus having a lower impact on T_g. In the case of NRVT, a second glass transition peak can be observed at even higher temperatures, but when deconvolution is applied, it matches well with the three merged peaks. This behavior can be explained by multiple processes that occur at the interface between components and in the volume of the matrix. One of the higher T_g peaks could be attributed to possible chemical binding to cellulose, as shown in Figure 1. However, this complex behavior needs more research. The lack of additional T_g peaks for NSVT indicates that it did not yield intensive interface interactions.

In our previous studies with vegetable oil-based resins, the broad tanδ peak has been attributed to inherent local variations in chain mobility, which result in various relaxation behaviors in the polymer matrix.[31] This just means that the vegetable oil-based polymer's structure has some random elements due to different fatty acid moieties and acrylation reactions not yielding complete conversion. According to Lei et al., the softening dispersion from the glassy state to the rubbery state involves at least three different modes of molecular motion.[32] Local segmental motion is the major transition that correlates well with various testing methods to yield what is considered a true glass transition, which in the case of DMA is the loss modulus peak.[33] Nevertheless, in the case of tanδ, enhanced mobility of local segments

contributes to higher sensitivity for Rouse modes that yield the main peak with a significantly higher temperature.[32,34] As a result, tanδ and loss modulus curves show peaks at different temperatures. The drop in tanδ peak values is attributed to composites being much stiffer than vegetable oil matrices.

3.5 | Dielectric spectroscopy

Figure 10 shows the dielectric permittivity, the dielectric loss tangent (tanδ), and the electric conductivity (σ) for NP, cured vegetable oils, NSVT, and NRVT. The dielectric permittivity from 10^{-3} to 10^{8} Hz characterizes the dipole orientation polarization and interfacial polarization processes. This covers the measured frequency range in this study. The orientation process takes time, which is reduced by increased frequency. The observed decrease in permittivity for all samples with an increase in frequency thus matches the theory. Two opposing effects were observed for composites compared to their cured vegetable oils. NSVT saw a decrease in the whole measured range compared to AESO, while NRVT increased compared to ARO. This could be related to the phase separation and poor interfacial interactions between hemp and AESO in NSVT, which introduced defects and decreased dielectric permittivity. In the case of NRVT, good polymer matrix adhesion was observed on hemp fibers. It could be explained by increased interfacial polarization due to the polar dipoles arising from the abundant hydroxyl groups in the cellulose.[35] This matches well with the proposed interactions by Li et al. for the glass fiber-reinforced phenol-formaldehyde epoxy composites.[36]

Loss tangent complements dielectric measurement results, indicating phase mobility and structural rearrangements. This, in turn, promotes the dissipation of electrical energy. The hemp fibers enhanced loss values for both vegetable oils due to a disrupted cross-linked network of modified oils. NSVT saw enhanced values for frequencies above 10^{2} Hz. However, in the case of ARO, a noticeable drop in loss tangent value was observed around 10^{2} Hz, which was almost eliminated in the NRVT composite structure. Interfacial interactions could limit structural rearrangements of fatty acid moieties, thus explaining the observed change. The conductivity values testify that both components and composites are dielectrics and serve as insulators. The composites show enhanced performance compared to NP. At the same time, they are comparable with various materials reported in the literature that are made from fossil-based epoxy and paper reinforcement.[35,37,38]

4 | CONCLUSIONS

The present study investigates how temperature, time, and pressure influence the impregnation of vegetable oil acrylates into hemp fiber-based NP. For comparison, we show that already commercialized AESO, indeed, struggles to produce competitive solutions due to its relatively high viscosity. Surprisingly, ARO, which we have prepared in a relatively simple one-step synthesis, shows almost no drawbacks compared to AESO. This is attested to by the more than 10-fold difference in viscosity. For optimal hemp fiber wetting, the elevated temperature showed a more significant impact than the application of just a vacuum. SEM micrographs show that the NRVT composite exhibited a well-formed structure with ARO properly adsorbed on the hemp fiber surface. Both mechanical testing methods further confirmed this observation. The highest results achieved in this work showed a Young's modulus of 1.3 GPa, a tensile strength of 35.6 MPa, a storage modulus of 4.4 GPa at 20°C, and elongation above 3% for all composites. If mechanical properties are not the main goal for the desired application, then all composites show potential for application as insulators.

There are different ways to prepare impregnated composites and achieve even higher properties. This study aimed to explore the compatibility between plant (hemp) fibers and vegetable oil-based resins. UV curing was selected as a potentially more energy-efficient solution to thermal curing. Studying the environmental impact of these novel composites and their performance in humid conditions is essential to fully evaluating their potential to substitute widely used glass and carbon fiber composites.

AUTHOR CONTRIBUTIONS

Conceptualization, formal analysis, investigation, writing – original draft, visualization: Oskars Platnieks. *Validation, investigation, writing – review & editing, visualization*: Sabine Briede. *Investigation*: Liga Grase. *Writing – review & editing*: Vijay Kumar Thakur. *Conceptualization, methodology, resources, writing – review & editing, supervision, project administration, funding acquisition*: Sergejs Gaidukovs.

ACKNOWLEDGMENTS

This research is funded by the Latvian Council of Science, project RealHLC, project No. lzp-2019/1-0390.

CONFLICT OF INTEREST STATEMENT

The authors declare no conflict of interest.

DATA AVAILABILITY STATEMENT

Data is available upon request from corresponding author as it is part of larger ongoing study.

ORCID

Oskars Platnieks https://orcid.org/0000-0001-5529-0912
Vijay Kumar Thakur https://orcid.org/0000-0002-0790-2264
Sergejs Gaidukovs https://orcid.org/0000-0001-8638-5009

REFERENCES

1. Rani M, Choudhary P, Krishnan V, Zafar S. A review on recycling and reuse methods for carbon fiber/glass fiber composites waste from wind turbine blades. *Compos B: Eng*. 2021;215:108768. doi:10.1016/j.compositesb.2021.108768
2. Song YS, Youn JR, Gutowski TG. Life cycle energy analysis of fiber–reinforced composites. *Compos Part A: Appl Sci Manuf*. 2009;40:1257. doi:10.1016/j.compositesa.2009.05.020
3. Ma S, Li T, Liu X, Zhu J. Research progress on bio–based thermosetting resins. *Polym Int*. 2016;65:164. doi:10.1002/pi.5027
4. Manian AP, Cordin M, Pham T. Extraction of cellulose fibers from flax and hemp: a review. *Cellulose*. 2021;28:8275-8294. doi:10.1007/s10570-021-04051-x
5. Wang B, Yan L, Kasal B. A review of coir fibre and coir fibre reinforced cement–based composite materials (2000–2021). *J Clean Prod*. 2022;338:130676. doi:10.1016/j.jclepro.2022.130676
6. Crini G, Lichtfouse E, Chanet G, Morin-Crini N. Applications of hemp in textiles, paper industry, insulation and building materials, horticulture, animal nutrition, food and beverages, nutraceuticals, cosmetics and hygiene, medicine, agrochemistry, energy production and environment: a review. *Environ Chem Lett*. 2020;18:1451. doi:10.1007/s10311-020-01029-2
7. Fike J. Industrial Hemp: renewed Opportunities for an Ancient Crop. *Crit Rev Plant Sci*. 2016;35:406. doi:10.1080/07352689.2016.1257842
8. Marrot L, Candelier K, Valette J, et al. Valorization of hemp stalk waste through thermochemical conversion for energy and electrical applications. *Waste Biomass Valorization*. 2022;13:2267-2285. doi:10.1007/s12649-021-01640-6
9. Sadrmanesh V, Chen Y. Bast fibres: structure, processing, properties, and applications. *Int Mater Rev*. 2019;64:381. doi:10.1080/09506608.2018.1501171
10. Wilson RF. Market driven research needs. In: Stacey G, ed. *Genetics and Genomics of Soybean*. Springer; 2008:3-15.
11. Yun H, Puyou J, Qianqian S, et al. Synthesis and application of UV–curable phosphorous–containing acrylated epoxidized soybean oil–based resins. *J Bioresour Bioprod*. 2019;4:183-191. doi:10.12162/jbb.v4i3.007
12. Rosace G, Rosa RP, Arrigo R, Malucelli G. Photosensitive acrylates containing bio–based epoxy–acrylate soybean oil for 3D printing application. *J Appl Polym Sci*. 2021;138:51292. doi:10.1002/app.51292
13. Su Y, Zhang S, Chen Y, Yuan T, Yang Z. One–step synthesis of novel renewable multi–functional linseed oil–based acrylate prepolymers and its application in UV–curable coatings. *Prog Org Coat*. 2020;148:105820. doi:10.1016/j.porgcoat.2020.105820
14. Liu Z, Knetzer DA, Wang J, Chu F, Lu C, Calvert PD. 3D printing acrylated epoxidized soybean oil reinforced with functionalized cellulose by UV curing. *J Appl Polym Sci*. 2022;139:51561. doi:10.1002/app.51561
15. Briede S, Barkane A, Jurinovs M, Thakur VK, Gaidukovs S. Acrylation of biomass: a review of synthesis process: Know–how and future application directions. *Curr Opin Green Sustain Chem*. 2022;35:100626. doi:10.1016/j.cogsc.2022.100626
16. Briede S, Jurinovs M, Nechausov S, Platnieks O, Gaidukovs S. State–of–the–art UV–assisted 3D printing via a rapid syringe–extrusion approach for photoactive vegetable oil acrylates produced in one–step synthesis. *Mol Syst Des Eng*. 2022;7:1434-1448. doi:10.1039/D2ME00085G
17. Lebrun G, Couture A, Laperrière L. Tensile and impregnation behavior of unidirectional hemp/paper/epoxy and flax/paper/-epoxy composites. *Compos Struct*. 2013;103:151. doi:10.1016/j.compstruct.2013.04.028
18. Åkesson D, Skrifvars M, Walkenström P. Preparation of thermoset composites from natural fibres and acrylate modified soybean oil resins. *J Appl Polym Sci*. 2009;114:2502. doi:10.1002/app.30773
19. Feigel B, Robles H, Nelson JW, Whaley JMS, Bright LJ. Assessment of mechanical property variation of as–processed bast fibers. 2019;11:2655. doi:10.3390/su11092655
20. Jyothi NS, Ramu TS, Mandlik M. Temperature distribution in resin impregnated paper insulation for transformer bushings. *IEEE Trans Dielectr Electr Insul*. 2010;17:931. doi:10.1109/TDEI.2010.5492269
21. Kolcunova I, Pavlik M, Lison L. Assessment of long thermal ageing on the oil–paper insulation. *Adv Electr Electron Eng*. 2016;14:506-511. doi:10.15598/aeee.v14i5.1836
22. Miao S, Liu K, Wang P, Su Z, Zhang S. Preparation and characterization of epoxidized soybean oil–based paper composite as potential water–resistant materials. *J Appl Polym Sci*. 2015;132:41575. doi:10.1002/app.41575
23. Dragonetti R, Napolitano M, Boccarusso L, Durante M. A study on the sound transmission loss of a new lightweight hemp/-bio–epoxy sandwich structure. *Appl Acoust*. 2020;167:107379. doi:10.1016/j.apacoust.2020.107379
24. Aitomäki Y, Moreno-Rodriguez S, Lundström TS, Oksman K. Vacuum infusion of cellulose nanofibre network composites: influence of porosity on permeability and impregnation. *Mater Des*. 2016;95:204-211. doi:10.1016/j.matdes.2016.01.060
25. Beluns S, Gaidukovs S, Platnieks O, et al. From wood and hemp biomass wastes to sustainable nanocellulose foams. *Ind Crops Prod*. 2021;170:113780. doi:10.1016/j.indcrop.2021.113780
26. Hasan W, Khan MN. *J Food Process Eng*. 2020;43:e13396. doi:10.1111/jfpe.13396
27. Kumar P, Singh J, Kumari N, Jurail SS, Verma D, Maurya AK. Study of mechanical and thermal behavior of alkali modified groundnut shell powder reinforced ABS composites. *Polym Compos*. 2022;43:4569-4587. doi:10.1002/pc.26713
28. Boccarusso L, Durante M, Langella A. Lightweight hemp/bio–epoxy grid structure manufactured by a new continuous process. *Compos B: Eng*. 2018;146:165. doi:10.1016/j.compositesb.2018.04.009
29. Ansari F, Sjöstedt A, Larsson PT, Berglund LA, Wågberg L. Hierarchical wood cellulose fiber/epoxy biocomposites –

Materials design of fiber porosity and nanostructure. *Compos Part A: Appl Sci Manuf*. 2015;74:60. doi:10.1016/j.compositesa.2015.03.024

30. Soni P, Sinha S. Synergistic effect of alkali and silane treatment on mechanical, flammability, and thermal degradation of hemp fiber/epoxy composite. *Polym Compos*. 2022;43:6204-6215. doi:10.1002/pc.26924
31. Barkane A, Platnieks O, Grase L, Gaidukovs S. Simultaneous wettability and stiffness control of UV–curing vegetable oil resin composites by lignocellulosic components. *Polymer*. 2022;255:125154. doi:10.1016/j.polymer.2022.125154
32. Lei Z, Xing W, Wu J, Huang G, Wang X, Zhao L. The proper glass transition temperature of amorphous polymers on dynamic mechanical spectra. *J Therm Anal Calorim*. 2014;116:447-453. doi:10.1007/s10973-013-3526-0
33. Rieger J. The glass transition temperature Tg of polymers—Comparison of the values from differential thermal analysis (DTA, DSC) and dynamic mechanical measurements (torsion pendulum). *Polym Test*. 2001;20:199. doi:10.1016/S0142-9418(00)00023-4
34. Ngai KL, Plazek DJ. Identification of different modes of molecular motion in polymers that cause thermorheological complexity. *Rubber Chem Technol*. 1995;68:376. doi:10.5254/1.3538749
35. Ning X, Feng H, Zhang H, Liu P, Xiang Z, Peng Z. Dielectric properties of multi–layer epoxy resinimpregnated crepe paper composites. *IEEE Trans Dielectr Electr Insul*. 2015;22:161. doi:10.1109/TDEI.2014.004526
36. Li Z, Zhou W, Yang L, et al. Glass fiber–reinforced phenol formaldehyde resin–based electrical insulating composites fabricated by selective laser sintering. *Polymers*. 2019;11:135. doi:10.3390/polym11010135
37. Chen Q, Yang H, Wang X, Liu H, Zhou K, Ning X. Dielectric properties of epoxy resin impregnated Nano-SiO_2 modified insulating paper. *Polymers*. 2019;11(3):393. doi:10.3390/polym11030393
38. Wang Y, Luo Y, Guan J, Ding R. Dielectric properties of epoxy resin impregnated paper insulation in different stages of partial discharge development. *Polym Compos*. 2020;41:360-368. doi:10.1002/pc.25375

How to cite this article: Platnieks O, Briede S, Grase L, Thakur VK, Gaidukovs S. Fully bio-based thermoset composites from UV curable prepregs: Vegetable oil acrylate impregnated hemp nanopaper. *Polym Compos*. 2023;44(9):5721-5733. doi:10.1002/pc.27521

Pielikums V

Appendix V

Greivule, S., Besprozvannaja I., Porcarello M., & Gaidukovs, S.

Reprocessable and Repairable Bio-Based Vitrimers from Acrylated Epoxidized Rapeseed Oil for Additive Manufacturing

Macromolecular Materials and Engineering, **2026**. (Accepted)

doi: 10.1002/mame.70228

Reprocessable and Repairable Bio-Based Vitrimers from Acrylated Epoxidized Rapeseed Oil for Additive Manufacturing

Sabine Greivule,[a] Inga Besprozvannaja,[a] Matilde Porcarello,[b] and Sergejs Gaidukovs[a]*

[a] Institute of Chemistry and Chemical Technology, Faculty of Natural Sciences and Technology, Riga Technical University, P. Valdena 3/7, Riga LV-1048, Latvia.

[b] Department of Applied Science and Technology (DISAT), Politecnico di Torino, Torino 10129, Italy

*Correspondance: Sabine.Greivule@rtu.lv; Sergejs.Gaidukovs@rtu.lv

Keywords: acrylated vegetable oils, rapeseed oil, vitrimers, reprocessing, repairability, 3D printing, UV curing, TGA-FTIR.

ABSTRACT

Thermosets are difficult to reprocess and often rely on petroleum-derived feedstocks, creating environmental and end-of-life challenges. This study addresses both issues by developing reprocessable bio-based vitrimers tailored for additive manufacturing. Acrylated epoxidized rapeseed oil (AERO) was synthesized as renewable UV curable precursor for constructing vitrimer networks capable of intrinsic and catalyst-assisted transesterification. The influence of transesterification catalyst $Zn(acac)_2$, AERO content, and reprocessing cycles was systematically studied through real-time curing behavior, stress relaxation, and thermo-mechanical characterization. Catalyst-free vitrimers exhibited notable stress relaxation of 34 min at elevated temperature due to the high density of *β*-hydroxyester groups, enabling intrinsic bond exchange. On the other hand, $Zn(acac)_2$-containing vitrimers demonstrated enhanced reprocessability with relaxation times as low as 10 min. Tensile strength recovery reached 98% after the first and 50% after the second reprocessing cycle. TGA-FTIR analysis indicated increased CO_2 and carbonyl-rich volatile release in catalyst-containing vitrimers, consistent with dynamic bond exchange reactions. Finally, the developed vitrimers exhibited excellent vat photopolymerization 3D printability and repairability, with repaired printed parts exceeding the original tensile properties by up to 2.9 times. These findings highlight the potential of vegetable oil-based vitrimers as promising customizable, repairable, and sustainable materials for next-generation advanced additive manufacturing and circular polymer design.

1. Introduction

Recycling and reprocessing of thermosets remain a significant challenge due to their permanent crosslinked network, which prevents reshaping once cured.[1] These challenges lead to waste accumulation and limit thermoset materials' circularity. Current approaches to improve reprocessability of thermosets include mechanical grinding followed by use as filler, chemical depolymerization into monomers, or partial thermal degradation.[2] However, these methods are often energy-intensive, inefficient, or degrade the polymer's properties, making the reprocessing of thermosets a persistent challenge.

Vitrimers have emerged as a promising solution to this problem, as they are a class of polymers featuring covalent adaptable networks (CANs) that undergo dynamic bond exchange reactions, thereby enabling stress relaxation, reprocessing, and repair without sacrificing network integrity.[3] This dynamic nature allows vitrimers to combine thermosets' mechanical robustness with thermoplastics' reprocessability, offering a pathway toward high-performance recyclable materials. Vitrimers can be made from renewable feedstocks, such as vegetable oils, enhancing environmental and economic sustainability.[4]–[6] The triglyceride structure in vegetable oils allows extensive chemical modification, and their abundance, low cost, and large-scale production make them ideal precursors for bio-based vitrimer resins.[7]–[9] Within this field, vitrimer research has focused on thermally cured systems, while UV-curable vitrimers are only beginning to

gain attention. This emerging class of materials offers the dual benefits of vitrimer reprocessability and the rapid, energy-efficient photopolymerization, opening opportunities for advanced manufacturing routes such as 3D printing.[10] For example, Fei *et al*. developed a 3D-printable vegetable oil-based vitrimer, achieving up to 68 wt% of bio-based content.[11] The prepared vitrimer demonstrated good reprocessability: samples were cut into small pieces and reprocessed by hot-pressing at 190 °C for 1 h. Repairability was confirmed by rheological experiments, where cracks were reduced by up to 65% after heating the damaged samples to 200 °C for 30 min. Interestingly, authors introduced a diepoxy extender to tailor the crosslink density and mechanical performance, which enabled the vitrimer properties to range from glassy plastics to ductile elastomers.

The dynamic bond exchange processes in vitrimers are driven by catalytic action in reactions such as transesterification,[12] or transamination.[13] By lowering the activation energy of these exchange reactions, catalysts such as zinc salts,[14] organophosphates,[15] or imidazoles[16] can significantly accelerate stress relaxation and network rearrangement.[17] The catalyst type and concentration are critical: insufficient catalysts may limit dynamic bond exchange, making the material behave more like a conventional thermoset; in contrast, excessive catalyst concentrations may increase viscoelastic flow and reduce mechanical properties.[18] Dynamic bond exchange without the catalyst is especially promising for *β*-hydroxyester-rich vitrimer networks.[19] In turn, Capiel *et al*. developed a bio-based catalyst-free vitrimer, using 30 wt% AESO and 70 wt% methacrylated oleic acid, enabling stress relaxation up to 80% at 170 °C in 2.5 h, and almost complete stress relaxation at 200 °C in less than 20 min.[20]

This work presents a systematic materials design framework based on controlled macromolecular network design for the development of UV-curable bio-based vitrimer resins tailored for vat photopolymerization additive manufacturing. Building on prior studies of vegetable oil-derived vitrimers, this work investigates the relationships between bio-based monomer architecture, dynamic exchange mechanisms, the influence of catalyst, and repair performance in 3D printing. Epoxidized acrylated rapeseed oil (AERO) was employed as the bio-based component to introduce renewable content and flexible aliphatic chains into the network while providing *β*-hydroxyester groups capable of participating in transesterification reactions. 2-Hydroxy-3-phenoxypropyl acrylate (HPPA) was selected as a reactive diluent to adjust viscosity for vat photopolymerization and to introduce additional *β*-hydroxyester groups that promote dynamic bond exchange. Additionally, the aromatic phenoxy moiety in HPPA contributes increased segmental rigidity, which can enhance the mechanical strength and thermal stability of the resulting network. Glycerol 1,3-diglycerolate diacrylate (GDA) was incorporated as a multifunctional crosslinker to control crosslink density and mechanical performance. The relative ratios of these components were chosen to systematically evaluate the influence of bio-based content and network architecture on the vitrimer properties and reprocessability. By optimizing catalyst loading, including catalyst-free options, we have achieved efficient network rearrangement while maintaining structural integrity. The developed vitrimers' reprocessability was tested by grinding pristine samples and hot-pressing them under pressure and temperature, ensuring mechanical performance recovery after two reprocessing cycles. Vitrimers demonstrated vat photopolymerization 3D printability with outstanding damage repairability, preserving mechanical performance more effectively due to thermally driven transesterification. The proposed vegetable oil-based UV-curable vitrimers are particularly relevant for applications requiring fast curing, high performance, and extended service life. Potential target utilities include protective and decorative coatings, additive manufacturing resins, and reprocessable thermoset composites.

2. Experimental section

2.1. Materials

Unrefined rapeseed oil was purchased from a local producer, "Iecavnieks" (Latvia). The rapeseed oil contained 62% oleic acid, 21% linoleic acid, and 11% linolenic acid, corresponding to 3.86 double bond equivalents per triglyceride. H_2O_2 (30 %), formic acid (reagent grade ≥ 95 %), acrylic acid (AA, anhydrous), triethyl amine (TEA, ≥ 99.5 %), ethyl acetate, $NaHCO_3$, Na_2SO_4, NaCl, 2-hydroxy-3-phenoxypropyl acrylate (HPPA), glycerol 1,3-diglycerolate diacrylate (GDA), zinc acetylacetonate ($Zn(acac)_2$), hydroquinone (HQ, ≥ 95 %), isopropanol, MeOH and glacial acetic acid were supplied by Sigma Aldrich. Ethyl phenyl(2,4,6-trimethylbenzoyl)phosphinate (TPOL, ≥ 95 %) was supplied by Arkema. All chemicals were used as received.

2.2. Synthesis of epoxidized rapeseed oil (ERO)

Epoxidation of rapeseed oil was carried out in a 250 ml flask equipped with a mechanical stirrer, thermometer, and dropping funnel. Rapeseed oil (100 g, 0.426 mol C=C, 1 eq) was mixed with HCOOH (5.88 g, 0.3 eq), and the reaction mixture was heated to 60 °C under continuous stirring. H_2O_2 (86.96 g, 1.8 eq) was added dropwise within 40 min. The reaction was allowed to proceed for 7 h. The reaction mixture was cooled to room temperature upon completion, and ethyl acetate was added to extract the organic components. The organic layer was washed with $NaHCO_3$ solution and brine until HCOOH was removed. The organic phase was then dried over anhydrous Na_2SO_4, filtered, and the solvent was removed under reduced pressure. Epoxidized rapeseed oil (ERO) was obtained as pale yellow resin. Epoxy value (EV) = 3.36 mmol epoxy/g resin (5.38 g O_2/g resin), indicating an epoxidation yield of approximately 89 %. The incomplete reaction may be attributed to partial hydrolysis of the formed epoxide groups or incomplete epoxidation of the triglyceride double bonds.

2.3. Synthesis of acrylated epoxidized rapeseed oil (AERO)

Acrylation of ERO was carried out in a 250 ml flask equipped with a mechanical stirrer, thermometer, and dropping funnel. ERO (94 g, 1 eq) was mixed with HQ as a polymerization inhibitor (300 ppm of AA) and TEA (1 wt% of total monomer mass), and the mixture was heated to 90-95 °C. AA (45.52 g, 2 eq) was then added dropwise, and the mixture was allowed to react for 18.5 h. Then the reaction was cooled to room temperature, diluted with ethyl acetate and washed with $NaHCO_3$ solution and brine to remove unreacted acrylic acid. The organic phase was then dried over anhydrous Na_2SO_4, filtered, and the solvent was removed under reduced pressure. Acrylated epoxidized rapeseed oil (AERO) was obtained as a dark yellow oil. AV = 1.4 mg KOH/g resin. OH value = 115 mg KOH/g resin. Figure 1a illustrates the two-step synthesis of AERO: epoxidation of rapeseed oil followed by epoxy ring-opening with acrylic acid. The synthesis of AERO was characterized by ^{1}H-NMR (Figure 1c) and confirmed successful rapeseed oil epoxidation and subsequent acrylation with the yield 1.97 mmol acrylic groups/g resin, indicating a yield of approximately 59 % (Figure S1). The incomplete reaction may be attributed to epoxy group hydrolysis and steric hindrance due to the bulky oil backbone. Three AERO signals appeared at δ = 5.79-5.90 ppm, δ = 6.05-6.20 ppm and δ = 6.35-6.47 ppm corresponding to **H_2**C-C**H**- of an acrylic group, and signals at δ = 3.37-3.64 ppm corresponding to the formed -OH groups, while ERO epoxy signals at δ = 2.82-3.23 ppm, δ = 1.65-1.84 ppm, and δ = 1.43-1.55 ppm corresponding to epoxy protons at α-position (-**H**COC**H**-), methylene protons between two epoxy groups (-COC-C**H_2**-COC-), and protons at β-position (-COC-C**H_2**-), respectively, disappeared.

2.4. Preparation, reprocessing, repairability and 3D printing of UV-curable vitrimers

For vitrimer resin formulations containing the catalyst (named as catalyst-vitrimers), 10 wt% (relative to total monomer mass) of $Zn(acac)_2$ was first dissolved in HPPA at 70 °C. Among the tested concentrations (1, 3, 5, and 10 wt%), 10 wt% of $Zn(acac)_2$ yielded the fastest stress relaxation and the most effective reprocessing performance (Figure S2). The solution was cooled to room temperature before adding AERO and GDA (Table 1). After cooling, slightly turbid formulations were obtained due to the limited solubility of $Zn(acac)_2$. The monomers were selected to provide sufficient β-hydroxyester groups to promote dynamic transesterification reactions. Subsequently, 3 wt% (relative to total monomer mass) of liquid photoinitiator TPOL was added to initiate UV curing, and the formulations were mixed for at least an hour. For catalyst-free vitrimers (abbreviated as “n/c”: no catalyst) all components were mixed directly at room temperature. The prepared resin formulations were applied onto a glass substrate using an open-bottom PTFE mold and covered with a fluorinated ethylene propylene (FEP) film to minimize oxygen inhibition during UV curing. UV curing was performed using a handheld 405 nm UV lamp at an intensity of 400 μW/cm^2 at a distance of 3 cm. The curing time was 30 s, as determined by preliminary tests from FTIR spectra. The used monomers, photoinitiator and catalyst are shown in Figure 1b.

To investigate the vitrimer reprocessability, the UV-cured films were first frozen in liquid N_2 and then ground into smaller particles using a conventional coffee grinder. The freezing and grinding were repeated three times to obtain fine vitrimer particles. The particles were then hot-pressed in a metal mold (dimensions: 60 × 10 × 0.5 mm) at 200 °C for 2 h under 1 ton load to form reprocessed films. The reprocessed vitrimer samples were named according to their processing cycle. For example, "AERO30_cycle_1" refers to a sample that was hot-pressed once, whereas "AERO30_cycle_2" refers to a sample that was hot-pressed, reground, and hot-pressed the second time. Catalyst-free samples are labelled with the abbreviation “n/c” (no catalyst), for example, “AERO30(n/c)_cycle_1”. A simplified schematic representation of the thermally

activated transesterification within the ester-hydroxyl network is shown in Figure 1d. Due to the multifunctional nature of the system, the dynamic exchange likely proceeds through multiple pathways.

As a proof of concept for vitrimer 3D printability, a sharp mountain structure ("Mountains 3D Printable (low Poly)" by Kaaa, obtained from the open-source 3D model repository Thingiverse) was printed using Elegoo Mars 2 Pro vat photopolymerization digital light processing (DLP) printer. The printer was equipped with a 6-inch monochrome LCD screen (2560 × 1440 resolution) and a UV-LED source (405 nm). Printing was performed with a layer height of 50 µm, 25 s exposure per layer (30 s for the four bottom layers). Following printing, samples were rinsed in isopropanol, air-dried at 25 °C for 15 min, and postcured for 3 min in a Prusa CW1 curing chamber (405 nm, 52.8 W) to ensure complete polymerization.

For the damage repairability investigation, strip film samples with a hole in the middle (dimensions: 50 × 10 × 0.8 mm, 5 mm hole diameter) were 3D printed to simulate mechanical damage. The same 3D printing parameters, resin formulation (AERO30), post-print washing and UV curing procedures were used. Then the hole was filled with fresh resin and cured for 60 s. To activate the thermally driven transesterification and promote repairability, samples were placed between PTFE sheets, compressed with a 5 kg counterweight, and thermally treated at 200 °C for 1 h. Tensile tests were performed on vitrimers before and after defect repair.

Table 1. Vitrimer formulations with different -COOR and -OH group ratios

Sample name	AERO, wt%	HPPA, wt%	GDA, wt%	$Zn(acac)_2$, wt%**	TPOL, wt%**	-COOR : -OH
AERO10	10	70	20	10	3	1 : 1.07
AERO20	20	70	10	10	3	1 : 0.95
AERO30	30	70	0	10	3	1 : 0.83
AERO10(n/c)*	10	70	20	0	3	1 : 1.07
AERO20(n/c)	20	70	10	0	3	1 : 0.95
AERO30(n/c)	30	70	0	0	3	1 : 0.83

* n/c: no catalyst.
** wt% calculated on total monomer mass.

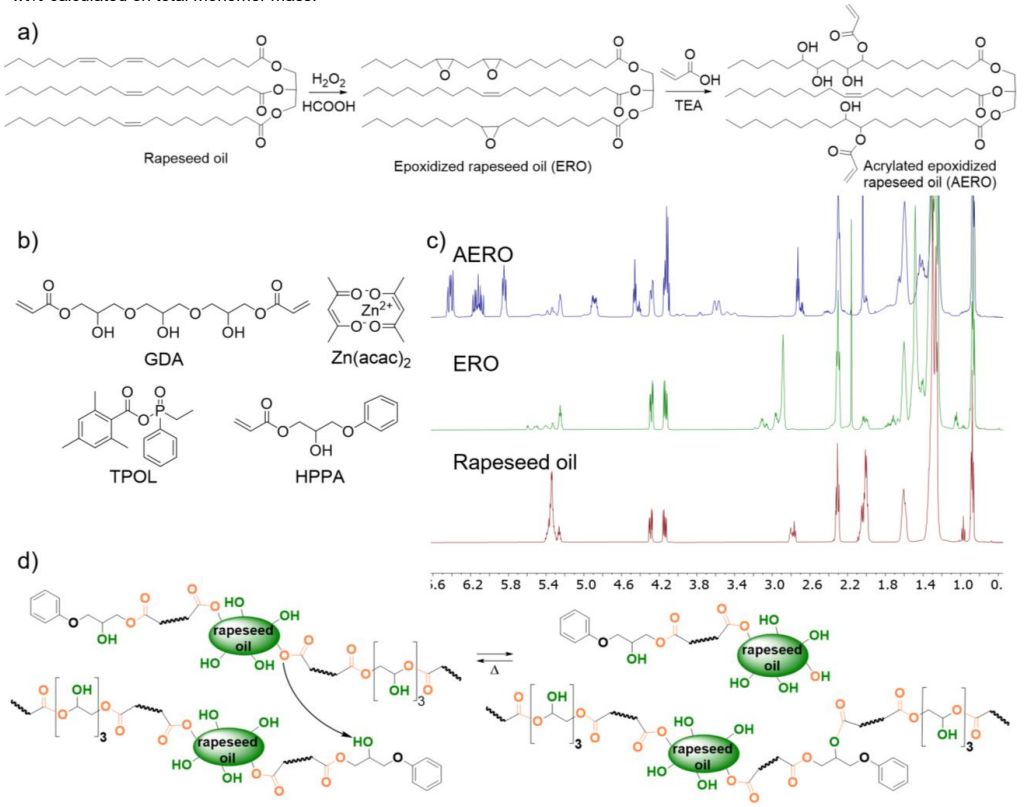

Figure 1. a) Synthesis of acrylated epoxidized rapeseed oil (AERO) through epoxidation and epoxy ring opening reactions; b) used monomers, photoinitiator and catalyst in vitrimer resin formulations; c) ^{1}H-NMR of rapeseed oil, ERO and AERO; d) possible dynamic bond exchange through thermally driven transesterification reaction.

2.5. Characterization methods

2.5.1. Epoxy value

Epoxy value (EV, mmol epoxy/g resin) was determined according to ASTM D1652 by titrating with 0.1 M $HClO_4$ in glacial acetic acid and using crystal violet as an indicator.

2.5.2. Hydroxyl value

The hydroxyl (OH) value (mg KOH/g resin) was determined according to DIN 53240 by titrating with 1 M KOH in MeOH.

2.5.3. Acid value

Acid value (AV, mg KOH/g resin) was determined by titration with 1 M KOH in MeOH.

2.5.4. ^{1}H-NMR spectroscopy

The ^{1}H-NMR spectra were recorded on a Bruker Avance 500 spectrometer (Bruker BioSpin, Switzerland) at 500 MHz, using the residual proton signal of $CDCl_3$ (δ = 7.26 ppm) as a chemical shift reference. Quantitative analysis was performed using 1,2,3-trimethoxybenzene as an internal standard. Based on the integration ratio between the acrylate vinyl protons (I_A = 54.2, m_{AERO} = 14.1 mg) and the aromatic proton signal of the internal standard (I_A = 100.0, $m_{1,2,3\text{-trimethoxybenzene}}$ = 8.6 mg), where I_A denotes the integral area of the corresponding ^{1}H-NMR signal, the acrylic group content was calculated to be 1.97 mmol of acrylic groups/g resin. The corresponding quantitative ^{1}H-NMR spectrum is provided in the Supporting Information (Figure S1).

2.5.5. FTIR spectroscopy

Fourier-transform infrared spectrometer (FTIR), Nicolet 6700 (ThermoScientific, Germany) measurements were held in the 400-4000 cm^{-1} region with 4 cm^{-1} resolution. Each spectrum was recorded from the bottom of the samples, in line with the work of Lacombe *et al*. who emphasized the impact of oxygen inhibition at the surface.[21] Double bond conversion (DBC) values were calculated using the Equation (1), based on the ratio of the vinyl bond out-of-plane deformation band at 810 cm^{-1} to the carbonyl band at 1733 cm^{-1} , as reported elsewhere [22]:

$$DBC = 1 - \frac{(\frac{I_{810}}{I_{1733}})_a}{(\frac{I_{810}}{I_{1733}})_b} \quad (1)$$

where *I* represents the absorbance intensities at the specified wavelengths before (b) and after (a) UV exposure.

2.5.6. TGA-FTIR combined analysis

Thermal decomposition products of vitrimers were analyzed using a TGA-FTIR setup, where the thermogravimetric analyzer was connected to an FTIR spectrometer via a heated transfer line maintained at 200 °C to prevent condensation of evolved gases. Approximately 10 mg of each sample was heated under a N_2 atmosphere at 10 °C/min up to 200 °C and then held isothermally for 150 min. The FTIR spectrometer was equipped with a heated gas cell, and the evolved gases were recorded.

2.5.7. Stress relaxation

The thermally activated dynamic bond exchange within the networks was studied using stress relaxation experiments on an Anton Paar rheometer MCR102 (Graz, Austria) with a parallel-plate measuring system (8 mm diameter of the top plate). The constant normal force of 1 N was applied to 3D printed samples with 0.4 mm thickness (3D printing parameters were set as described in Materials and methods section). The samples were heated to the test temperature and equilibrated for 15 min. A constant strain of 3% was applied to the samples and the change of relaxation modulus versus time was recorded.

2.5.8. Photo-DSC

Photo-differential scanning calorimetry (photo-DSC) analysis was performed using a Mettler Toledo DSC-1 instrument (Milano, Italy), equipped with a GC100 gas control unit and a Hamamatsu Lightningcure LC8 mercury lamp (Hamamatsu Photonics, Japan). The lamp was operated at 2% of its maximum output, corresponding to a UV intensity of 5 mW/cm^2 at the sample surface, as measured by a radiometer. An optical fiber directed the radiation (λ = 365 nm) onto the sample. Approximately 8–10 mg of sample was weighed

into an open aluminum crucible, with an identical open pan used as a reference. All measurements were conducted at room temperature (25 °C). Each sample was tested in duplicate to ensure repeatability.

2.5.9. DMA

The storage modulus, loss modulus, and loss factor (tanδ) of the UV-cured and reprocessed vitrimer samples were measured using a Triton Technology dynamic mechanical analyzer (DMA). The dimensions of the samples were 0.86 × 10 × 10 mm. The analysis was performed over a temperature range from −60 °C to 100 °C in a tensile mode at a heating rate of 3 °C/min and a frequency of 1 Hz. The glass transition temperature (T_g) was determined as the temperature corresponding to the peak of the tanδ curve.

2.5.10. Gel fraction

The gel fraction was determined using Soxhlet extraction. Three parallel samples were weighed and immersed in boiling acetone for 48 h. After extraction, the insoluble residue was dried and weighed to calculate the gel fraction.

2.5.11. Tensile properties

Tensile tests were conducted using a Tinius Olsen 25ST universal testing machine (Tinius Olsen, USA) to evaluate the mechanical properties of the samples. The tests were carried out at a 1 mm/min strain rate up to 2% elongation, followed by 5 mm/min beyond that point. Each measurement was repeated at least three times, and the average values are reported.

2.5.12. Optical Microscopy

Ivesta 3 stereo microscope (Leica Microsystems, Germany) with integrated camera was used to obtain images of the 3D printed structure.

3. Results and discussion

3.1. Photo-DSC, and FTIR

The UV curing process of the bio-based formulations was investigated through photo-DSC and FTIR spectroscopy. Photo-DSC analysis was used to monitor the exothermic heat flow during polymerization. As photopolymerization proceeds, exothermic heat raises the resin temperature, temporarily enhancing reactive species' molecular mobility and diffusion.[23] However, this thermal effect is insufficient to offset the dramatic viscosity increase due to full crosslinking. The measurements revealed notable differences in photopolymerization behavior between vitrimer samples depending on the amount of the transesterification catalyst (Figure 2a). Catalyst-free samples exhibited higher polymerization enthalpy (235-241 J/g) and a rapid exothermic peak at approximately 5 s. In contrast, catalyst-vitrimers exhibited lower enthalpy values (167-203 J/g) and a delayed exothermic peak around 12 s, indicating a slower and less exothermic polymerization process. This is supported by the gel fraction measurements, which showed higher values for photopolymerized catalyst-free vitrimers compared to catalyst-vitrimers (Figure 3e). Additionally, the delayed onset of polymerization may indicate that the catalyst absorbs or scatters UV light, thereby reducing monomer mobility and hindering the initiation and propagation of reactive radical species. A similar trend was observed with increasing acrylated epoxidized rapeseed oil (AERO) content.[24] Higher AERO concentrations led to a slight reduction in both the polymerization rate and the total heat released. This behavior is attributed to increased resin viscosity (Figure S3), which limits the mobility of reactive species and thus slows down the polymerization process.[25]

FTIR data further confirmed a high degree of conversion for catalyst-free vitrimers (Figure 2b). AERO10 showed the highest DBC value of 75% due to the high crosslinking density. The DBC graph also indicated that the optimal curing time of resins was approximately 20-30 s. Thereto, all the films were cured for 30 s to facilitate complete crosslinking. However, incomplete crosslinking may also result from surface effects such as the screening, which can influence the interpretation of crosslinking efficiency, i.e., rapid surface curing absorbs most of the UV light, limiting its penetration into deeper layers.[26] Rusu *et al.* studied this using photo-DSC and reported higher conversion at the top of irradiated samples.[23] It was found that the influence of oxygen inhibition is dependent on curing conditions, e.g., at temperatures below 50 °C, when the inhibitory effect of oxygen appeared more pronounced.

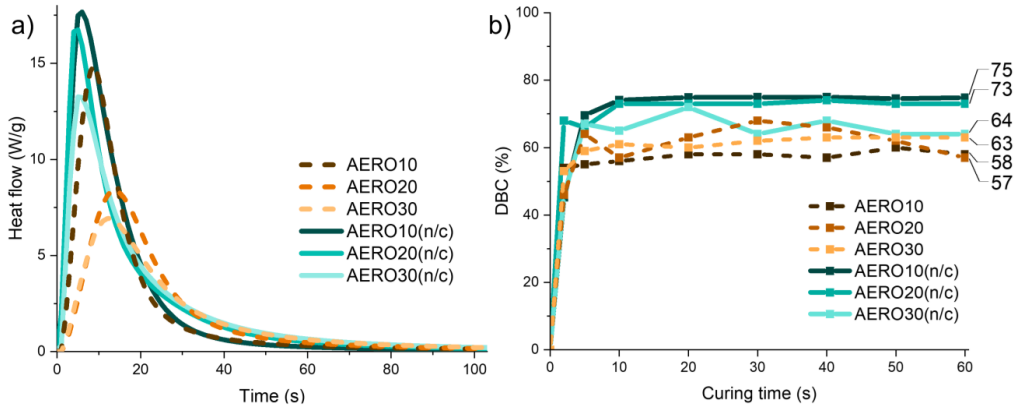

Figure 2. Comparison of catalyst- and catalyst-free AERO formulations: a) photo-DSC curves; b) double bond conversion (DBC) values at different UV curing times.

3.2. Thermal reprocessing

For the thermal reprocessing experiments as shown in Figure 3a, the UV-cured AERO vitrimer films were ground into fine particles and then molded into bulk samples using hot-pressing as described in the Materials and methods section. Initial reprocessing trials were carried out with AERO30 at 180 °C for 2.5 h and yielded successful reprocessing; however, the vitrimer appeared visually hazy and lacked full transparency (Figure 3b). Enhanced visual appearance and integrity of reprocessed film samples were achieved when the reprocessing temperature was increased up to 200 °C, while the reprocessing time was reduced to 2 h (Figure 3b). Using the optimized conditions two consecutive reprocessing cycles were investigated, while the vitrimer performance was assessed after each cycle.

The same experimental conditions were used to examine the transesterification catalyst's role in vitrimers' reprocessability. For the catalyst-free vitrimer (AERO30(n/c)_cycle1), multiple cracks were developed during reprocessing, thus, bringing reduced mechanical integrity of the film (Figure 3c). Wu *et al*. reported that such crack formation during vitrimer processing can be influenced by the high hydroxyl-to-ester group ratio, which may slow down transesterification reaction and ultimately decrease crack-healing efficiency.[27] In contrast, the catalyst-vitrimer (AERO30_cycle1) remained smooth and intact, confirming its good reprocessability performance. Summarizing the obtained results demonstrate that the catalyst efficiently enables network rearrangement and improves structural recovery in vitrimer materials.

Similar observation was also revealed in FTIR spectra (Figure 3d), where solid lines represent catalyst-vitrimer formulations, while dashed lines correspond to catalyst-free formulations. Given the negligible spectral differences observed among AERO30, AERO20, and AERO10 (attributable to their identical chemical compositions aside from slight variations in concentration), the spectra of the latter are not shown. No significant spectral changes were observed after the first reprocessing cycle, indicating the material retains its crosslinked structure. Only a complete disappearance of a small band at 1637 cm^{-1} suggests additional thermally induced crosslinking, likely due to incomplete UV curing or limited monomer conversion caused by steric hindrance in highly functional acrylates.[28] Elevated thermal mobility may have enabled further reactions of previously inaccessible groups.[29], [30] After the second thermally driven transesterification reprocessing cycle (AERO30_cycle2), a distinct absorbance band appeared at 963 cm^{-1}, which could correspond to newly formed double bond vibrations. TGA-FTIR spectra data also confirm this observation in the following section. The observed band at 963 cm^{-1} can be attributed to out-of-plane C-H deformation of vinyl ethers, rotational isomerism in alkyl acrylates, or acrylate ester fragments.[31] Given the distinct nature of the band, it is likely assigned to primary alkyl vinyl ether. This band's absence in FTIR spectra for the catalyst-free sample (AERO30(n/c)_cycle2) confirms that both catalyst and heat cause polymer chain network rearrangement, influencing the decomposition pathways.

The gel fraction (Figure 3e) represents the insoluble part of the developed macromolecular chain network, which is directly related to its crosslinking mesh density and complemented the curing efficiency.[32] After each reprocessing cycle, the gel fraction showed only minor variations, indicating that the chain network structure was well preserved and that the vitrimer retained a high degree of crosslinking during reprocessing.

For the catalyst-vitrimers, gel fraction values ranged from 73 to 79%, whereas values of 85 to 96% were observed for the catalyst-free vitrimers, which is consistent with the obtained higher DBC values (Figure 2b).

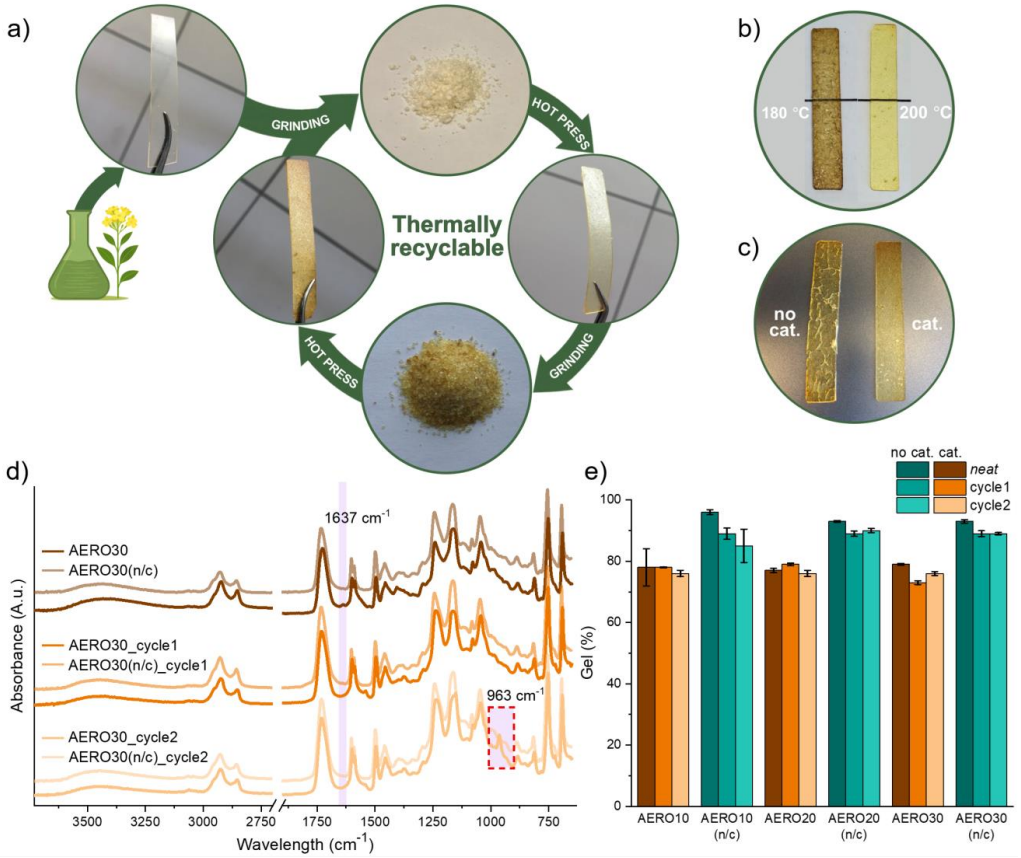

Figure 3. Vitrimer reprocessing and characterization: a) reprocessability and circularity of the developed AERO vitrimers; b) temperature influence on AERO30 during hot-pressing; c) catalyst influence on AERO30 during hot-pressing; d) FTIR spectra of UV-cured and reprocessed AERO30: dark lines represent catalyst-vitrimers; lighter semi-transparent lines represent catalyst-free vitrimers; e) gel content of UV-cured and reprocessed vitrimers after Soxhlet extraction.

3.3. TGA and TGA-FTIR

Thermal stability is often assessed using temperature ramp measurements, which typically reveal that the onset of weight loss occurs at temperatures higher than those required for transesterification. Reprocessing below this threshold is commonly assumed as thermally safe process with negligible decomposition at stress relaxation.[11], [33], [34] However, this approach is criticized due to non-accurate reflection of real processing conditions as vitrimer reprocessing at elevated temperatures can take several hours.[35] Therefore, isothermal thermogravimetric analysis is more accurate choice to evaluate the long-term thermal behavior of vitrimers during hot-pressing. Figure 4 presents measurements performed under N_2 atmosphere.

TGA revealed that GDA monomer was likely responsible for the initial thermal decomposition, as higher concentrations in the formulation resulted in a slight decrease in thermal stability of all vitrimer materials (Figure S4). The subsequent thermal decomposition of the remaining crosslinked network occurred between 300 and 480 °C, similarly as reported for vegetable oil-based systems.[36]–[38] Up to 480 °C, no significant differences were observed in the decomposition behavior of the samples under N_2 and air atmospheres, except in the presence of air, an additional degradation stage occurred above 480 °C (Figure S5), resulting in near-complete degradation, similar to that reported elsewhere.[39] The decomposition mechanism of acrylated vegetable oils is complex and proceeds through multiple steps, including

dehydration, decarboxylation, and the breakdown of ester and acrylate functionalities, ultimately yielding a range of intermediate and volatile products.[40] Volatile products characteristic of our prepared vitrimers may include *β*-hydroxy esters,[41] diesters, glycol derivatives, or ethers.[42], [43] TGA-FTIR analysis of UV-cured AERO30 and AERO30(n/c) was performed to identify some evolved gaseous products. The respective 3D FTIR spectra (Figure 4a, b) implied that volatile fragments formed much faster for AERO30 due to dynamic bond exchange.[41] AERO30 also showed higher absorbance, especially in the CO_2 and C=O regions, confirming enhanced decomposition (Figure 4c).[44], [45]

Transesterification catalyst-free samples exhibited higher thermal stability (Figure 4d, e) with a single-stage decomposition peaking at 410 °C (Figure 4f), whereas catalyst-vitrimers peaked at 370 °C, indicating a more heterogeneous structure.

Regarding reprocessing, thermal stability increased with each reprocessing step (Figure 4d, e, f). This was likely because the thermally unstable, low-molecular-weight or unreacted components volatilized during the hot-pressing process, leaving behind the material mainly consisting of the more stable, crosslinked network. Vilanova-Perez *et al*. compared UV-cured vitrimers using a radical photoinitiator vs thermally cured vitrimers using a radical thermal initiator and observed that photocured vitrimers degraded at lower temperatures than thermally cured vitrimers, attributed to lower crosslinking density.[46]

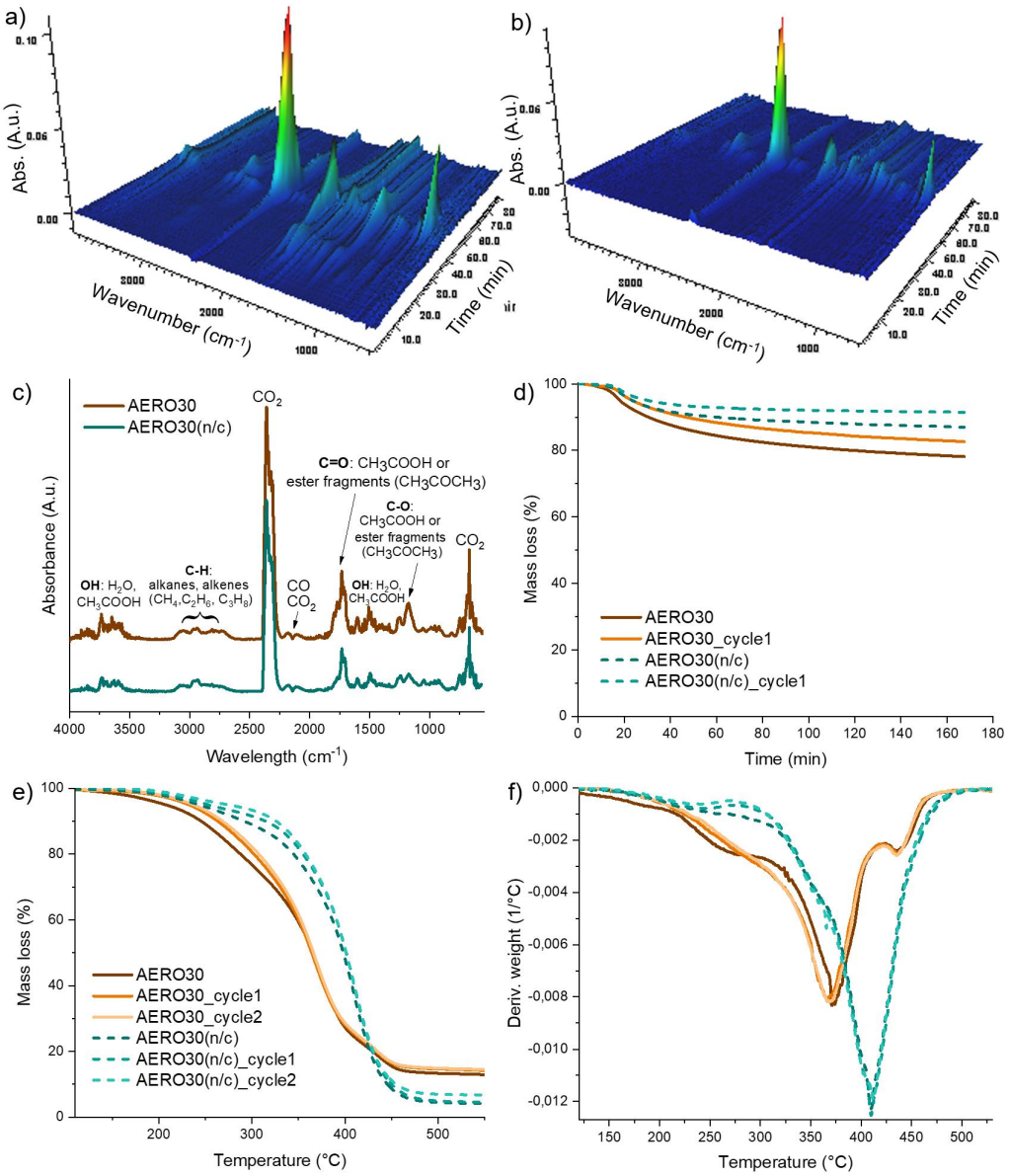

Figure 4. The 3D surface graphs for the FTIR spectra of the evolved gases produced by a) AERO30 and b) AERO30(n/c); c) FTIR spectra of evolved gases during thermal decomposition of UV-cured catalyst- and catalyst-free AERO30 vitrimers at the time of maximum absorbance (T = 370 °C and T = 410 °C, respectively); d) isothermal curves for UV-cured and reprocessed catalyst- and catalyst-free AERO30 vitrimers; e) temperature ramp curves for UV-cured and reprocessed catalyst- and catalyst-free AERO30 vitrimers; f) the respective DTG curves.

3.4. Stress relaxation

The relaxation time for vitrimers was monitored by isotherms ranging from 180 to 200 °C (Figure S6). The stress relaxation rate in vitrimers is influenced by temperature, catalyst type and concentration, polymer network structure, and crosslinking density.[41] It is commonly denoted by the characteristic relaxation time (τ*), which is the time it takes for the sample to relax to 1/e (~37%) of its initial modulus.[47] When subjected to an external stimulus, the dynamic bonds within CANs reorganize reversibly, allowing the network to relax

stress and exhibit macroscopic flow behavior without compromising the overall integrity of the material.[48] The stress relaxation rates of cured AERO vitrimers increased with increasing temperature because of thermally activated dynamic bond exchange reactions.[49] For example, when the temperature was 180 °C, the network of cured AERO30 exhibited a relaxation time of 20 min, but dropped to 14 min at 200 °C (Figure S6). Adding $Zn(acac)_2$ catalyst lowered the activation energy for the dynamic bond exchange reactions between ester and hydroxyl groups. Stress relaxation for AERO10, AERO20 and AERO30 at 200 °C was observed after 10, 16 and 14 min, respectively (Figure 5a). Notably, catalyst-free samples demonstrated a distinct stress relaxation behavior at 200 °C; however, at significantly slower rates i.e. after 31, 34, and 33 min, respectively, which is 2-3 times slower than catalyst-vitrimer. Figure 5b schematically illustrates dynamic -COOR and -OH exchange reactions, where i) slower exchange occurs in a more crosslinked AERO-based network whereas ii) the presence of $Zn(acac)_2$ accelerates transesterification within a less crosslinked AERO-based network. The same effect of the catalyst was also observed at lower temperatures (Figure S6). Similar results were reported by Capelot *et al*., who observed that a stress relaxation time of catalyst-free epoxy-acid vitrimer was 15 h at 150 °C, but dropped to 2 h when zinc acetate or $Zn(acac)_2$ was used.[41] Beside the catalyst, the authors demonstrated that an excess of OH groups promotes transesterification, and that their concentration controls the vitrimer reprocessing behavior. Shaukat *et al*. demonstrated that the presence of ester moieties, whilst keeping the concentration and ratio of -OH functional acrylate monomers constant, accelerated both the curing process and the stress relaxation rate of related thiol-acrylate vitrimers.[50] While Vilanova-Perez *et al*. suggested that the photoinitiator (phosphine oxide) could enhance dynamicity by promoting the exchange reaction in vitrimers.[46]

When comparing the stress relaxation of cured AERO10, AERO20, and AERO30, it was found that cured AERO10 relaxed slightly faster near the 1/e threshold. The increase of -OH group total concentration, that are available for transesterification complementing lower viscosity, is relevant to the observed phenomena.[51] Despite this, the differences in stress relaxation between samples with varying AERO content were minimal, which aligns well with the gel fraction representing negligible differences in crosslinking density (Figure 3e). Catalyst-free samples presented higher gel fraction, representing higher crosslinking density, which slows the overall relaxation rate.[52], [53] It is worth reminding that stress relaxation can be attributed not only to dynamic bond exchange, but also to the gradual release of internal stresses accumulated during polymerization, mainly due to volumetric shrinkage.[54]

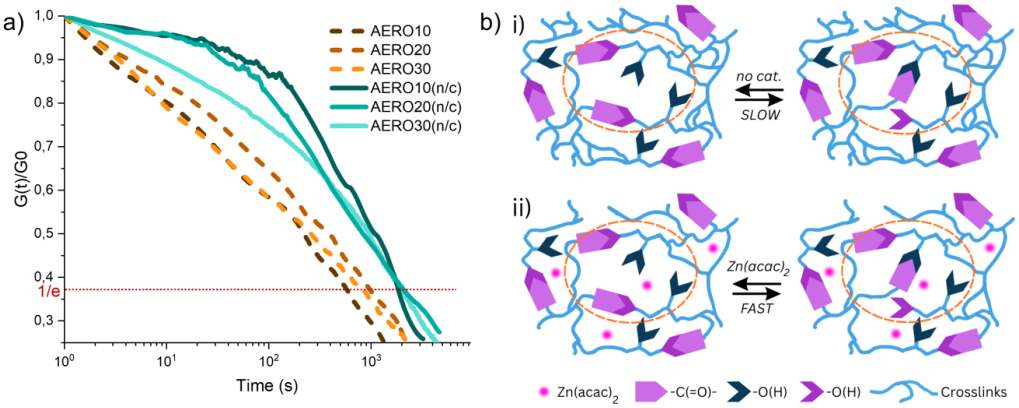

Figure 5. a) Stress relaxation at 200 °C of catalyst-free and catalyst-vitrimers with different amounts of AERO; b) schematic representation of dynamic bond exchange during transesterification: i) higher network crosslinking density without the transesterification catalyst, ii) lower network crosslinking density with $Zn(acac)_2$ as transesterification catalyst.

3.5. Mechanical and thermomechanical properties

DMA was conducted to evaluate the effect of reprocessing on the thermomechanical properties of the materials (Figure 6a). All vitrimers exhibited similar dynamic stiffness values. AERO30 showed the higher storage modulus in the glassy and rubbery regions (below and above T_g), indicating a rigid crosslinked network.[46] After reprocessing, the storage moduli absolute values decreased, reflecting a loss of stiffness and elasticity, likely due to network rearrangement, partial degradation, and minor chain scission.[55]

Tanδ, which reflects the damping properties of a material, showed the sharpest and highest peak for UV-cured AERO30 specifying glass transition temperature T_g and indicating a more homogeneous macromolecular chain network. In contrast, the broader and lower intensity peaks of reprocessed samples suggest increased heterogeneity due to uneven bond exchange through transesterification.[20] T_g decreased from 18 °C (AERO30) to 13 °C and 14 °C (AERO30_cycle1, AERO30_cycle2) after reprocessing cycles. Cuminet *et al*. also reported a drop of T_g from 47 to 30 °C for vitrimer after reprocessing at 150 °C for 1.5 h, suggesting moisture-induced hydrolysis or plasticization under constrained conditions that hindered water evaporation from the samples.[19]

Tensile tests were conducted to evaluate the reprocessing efficiency further. Although the tensile strength absolute values of reprocessed samples were not fully restored in comparison to the initial material, a considerable strength recovery was observed (Figure 6b, Table 2). UV-cured AERO10, AERO20, and AERO30 recovered 67, 71, and 98 % of the initial tensile strength after the first cycle. Subsequently, 41%, 50 % and 44 % of the initial tensile strength were recovered after the second cycle, respectively. The decreased mechanical strength after reprocessing was inevitable due to the broken covalent networks during vigorous grinding.[56], [57] Interestingly, AERO30 also demonstrated the highest recovery efficiency after the first cycle, despite having the lowest OH group content. It is suggested that with fewer multifunctional alcohols (GDA), the network in AERO30 is less heterogeneous, allowing smoother bond rearrangement during reprocessing.[56] The tensile modulus values remained essentially unchanged after reprocessing, suggesting that the stiffness of the network backbone was maintained even as ultimate strength and elongation decreased. In terms of formulations, increasing AERO content decreased both tensile strength and elongation at break, consistent with the lower crosslink density and higher aliphatic chain flexibility typically associated with higher renewable feedstock content such as vegetable oils.[58]

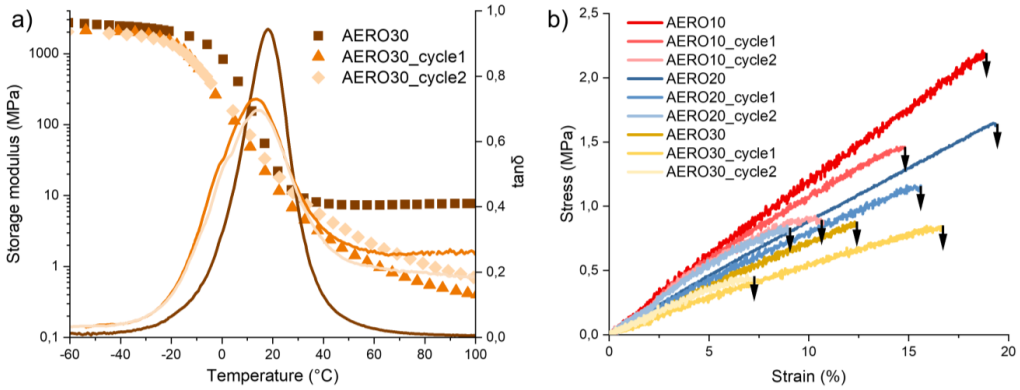

Figure 6. a) Storage modulus and tanδ curves of UV-cured and reprocessed catalyst-vitrimer AERO30; b) tensile stress-strain curves of UV-cured and reprocessed catalyst-vitrimers.

Table 2. Tensile data of vitrimers before and after reprocessing

	Stress, MPa	Elongation at break, %	Tensile modulus E, MPa
AERO10	2.19 ± 0.09	18.2 ± 2.0	12.5 ± 0.4
AERO10_cycle1	1.46 ± 0.09	14.8 ± 2.0	12.4 ± 0.6
AERO10_cycle2	0.90 ± 0.03	10.6 ± 0.3	12.4 ± 0.3
AERO20	1.64 ± 0.27	19.2 ± 2.8	9.1 ± 0.7
AERO20_cycle1	1.16 ± 0.20	15.6 ± 2.9	8.6 ± 0.5
AERO20_cycle2	0.82 ± 0.20	9.1 ± 2.9	11.5 ± 0.4
AERO30	0.86 ± 0.06	12.3 ± 1.2	7.6 ± 0.3
AERO30_cycle1	0.84 ± 0.11	16.7 ± 2.1	5.6 ± 0.3
AERO30_cycle2	0.43 ± 0.04	7.3 ± 0.2	7.0 ± 0.2

3.6. Repairability

Further catalyst-vitrimers were investigated for the material's repairability. The photos in Figure 7a demonstrate the vitrimer repairability testing for rectangular samples: initially, vitrimer resins were printed with a hole to simulate damage (e.g., “AERO10 3D | defect”), and their tensile properties were measured. In early repair trials, a 3D printed circular insert was placed into the hole, followed by thermal treatment to

activate the dynamic bond exchange. However, this approach failed due to insufficient interfacial contact between the two parts. A second approach proved more effective – fresh liquid resin was poured into the hole, then UV-cured and thermally treated at 200 °C for 1 h (e.g., “AERO10 3D | repaired”). This approach succeeded in repairing the vitrimer.

Among the damaged vitrimers, AERO20 3D | defect showed the highest tensile strength and elongation, reaching 1.56 MPa and 20.4%, respectively. After repair, these values increased to 2.56 MPa and 48.3%, indicating substantial recovery of mechanical performance. At the same time, AERO10 3D | defect exhibited the highest tensile modulus, reaching 11.5 MPa, which decreased to 7.1 MPa after repair.

The tensile property ratios (after repair to before repair) are summarized in Figure 7c. The AERO30 3D vitrimers demonstrated the largest relative improvement, with tensile strength and elongation increasing by up to 2.0- and 2.9-fold, respectively. However, this enhancement in strength and ductility was accompanied by a reduction in tensile modulus across all formulations, indicating a trade-off between stiffness and repair-induced network rearrangement. The recovery of mechanical performance after repair highlights the effective dynamic behavior and improved interfacial integration of the developed vegetable oil-based UV-curable vitrimer system.

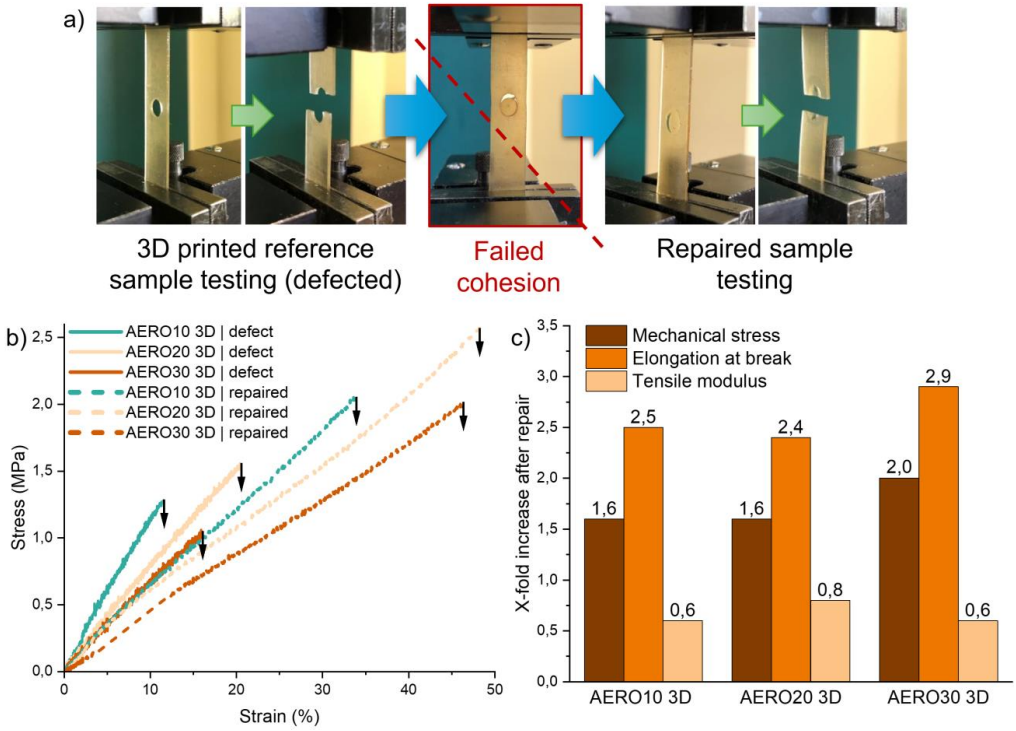

Figure 7. 3D printed vitrimers before and after damage (hole) repair: a) photos of damaged and repaired sample testing; b) the obtained stress-strain curves; c) calculated ratios of tensile properties.

3.7. 3D printing

To assess the printability of the developed vitrimers, the resin with the highest AERO content (AERO30) was selected for testing. The selection of AERO30 resin considered viscosity as a key parameter influencing the flow behavior within the vat of the DLP printer. All vitrimer resins possessed relatively low viscosities, making them well-suited for vat polymerization-based 3D printing (Figure S2). The obtained vitrimer resin viscosity was in the range of 458 to 939 mPa·s, which ensures proper resin leveling between layers, promoting consistent layer adhesion and directly affecting the printed object's dimensional accuracy and surface quality in agreement with our earlier findings.[22] The 3D printed sharp mountain structure demonstrated great accuracy, high precision, and fine resolution at different magnifications (Figure 8). The object exhibited precise, straight faces and smooth curves, with a layer height of 50 µm. The absence of visible defects such as delamination or surface irregularities confirms the vitrimer resin’s suitability for high-resolution 3D printing.

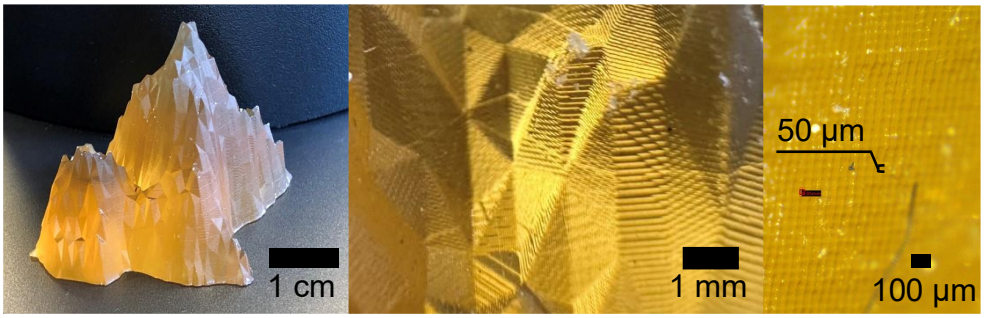

Figure 8. Validation of AERO30 vitrimer resin 3D-printing by vat photopolymerization.

4. Conclusions

This study establishes a comprehensive understanding of structure-property relationships in UV-curable AERO-based vitrimer networks by systematically comparing catalyst-free and $Zn(acac)_2$-catalyzed systems within a unified bio-based resin platform. The findings highlight the developed AERO vitrimer material's efficient performance, repairability and potential to become mechanically reinforced during the repairing process – an advantage for extending service life and performance.

It was observed that catalyst-vitrimers exhibited lower photopolymerization enthalpy, leading to lower crosslinking macromolecular chain network densities. On the other hand, lower crosslinking density facilitated stress relaxation for transesterification catalyst-free vitrimers, highlighting the role of hydroxyl and ester group concentration and expanding the design space for catalyst-free vitrimer systems. Catalyst-free vitrimers possessed higher thermal stability, while catalyst-vitrimers offered superior reprocessability. TGA-FTIR analysis supported this observation by revealing higher CO_2 and carbonyl-rich volatile emissions for catalyst-vitrimers. Under optimized conditions, catalyst-vitrimers maintained excellent optical visual transparency and structural integrity, recovering up to 98% of tensile strength after the first and up to 50% after the second reprocessing cycle.

Vitrimer transesterification during damage repair led to material's final outstanding mechanical performance – excellent repairability of 3D printed parts, reaching up to 2.9-fold increase in tensile properties, which is a valuable trait for extending the lifespan of 3D-printed vitrimer components. Meanwhile, the developed AERO vitrimer resins exhibited excellent 3D printing performance with high resolution and accuracy for a more detailed geometrical structure.

These findings establish a framework for designing customizable, reprocessable, and sustainable vegetable oil-based vitrimers, paving the way for developments in advanced vat photopolymerization additive manufacturing resin materials. Future efforts could focus on optimizing the balance between reprocessability and thermal stability while exploring novel formulations for advanced additive manufacturing applications.

CRediT authorship contribution statement

Greivule Sabine: Writing – original draft, Writing – review & editing, Methodology, Investigation, Formal analysis, Data curation, Visualization, Conceptualization. **Besprozvannaja Inga**: Formal analysis, Data curation. **Porcarello Matilde**: Formal analysis. **Gaidukovs Sergejs**: Writing – review & editing, Validation, Conceptualization, Funding acquisition, Supervision.

Conflicts of Interest

The authors declare no conflicts of interest.

Acknowledgment

This work was supported by the EU Recovery and Resilience Facility within the Project No 5.2.1.1.i.0/2/24/I/CFLA/003 "Implementation of consolidation and management changes at Riga Technical University, Liepaja University, Rezekne Academy of Technology, Latvian Maritime Academy and Liepaja

Maritime College for the progress towards excellence in higher education, science and innovation" academic career doctoral grant (ID 1097).

Data Availability Statement
The data that support the findings of this study are available from the corresponding author upon reasonable request.

Supporting Information
Additional supporting information can be found online in the Supporting Information section.

References

[1] M. Galià, L. M. de Espinosa, J. C. Ronda, G. Lligadas, and V. Cádiz, "Vegetable oil-based thermosetting polymers," *Eur. J. Lipid Sci. Technol.*, vol. 112, no. 1, pp. 87–96, Jan. 2010, doi: 10.1002/ejlt.200900096.

[2] E. Morici and N. T. Dintcheva, "Recycling of Thermoset Materials and Thermoset-Based Composites: Challenge and Opportunity," *Polymers*, vol. 14, no. 19. 2022, doi: 10.3390/polym14194153.

[3] C. J. Kloxin and C. N. Bowman, "Covalent adaptable networks: Smart, reconfigurable and responsive network systems," *Chem. Soc. Rev.*, vol. 42, no. 17, pp. 7161–7173, 2013, doi: 10.1039/c3cs60046g.

[4] H. Nabipour *et al.*, "A bio-based intrinsically flame-retardant epoxy vitrimer from furan derivatives and its application in recyclable carbon fiber composites," *Polym. Degrad. Stab.*, vol. 207, p. 110206, Jan. 2023, doi: 10.1016/j.polymdegradstab.2022.110206.

[5] B. Trinh, P. Owen, A. VanderHeide, A. Gupta, and T. H. Mekonnen, "Recyclable and Self-Healing Natural Rubber Vitrimers from Anhydride-Epoxy Exchangeable Covalent Bonds," *ACS Appl. Polym. Mater.*, vol. 5, no. 11, pp. 8890–8906, Nov. 2023, doi: 10.1021/acsapm.3c01258.

[6] J. Peng *et al.*, "High-performance epoxy vitrimer with superior self-healing, shape-memory, flame retardancy, and antibacterial properties based on multifunctional curing agent," *Compos. Part B Eng.*, vol. 242, p. 110109, Aug. 2022, doi: 10.1016/j.compositesb.2022.110109.

[7] Y.-Y. Liu, J. He, Y.-D. Li, X.-L. Zhao, and J.-B. Zeng, "Biobased epoxy vitrimer from epoxidized soybean oil for reprocessable and recyclable carbon fiber reinforced composite," *Compos. Commun.*, vol. 22, p. 100445, Dec. 2020, doi: 10.1016/j.coco.2020.100445.

[8] C. Li, B. Ju, and S. Zhang, "Fully bio-based hydroxy ester vitrimer synthesized by crosslinking epoxidized soybean oil with doubly esterified starch," *Carbohydr. Polym.*, vol. 302, p. 120442, Feb. 2023, doi: 10.1016/j.carbpol.2022.120442.

[9] X.-L. Zhao, Y.-Y. Liu, Y. Weng, Y.-D. Li, and J.-B. Zeng, "Sustainable Epoxy Vitrimers from Epoxidized Soybean Oil and Vanillin," *ACS Sustain. Chem. Eng.*, vol. 8, no. 39, pp. 15020–15029, Oct. 2020, doi: 10.1021/acssuschemeng.0c05727.

[10] S. Briede, A. Barkane, M. Jurinovs, V. K. Thakur, and S. Gaidukovs, "Acrylation of biomass: A review of synthesis process: Know-how and future application directions," *Curr. Opin. Green Sustain. Chem.*, vol. 35, p. 100626, Jun. 2022, doi: 10.1016/j.cogsc.2022.100626.

[11] M. Fei, T. Liu, B. Zhao, A. Otero, Y. C. Chang, and J. Zhang, "From Glassy Plastic to Ductile Elastomer: Vegetable Oil-Based UV-Curable Vitrimers and Their Potential Use in 3D Printing," *ACS Appl. Polym. Mater.*, vol. 3, no. 5, pp. 2470–2479, 2021, doi: 10.1021/acsapm.1c00063.

[12] C. Hao, T. Liu, S. Zhang, W. Liu, Y. Shan, and J. Zhang, "Triethanolamine-Mediated Covalent Adaptable Epoxy Network: Excellent Mechanical Properties, Fast Repairing, and Easy Recycling," *Macromolecules*, vol. 53, no. 8, pp. 3110–3118, Apr. 2020, doi: 10.1021/acs.macromol.9b02243.

[13] C. Taplan, M. Guerre, C. N. Bowman, and F. E. Du Prez, "Surface Modification of (Non)-Fluorinated Vitrimers through Dynamic Transamination," *Macromol. Rapid Commun.*, vol. 42, no. 7. 2021, doi: 10.1002/marc.202000644.

[14] W. Cai *et al.*, “A Multifunctional Biomass Zinc Catalyst for Epoxy-Based Vitrimers and Composites,” *Eur. Polym. J.*, vol. 188. 2023, doi: 10.1016/j.eurpolymj.2023.111936.

[15] K. Moazzen, E. Rossegger, W. Alabiso, U. Shaukat, and S. Schlögl, “Role of Organic Phosphates and Phosphonates in Catalyzing Dynamic Exchange Reactions in Thiol-Click Vitrimers,” *Macromol. Chem. Phys.*, vol. 222, no. 12. 2021, doi: 10.1002/macp.202100072.

[16] S. Bhusal *et al.*, “Transesterification in Vitrimer Polymers Using Bifunctional Catalysts: Modeled with Solution-Phase Experimental Rates and Theoretical Analysis of Efficiency and Mechanisms,” *J. Phys. Chem. B*, vol. 125, no. 9, pp. 2411–2424, Mar. 2021, doi: 10.1021/acs.jpcb.0c10403.

[17] J. Casado, O. Konuray, A. Roig, X. Fernández-Francos, and X. Ramis, “3D printable hybrid acrylate-epoxy dynamic networks,” *Eur. Polym. J.*, vol. 173, no. May, 2022, doi: 10.1016/j.eurpolymj.2022.111256.

[18] A. K. Biswal, A. Nandi, H. Wang, and A. Vashisth, “Ultrasonic Welding of Glass Fiber Reinforced Vitrimer Composites,” *Proc. Am. Soc. Compos. - 38th Tech. Conf. ASC 2023*, vol. 242, no. July, pp. 149–158, 2023, doi: 10.12783/asc38/36527.

[19] F. Cuminet *et al.*, “Synthesis of a transesterification vitrimer activated by fluorine from an α,α-difluoro carboxylic acid and a diepoxy,” *Eur. Polym. J.*, vol. 182, p. 111718, 2023, doi: 10.1016/j.eurpolymj.2022.111718.

[20] G. Capiel, E. Hernández, N. E. Marcovich, and M. A. Mosiewicki, “Stress relaxation behavior of weldable crosslinked polymers based on methacrylated oleic and lauric acids,” *Eur. Polym. J.*, vol. 132, no. March, p. 109740, 2020, doi: 10.1016/j.eurpolymj.2020.109740.

[21] J. Lacombe and C. Soulié-Ziakovic, “Controlling self-patterning of acrylate films by photopolymerization,” *Polym. Chem.*, vol. 8, no. 7, pp. 1129–1137, 2017, doi: 10.1039/c6py02072k.

[22] M. Jurinovs *et al.*, “Sustainable 4D Printable Biobased Shape Memory Polymers with Linear Tunability and Multistimuli Actuation for Advanced Applications,” *Small Sci.*, vol. 2500104, pp. 1–13, 2025, doi: 10.1002/smsc.202500104.

[23] M. C. Rusu, C. Block, G. Van Assche, and B. Van Mele, “Influence of temperature and UV intensity on photo-polymerization reaction studied by photo-DSC,” *J. Therm. Anal. Calorim.*, vol. 110, no. 1, pp. 287–294, 2012, doi: 10.1007/s10973-012-2465-5.

[24] M. Bodor, A. Lasagabáster-Latorre, G. Arias-Ferreiro, M. S. Dopico-García, and M. J. Abad, “Improving the 3D Printability and Mechanical Performance of Biorenewable Soybean Oil-Based Photocurable Resins,” *Polymers*, vol. 16, no. 7. 2024, doi: 10.3390/polym16070977.

[25] J.-T. Lin, H.-W. Liu, K.-T. Chen, and D.-C. Cheng, “Modeling the Kinetics, Curing Depth, and Efficacy of Radical-Mediated Photopolymerization: The Role of Oxygen Inhibition, Viscosity, and Dynamic Light Intensity,” *Front. Chem.*, vol. 7, Nov. 2019, doi: 10.3389/fchem.2019.00760.

[26] S. Asmussen and C. Vallo, “Light absorbing products during polymerization of methacrylate monomers photoinitiated with phenyl-1,2-propanedione/amine,” *J. Photochem. Photobiol. A-Chem.*, vol. 202, no. 2–3. pp. 228–234, 2009, doi: 10.1016/j.jphotochem.2008.12.007.

[27] P. Wu, L. Liu, and Z. Wu, “A transesterification-based epoxy vitrimer synthesis enabled high crack self-healing efficiency to fibrous composites,” *Compos. Part A Appl. Sci. Manuf.*, vol. 162, no. May, 2022, doi: 10.1016/j.compositesa.2022.107170.

[28] B. Yamada, P. B. Zetterlund, and E. Sato, “Utility of propenyl groups in free radical polymerization: Effects of steric hindrance on formation and reaction behavior as versatile intermediates,” *Prog. Polym. Sci.*, vol. 31, no. 10. pp. 835–877, 2006, doi: 10.1016/j.progpolymsci.2006.08.005.

[29] A. Endruweit, M. S. Johnson, and A. C. Long, “Curing of composite components by ultraviolet radiation: A review,” *Polym. Compos.*, vol. 27, no. 2. pp. 119–128, 2006, doi: 10.1002/pc.20166.

[30] Y. Ren, Y. Dong, R. Yang, and Y. Yao, “Preparation and properties of ultraviolet/thermal dual-curable polyurethane acrylate,” *Int. J. Adhes. Adhes.*, vol. 99, no. February, p. 102580, 2020, doi: 10.1016/j.ijadhadh.2020.102580.

[31] G. E. McManis and L. E. Gast, “IR spectra of long chain vinyl derivatives,” *J. Am. Oil Chem. Soc.*, vol. 48, no. 11. pp. 668–673, 1971, doi: 10.1007/BF02638515.

[32] Y. Y. Liu, J. He, Y. D. Li, X. L. Zhao, and J. B. Zeng, “Biobased, reprocessable and weldable epoxy vitrimers from epoxidized soybean oil,” *Ind. Crops Prod.*, vol. 153. 2020, doi: 10.1016/j.indcrop.2020.112576.

[33] S. Zhang, T. Liu, C. Hao, A. Mikkelsen, B. Zhao, and J. Zhang, “Hempseed Oil-Based Covalent Adaptable Epoxy-Amine Network and Its Potential Use for Room-Temperature Curable Coatings,” *ACS Sustain. Chem. Eng.*, vol. 8, no. 39, pp. 14964–14974, 2020, doi: 10.1021/acssuschemeng.0c05223.

[34] E. Rossegger *et al.*, “Digital light processing 3D printing with thiol-Acrylate vitrimers,” *Polym. Chem.*, vol. 12, no. 5, pp. 638–644, 2021, doi: 10.1039/d0py01520b.

[35] B. Sölle, U. Shaukat, E. Rossegger, and S. Schlögl, “Synthesis and characterization of bio-based transesterification catalysts for green 3D-printable dynamic photopolymers,” *Polym. Chem.*, vol. 14, no. 44, pp. 4994–5003, 2023, doi: 10.1039/d3py00989k.

[36] D. Behera and A. K. Banthia, “Synthesis, characterization, and kinetics study of thermal decomposition of epoxidized soybean oil acrylate,” *J. Appl. Polym. Sci.*, vol. 109, no. 4, pp. 2583–2590, Aug. 2008, doi: 10.1002/app.28350.

[37] F. Habib and M. Bajpai, “Synthesis and Characterization of Acrylated Epoxidized Soybean Oil for UV-Cured Coatings,” *Chem. Chem. Technol.*, vol. 5, no. 3, pp. 317–326, 2011, doi: 10.23939/chcht05.03.317.

[38] S. Briede, M. Jurinovs, S. Nechausov, O. Platnieks, and S. Gaidukovs, “State-of-the-art UV-assisted 3D printing via a rapid syringe-extrusion approach for photoactive vegetable oil acrylates produced in one-step synthesis,” *Mol. Syst. Des. Eng.*, vol. 7, no. 11, pp. 1434–1448, 2022, doi: 10.1039/D2ME00085G.

[39] J.-H. Chen, J.-H. Lu, X.-L. Pu, L. Chen, and Y.-Z. Wang, “Recyclable, malleable and intrinsically flame-retardant epoxy resin with catalytic transesterification,” *Chemosphere*, vol. 294, p. 133778, May 2022, doi: 10.1016/j.chemosphere.2022.133778.

[40] A. Barkane, O. Platnieks, M. Jurinovs, and S. Gaidukovs, “Thermal stability of UV-cured vegetable oil epoxidized acrylate-based polymer system for 3D printing application,” *Polym. Degrad. Stab.*, vol. 181, 2020, doi: 10.1016/j.polymdegradstab.2020.109347.

[41] M. Capelot, D. Montarnal, F. Tournilhac, and L. Leibler, “Metal-catalyzed transesterification for healing and assembling of thermosets,” *J. Am. Chem. Soc.*, vol. 134, no. 18, pp. 7664–7667, 2012, doi: 10.1021/ja302894k.

[42] H. Matsubara, A. Yoshida, H. Ohtani, and S. Tsuge, “Compositional analysis of UV-cured acrylic ester resins by pyrolysis-gas chromatography in the presence of organic alkali,” *J. Anal. Appl. Pyrolysis*, vol. 64, no. 2. pp. 159–175, 2002, doi: 10.1016/S0165-2370(02)00028-1.

[43] H. Matsubara, A. Yoshida, Y. Kondo, S. Tsuge, and H. Ohtani, “Characterization of network structures in UV-cured acrylic ester resin by pyrolysis-gas chromatography in the presence of organic alkali,” *Macromolecules*, vol. 36, no. 13, pp. 4750–4755, 2003, doi: 10.1021/ma0217837.

[44] J. Li, J. Guo, and H. Dai, “Probing dissolved CO2(aq) in aqueous solutions for CO2 electroreduction and storage,” *Sci. Adv.*, vol. 8, no. 19. 2022, doi: 10.1126/sciadv.abo0399.

[45] G. C. de Carvalho *et al.*, “Influence of the atmosphere on the decomposition of vegetable oils: study of the profiles of FTIR spectra and evolution of gaseous products,” *J. Therm. Anal. Calorim.*, vol. 140, no. 5, pp. 2247–2258, 2020, doi: 10.1007/s10973-019-08960-9.

[46] A. Vilanova-Pérez, S. De la Flor, X. Fernández-Francos, À. Serra, and A. Roig, “Biobased Imine Vitrimers Obtained by Photo and Thermal Curing Procedures─Promising Materials for 3D Printing,” *ACS Appl. Polym. Mater.*, vol. 6, no. 6, pp. 3364–3372, 2024, doi: 10.1021/acsapm.3c03234.

[47] M. Capelot, M. M. Unterlass, F. Tournilhac, and L. Leibler, “Catalytic Control of the Vitrimer Glass Transition,” *ACS Macro Lett.*, vol. 1, no. 7, pp. 789–792, Jul. 2012, doi: 10.1021/mz300239f.

[48] M. Chen, L. Zhou, Y. Wu, X. Zhao, and Y. Zhang, “Rapid Stress Relaxation and Moderate Temperature of Malleability Enabled by the Synergy of Disulfide Metathesis and Carboxylate Transesterification in Epoxy Vitrimers,” *ACS Macro Lett.*, vol. 8, no. 3, pp. 255–260, Mar. 2019, doi: 10.1021/acsmacrolett.9b00015.

[49] B. M. El-Zaatari, J. S. A. Ishibashi, and J. A. Kalow, “Cross-linker control of vitrimer flow,” *Polym. Chem.*, vol. 11, no. 33, pp. 5339–5345, 2020, doi: 10.1039/D0PY00233J.

[50] U. Shaukat, E. Rossegger, and S. Schlögl, “Thiol–acrylate based vitrimers: From their structure–property relationship to the additive manufacturing of self-healable soft active devices,” *Polymer (Guildf).*, vol. 231, p. 124110, Sep. 2021, doi: 10.1016/j.polymer.2021.124110.

[51] A. Campanella, M. Fahimian, R. P. Wool, and J. Raghavan, “Synthesis and Rheology of Chemically Modified Canola Oil,” *J. Biobased Mater. Bioenergy*, vol. 3, no. 1, pp. 91–99, Mar. 2009, doi: 10.1166/jbmb.2009.1012.

[52] E. Rossegger *et al.*, “High resolution additive manufacturing with acrylate based vitrimers using organic phosphates as transesterification catalyst,” *Polymer (Guildf).*, vol. 221, no. February, 2021, doi: 10.1016/j.polymer.2021.123631.

[53] Y. Liu *et al.*, “Tuning the mechanical and dynamic properties of imine bond crosslinked elastomeric vitrimers by manipulating the crosslinking degree,” *Polym. Chem.*, vol. 11, no. 7, pp. 1348–1355, 2020, doi: 10.1039/C9PY01826C.

[54] H. Fang and C. A. Guymon, “Recent advances to decrease shrinkage stress and enhance mechanical properties in free radical polymerization: a review,” *Polym. Int.*, vol. 71, no. 5, pp. 596–607, May 2022, doi: 10.1002/pi.6341.

[55] L. Li, X. Chen, K. Jin, and J. M. Torkelson, “Vitrimers Designed Both to Strongly Suppress Creep and to Recover Original Cross-Link Density after Reprocessing: Quantitative Theory and Experiments,” *Macromolecules*, vol. 51, no. 15. pp. 5537–5546, 2018, doi: 10.1021/acs.macromol.8b00922.

[56] Y. You, W. L. Peng, P. Xie, M. Z. Rong, M. Q. Zhang, and D. Liu, “Topological rearrangement-derived homogeneous polymer networks capable of reversibly interlocking: From phantom to reality and beyond,” *Mater. Today*, vol. 33, pp. 45–55, Mar. 2020, doi: 10.1016/j.mattod.2019.09.005.

[57] H. Hinsken, S. Moss, J. R. Pauquet, and H. Zweifel, “Degradation of polyolefins during melt processing,” *Polym. Degrad. Stabil.*, vol. 34, no. 1–3. pp. 279–293, 1991, doi: 10.1016/0141-3910(91)90123-9.

[58] A. Ritere, M. Jurinovs, O. Platnieks, A. Barkane, and S. Gaidukovs, “A super-tough plant oil based elastomer for UV-light assisted 3D printed soft robotics and shape-memory,” *J. Mater. Chem. A*, vol. 12, no. 27. pp. 16569–16582, 2024, doi: 10.1039/d4ta02218a.

Sabīne Greivule dzimusi 1997. gadā Talsos. Rīgas Tehniskajā universitātē (RTU) ieguvusi bakalaura grādu ķīmijas tehnoloģijā (2020) un maģistra grādu ķīmijā un ķīmijas tehnoloģijā (2022). Strādājusi un praktizējusies RTU Organiskās ķīmijas tehnoloģijas institūta, SIA "*Tenax Panel*", W*orlée-Chemie GmbH* (Lauenburga, Vācija), *WKI Fraunhofer* (Brunsvika, Vācija) laboratorijās. Kopš 2022. gada strādā RTU Ķīmijas un ķīmijas tehnoloģijas institūtā, ieņemot zinātniskā asistenta amatu, patlaban ir šī institūta pētniece. Zinātniskās intereses saistītas ar akrilātu sintēzi un fotopolimerizācijas procesu izpēti.

Sabīne Greivule was born in 1997 in Talsi. She obtained a Bachelor's degree in Chemical Technology (2020) and a Master's degree in Chemistry and Chemical Technology (2022) from Riga Technical University (RTU). She has worked and completed internships in the laboratories of the Institute of Technology of Organic Chemistry, SIA "Tenax Panel", Worlée-Chemie GmbH (Lauenburg, Germany), and Fraunhofer WKI (Braunschweig, Germany). Since 2022, she has been working at the RTU Institute of Chemistry and Chemical Technology, initially as a Scientific Assistant and currently as a Researcher. Her scientific interests are focused on acrylate synthesis and the study of photopolymerization processes.